POLYTECHNIQUE MONTRÉAL

affiliée à l'Université de Montréal

An Innovative Bio-engineered 3D Interface Model for the Study of Cancer Metastasis

MANSOUREH MOHSENI GARAKANI

Institut de génie biomédical

Thèse présentée en vue de l'obtention du diplôme de *Philosophiae Doctor*

Génie biomédical

Mai 2022

© Mansoureh Mohseni Garakani, 2022.

POLYTECHNIQUE MONTRÉAL

affiliée à l'Université de Montréal

Cette thèse intitulée :

An Innovative Bio-engineered 3D Interface Model for the Study of Cancer Metastasis

présentée par **Mansoureh MOHSENI GARAKANI**

en vue de l'obtention du diplôme de *Philosophiae Doctor*

a été dûment acceptée par le jury d'examen constitué de :

Thomas GERVAIS, président

Abdellah AJJI, membre et directeur de recherche

Michael WERTHEIMER, membre et codirecteur de recherche

Derek ROSENZWEIG, membre et codirecteur de recherche

Géraldine MERLE, membre

Veena SANGWAN, membre externe

DEDICATION

To my precious parents,

My beloved son, Amir Hossein,

and

Love of my life, Mohammad,

For unconditional love, constant patience, and support

ACKNOWLEDGEMENTS

Before everything, I am thankful of God for all that he gave and did for me in my life.

During the course of my PhD, I had the chance to meet many incredible and exceptional people who massively helped me with my project and made everything possible for me. I first of all would like to thank my amazing supervisors: Prof. Abdellah Ajji, Prof. Michael Wertheimer, and Prof. Derek Rosenzweig for their unceasing support, encouragement, and guidance throughout my PhD studies. I am truly honored to be their student in the past few years.

I am profoundly thankful to my main supervisor, Prof. Abdellah Ajji, who always made sure that everything went well with my project and has always generously been there for me whenever I needed support during my research. Prof. Ajji was not only a very dignified and prominent professor, but he was also a great mentor for me. I have not only been learning from him in the scientific field, but also in my life; from his great attitude and patience towards others.

I am also deeply grateful to Prof. Michael Wertheimer, a distinguished professor in his field, for his invaluable advice and excellent guidance in bringing the best out of me. Prof. Wertheimer's supervision immensely affected my thesis to be the best it could be. I could always count on his helpful support whenever I needed it. Prof. Wertheimer's constant constructive comments greatly helped me to improve especially my writing skills during my PhD studies.

My sincere gratitude to Prof. Derek Rosenzweig, who tremendously helped me in the biology field throughout my studies with his energetic and kind nature. I learned everything I now know about cell biology from Prof. Rosenzweig. He was a big part of my research project with his constant support, insightful suggestions, and invaluable guidance. He enabled me to significantly expand my knowledge with what he taught me in the past few years. The impact that Prof. Rosenzweig had in my studies will substantially help me in my future careers.

I am truly grateful to my thesis committee members for their time to read and evaluate this thesis and their valuable and helpful suggestions: Prof. Thomas Gervais, Prof. Veena Sangwan, and Prof. Géraldine Merle.

I am also sincerely thankful to Prof. Mark Lavertu, Prof. Nick Virgilio, Prof. Stephan Reuter, Prof. Anie Philip, and Dr. Josianne Lefebvre for giving me the opportunity to be trained and work in their laboratory to accomplish some tests and analysis for this research.

I would like to express my deep gratitude to Dr. Linda Peltier at McGill University Health Center (MUHC) for her generous and invaluable support and insightful advice before and during my comprehensive exam. Many thanks to Dr. Amir Yadghar, Dr. Maryam Heidari, Dr. Haniyeh Molaei, and Dr. Maryam Nadimi to kindly support and help me a lot before my predoc exam.

I would like to sincerely thank Mr. Sean Watson, Dr. Bernard Nisol, and Dr. Cédric Pattyn for their valuable assistance, technical support, and insightful suggestions during the experimental works in the plasma laboratory and also special thank to Dr. Pouyan Ahangar to train me in the cell/tissue culture laboratory and Dr. Megan Cooke for always being there to kindly support and help. I would also like to deeply acknowledge Mr. Ateeque Siddique for editing the chapters of this thesis and for the French translation of the Abstract.

I am sincerely thankful to all my amazing colleagues and friends at the Institute of Biomedical Engineering, Chemical Engineering Department and Engineering Physics Department at Ecole Polytechnique Montreal for their valuable assistance, technical support and perceptive suggestions during this journey: Mr. Matthieu Gauthier, Mrs. Clair Cerclé, Mr. Richard Silverwood, Dr. Ebrahim Jalali, Mr. Dariush Alavijeh, Mrs. Neda Azizipour, Mr. Amirhossein Moslehi, Mrs. Anik Chevrier, Mr. Yves Leblanc, Mr. Julien Bissonnette-Dulude, and many thanks to Mrs. Amal Bennani for her constant support and help. I am also truly grateful to my wonderful colleagues and friends at Montreal General Hospital, Department of Surgery, Division of Orthopaedic Surgery for their practical supports: Dr. Li Li, Dr. Elie Akoury, Dr. Hyeree Park, Mr. Ateeque Siddique, Mrs. Meryem Blati, and also many thanks to all nice students in Prof. Rosenzweig's team for their warm friendships since summer 2018.

I do not know how to express my gratitude and profound appreciation to my beloved parents, Aghdas and Ahmad, for their unwavering love and supports. They taught me this key phrase: "Fight for your dream!" and I saw it in how they live. Also, many Thanks to my supportive and kind family members for their unconditional love and emotional supports from overseas.

At the end, a very special and profound thanks to the pillars of my life, two precious treasures, my lovely son and husband, this long journey would not have been possible without their constant patience and moral support.

My son, Amir Hossein! I am so thankful of God for having you. Thank you for bringing joy and happiness into my life and making it brilliant and colorful. I am so proud of who you are and becoming. You have unlimited potential to achieve your dreams. Be positive and strong!

Love of my life, my patient and kind husband, Mohammad! There are not enough words to express how appreciative I am to you! I am truly blessed to have you as a constant source of love, strength, and motivation during the past 21 years! Thank You, My MAN!

RÉSUMÉ

Les cancers métastatiques et leurs microenvironnements sont de nature complexe et très hétérogènes, présentent une grande variabilité entre les patients et sont généralement difficiles à traiter avec des agents thérapeutiques en raison de la chimiorésistance. Une telle complexité dans la composante cellulaire du microenvironnement tumoral est intensifiée par les relations entre les cellules cancéreuses métastatiques et les cellules stromales, affectant leur sensibilité/résistance aux médicaments thérapeutiques anticancéreux, et il est compliqué de la récapituler. Les chimiothérapies standards actuelles ne sont pas efficaces pour tous les patients et s'accompagnent généralement d'effets secondaires graves. Ainsi, l'identification de nouvelles thérapeutiques spécifiques au patient est un axe majeur de la recherche sur le cancer métastatique, pour tendre vers l'objectif de thérapies personnalisées et améliorer la qualité de vie des patients. Cependant, y parvenir reste un défi majeur en raison de l'état actuel des plateformes de culture *in vitro* non physiologiques. Actuellement, les tests de médicaments sont principalement effectués sur des modèles 2D conventionnels qui ne peuvent pas représenter les interactions critiques cellule-cellule et cellule-matrice extracellulaire, qui jouent un rôle essentiel dans la tumorigènes et la progression tumorale. Par conséquent, des modèles 3D *in vitro* plus complexes et physiologiquement plus pertinents imitant le microenvironnement du cancer humain pourraient considérablement aider au développement de nouvelles chimiothérapies pour des traitements personnalisés. De nombreux modèles de cancer 3D avancés et prometteurs ont été proposés ces dernières années pour simuler l'hétérogénéité tumorale, et ont été appliqués à la découverte et aux tests de médicaments. Néanmoins, peu de ces modèles ont été conçus sur la base de compartiments séparés du stroma et de la tumeur, en particulier ceux avec des caractéristiques mécaniques différentes imitant les interfaces des tissus mous-durs comme dans les microenvironnements tumoraux naturels.

Dans cette recherche doctorale, un nouveau modèle de co-culture *in vitro* 3D (nommé « PP-3D-S », pour « *Plasma Polymerized 3-Dimensional Scaffold* ») a été développé pour un tel dépistage chimiothérapeutique personnalisé ; il est personnalisable, reproductible, rentable et convivial, bien plus que les produits commerciaux existants tels que Matrigel®. Il peut représenter un modèle d'interface 3D du microenvironnement tissu-tumeur normal. Le PP-3D-S est généré en

combinant (A) un échafaudage de polymère nanofibreux électrofilé traité par décharge électrique (souvent de l'acide polylactique - APL) qui est pré-ensemencé avec des ostéoblastes ou des fibroblastes humains en tant que cellules stromales ; et (B) une surcouche d'hydrogel à base d'alginate/gélatine sur (A) qui est incorporée avec des lignées cellulaires cancéreuses (par exemple du cancer du sein humain) avec une agressivité différente, ou des cellules cancéreuses dérivées du patient (par exemple des cellules métastasées osseuses), pour créer un système 3D physiologiquement réaliste représentant une interface tissulaire stroma-tumeur. Ce modèle est appliqué comme outil d'essai de migration et permet de quantifier la migration et la réponse chimiothérapeutique de différentes cellules cancéreuses immortalisées ou dérivées de patients vers un compartiment stromal.

Le modèle PP-3D-S peut être adapté pour cibler divers types de tissus et de cancers, en modifiant les propriétés biophysiques et mécaniques du polymère, la morphologie de l'échafaudage et la composition de l'hydrogel. Le modèle hybride 3D a été caractérisé pour les types de traitement au plasma optimaux, les matériaux polymères et la morphologie des échafaudages, y compris le diamètre des fibres et la taille des pores. Il a été constaté que les tapis de APL modifiés au plasma, mais aussi le polyuréthane et le polycaprolactone, amélioraient considérablement l'adhésion et la croissance cellulaires initiales par rapport aux témoins non traités. Il a été démontré que les traitements au plasma, y compris la fonctionnalisation au plasma et la polymérisation au plasma à basse pression et à pression atmosphérique, stimulent considérablement l'adhésion, la prolifération, la migration et l'invasion des cellules tumorales. De plus, des différences significatives dans la migration des cellules tumorales entre les échafaudages de petite taille (diamètre des fibres) et de taille moyenne ou grande ont été observées pour tous les tapis traités et non traités. L'impact de deux médicaments chimiothérapeutiques différents, la Doxorubicine (Dox) et le Cisplatine (Cis), sur la migration et l'activité métabolique des cellules cancéreuses des patients et de leurs homologues de lignées cellulaires immortalisées a été évalué. Différents comportements migratoires ont été trouvés, avec des valeurs de CI50 qui étaient pour la plupart conformes aux caractéristiques cellulaires attendue. Dox et Cis se sont révélés capables de réduire les activités métaboliques et de bloquer la migration, mais une efficacité plus élevée (ou une CI50 inférieure) a été observée avec Dox. De plus, dans deux ensembles différents de tests de dépistage de Dox, les performances du PP-3D-S

ont été comparées à celles du Matrigel® dans les tests de migration après exposition à différentes doses de Dox, avec des résultats numériques très similaires. Dans l'ensemble, ces données indiquent que PP-3D-S est un modèle de tumeur (migration) 3D efficace, adapté au dépistage de médicaments pour des thérapies personnalisées dans le traitement du cancer métastatique.

Mots-clés : Système de co-culture 3D, Échafaudages nanofibreux, Traitement de surface plasmatique, Modèles tissulaires d'interface, Dépistage de médicaments, Cancer du sein, Métastase osseuse, Médecine personnalisée

ABSTRACT

Metastatic cancers and their microenvironments are complex and highly heterogeneous in nature, show large patient variability, and are usually difficult to treat with therapeutic agents due to chemoresistance. Such complexity in the cellular component of the tumor microenvironment is intensified by the relations between metastatic cancer cells and stromal cells, affecting their sensitivity/resistance to anti-cancer therapeutic drugs, and it is complicated to recapitulate. Current standard chemotherapeutics are not effective for every patient and are typically accompanied with severe side effects; thus, identifying new patient-specific therapeutics is a main focus of research into metastatic cancer, to move towards the goal of personalized therapies and to enhance quality of life for patients. However, achieving this remains a major challenge owing to the current state of non-physiological *in vitro* culture platforms: Currently, drug testing is mainly performed on conventional 2D models that cannot represent critical cell-cell and cell-extracellular matrix (ECM) interactions, which play essential roles in tumorigenesis and tumor progression. Therefore, more complex, and physiologically more relevant *in vitro* 3D models mimicking human cancer microenvironment could considerably help in the development of new chemotherapeutics for personalized treatments. Many advanced and promising 3D cancer models have been proposed in recent years to simulate tumor heterogeneity and then been applied in drug discovery and testing. Nevertheless, few of these models have been designed based on separate stroma and tumor compartments, particularly ones with different mechanical characteristics mimicking soft-hard tissues interfaces as in natural tumor microenvironments.

In this PhD research, a novel 3D *in vitro* co-culture model (named “PP-3D-S”, for “Plasma Polymerized 3-Dimensional Scaffold”) was developed for such personalized chemotherapeutic screening; it is customizable, reproducible, cost-effective, and user-friendly, far more so than existing commercial products such as Matrigel®. It can represent a 3D interface model of normal tissue-tumor microenvironment; PP-3D-S is generated by combining (A) an electric discharge plasma-treated electrospun nanofibrous polymer (often polylactic acid – PLA) scaffold that is pre-seeded with human osteoblasts or fibroblasts as stromal cells; and (B) an alginate/gelatin-based hydrogel overlayer on (A) that is embedded with either (for example human breast-) cancer cell lines with different aggressivity, or patient-derived (e.g. bone-metastasized) cancer cells, to

create a physiologically realistic 3D system representing a stroma-tumor tissue interface. This model is applied as a migration assay tool and enables quantifying migration and chemotherapeutic response of different immortalized or patient-derived cancer cells towards a stromal compartment. The PP-3D-S model can be tailored to target various tissue and cancer types, through altering the biophysical and mechanical properties of the polymer, scaffold morphology, and hydrogel composition. The 3D hybrid model was characterized for optimal plasma treatment types, polymer materials, and scaffolds morphology including fiber diameter and pore size. It was found that plasma-modified PLA mats, but also polyurethane (PU) and polycaprolactone (PCL), considerably improved initial cell adhesion and growth compared with non-treated controls. Plasma treatments including plasma functionalization and low- and atmospheric pressure plasma polymerization were shown to greatly stimulate the adhesion, proliferation, migration, and invasion of tumor cells. Moreover, significant differences in tumor cell migration between small-sized (fiber diameter) and either medium- or large-sized scaffolds were observed for all treated and untreated mats. The impact of two different chemotherapeutic drugs, Doxorubicin (Dox) and Cisplatin (Cis), on migration and metabolic activity of patient cancer cells and their immortalised cell line counterparts was assessed. It was found different migratory behaviors, with IC50 values that were mostly in accordance with expected cell characteristics. Both Dox and Cis were found to be able to reduce metabolic activities and to block migration, but higher efficiency (or lower IC50) was observed with Dox. In addition, in two different sets of Dox screening tests, PP-3D-S performance was compared with that of Matrigel® in migration assays after exposure to varying Dox dosages, with very similar numerical outcomes. Taken altogether, these data indicate that PP-3D-S is an effective 3D tumor (migration) model, suitable in drug screening for personalized therapies in metastatic cancer treatment.

Keywords: 3D Co-culture system, Nanofibrous scaffolds, Plasma surface treatment, Interface tissue models, Drug screening, Breast cancer, Bone metastasis, Personalized medicine

TABLE OF CONTENTS

DEDICATION III

ACKNOWLEDGEMENTS IV

RÉSUMÉ VII

ABSTRACT X

TABLE OF CONTENTS XII

LIST OF TABLES XVI

LIST OF FIGURES XVII

LIST OF APPENDICES XX

LIST OF SYMBOLS AND ABBREVIATIONS XXI

CHAPTER 1 INTRODUCTION 1

1.1 Motivation 1

1.2 Thesis organization 3

CHAPTER 2 LITERATURE REVIEW 5

2.1 Metastatic cancer: incidence and clinical significance 5

2.1.1 Bone metastasis 6

2.2 Current cancer therapies and limitations 7

2.2.1 Local treatments 7

2.2.2 Systemic treatments 8

2.3 Drug discovery and screening in cancer research 9

2.3.1 Limitations and Challenges 9

2.3.2 Current therapeutic research in oncology and limitations 10

2.3.3 Approach of precision/personalized medicine 12

2.4 From 2D to 3D culture models 12

2.5 3D cancer models for chemotherapeutic screening 14

2.5.1 Spheroid generation 14

2.5.2 Microfluidic systems 15

2.5.3 Scaffolds, hydrogels, and bioprinting 16

2.6 Electrospinning technology 21

2.6.1 Basics of the technique 21

2.6.2 Natural and synthetic materials used in electrospinning 23

2.6.3 Effect of processing parameters on scaffolds morphology and structure 24

2.6.4 Effect of electrospun nanofiber morphology on cell adhesion and growth 26

2.6.5 New advances in electrospun scaffolds as 3D models in cancer research 27

2.7 Surface modification of 3D polymeric scaffolds 29

2.7.1 Surface treatment of 3D scaffolds by plasma techniques 30

2.7.2 Plasma treatment of electrospun nanofibrous scaffolds 34

2.8 Previous related work in our laboratories 35

2.9 Knowledge gap and significance 35

CHAPTER 3 HYPOTHESES AND OBJECTIVES 37

CHAPTER 4 ARTICLE 1: A NOVEL 3D CO-CULTURE PLATFORM FOR INTEGRATING TISSUE INTERFACES FOR TUMOR GROWTH, MIGRATION AND THERAPEUTIC SENSITIVITY: “PP-3D-S” 42

4.1 Introduction 44

4.2 Experimental Section 46

4.2.1 Preparation of plasma-treated electrospun nanofibrous scaffold 46

4.2.2 Scaffolds characterization 48

4.2.3 Biological experiments 50

4.2.4 Statistical analysis 52

4.3 Results and Discussion 53

4.3.1 Physical properties and morphology evaluation of nanofibrous mats 53

4.3.2 Surface characterization of bare and plasma-treated scaffolds 57

4.3.3 Investigation of initial cell adhesion 58

4.3.4 Tumor-cell migration 59

4.3.5 Penetration depth of tumor cells 65

4.3.6 Drug screening experiments with PP-3D-S and Matrigel® models 66

4.4 General Discussion and Conclusions 68

CHAPTER 5 ARTICLE 2: A NOVEL 3D *IN VITRO* TISSUE MODEL FOR BONE-METASTASIZED BREAST CANCER: A PRECLINICAL TOOL IN DRUG DISCOVERY AND TESTING 71

5.1 Introduction 73

5.2 Experimental Section 75

5.2.1 Fabrication of plasma-treated electro-spun nanofibrous scaffolds 75

5.2.2 Physico-chemical characterization of 3D NF scaffolds 78

5.2.3 Biological experiments 81

5.2.4 Statistical analysis 83

5.3 Results and Discussion 83

5.3.1 Surface-related characteristics of 3D NF scaffolds 83

5.3.2 Biological test results 85

5.4 General Discussion and Conclusion 92

CHAPTER 6 ARTICLE 3: A 3D, COMPARTMENTAL TUMOR-STROMAL MICROENVIRONMENT MODEL OF PATIENT-DERIVED BONE METASTASIS 97

6.1 Introduction 99

6.2 Experimental Section 101

6.2.1 Fabrication of plasma-treated electrospun nanofibrous scaffold 101

6.2.2 Biological experiments 103

6.2.3 Statistical analysis 106

6.3 Results and Discussion 107

6.3.1 Invasion behavior of patient-derived spine-metastasized cells in the PP-3D-S model 107

6.3.2 Screening of patient-derived bone-metastasized cells with Doxorubicin 109

6.3.3 Treatment of bone-metastasized secondary to breast tumor cells with different chemotherapy drugs 111

6.3.4 Gene expression profile of breast cancer cell lines in the PP-3D-S model 113

6.4 Conclusion 114

CHAPTER 7 GENERAL DISCUSSION 116

7.1 Combination of electrospinning, plasma treatment, and hydrogel technologies for 3D culture applications 116

7.2 Evaluation of migration and drug sensitivity/resistance of immortalized cancer cell lines with different aggressivity through the PP-3D-S model 120

7.3 Evaluation of migration and drug sensitivity/resistance of patient-derived metastasized cancer cells using the PP-3D-S model 122

CHAPTER 8 CONCLUSIONS AND RECOMMENDATIONS 126

REFERENCES 129

APPENDICES 158

LIST OF TABLES

Table 2.1 Advantages and disadvantages of different 3D culture models 20

Table 4.1 Comparison of average pore size (µm) and porosity (%) of PLA electrospun mats in different sizes calculated by three techniques including ImageJ, eq. (2) and MIP test 56

Table 4.2 Surface chemical compositions of pure PLA and PLA mats modified with L-PPE:N coating or O_2 plasma, determined from XPS survey spectra 57

Table 4.3 Static water contact angles of plasma-treated and non-treated PLA mats 58

Table 5.1 Mean fiber diameter, pore size and overall porosity of PLA electrospun mats for small, medium and large nano-fiber sizes, n=3 79

Table 5.2 Surface chemical compositions of untreated and plasma-modified PLA mats; plasma treatments with O2 and NH3, or L-PPE:N, L-PPE:O, PP-EL and PP-AAm coatings (data from XPS survey spectra) 80

Table 5.3 Aging effect in O2 plasma-treated NF mats over 7 days, from XPS survey scans.....81

Table 6.1 Detailed information of primer sequences used for qRT-PCR analyses.....106

Table A.1 Process parameters applied to fabricate electrospun mats 158

LIST OF FIGURES

Figure 2.1 Schematic of the metastatic cascade, including migration, invasion, intravasation, circulation, extravasation, and colonization 5

Figure 2.2 Schematic of the primary tumor microenvironment, consisting of cellular and non-cellular components 6

Figure 2.3 Schematic of the types of 3D culture models used in cancer study 19

Figure 2.4 Schematic diagram of electrospinning process, along with a typical SEM micrograph of an electrospun mat 22

Figure 2.5 SEM micrographs of bead-free and beaded PLA nanofibers mats 24

Figure 2.6 Types of surface treatment of 3D electrospun scaffolds: (A) plasma treatment or wet-chemical technique; (B) surface grafting 32

Figure 2.7 A schematic diagram of the low-pressure, capacitively coupled r.f. plasma reactor ... 33

Figure 4.1 Schematic diagram of the main steps that comprise the current innovative methodology 46

Figure 4.2 SEM micrographs and fiber diameter distribution curves of PLA electrospun mats of different fiber diameter sizes 54

Figure 4.3 SEM micrographs of electrospun mats with different fiber sizes and porosities. 56

Figure 4.4 Percentages of initially-seeded RFP cancer-associated fibroblasts adhering to plasma - treated and non-treated PLA scaffolds 59

Figure 4.5 Tumor cell migration in the PP-3D-S model 61

Figure 4.6 Numbers of tumor cells having migrated into the volume of different-sized and differently plasma-treated scaffolds 63

Figure 4.7 Effect of polymer type on tumor cell migration 64

Figure 4.8 Tumor cell migration and growth in depth of the PP-3D-S model 66

Figure 4.9 Drug screening experiments with PP-3D-S and Matrigel® models 67

Figure 5.1 Schematic diagram of the steps that comprise the current methodology 76

Figure 5.2 SEM micrograph and fiber diameter distribution curve of electrospun PLA NF mats of medium (600-800 nm) fiber diameter sizes 79

Figure 5.3 Static water contact angles of plasma-treated and untreated PLA mats 85

Figure 5.4 Numbers of tumor cells having migrated/proliferated in the volume of different-sized and differently plasma-treated scaffolds 87

Figure 5.5 Numbers of variably-aggressive breast tumor cells and benign breast epithelial cells having migrated into osteoblast-seeded plasma-treated medium-sized PLA scaffolds 88

Figure 5.6 Metabolic activity/ proliferation evaluation of the different cancerous and benign breast cells growing in 2D, 3D hydrogel (A1G7), and 3D nano-fibrous mats 90

Figure 5.7 Metabolic activities of different cancer- and non-cancerous breast cells by increasing doses of Doxorubicin (Dox).....91

Figure 5.8 Effect of Doxorubicin on migration and metabolic activities of MDA-MB 231 92

Figure 6.1 (a): Schematic diagram of the main steps of the current "PP-3D-S" 3D interface model; (b): SEM micrographs of medium-sized electrospun PLA mats 102

Figure 6.2 Migration of patient-derived bone/spine-metastasized tumor cells in PP-3D-S.....108

Figure 6.3 Metabolic activities and Dox response of patient-derived bone/spine-metastasized tumor cells and their equivalent immortalized cell lines.....110

Figure 6.4 . Metabolic activities of patient-derived bone-metastasized tumor cells and MDA-MB 231 breast cancer cell lines screened with Doxorubicin and Cisplatin 112

Figure 6.5 Gene expression profile of MDA-MB231 aggressive breast cancer cells cultured in PP-3D-S model.....114

Figure A.1 Spheroid formation in hydrogel over 7 days of culture of MDA-MB 231.....159

Figure A.2 Cell proliferation over 7 days of culture in plasma-treated PLA electrospun mats...160

Figure A.3 Live/Dead assay on Osteoblasts culture on NH3 plasma-treated PLA mats.....161

Figure A.4 Effect of Doxorubicin on tumor cell (MDA-MB 231) migration.....162

Figure A.5 applying two mats technique to investigate tumor cell (MDA-MB 231) migration across the 3D model 163

Figure A.6 Effect of gravity and presence/lack of fibroblast on tumor cell (MDA-MB 231) migration by inverting the PP-3D-S model.....163

Figure A.7 A representative images of fully covered cell adhesion on the NH3 plasma-treated PLA mats.....164

Figure A.8 Photographs of the scaffolds and hydrogels used in this thesis.....165

LIST OF APPENDICES

Appendix A Supplementary data 158

LIST OF SYMBOLS AND ABBREVIATIONS

AC	Alternating current
AG	Alginate-gelatine
AP	Atmospheric pressure
Ar	Argon
BCS	Breast-Conserving Surgery
BE	Binding energy
BMB	Bone Met Breast
BME	Basement membrane extract
BMK	Bone Met Kidney
BML	Bone Met Lung
BMP	Bone Met Prostate
Cis	Cisplatin
DBD	Dielectric barrier discharge
DC	Direct current
DMEM	Dulbecco's modified Eagle medium
DMF	Dimethylformamide
Dox	Doxorubicin
ECM	Extracellular matrix
EMT	Epithelial-to-mesenchymal transition
ER	Estrogen receptor
FBS	Fetal bovine serum
GAG	Glycosaminoglyca

GFP	Green-fluorescent protein
HUVEC	Human umbilical vein endothelial cells
HV	High voltage
LP	Low pressure
L-PPE:N	Low-pressure plasma-polymerized of ethylene, N doped
L-PPE:O	Low-pressure plasma-polymerized of ethylene, O doped
MET	Mesenchymal-to-epithelial transition process
Mfp	Mean free paths
MIP	Mercury Intrusion Porosimetry
NF	Nanofibrous
PAM	polyacrylamide
PBS	Phosphate buffered saline
PCL	Polycaprolactone
PDMS	Polydimethylsiloxane
PECVD	Plasma enhanced chemical vapor deposition
PEG	Polyethylene glycol
PET	Poly (ethylene terephthalate)
PFA	Paraformaldehyde
PGA	Poly (glycolic acid)
PLA	Poly (lactic acid)
PLG	Poly (lactide-co glycolide)
PLGA	Poly (lactic-*co*-glycolic acid)
PLLA	Poly-L-lactic acid
PMAA	Polymethacrylic acid

poly-HEMA	Poly-2-hydroxyethyl methacrylate
PP-3D-S	Plasma Polymerized 3-Dimensional Scaffold
PP-AAm	Plasma Polymerized-Allyl Amine
PP-EL	Plasma Polymerized-Ethyl Lactate
PR	Progesterone receptor
PS	Polystyrene
PS	Penicillin-Streptomycin
PTFE	Polytetrafluoroethylene
PU	Polyurethane
r.f.	Radio-frequency
RFP	Red-florescent protein
RH	Relative humidity
SCA	Static contact angles
Sccm	Standard cubic centimeters per minute
SD	Standard deviation
SE	Standard error
SEM	Scanning electron microscope
Slm	10 standard liters per minute
TFE	Trifluoroethanol
THF	Tetrahydrofuran
TME	Tumor microenvironment
XPS	Surface chemical analyses
2D	two Dimensions
3D	three Dimensions

CHAPTER 1 INTRODUCTION

1.1 Motivation

Cancer is the leading cause of death in Canada, as nearly 50% of Canadians will develop cancer in their lifetime, and close to half of these will die of the disease. Based on a report from The Canadian Cancer Society, 229,200 Canadians were diagnosed with cancer and 84,600 died only in 2021. The most frequently diagnosed cancers were lung, breast, colorectal and prostate cancers, accounting for almost half of all cases in 2021 [1]. Metastatic or secondary cancer is a type that has spread from the original so-called primary tumor to another part of the body [2, 3]. Bone tissue is a frequent site to be affected by metastatic cancer, termed as bone metastasis, and tumors arising from the breast, prostate, lung, and kidney are the most common sources [4]. Therefore, the importance of research activities in cancer disease and its cure is obvious. In oncology, current treatments such as surgery, radio-therapy and chemotherapy frequently lead to severe side effects, greatly decreasing the quality of life of patients [5]. Development of novel therapeutics based on personalized treatment strategies is therefore essential to treat cancers more effectively and specifically, while also improving overall patient outcomes. However, developing new therapeutic drugs is a long and costly path when using (inappropriate) current *in vitro* and *in vivo* models, as 75-90% of new drug candidates fail to pass phase 3 clinical trials [6-8].

Current culture methods for testing new chemotherapy drugs commonly involve two-dimensional (2D) flat polystyrene culture dishes that neither realistically portray the behaviour of living cells in their normal three-dimensional (3D) environment of natural tissues, nor reproduce complexities of cell-cell and cell-extracellular matrix (ECM) interactions *in* vivo [9-11]. Different types of cancers may present variations in complexity of tumor microenvironments, and it is challenging to mimic intercellular interactions *in* vitro [10, 11]. It is noteworthy that the microenvironment of neoplasia, specifically stromal-epithelial interactions which are critical and essential for cancer therapy, are still underexplored due to insufficient understanding of stromal-epithelial crosstalk [12, 13]. Standard 2D culture often fails to recapitulate interactions between cancer epithelial cells and stromal compartment, which play a crucial role in tumorigenesis and progression. This has directly led to a rise in developing 3D culture and co-culture models of cancer microenvironments [10, 14], to simulate the complexity and heterogeneity of tissues and

organs in tissue engineering and regenerative medicine, and/or as *in vitro* 3D models for drug discovery [15-17]. Cancer cells in a 3D network can better mimic *in vivo* tumor growth [9-11, 14], so that this allows for long-term investigation and medium throughput screening of novel therapeutic drugs using either cell lines or patient derived cells [11, 12, 18].

Several different 3D culture systems have been proposed to simulate the tumor microenvironment, both scaffold-free and scaffold-based ones such as hydrogels, ceramic or polymeric 3D-printed scaffolds, electrospun nanofiber scaffolds [19], and cell spheroids [20-23] or organoids [24]. Other new approaches including bioprinting and microfluidic devices have been trending in cancer research in recent years, while proving meaningful differences in cellular responses to new and existing therapeutics, and they have opened doors towards personalized medicine [25]. However, few, if any, 3D models have addressed simulation based on separate stroma/tumor compartments, with different mechanical characteristics to portray hard-soft tissues interfaces as in the real tumour microenvironment. To address this gap, such future 3D models need to be introduced through the combination of suitable technologies.

Electrospun nanofibrous scaffolds made of synthetic materials such as polyethylene glycol (PEG), poly(lactide-co glycolide) (PLG), polycaprolactone (PCL), polyurethane (PU) and poly(lactic acid) (PLA) have advantages of reproducibility, being inert, with “tunable” biodegradability, and more specifically, control on tuning chemical composition, mechanical properties, porosity, and fiber size for realistically mimicking the ECM of tumors [26-33]. However, these and other synthetic polymers are characterized by low surface energy and poor wettability. To increase surface energy / wettability and improve their biocompatibility, plasma-based surface functionalization or plasma-polymer deposition are used as remarkably powerful techniques to greatly enhance those performance criteria for biomedical applications. By employing plasma-generated reactive species, different surface-near polar functional groups and/or polymer-like coatings containing various selected hydrophilic groups such as hydroxyl-, carboxyl-, or primary amines, etc. are introduced/deposited on the surface to enable immobilization of biomolecules such as proteins and thereby promote cell adhesion. Of course, the latter takes place through covalent bonding between those adsorbed proteins and integrin receptors on the cell membrane [34-37]. On the other hand, natural components of the ECM such as collagen, fibronectin, and hyaluronic acid, as well as alternates such as gelatin, and alginate,

have been developed as hydrogels to provide structural support for cell interactions in 3D systems. They have been the most commonly used materials due to their inherent cytocompatibility, intrinsic cell adhesion properties and capability of being remodelled by cells [14, 38, 39]. Therefore, this thesis has aimed at combining (A) plasma-treated electrospun nanofiber mats with (B) alginate/gelatin-based hydrogel to develop a 3D co-culture interface model based on separate (A) stroma- (B) tumor compartments, a combination that can truly mimic the microenvironment of human cancers.

1.2 Thesis organization

This highly interdisciplinary research project has been performed through close collaboration of three laboratories in different fields, each bringing their own expertise:

- Electrospinning laboratory at Polytechnique, led by Prof. Abdellah Ajji, expertise in electrospun nanofiber polymeric matrices for biomedical applications;
- Plasma laboratory at Polytechnique, led by Prof. Michael R. Wertheimer, expertise in polymeric surface modification by plasma for biomedical applications;
- Cell biology laboratory at Montreal General Hospital, Research Institute of the McGill University Health Centre (RI-MUHC), led by Prof. Derek H. Rosenzweig, expertise in 3D tumor modeling for cancer metastases;

In **Chapter 2**, an overview of the literature is provided, addressing the incidence and clinical significance of metastatic cancer including bone metastasis. A brief review of current cancer therapies and limitations, including local and systemic treatments are presented. Then, challenges and limitations in drug discovery and screening are discussed, followed by an introduction of precision/personalized medicine approaches. Comparison of 2D with 3D models, then a review of 3D cancer models for chemotherapeutic screening comprising spheroid models, microfluidic systems, scaffolds, hydrogels, and bioprinting techniques are presented. Then, electrospinning technology including basics of the technique, materials, morphology, and processing parameters optimization, new advances in electrospun scaffolds as 3D models in cancer research are discussed in more detail. Surface modification of 3D polymeric scaffolds, particularly focused on plasma techniques to improve cell adhesion and growth, are also reviewed. Finally, the knowledge gap and significance of the present work are discussed. **Chapter 3** presents

hypotheses and research-specific objectives which were defined based on the literature review. The three articles forming the core of this thesis are presented in the next three chapters. **Article 1** (published in *Materials Science and Engineering* [40]), presented in **Chapter 4**, focuses on the development, characterization, and optimization of 3D electrospun nanofibrous scaffolds with different materials and morphologies, coupled with the benefit of plasma functionalization or plasma polymer coatings to provide a biocompatible 3D system that is morphologically, mechanically, and biologically suitable for cellular activities in biological tests. The optimized 3D scaffolds combined with hydrogel were used as a 3D tumor model for subsequent migration assays and chemotherapy screening tests. **Chapter 5** presents **Article 2** (published in *Plasma Processes and Polymers* [41]), which deals with the microenvironment of breast cancer metastasis in bone-like tissue. Our 3D hybrid model was employed to investigate the response of more- or less-aggressive breast tumor cell lines and non-cancerous epithelial breast cells to Doxorubicin. A greater variety of plasma treatments extends the content well beyond that covered in **Chapter 4**. **Chapter 6** which presents **Article 3** (submitted to *Biomedical Engineering Advances*), aims to replicate a real cancerous tissue based on patient-derived spine-metastasized tumor cells, initially separated by the interface from human primary bone cells. The performance of two different chemotherapeutics, Doxorubicin (Dox) and Cisplatin (Cis), on both patient cells and immortalized cell lines was investigated, along with their gene expression profiles. A general discussion, along with recommendations for future works, followed by a conclusion are presented in **Chapter 7**.

CHAPTER 2 LITERATURE REVIEW

2.1 Metastatic cancer: incidence and clinical significance

According to the statistics of incidence and mortality of cancer reported by the Canadian cancer society in 2021, among 229,200 new cancer cases, 84,600 will die from cancer. Thus, cancer is still the leading cause of death in Canada, which is responsible for 28.2% of all deaths. The most diagnosed types of cancer are breast, prostate, lung, and colorectal, accounting for 46% of all diagnoses [1]. When cancer spreads from its primary site to surrounding tissues and to other parts of the body it is called metastatic cancer [42-45]. Metastasis is the main reason of cancer morbidity, as it is the cause of death in about 90% of patients with cancer [42, 44]. Metastatic process includes a number of sequential and interrelated events including cell migration, invasion and adhesion to reach distant peripheral organs [45], which is termed metastatic cascade. Indeed, tumor cells must have the ability to attach and degrade basement membranes to follow this consecutive process [44, 45]. Metastatic cascade occurs when cancer cells detach from the primary tumor, intravasate into blood vessels and lymphatic systems; circulating, they evade immune attacks, extravasate at distant capillaries and invade the blood vessel walls, proliferate, and colonize into surrounding tissues of the new organ. The result is the formation of a secondary tumor, which can cause severe and irreversible damage to these distant organs [42-44]. An overview of the metastatic cascade is shown in **Figure 2.1**.

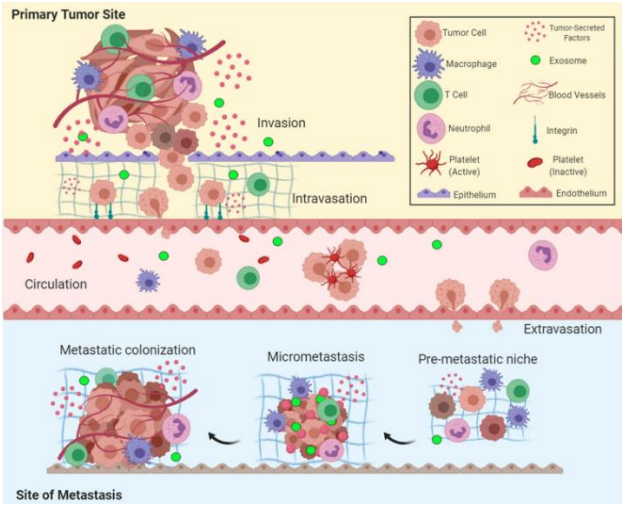

Figure 2.1 Schematic of the metastatic cascade, including migration, invasion, intravasation, circulation, extravasation, and colonization [43]

In this context, the primary tumor microenvironment (TME) plays a critical role in controlling tumor development and metastatic potential. It is an environment surrounding a tumor, comprising cellular (stromal) and non-cellular components including fibroblasts, epithelial cells, immune cells, blood and lymphatic vascular networks, signaling molecules, and extracellular matrix (ECM), all having dynamic and continuous interactions with tumor cells [46-48], as illustrated in **Figure 2.2**. It was found that each component of the TME, particularly non-malignant cells, is able to promote tumorigenesis at every stage of initiation, progression, and invasion [47-49]. Such a complex crosstalk between the tumor and the components of TME contributes to drug resistance and failure in cancer therapy [48]. Thus, it is essential to have a better understanding of the underlying cellular and molecular mechanisms involved in this heterogeneous disease for the further development of efficient therapeutic strategies.

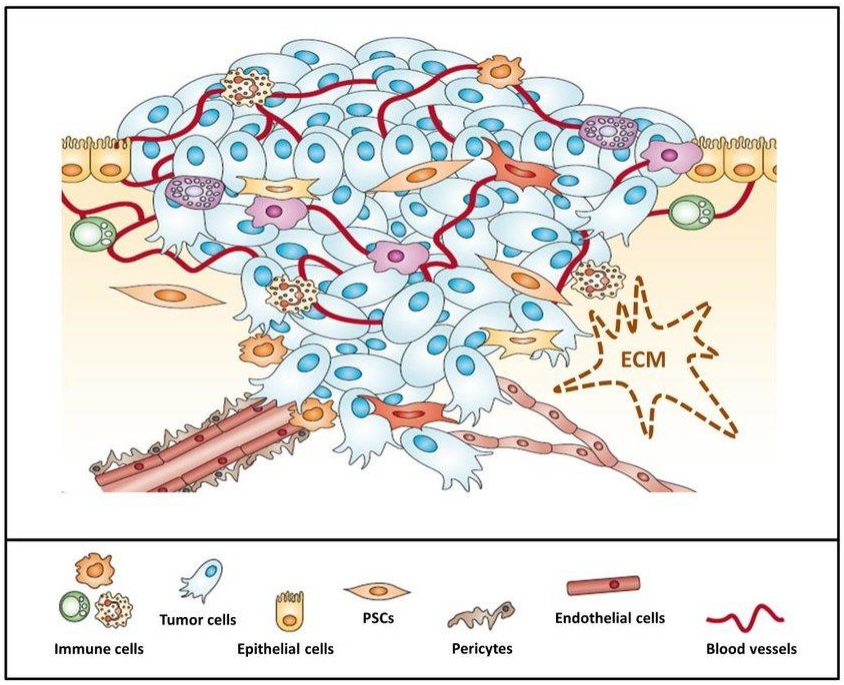

Figure 2.2 Schematic of the primary tumor microenvironment, consisting of cellular and non-cellular components [50]

2.1.1 Bone metastasis

Bone is a frequent site to be affected by tumor metastasis, in which primary tumors spread from their original site to the bone [2, 4, 51]. The relative incidence of bone metastases is as follows:

65-75% in breast cancer, 65-75% in prostate cancer, 60% in thyroid cancer, 30-40% in lung cancer, 40% in bladder cancer, 20-25% in kidney; thus, breast and prostate cancer indicate the highest prevalence, accounting for about 70% of bone metastasis [2, 51]. Moreover, in the United States it was estimated that around 60% of the Americans that are diagnosed with breast, lung, and prostate cancer (750,000 in 2021), will develop metastatic bone disease [52]. Unfortunately, bone metastases are not usually curable, as 20% of patients with breast cancer survive only limited time (up to five years) after the disease diagnosis [2, 53]. When there is a dysregulation of the normal bone remodeling process, two types of bone metastasis occur including osteoblastic, osteolytic, or even a mixture of both. The former is characterized by deposition of the new dense bone and the latter by destruction of the bone [51, 53]. Most patients with breast cancer indicate predominantly osteolytic, while prostate cancer metastases are mainly osteoblastic [53]. Both osteolytic and osteoblastic are caused through factors secreted by tumor cells which affect the normal homoeostasis of bone formation and resorption, followed by changes to the structure and function of the bone. Bone metastasis is characterized by severe pain, vertebral instability, fractures, high blood calcium levels, and spinal cord compression [51].

2.2 Current cancer therapies and limitations

Treatment of cancer cells with certain characteristics of uncontrolled growth, immortality, and metastatic potential is one of the challenging issues in medical oncology management. Current approaches for cancer therapy are discussed below.

2.2.1 Local treatments

2.2.1.1 Surgery

Tumor removal, also called “resection”, is a common type of cancer surgery which is used to treat many types of cancer. Depending on the type of cancer and its stages, curative, also called primary, surgery can be used to remove the entire tumor that is found in one part of the body and probably some of the healthy tissue surrounding it, or to debulk a tumor in which some, but not all, is removed. Debulking is used when taking out the entire tumor might damage an organ or the whole body [54, 55]. For example, for breast cancer, there are two main types of procedures comprised of Breast-Conserving Surgery (BCS), and mastectomy, which are defined for

partially- or entirely-removed techniques, respectively [56]. Commonly, surgery might be combined with other treatments like radiation therapy before or after the operation.

2.2.1.2 Radiation Therapy

Radiation therapy is another type of local treatment, in which high energy rays are used to destroy cancer cells locally. To reduce cancer recurrence chances or metastases, radiotherapy may usually be pursued after surgery. External beam radiation therapy and localized internal irradiation are the two major types of radiotherapy. This strategy can also be combined with chemotherapy treatment to enhance the radiation efficacy [57].

2.2.2 Systemic treatments

2.2.2.1 Chemotherapy

Systemic chemotherapy is the most extensively used strategy to treat any cancer in which cytostatic medications are administered to target DNA synthesis or cell division, to kill quickly-dividing cells [58]. However, during the process of treatment, normal fast-proliferating cells such as immune cells, hematopoietic progenitor cells in bone marrow, hair follicles, skin epithelial cells are also targeted. This limitation in cancer-specificity leads to severe side effects for cancer patients undertaking this treatment [59, 60]. Those side effects are different from patient to patient, types of chemotherapeutics and cancer. A list of well-known side effects is as follows: hair loss, nail changes, nausea, diarrhea, loss of appetite or weight, early menopause, changes in sex hormones, infertility, mouth sores, fatigue, iron deficiency, low hemoglobin level, etc. [61, 62]. Around 50 approved commercial drugs, including both natural and synthetic ones, have been introduced into the market. Depending on the type of cancer cells, there would be some important criteria to choose the proper chemotherapy drugs or their combination during the treatment process [63].

2.2.2.2 Immunotherapy

In order to stop cancer cells from growing, migrating, and invading other organs, immunotherapy is used [64]. In this technique, the immune system of patients is stimulated by targeted drugs, to damage cancer cells and consequently induce cell death [65].

2.2.2.3 Hormone therapy

For those tumors which are hormone receptor-positive, a hormone therapy technique is recommended. To decrease the risk of cancer recurrence or in the case of metastases, this strategy might be used after or even before surgery. For patients with low risk of recurrence, hormone therapy is advantageous. Hormone therapy, also called endocrine therapy, relies on blocking the capability of the body to produce hormones or disrupt hormones to slow/stop cancer cells growth [66].

The metastatic potential of tumor cells contributes to poor prognosis in patients with cancer, as their resistance to chemotherapeutics and possibility of recurrence are the main causes of failure in treatment. Numerous complex molecular mechanisms are involved in continuous growth and migratory behaviour of these metastatic cells, while deceiving or eluding the immune response [67, 68]. Although some cancers are sensitive and responsive to surgery, radiotherapy or chemotherapy, their diverse locations and mutations cause them to become resistant to some of these therapies. For all these reasons, there is still growing interest in exploring highly effective anti-cancer drugs, as well as in developing suitable 3D platforms to be adopted as screening models in drug discovery and testing.

2.3 Drug discovery and screening in cancer research

2.3.1 Limitations and Challenges

When a potential anti-cancer drug is identified, pre-clinical testing is performed with the use of *in vitro* and later *in vivo* studies [69]. This testing is done to screen for drugs, and to determine their toxicity and pharmacological characteristics. Despite there being an increase in the number of potential anti-cancer drugs, few make it successfully through clinical development [69]. The overall clinical development success rate for oncology products is approximately 10%, with an associated cost of bringing a drug to market being over US$1 billion [70]. Over 95% of compounds that have been shown to kill cancer cells in culture, or to regress tumors in animals, end up failing in phase I clinical trials [71]. The main causes of failure are lack of clinical efficacy and unacceptable toxicity. This points to the inadequacy of pre-clinical models of cancer. It is critical for *in vitro* assays to generate information for drug development; however, the

conventional 2D cell culture model to mimic native tissues is incomplete. Nearly 75% of publications in oncology research utilize various cell lines because they are cost-effective, immortalized, homogenous, and easy to work with. However, genomic instability may give rise to differences between the cells and the original tumor; cell culture conditions can alter the morphology of the cells and cellular pathways, and propagation of these cells results in further genetic and epigenetic changes [71, 72]. Traditional monolayer culture lacks the ECM signaling that occurs in a 3D environment, as well as the interactions with other cell types (e.g., endothelial, fibroblasts, immune cells) and does not recapitulate the TME [69, 72-75]. *In vivo* tumor models present challenges associated with graft failures, technical skill, time, cost, availability of animals and resources, and inconsistent responses between animal strains [71, 72, 76-79]. Due to these limitations in 2D *in vitro* and *in vivo* research, 3D culture models are becoming increasingly popular for their ability to study cells in a more *in vivo*-like environment [80].

2.3.2 Current therapeutic research in oncology and limitations

2.3.2.1 *In vitro* adherent monolayer (2D)

The most common *in vitro* mammalian cell culture model is a 2D monolayer of cells. The inherent limitation of this technique is that cells do not grow in 3D as they would in their natural *in vivo* environment. It is lacking in the microenvironmental cues that can influence molecular and cellular events [75]. Developed in the early 20th century, monolayer cells are grown on rigid plastic surfaces optimized for cell attachment and growth (e.g., cell culture dishes) with cell medium as a source of nutrients and are incubated at 37ºC. Differences have been observed between cells grown as monolayers and cells found *in vivo* in terms of morphology, polarity, receptor expression, oncogene expression, interaction with the ECM, and overall cellular architecture [69, 81]. The unnatural plastic for cell attachment may lead to questionable conclusions as cells may lose their ability to respond to anti-cancer drugs [82]. 2D monolayers are severely limited by the absence of stromal cells. In mammary glands, for example, over 80% of the breast volume is comprised of stromal cells [83], demonstrating the importance of recreating a complex architecture to represent native tissue. Human tissues require: 1) the colocalization of various cell types, their interactions, and exchange of growth and other

biological factors; 2) mechanical stability via an ECM; 3) fabrication of interstitial fluid containing nutrients and biological effectors necessary for tissue maturation and differentiation [83, 84]. 2D monolayer cultures fail to provide these requirements and therefore cannot serve as rigorous and reliable pre-clinical drug screening platforms.

2.3.2.2 *In vivo* models

Animal models provide us with important insights into tumor biology and drug screening and are considered the gold standard. However, they are costly, come with logistical issues, possess limited bioavailability, and cannot accurately recapitulate human tumors, as demonstrated by poor clinical translatability [74]. Furthermore, animal models are increasingly subject to ethical concerns regarding discomfort and pain, and the feasibility of high-throughput screening is extremely limited with animal models [75]. The most used animal model for cancer drug screening is the athymic nude mouse, which is unable to reject human tumors due to an inhibited immune system [71]. These mice can be used for orthotopic, heterotopic, and metastatic models. The metastatic tumor models do not recapitulate the early steps involved in carcinogenesis [85] and cannot recreate spontaneous bone metastases [86]. Intraosseous injection models of metastasis skip over the initial homing, extravasation, and dormancy of the tumor cells and go directly to the final stages of bone colonization and are therefore more analogous to primary bone tumors. Intracardiac injection of osteotropic cancer cells can result in the quick generation of bone metastases. However, this requires the use of immunocompromised animals (nude, SCID, NOD/SCID) to avoid xenograft rejections [87-89]. By doing so, the immune system's role in the TME is eliminated and no longer representative of a native *in vivo* bone metastasis [85, 86, 90].

Syngeneic rodent tumor and human cancer xenograft models in *in vivo* prostate and breast cancer models are common; however, the development of bone metastases is rare. Cells often lose their heterogeneity after multiple passages and can no longer represent the primary tumor [91]. Cancer cell lines injected or implanted *in vivo* lack the heterogeneity of the primary tumor and may possess genomic and phenotypical modifications compared to the original primary cells harvested [85]. Patient-derived xenografts have a high transplantation failure rate, and not all models can be used for drug screening as tumor growth can be slow, inconsistent, or may present with cystic necrotic areas even at small tumor volumes [77]. Zebrafish have also been used to

study drug responses; however, they are faced with similar challenges of inappropriate xenograft tumor-host interactions that reduce the translatability and true clinical relevance [92]. *In vivo* models for cancer drug screening are indispensable tools; however, they are limited in their ability to accurately replicate native metastatic tumors. Nonetheless, each model can add its unique value in the pre-clinical stage of drug screening to better predict clinical outcomes.

2.3.3 Approach of precision/personalized medicine

To define personalized drug regimens for patients, patient-derived models have been proposed and drug screening is primarily conducted in 2D cultures [74, 93]. This approach intends to develop patient-centric treatments and considers patient-to-patient variations in genes, environment, and lifestyle. Inter- and intra-patient variability exists in response to treatment, and it can be difficult to predict biological responses within a reasonable time frame [93]. Therefore, personalized technologies can recapitulate the heterogeneity of the patient tumors for functional drug testing. This means replacing traditional cell lines with patient-derived cells and generating patient-derived xenograft and organoid models. As discussed previously, patient-derived xenografts are limited by the variable success rates of tumor engraftment [77, 94]. Furthermore, patient-derived tumor organoids lack TME control and stromal cells. For these reasons, 3D models are gaining traction for more physiologically relevant cancer models with the ability to bring personalized medicine into reality [94]. With any particular class of anti-cancer drug being ineffective in an estimated 75% of patients, personalized medicine aims to move away from the "one size fits all" approach and towards a more effective model to minimize patient suffering and unnecessary side effects [95].

2.4 From 2D to 3D culture models

The value of 2D *in vitro* tissue models lies in the systematic, reproducible, and quantitative investigations that have contributed greatly to biological research and drug discovery [75]. 3D *in vitro* tissue models offer a cellular microenvironment that is closer to the microenvironment found in native tissues, and this is a key component for drug screening [75]. Microenvironments crosstalk with cells through soluble factors, cell-cell, or cell-ECM interactions, and by mechanical forces. In turn, these result in a cascade of cell and molecular events that can range

from a change in gene expression to cellular differentiation [75]. Furthermore, 3D models allow for a complex mimicking of the interactions between stromal and parenchymal cells in terms of concentration gradients of signaling molecules and drugs, composition and structure of ECM, as well as morphology and arrangement of individual cells [75]. 3D models allow for the investigation of morphogenesis of cellular or tissue structures which can hinder transport of drugs to target cells, thereby mimicking physiological barriers to drug delivery *in vivo* [96]. 2D models lacking these barriers may lead to drug candidates that cannot reach target cells *in vivo* or that aren't effective [75].

When cells from the MCF-7 breast cancer cell line were cultured on a 3D chitosan scaffold, 10-fold higher tamoxifen concentrations were required to inhibit the cells [97]. Additionally, MCF-7 cells in 3D culture produced similar lactate levels to what is observed *in vivo*, unlike 2D culture [97]. Similarly, colon cancer HCT-116 cells in 3D culture were more resistant to melphalan, fluorouracil, oxaliplatin, and irinotecan, as compared to 2D culture [98]. While 2D cancer models have produced invaluable data and continue to be highly used, there is a progressive shift towards 3D culture models to more closely reproduce tumors and improve anti-cancer drug screening [99]. It was found that in 3D-cultured breast cancer cells, dense multicellular spheroids were more representative of tumor characteristics (hypoxia, dormancy, anti-apoptotic features) *in vivo* when compared to 2D culture [73]. The cellular fraction of tumors contains a heterogenous population of cells consisting of tumor cells, cancer stem cells, cancer-associated fibroblasts, endothelial cells, adipocytes, and immune cells [93]. With the addition of the ECM, growth factors, cytokines, chemokines, and exosomes, it is easy to see that there is a large combination of interactions that are possible which are not captured by 2D culture. In co-cultures of breast cancer cells with fibroblasts, the fibroblasts secrete cytokines that increase the malignancy of the breast cancer cells, thereby leading to drug resistance [100]. In a 3D polyethylene glycol hydrogel co-culture of LNCaP prostate cancer cells with osteoblasts, osteoblasts exerted a paracrine effect that promoted osteomimicry of the LNCaP cells. The 3D co-culturing demonstrated cellular and molecular changes that are relevant to the metastatic colonization of bone and shed light on the crosstalk between prostate cancer and bone [101]. Many researchers are turning to 3D culture models for pre-clinical anti-cancer drug screening as it becomes more appealing due to their improved ability to represent the TME of *in vivo* tumors [74] and thereby

enhance the predictive power and efficacy of drug screening [102]. A variety of 3D culture models can be used for chemotherapeutic screening, for example, suspension cultures, hydrogel scaffolds, organ-on-chip devices, and bioprinting. These models will be discussed in the following section.

2.5 3D cancer models for chemotherapeutic screening

2.5.1 Spheroid generation

There exist four common approaches to generate 3D spheroids. The first is forced-floating culture models which generate spheroids by using surfaces treated to prevent the attachment of cells. Low cell adhesion plates can be purchased commercially, however, they can be costly. Alternatively, researchers can coat their own plates with poly-2-hydroxyethyl methacrylate (poly-HEMA) which prevents cell attachment [69, 103]. Briefly, cell suspensions are added to these plates which are then centrifuged to aggregate the cells, allowing for cell-cell interactions. This method for spheroid generation is simple and reproducible and allows for high-throughput drug screening. Another type of coating that can be used is agarose in cell culture medium. Like poly-HEMA, agar prevents the attachment of cells to the surface and encourages the formation of spheroids [104]. These are simple and inexpensive methods to produce low-attachment plates that can form spheroids, however, coating the plates takes time [69]. The second method is the hanging drop method which uses a small aliquot of a cell suspension that is plated and subsequently, the plate is inverted. The aliquot droplets hang down and are held up by surface tension, and the cells accumulate at the droplet's tip where they proliferate [105]. Once ready, the spheroids can be transferred to a second plate for assays. It is difficult to change the spent cell medium for the hanging drop technique without disturbing the spheroid [69]. For both forced-floating and hanging drop techniques, the size of the spheroids can easily be controlled by the number of cells initially seeded. The third method of generating spheroids is by agitation, such as with gyratory rotation and spinner flasks. These utilize continuous rotation or stirring motions to prevent the cells from attaching to the surface, enabling them to form spheroids. For gyratory rotation, a cell suspension is placed in a spinner flask, and it is placed in a gyratory motion incubator until spheroids are formed. Spinner flasks have an impeller which continuously maintains cells in suspension. The movement of fluid facilitates transport of nutrients and

removal of waste from the spheroids [69, 81, 84]. However, this method is not feasible for high-throughput screening [80]. The fourth method to generate spheroids is by using micro-/nano-patterned surfaces. Nanoscale scaffolds imprinted onto a flat substrate control the adhesion and migration of cells, thereby enabling the formation of spheroids. This generates spheroids enabling high-throughput screening like low-attachment plates, however, these surfaces are susceptible to damage from pipetting, and can generate air bubbles [81]

Spheroids can recapitulate certain physiological characteristics such as oxygen and nutrient gradients, they can synthesize their own ECM and possess cell-cell contact. The gradients can allow spheroids to develop a heterogenous population of cells; the external layers are highly proliferative, the middle layer is formed of senescent cells, and the core contains necrotic cells [106]. Tofani et al. utilized both hanging drop and ultra-low attachments plates to compare drug responses between 3D ovarian cancer spheroids and 2D monolayer culture. They observed the presence of microvilli on the surface of the spheroids, as well as higher apoptotic activity of spheroids assessed by caspase 3/7 activity, and higher drug resistance compared to monolayer culture. Furthermore, they claim that the forced-floating method was more suitable and straight-forward to use [104]. Similarly, Amaral et al. found that the forced-floating method was superior in generating bladder cancer spheroids compared to the hanging drop method, and that spheroids had a higher drug resistance compared to 2D culture [107]. 3D spheroids better represent patient responses than 2D culture, as they also mimic gene expression profiles seen in tissues [108].

2.5.2 Microfluidic systems

In microfluidic systems, cells are embedded in a network of channels subject to continuous flow, providing fresh medium allowing for the diffusion of nutrients, metabolites, drugs, or chemokines. This allows for a controllable, reproducible, and easy to handle cell environment [109, 110]. Microfluidic tumor-on-chip devices can mimic the body's environment, but it is challenging to recreate the *in vivo* TME in a chip. However, the devices can be applied for high-throughput drug screening in a cost-effective manner [111]. The common technique for microfluidic device preparation involves the casting of a polydimethylsiloxane (PDMS) which is cured to construct a wide range of channels of various patterns [112, 113]. Chang et al. constructed a microfluidic device consisting of a thin-gel cell culture chamber sandwiched

between two drug chamber layers, with a porous membrane cell medium chamber. They were able to successfully perform an 8 x 8 combination treatment of doxorubicin and paclitaxel drug screening on breast cancer cells lines. The advantage of microfluidic devices is that they can reduce operational time and the number of samples required, while allowing for combinatorial drug screening [114]. They also require 10 to 1000 times less sample volume than conventional methods and can rapidly test drug compounds on live patient cells due to the requirement of a small cell number [115]. However, PDMS requires surface modification due to its hydrophobicity, and the fabrication of the chip itself in a high throughput manner remains a challenge. It is also difficult to remove the 3D tumors from the chips once they are formed, and analysis relies primarily on imaging (e.g., immunofluorescence) [116].

2.5.3 Scaffolds, hydrogels, and bioprinting

ECM can be purchased commercially to support 3D cell cultures. Matrigel® is a common example, consisting of Engelbreth-Holm-Swarm mouse tumor cell-derived basement membrane proteins (collagen-IV, laminin, perlecan, entactin, matrix metalloproteinase-2 and growth factors) [117, 118]. Matrigel® was among the first and still the most commonly used ECM material for the 3D culture of cancer cells because of the cytocompatibility, cell adhesion, and ability to be remodeled by cells [119]. Reconstituted Matrigel® undergoes gelation at 22-37ºC. The entactin crosslinks laminin and collagen IV to create a hydrogel [117]. Badea et al. compared breast cancer spheroids formed with and without Matrigel®. They observed that with the addition of a 2.5% concentration of Matrigel® in the cell suspension, the resulting spheroids had a uniform circular morphology, increased diameter, and increased PCNA proliferation marker expression compared to non- Matrigel® spheroids [120]. Matrigel® is seen as the gold standard, however, like all natural scaffolds, it is limited by its poorly defined and variable composition, both within and between batches, which poses a challenge for experimental reproducibility [117]. In essence, Matrigel® is a basement membrane extract, and is among the natural ECM-derived biomaterials that can support cells in 3D culture. Others are collagen, laminin, and hyaluronic acid.

An increasingly used category of biomaterials for 3D culture are naturally derived polysaccharides such as alginate and chitosan. However, they lack mammalian cell adhesion sites and require chemical modification for crosslinking to be able to provide the desirable physical

properties [119]. Synthetic materials may also be used, such a polyacrylamide (PAM) and polyethylene glycol (PEG). PAM hydrogel is formed through the copolymerization of acrylamide and *N,N'* methylenebis (acrylamide), a slow reaction that required 20-30 min to complete in a deoxygenated environment [121]. PEG-based polymers are of interest due to their thermal responsiveness, ability to be functionalized and attached to planar surfaces, and ability to form nanoparticles. These synthetic hydrogels are physically crosslinked, allowing for responsiveness to temperature and pH [122]. Gelatin is derived from collagen and has also been widely used in hydrogel biomaterials to provide cells with an environment which they can remodel. This is essential for the regulation of cell behaviour [123]. Alginate is a polysaccharide available commercially and extracted from brown seaweeds. Alginate scaffolds can be tuned and optimized for 3D culture and can be made to replicate the elasticity of most tissue types. It can be crosslinked ionically in the presence of divalent cations (except magnesium ion), or covalently in the presence of a photo-initiator and UV light [124]. Natural (e.g., alginate, gelatin, chitosan, etc.) or synthetic (e.g., PAM, PEG, polyvinyl alcohol, etc.) hydrophilic hydrogels can provide a scaffold for 3D tumor models, allowing for the diffusion of nutrients and metabolites, given their high percentage of water content and porous structure [109]. Fong et al. utilized a hyaluronan-based hydrogel to encapsulate prostate cancer cells, resulting in maintained cell viability and continued native androgen receptor expression. This was not possible in standard culture as the cells that were used are poorly adherent [125]. With hydrogel scaffolds, it is possible to observe the migration of cells in a physiologically relevant model. Cavo et al. cultured MDA-MB-231 breast cancer cells in a 50% alginate, 50% Matrigel® gel and observed that the cells exhibited a distinct morphology characteristic of their malignancy, the formation of invadopodia (actin structures allowing cells to cross extracellular barriers), and were able to migrate through the gel and attach to a membrane mimicking vascular walls [126]. Hydrogels can be made more complex with components such as fibronectin to produce a diverse TME, and co-cultures can allow for cellular crosstalk between various cell types. The stiffness of hydrogels can be modified to replicate native tissues. This can allow for anti-cancer drug screening with a more representative model [127]. Lam et al. formed breast cancer cell spheroids in a collagen hydrogel and determined that in stiffer hydrogels, cells were less invasive and were less susceptible to the

chemotherapy drug, paclitaxel [128]. This demonstrates the potential applicability of 3D hydrogel culture for cancer drug screening.

Nanofibrous scaffolds can also be used for 3D culture. A low-cost and rapid method to achieve highly porous and large surface area-to-volume ratio is electrospinning. Electrospun scaffolds can be prepared from synthetic materials such as polylactic acid (PLA), polycaprolactone (PCL), and polystyrene (PS), as well as natural materials such as alginate and gelatin [123, 129-131]. Briefly, electrospinning uses electrostatic forces to generate nanometer to micrometer fibers from polymer solutions, typically requiring a DC voltage in the tens of kV. Key components include the power supply, spinneret, and a grounded collecting plate. As the diameter of the fibers is similar to ECM fibers, the mats created by electrospinning can be used to mimic a natural tissue environment for 3D cell culture [132]. Hartman et al. used the electrospinning technique to produce both nano- and microfibrous collagen membranes for the culture of nonadherent C4-2B prostate cancer cells. The cells grown on the electrospun membranes were more resistant to anti-cancer drugs docetaxel and camptothecin compared to cells on collagen-coated tissue culture polystyrene [133]. Furthermore, Nelson et al. determined that the alignment of electrospun PCL scaffold nanofibers influenced the migration of breast cancer cells. They observed that cells traveled greater distances with more aligned fibers. Additionally, when gradients of CXCL12 chemotaxis factor were applied, they observed an increase in cell migration distance [134].

Bioprinting is the combination of 3D printing techniques and a bio-ink, that is, a printable biomaterial into which cells are mixed. The layer-by-layer deposition of the bio-ink creates a 3D structure. A challenge of this technique lies in the maintenance of cell viability during printing. The bio-ink is a hydrogel usually made of agarose, fibrinogen, alginate, hyaluronic acid, or gelatin. The physical, chemical, and mechanical properties of bio-inks can be tuned to recapitulate the target tissue [109]. Bioprinting is either inkjet-based, extrusion-based, or light-assisted. Cells can either be seeded onto printed scaffolds or be mixed with the carrier matrix to produce the bio-ink before printing. Primary cells, cell lines, and stem-cell derived cells are commonly used. To take advantage of both natural and synthetic biomaterials, composite hydrogels have been used since synthetic materials provide a role in mechanical strength, while natural materials play a role in mimicking the ECM to improve cell viability and functionality [135]. As a proof of concept, Ling et al. used a custom-built bioprinting system to bio-print

droplets of breast cancer cells in a gelatin carrier/bio-ink. From the printed droplets, they rapidly obtained uniform array of 3D spheroids that allow for high-throughput drug screening [136]. Gebeyehu et al. demonstrated that bio-printed scaffolds of non-small-cell lung cancer patient-derived xenograft cells underwent rapid spheroid growth and TME formation within a week. The 3D bio-printed model exhibited higher chemotherapy resistance compared to 2D monolayers in lung and breast cancer cells [137]. Bioprinting offers the notable advantage of developing complex-geometry 3D tumor structures to conduct drug screening in a high-throughput manner. The bio-ink can be customized with the type of cells, ECM components, and biochemical factors to produce the desired physiologically relevant cell-cell and cell-matrix interactions [138].

The above-mentioned 3D models along with their advantages and disadvantages are briefly listed in **Table 2.1** and also illustrated in **Figure 2.3**.

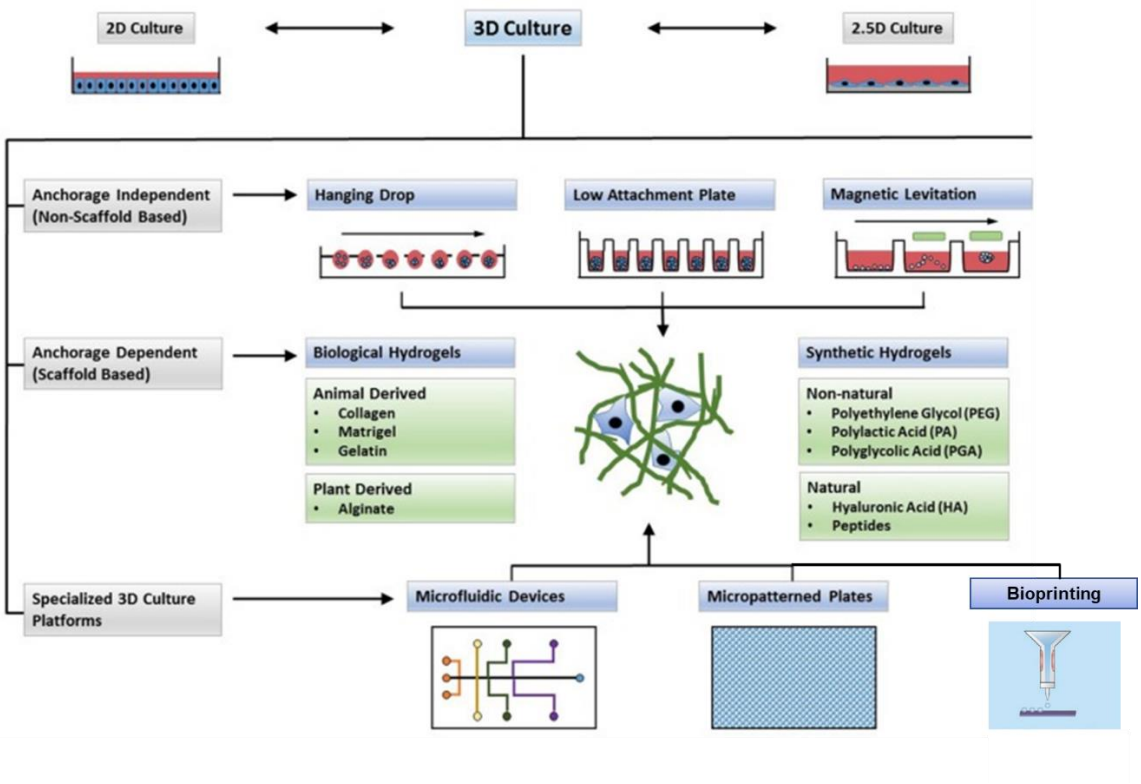

Figure 2.3 Schematic of the types of 3D culture models used in cancer study [139]

Table 2.1 Advantages and disadvantages of different 3D culture models [74, 140]

3D Culture Models	**Advantages**	**Disadvantages**
Spheroids (Suspension culture)	Easy to generate along with standardized protocol (can be automated) Reproduce gradients of nutrients/oxygen Cheap and simple Adaptable for high-throughput screening (HTS) Allows co-culture High reproducibility	Simplified architecture (TME) No cell-ECM interaction Static condition Variation in spheroid sizes depending on technique
Hydrogel/Scaffold	Relatively cheap and simple Cell-ECM interaction Adaptable for high-throughput screening Co-culture ability High reproducibility Versatile (hydrogel/synthetic polymer availability) Tunable properties	Simple architecture Batch-to batch variability of natural hydrogel Need to biofunctionalization of synthetic scaffolds Static condition May be difficult to retrieve cells
Microfluidics	Resemble diffusion/gradients/perfusion Simulate physiological process Vascularized Precise control over microenvironment Co-culture ability	Difficult to scale-up Required high expertise and specialized equipment Difficult to be adapted to HTS Not suitable for long-term experiments
3D Bioprinting	Generate highly complex tissue structure Customized architecture High precision Can be automated Adaptable to HTS Co-culture ability	Cell viability may be difficult depending on technique Difficult to scale-up Required high expertise and specialized equipment Expensive

As indicated, a growing number of studies are being performed to develop improved 3D culture models, to better mimic the native ECM and the tumor microenvironment in cancer studies. Among different above-mentioned strategies considered to produce 3D scaffolds to this aim,

electrospinning is one of the most promising techniques to generate nanofibrous scaffolds comparable to natural ECM with fibrous structures in human tissues. These scaffolds have unique properties such as high surface area to volume ratio and inter-/intra-fibrous porosity. They are categorized in the group of porous structures and have been successfully integrated at the industrial level, particularly in tissue engineering applications in clinical trials. Thus, we focus on this technique in more detail in the following section.

2.6 Electrospinning technology

The extracellular matrix of human tissues and organs is characterized by nanofiber structures; thus, to properly mimic those fibrous networks, electrospinning is an interesting process used to improve the interaction of materials with cellular and biological environment [92, 132]. In the literature, this technique has been widely used in diverse biomedical applications including drug delivery systems, wound dressings, developments of artificial implants in tissue engineering, and 3D cell culture modeling in cancer studies [141]. Flexibility in choosing materials, adaptability of manufacturing parameters, control of mechanical properties and morphology of the final products are outstanding potential attributes of this strategy [142, 143]. Adequate mechanical properties based on the chosen polymeric materials and the porous structure of electrospun mats makes them suitable environments for cellular metabolic exchange, cell adhesion, diffusion, and growth in biological assays, and that is why this technique was preferred to be applied in our 3D model of this research.

2.6.1 Basics of the technique

Electrospinning is a common and versatile method to synthesize nano/micro fibrous scaffolds, highly porous (>80% porosity) networks of ultrafine fibers with diameters ranging from nano- to micrometer (nm to µm) that have great potential in providing a biological microenvironment for subsequent cellular residence and activities like a natural ECM [132, 144]. A high voltage (HV) is used to create a strong electric field between a droplet of polymer solution or melt at the tip of a metallic needle coupled with a syringe and a collector connected to the ground, in the form of either a plate or a rotating mandrel with variable diameter. It causes induction of positive charges in the polymer solution, resulting in repulsive interactions within the solution, then overcome

surface tension, draw polymer droplets from the spinneret, and form a cone known as “Taylor cone”. The narrow jet is finally projected towards the oppositely charged collector, while the solvent evaporates, and polymeric nanofibers are collected on the collecting target [32, 145, 146]. A schematic of the electrospinning setup, along with a typical SEM micrograph of electrospun mat, is shown in **Figure 2.4**.

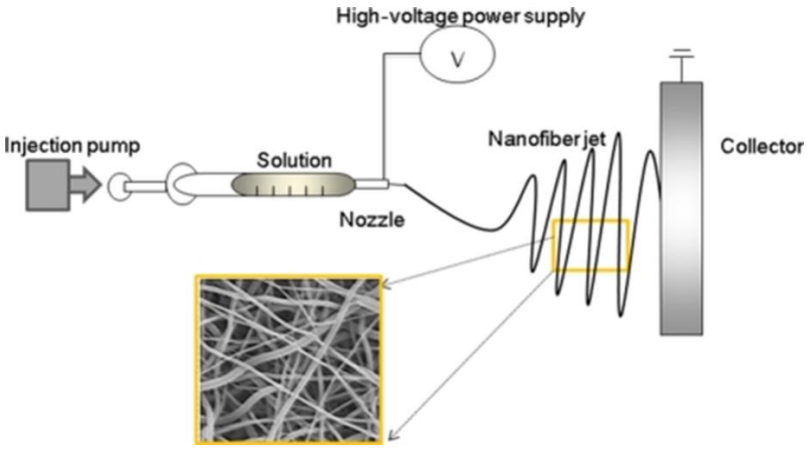

Figure 2.4 Schematic diagram of electrospinning process, along with a typical SEM micrograph of an electrospun mat [147]

It is possible to produce random and partially-aligned fibers during the process by changing the speed of the rotating cylindrical mandrel from low to high, respectively [148]. Also, nano/micro fibers with different morphologies such as core-sells, ribbon-, beaded-, and porous fibers are manufactured based on a broad range of polymers and co-polymers [149] through the classical techniques of electrospinning, including melt electrospinning (polymer is melted at high temperature), co-electrospinning (polymer solutions in different syringes are electrospun at the same time), and co-axial electrospinning (two solutions are electrospun simultaneously by coaxial needles) [150]. In order to have reproducibility and good control on morphology of the fabricated defect-free nanofibers, some critical parameters are involved in the manufacturing process: i) processing conditions including flow rate of solutions, applied voltage, collector geometry, and distance between needle tip and collector; ii) polymer solution characteristics such as polymer concentration, polymer conductivity, molecular weight of polymer, and type of solvent; iii) ambient conditions include temperature and humidity of the electrospinning setup [149, 151, 152].

2.6.2 Natural and synthetic materials used in electrospinning

As we mentioned before, electrospinning is the most powerful method to fabricate fibrous scaffolds and there already exists a considerable amount of literature concerning their biomedical applications [26, 29-33, 153]. The polymers being used in electrospinning processes are basically classified into natural and synthetic polymers. To better reproduce the biological constituents, electrospun mats based on natural polymers are usually fabricated from collagen, alginate, fibrin, chitosan, silk fibroin, gelatin, elastin, glycosaminoglycan (GAG), etc. [154, 155] similar to the components of natural extracellular matrix. Commonly used synthetic polymers employed in electrospinning are polycaprolactone (PCL), poly-lactic acid (PLA), poly(glycolic acid) (PGA), poly(lactic-*co*-glycolic acid) (PLGA), polyethylene glycol (PEG), polyurethane (PU), polypropylene, etc., and have the benefits of reproducible, being inert, with tunable biodegradability and control over tuning their mechanical properties and chemical composition for realistically mimicking the ECM of natural tissues [156]. Although natural polymers show better biocompatibility than synthetic polymers, their mechanical properties and processability are weaker when compared to synthetic polymers. On the other hand, synthetic polymers are generally characterized by good mechanical strength, great flexibility in synthesis and modification, but poor biocompatibility and cell affinity due mainly to low surface hydrophilicity and wettability [156-158]. Therefore, in order to address all of these requirements to make electrospun scaffolds for biomedical applications, blending of two synthetic/two natural polymers or favourably synthetic and natural polymers would be a promising approach to produce an electrospun mat with improved required properties like mechanical strength or biocompatibility [158, 159]. Among many polymeric blends studied in the literature for the development of electrospun mats, PCL/PU, PCL/PLA, silk fibroin/collagen, PCL/gelatin, polydioxanone/elastin, PCL/PEG, etc. are the commonly used ones, but few [160-162]. PLGA is also a very promising copolymer used for tissue engineering application with tunable biodegradability, biocompatibility, and flexibility in surface modification, however, its mechanical properties still need to be improved for biomedical uses through combination with other polymers that have reported in several studies in this field [163]. PLA a versatile biocompatible polymer with widely accepted applications has gained much attraction in cancer studies due to its properties such as biocompatibility, biodegradability, mechanical strength and processability [164]. In the field of

cancer therapy, electrospun scaffolds based on PLA have been widely used as drug delivery systems with having adaptable degradation rate through copolymerization with other polymers such as PGA, as it permits for the study of long-term drug release [165, 166].

2.6.3 Effect of processing parameters on scaffolds morphology and structure

Fiber diameter, porosity and pore size are three important morphological features of electrospun mats that are influenced by processing parameters. In order to have uniform bead-free nanofibers, those parameters should be optimized during the process. A comparison between the structure of uniform bead-less and beaded nanofibers is shown by SEM micrographs in **Figure 2.5**.

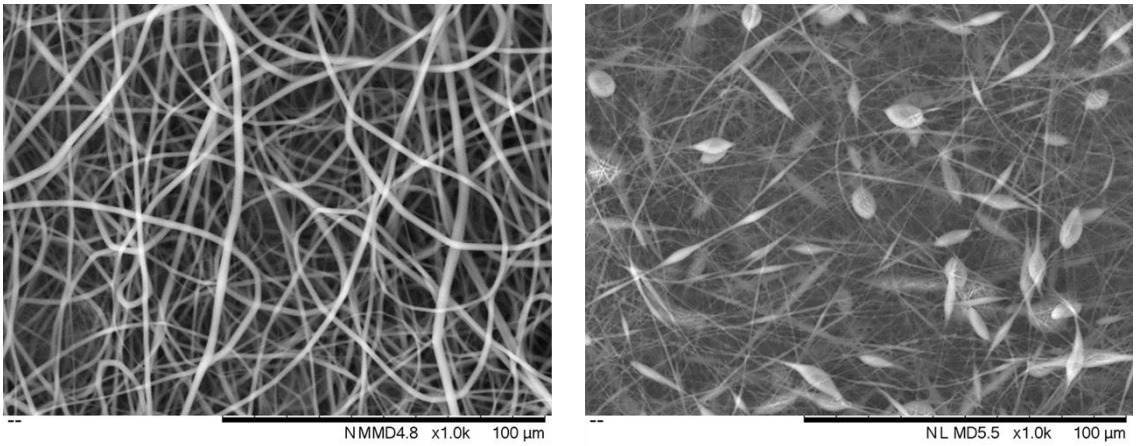

Figure 2.5 SEM micrographs of bead-free and beaded PLA nanofibers mats

Numerous studies have been carried out to determine the links between these parameters and the morphology of the resulting fibers. There is a critical value of the applied voltage to produce nanofiber that beyond those values renders bead formation probable [167, 168]. Depending on the polymer type, an increased voltage will result in higher jet velocity and reduced fiber diameter [169]. There is also an optimal point for the distance between the needle tip and collector to properly collect fibers on the collector while getting dried. It has significant effect on morphology of nanofibers since it depends on the deposition time and evaporation rate of solvent [170]. The more the distance is increased, the more the fiber diameter is reduced [169]. Fiber diameter and pore size of the electrospun nanofibers are also affected by the flow rate of polymer

solution at a critical point to achieve uniform fibers. Increasing the flow above this critical value will lead to increase in the pore size and fiber diameter and also formation of beads [171].

Effect of polymer concentration and viscosity of the solution are also significant on the fiber diameter and pore size of the electrospun nanofibers. A higher viscosity creates fibers with larger diameters and pore size; however, an optimal viscosity needs to produce smooth nanofibers since below the critical point of viscosity, nanofibers full of beads will be produced [146, 168, 169]. A minimum polymer concentration is essential to produce continuous beadless nanofibers because when it is low, the electric field and surface tension make the polymeric chains and their entanglement break into fragments and eventually cause bead formation. Increasing the polymer concentration will lead to an increase in fiber diameter and pore size and also produce smooth nanofibers without beads. Because the polymer concentration is proportional to the solution viscosity, higher concentration causes an increase in viscosity and then chain entanglements that are able to overcome surface tension [172, 173]. Similarly, polymers with higher molecular weight generate nanofiber mats in larger fiber diameters and pore size, whereas lower one produces nonuniform beaded nanofibers [174, 175]. Moreover, the choice of the solvent type plays an important role in structural features of nanofibrous mats and formation of uniform defect-free nanofibers [176]. Having moderate boiling point or optimal evaporation rate and polymer solubility are considered crucial characteristics that should be taken into account before selecting the solvent [167, 177]. Conductivity of polymer solution is another key factor that is mostly affected by the type of polymer and solvent, as reduction in fiber diameter and pore size is obtained by an increase in solution conductivity [178].

Ambient conditions including temperature and relative humidity have also an effect on fiber diameter and morphology of electrospun nanofibers [179, 180]. Increasing temperature leads to a decrease in the viscosity of the solution and increase in the evaporation rate of the solvent, and both result in smaller fiber diameter and pore size of nanofibers [181, 182]. Change in humidity influences the solidification process of the polymeric jet at the needle tip, and subsequently the nanofiber diameter and pore size will get changed as higher humidity leads to more reduction in fiber diameter and pore size [180, 183]. Furthermore, high humidity causes creation of porous nanofibers when two solvents are used in the solution system. It is attributed to the different evaporation rates of the two solvents [184].

2.6.4 Effect of electrospun nanofiber morphology on cell adhesion and growth

Essential cellular properties such as adhesion, spreading, diffusion, proliferation, and differentiation are significantly influenced by the surface topography and morphology of nanofibers, including fiber orientation, diameter, and pore size. There have been a growing number of research papers in the literature dedicated to the effect of those parameters on the cellular activity [185-188]; however, when reviewing them, it can be concluded that this is a controversial topic. Some researchers found great initial cell adhesion, proliferation, and following cell penetration into the depth of electrospun mats with fiber diameters of less than 1 μm because they have higher specific surface area than mats with larger fibers [189-191]. On the other hand, some studies have indicated that electrospun nanofibrous scaffolds with fiber diameter <1 μm prevent inward cell growth and penetration [192-194]. It is also reported that pore size has greater effect on cell proliferation than fiber diameter [185, 195]; this proves that the pores of nanofiber mats do not need to be larger than the cell diameters, as cells could diffuse into electrospun mats with pores size of around 1.5 μm (fiber diameter of 200 nm) which is much smaller than the original size of cells. It is explained by the fact that the cells are able to move through those small pores by pushing the neighboring fibers away [196, 197].

Similarly, the effect of fiber orientation, including random and aligned nanofibers, on cell organization and alignment is considered another debatable issue in the literature. Some researchers reported significant influence on cell proliferation and orientation as well as metabolic activity, by applying electrospun mats based on aligned nanofibers [190, 198]. Conversely, it was found that random nanofibrous mats showed substantial cell adhesion and growth when cultured with cells, in contrast with scaffolds made of oriented nanofibers [199]. Moreover, it has been reported in the literature that fiber surface topography, another key player, has substantial effect on the cell-scaffold interaction, as the presence of nanopores and different features of roughness on the surface of nanofibers seem to make great improvement in cell adhesion, proliferation, and infiltration; however, this area of research with promising results should be studied further [188].

2.6.5 New advances in electrospun scaffolds as 3D models in cancer research

Over the past few years, numerous studies have been performed based on implementation of a vast variety of electrospun nanofibrous 3D scaffolds in cancer research, particularly in drug delivery systems as local cancer therapy methods and tissue engineering approaches. As stated earlier, they have outstanding features such as high surface area to volume ratio, flexibility, simplicity of manufacturing, and high capacity of drug loading, enabling them to be used as drug/gene delivery devices and 3D engineered tissue models in local cancer therapy. Targeted drug delivery systems developed by biodegradable and biocompatible nanofibrous scaffolds can deliver a variety of anti-cancer therapeutics and also different combinations of drugs and agents like nanoparticles and release them in a sustained manner for a long time to control cancer recurrence [29, 200-203]. When loaded with various anti-cancer drugs to treat different breast cancer cell lines, those nanofiber scaffolds, produced with advanced technologies like core/sheath or coaxial electrospinning, caused a great reduction in the recurrence of breast cancer cells through releasing the chemotherapeutics in a time-dependent manner, consequently preventing radiotherapy and the severe side effects of systemic chemotherapy, specially on healthy cells of patients [204-208]. Moreover, termed as cancer theragnostics, a new cutting-edge area of research in drug delivery systems is focused on cancer cell detection or sensing for fast diagnosis of cancers. It is based on using an external stimulus such as light, temperature, and magnetic fields that are applied on smart polymeric nanofibers loaded with encapsulated drugs or other agents [209, 210]. For example, high loads of magnetic nanoparticles can be incorporated into polymeric nanofibrous mats, named magnetic nanofibers, and then implanted directly in the tumor location as a sensor platform to detect and treat cancer at early stages without causing severe side effects [203]. There would be another approach considering the combination of two concepts of local drug delivery and tissue regeneration based on using electrospun nanofiber mats due to their excellent biomimicry. It may be designed based on using nanofibrous scaffolds as a patch at the tumor site, releasing drugs in a sustained manner while promoting tissue regeneration simultaneously in order to treat and renew the resected void space after surgery [29].

A growing number of research papers in the literature are based on the application of electrospun nanofibrous mats as 3D *in vitro* cancer models due to their biomimicry of the structure of ECM. It is a powerful tool to study cancer microenvironment and underpinning molecular mechanisms

of tumor growth and metastasis and then adopt them as proper platforms for drug screening applications. These 3D nanofibrous scaffolds cultured with different types of tumor cells provide a 3D microenvironment, enabling complex and dynamic cell–cell communications and cell–ECM matrix interactions that occur during cancer metastasis [29, 201]. They are essentially fabricated with different morphologies (fiber diameter and porosity), topography and orientations, providing a 3D microenvironment with a more physiologically relevant cell phenotype than 2D conventional cultures; thus, they more appropriately portray metastasis phenomena including tumor cell growth, migration, and invasion [29]. Some studies indicated that, in comparison with 2D culture, tumor cells seeded on 3D electrospun nanofibers are able to grow in an elongated or stellar shape depending on the fibers orientation (aligned/random), showing different behaviours and characteristics [211, 212]; they can grow in the form of irregular aggregates/clusters like *in vivo* tumoroids, along with upregulation and/or downregulation of EMT markers such as E-cadherin and N-cadherin [213]; they present different anti-cancer drug sensitivity compared with 2D collagen-coated culture plates [133]. Another published work developed a co-culture of tumor cells and immune cells on electrospun scaffolds, yielding efficient cellular adhesion, spreading, infiltration, and migration, thus, better recapitulation of the *in vivo* cross-talk between these two cell types in the microenvironment [214]. Surface immobilization of 3D nanofibrous scaffolds by using ligand/peptide is another technique to create 3D tumor models appropriate for chemosensitivity test, in which tumor cells respond to these biochemical stimuli through their specific receptors and indicate higher drug resistance in 3D scaffold than 2D models [215]; in another work, peptide-conjugated scaffolds supported proliferation, survival, and migration of cancer cells [216]. Development of an engineered 3D bone tissue model can be promising to study cancer metastasis to bone since it has been suggested that bone matrix proteins may promote cancer cell adhesion, growth, migration, and invasion [217, 218]. For example, Ewing sarcoma, a bone tumor, was modeled by applying electrospun scaffolds and represented significant upregulation of insulin-like growth factor-1 receptor (IGF-1R) pathway, which is a commonly expressed in Ewing sarcomas and an essential target in drug development and testing [219]. In yet another 3D model of Ewing sarcomas, in order to better mimic *in vivo* tumor microenvironment and drug sensitivity, biomechanical stimulation was added to the 3D cancer model as a new feature. It can be a flow perfusion bioreactor adopted as mechanical stimulus,

providing fluidic shear stress which may cause better cell distribution and increased proliferation due to higher nutrient supply. In addition, it was found that the fluid flow leads to a greater expression of IGF1R by tumor cells and enhanced drug sensitivity [220].

Although the current 3D cancer models have shown considerable contribution in cancer therapy, there is still an open avenue to explore in terms of optimization and improvement of such models in cancer research. Future perspective might be focus on producing 3D electrospun nanofiber scaffolds with hierarchical structure and their combination with either hydrogels or 3D bio-printed scaffolds for better recapitulating the heterogeneity and complexity of the tumor microenvironment and expectantly translation of new chemotherapeutics to clinical trials.

2.7 Surface modification of 3D polymeric scaffolds

In the field of tissue engineering and regenerative medicine, polymeric three-dimensional (3D) matrix referred to as “scaffolds” play an essential role to support cell adhesion, proliferation and differentiation. Cells interact with their microenvironment through adhering to extracellular matrix (ECM) proteins such as collagen, fibronectin, vitronectin, laminin via special receptors named integrins [221, 222]. The surface of biomaterials should mimic the same mechanism after initial contact with cell culture medium consisting of various proteins, as proteins are adsorbed on the biomaterial surface, mediating its interaction with living cells in culture. Thus, recognition of biomaterials relies on the interaction of adsorbed proteins with cell receptors, leading to the modulation of the host immune system, integration of the scaffold with nearby tissue microenvironment and consequent inflammatory and wound healing responses [223]. To better understand cell interactions with scaffolds, focus on surface properties of scaffolds is crucial since it has an extensive impact on cellular response *in vitro* and *in vivo*. As stated earlier, polymeric scaffolds are fabricated from i) natural biomaterials include collagen, chitosan, gelatin and decellularized tissues ii) synthetic polymers such as poly (lactic acid) (PLA), poly(L-lactic-co-glycolic acid) (PLGA), and poly(ε-caprolactone) (PCL) [224]. Although natural polymers generally induce interaction between cell and ECM due to their intrinsic characteristics, they suffer from poor and unsatisfactory mechanical properties as well as batch-to-batch variation. On the other hand, most synthetic polymers used as scaffolds, despite being mechanically and chemically stable with reasonable degradation rate, mostly possess inert hydrophobic surfaces

with low surface energy, which cause poor cell adhesion, proliferation and growth [225]. Thus, changes to surface characteristics of synthetic scaffolds and tuning their biomimetic behaviour is necessary and relies on surface engineering via several surface modification approaches [224]. In recent years, surface modification has been widely studied [226-228] and can be categorized into: i) physical modification methods [229], through changing surface roughness and inducing specific topographical features to physically modulate cell behavior, ii) bio-functionalization by immobilizing bioactive molecules like ECM proteins, peptides and growth factors onto the surfaces through physical adsorption or chemical immobilization [230, 231]; and iii) chemical treatment techniques, to modify surface chemical composition and introducing functional groups to promote cell attachment and improved wettability by using some chemical mixtures like NaOH [232], hydrogen peroxide (H_2O_2) [233] or graft polymerization [234]. However, despite being simple techniques, wet chemistry approaches are harsh and environmental-unfriendly processes which cause undesirable loss of mechanical properties as well as a toxicity issues [225]. In contrast, non-thermal plasma treatment techniques have been considered in the literature as powerful dry, solvent-free techniques with capability of treating the surface of complex shaped scaffolds through providing chemical cues and/or roughness without compromising the bulk properties of the substrate [235]. Considering these advantages, plasma surface modification is acknowledged as a promising method with great potential in surface engineering field, and will therefore be reviewed briefly in this section.

2.7.1 Surface treatment of 3D scaffolds by plasma techniques

Plasma, referred as the “fourth state of matter”, can be generated through energy being supplied by an external source like electrical energy with the capability of ionization of gas molecules. The most common source of energy required for gas ionization is alternating current (AC) at different frequencies including low- (60 Hz), audio- (20 kHz), radio- (13.56 MHz), and microwave frequency (2.45 GHz) [236]. Plasma is an electrically quasi-neutral, extremely reactive multi-component system in which charged particles (electrons, negative and positive ions), excited atoms and molecules, reactive atoms and radicals are created by the applied electric field [236]. Plasma can include thermal (equilibrium) plasma, with gas temperatures of several thousand degrees K, and cold (non-equilibrium) plasma in which only the electrons have high

temperatures, but gas temperature (neutral atoms, molecules and ions) is low, near room temperature. Thus, heat-sensitive materials like polymers are destroyed by thermal plasma, and so only non-destructive cold plasma is suitable for surface modification of such materials [236]. The benefits of employing plasma on polymers' surface is that surface properties of polymers are changed through breaking covalent bonds on the surface and then reacting with reactive plasma species without changing their bulk properties. The resulting functional groups on the surface depend on some important parameters including power (voltage and frequency), time of exposure, gas composition and flow rate [237]. When the surface of polymers is exposed to a non-thermal plasma, beside introduction of functional groups, etching and cleaning, and plasma polymerization can also occur, which are briefly explained in the following sub-sections.

2.7.1.1 Surface functionalization

Plasma functionalization occurs when highly reactive species generated by plasma including electrons, ions, atoms and free radicals are in direct contact with the polymer surface; this leads to breakage of covalent bonds, removing hydrogen and chain fragments, which can be replaced by radicals containing oxygen or nitrogen atoms when the feed gas or vapour contains these elements. This process therefore results in the formation of polar hydrophilic groups such as hydroxyl, carbonyl, carboxyl and primary amine groups on the polymer substrate [238]. As mentioned, the types of these chemically reactive functional groups depend on the selection of process gas (or vapour) like air, argon, oxygen, nitrogen and ammonia, for example [239]; it is intended to change wettability (increase the surface free energy), thereby improving adhesion characteristics and biocompatibility [222]. In other words, this change in surface properties can result in the benefits of subsequent covalently immobilizing a variety of bioactive molecules like proteins, peptides, growth factors, etc. which enhance cell adhesion, proliferation and growth in diverse biomedical applications [224]. However, this high surface energy is only temporary, due to a mechanism named "hydrophobic recovery" or "aging" over the course of time, because surface polymer chains tend towards a thermodynamically stabler state by "reptation" (rotational motion), whereby polar functional groups bury below the surface [240-242]. It is also found that types of materials and plasma conditions can greatly influence ageing characteristics [36]. Surface graft polymerization (**Figure 2.6**) can also be induced under plasma and radiation in two steps: i) incorporation of specific functional groups on the surface by plasma functionalization ii)

plasma activated surface can be brought into direct contact with monomers in the liquid or gas phase and polymerization is initiated under radiation [241]. Contrary to plasma functionalization, grafting is supposed to be permanent [243].

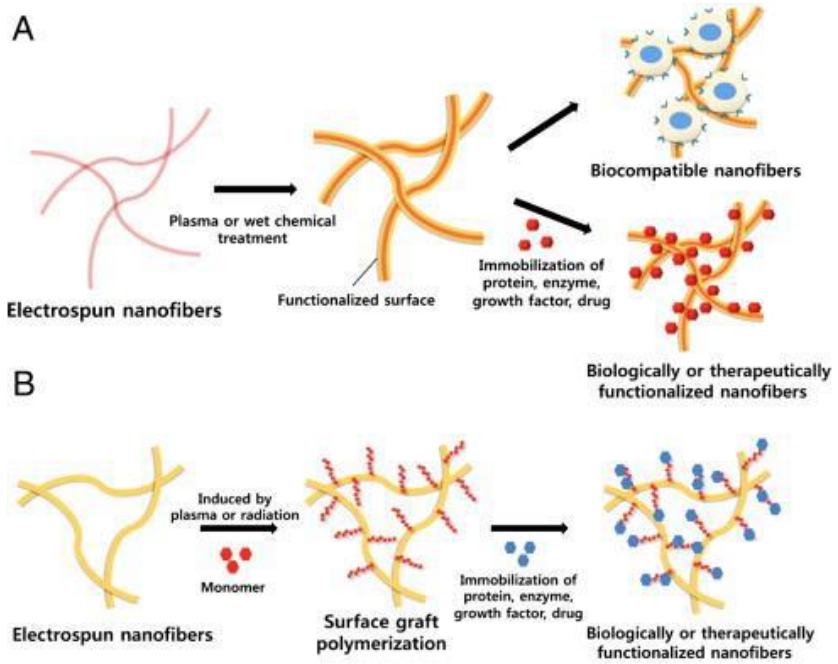

Figure 2.6 Types of surface treatment of 3D electrospun scaffolds: (A) plasma treatment or wet-chemical technique; (B) surface grafting [244]

In addition, etching or physical sputtering happens when microscopic particles are ejected from the surface, after being bombarded by plasma-generated energetic ions of inert gases like argon and helium, leading to change of surface physical properties and roughness [245]. Plasma cleaning is also a form of etching in which organic bonds of surface contaminants are broken and react with energetic plasma species to form some by-products like H_2O, CO, CO_2 which are evacuated from the chamber during the process. The resulting surface is ultra clean with significant efficiency of microorganisms' mortality [246].

2.7.1.2 Plasma-induced deposition of polymer-like coatings (Plasma polymerization)

Plasma enhanced chemical vapor deposition (PECVD) is a well-known technique for surface modification, for example of polymers, that can be done in a capacitively-coupled parallel-plate

radio-frequency (r.f.) plasma reactor (**Figure 2.7**). By this technique, various types of thin layers of polymer-like film coatings can be deposited on the substrate surface within a plasma reactor. Chemical bonds in precursor gases or vapours of monomers, specially selected organic compounds, are broken under electron bombardment in the plasma chamber at low pressure (ca. 20 Pa) and undergo plasma polymerization via free radical reactions. In PECVD, there is the possibility not only of adding one or more co-monomers to the process gas so as to change the coating structure, but also of using saturated organic compounds like methane or ethane, which is impossible by conventional polymerization. Depending on the types of "monomers" used, a variety of functional groups such as hydroxyl, carboxyl, carbonyl, amine etc. can be introduced into the film structure [239]. Among these functional groups, nitrogen-rich ones, particularly primary amines ($-NH_2$), have proven to be attractive for cellular response and immobilization of biomolecules in biomedical applications [227, 247-257].

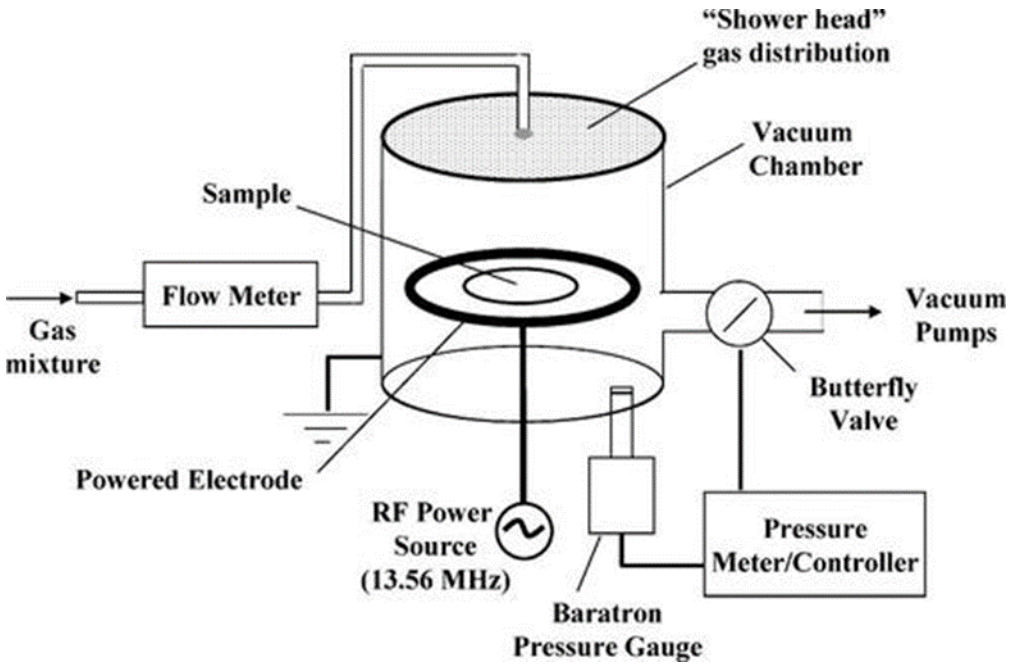

Figure 2.7 A schematic diagram of the low-pressure, capacitively coupled r.f. plasma reactor [248]

2.7.2 Plasma treatment of electrospun nanofibrous scaffolds

Plasma modification of 3D fibrous structures efficiently occurs because the plasma species penetrate readily inside the highly porous nanofibrous mats (ca. 90% void), but most characterization techniques only permit access to the outermost surface [258]. Several studies have investigated cell interactions with plasma-modified fibrous structures or fabrics after immobilization of various bioactive molecules, including proteins such as gelatin, collagen, laminin, fibronectin, etc. [259-262]. Electrospun nanofibers composed of biodegradable polymers such as PGA, PLLA, or PLGA were modified using oxygen and acrylic acid plasma treatment to promote fibroblast adhesion and proliferation, without significant change in mechanical properties [263, 264]. Air or argon plasma treatment has also been extensively used to create carboxylic acid groups on electrospun nanofibers, leading to enhanced cellular activity [265, 266]. In another study, gelatin was covalently attached on PMAA-grafted PET nano-fibrous scaffolds using water-soluble carbodiimide chemistry, leading to a significant increase in endothelial cell adhesion and growth [267]. A similar result was achieved after deposition of a thin layer of plasma-polymerized allylamine (PP-AAm) on electrospun polylactide nanofiber mat, as human osteoblasts primary cells showed improved spreading and quick filopodia formation along and between the nanofibers [268]. Enough amine groups are introduced on the surface of nanofibers by plasma polymerization of allylamine monomer to yield highly hydrophilic scaffolds, which can also be more bioactive by immobilizing suitable biomolecules for enhanced cell adhesion and differentiation, or even for new tissue development [269].

As discussed in this section, non-thermal (cold) plasma technology has been widely recognized as a promising technique in surface modification of biodegradable polymers used in biomedical applications, including 3D cell culture systems, drug delivery and tissue engineering. Outstanding features including selectively modifying the physical and chemical properties of surfaces, short time of process, being applicable to complex geometries and porous scaffolds, being non-hazardous and environmentally friendly, have all contributed to make plasma a preferred, leading technique in surface modification of polymers compared with other methods. In this thesis we focus on plasma functionalization at low pressure, and plasma polymerization at both low and atmospheric pressure.

2.8 Previous related work in our laboratories

In 2008, low-pressure plasma-polymerized coatings based on a binary gas mixtures of ethylene and ammonia (so-called L-PPE:N) were deposited on different substrates, amine-rich plasma polymer coatings for biomedical applications [248]. The same coating, deposited on PET and PTFE, showed a great improvement in endothelial cell adhesion and adhesion rate, spreading, focal adhesion, and resistance to flow-induced shear compared to pristine and gelatin-coated PET and PTFE [249]. Thus, L-PPE:N coating showed much promise in developing electrospun or woven bioactive prostheses, vascular grafts, for which the adhesion of a continuous endothelial cell layer is crucial. Savoji et al (2014) combined electrospinning and plasma polymerization for the case of PET mats with L-PPE:N coatings, which revealed significantly increased adhesion and resistance to flow-induced shear stress of human umbilical vein endothelial (HUVEC) cells, for endothelialization of the luminal side of small-diameter vascular prostheses [270]. Moreover, that ability was increased by L-PPE:N covered with chondroitin sulphate (CS), resulting in bioactive coating with demonstrated ability to form a complete, flow-resistant monolayer of HUVEC [271]. Bouchet et al. developed similarly coated electrospun tubular PU/PCL scaffolds, but with superior compliance compared to commercial ones; these also possessed suitable saturability and burst pressure profiles but no deterioration in saline solution over a 6-month period *in vitro* [272].

2.9 Knowledge gap and significance

Chemotherapeutic drugs are powerful chemicals to destroy fast-growing cancer cells and are essential in treating or regulating tumor progression in patients with cancer. However, some patients' cells resist the drugs and continue to progressively evolve. As there is no standard for drug sensitivity among patients, a reactive approach named "one-size-fits-all" is currently applied, accompanied with undesirable side effects. To mitigate this challenge, the approach of "personalized medicine" as predictive and precise care has been proposed, based on specific patients' needs. The improvements in 3D culture *in vitro* models offer potential avenues to explore and to move towards this latter strategy. However, these 3D advanced cancer models are mainly designed in one specific medium, while the tumor microenvironment is characterized as a multi-phase structure with high level of complexity and heterogeneity. It is comprised of a

heterogeneous population of cells distributed in different phases of tumor mass, epithelium, stroma, blood vessels, and ECM, all have close interactions through signaling molecules in TME. Thus, the study of cellular activities and communications at the interface of those mediums in such a complex microenvironment is essential. Few works have been found in the literature focusing on the development of interface 3D cancer models constructed based on the separate stroma/tumor compartments, particularly the ones with different mechanical characteristics to mimic soft-hard tissues interfaces in the tumor microenvironment. In this context, patient-derived 3D cancer models are more favorable for *in vitro* drug screening of anti-cancer therapeutics to develop personalized treatments. In this PhD thesis, we propose and develop such a methodology, by utilizing plasma-treated electrospun PLA scaffolds seeded with stromal cells as the stroma compartment combined with alginate-gelatin hydrogels containing either patient-derived metastasized tumor cells or cancer epithelial cell line as the tumor compartment to better mimic the native TME and assess the effect of stromal cells on the behaviour of tumor cell migration and progression. In other words, it can be measured how cancer cells manage to metastasize from the hydrogel representing the primary tumor site to the nanofibrous scaffold as representative of a normal tissue. Moreover, there is a potential to apply this cost-effective hybrid model in drug screening as a personalized treatment platform and evaluate how the patient-specific tumor cells respond to different chemotherapeutics. This then enables a better treatment plan tailored to the patients for both pre- and post-operative care.

CHAPTER 3 HYPOTHESES AND OBJECTIVES

As indicated in the literature review, 3D models are commonly generated only from epithelial tumor cells; obviously, this cannot explain the molecular underpinnings of stromal-epithelial interactions and their complexity in the tumor microenvironment. Therefore, 3D models that include both stromal and epithelial tumor cells must contribute to any major improvement of cancer study. In this thesis, we hypothesize that developing a 3D interface model comprised of both stromal and epithelial cancer cells through combining (A) plasma-treated electrospun mats and (B) hydrogel can yield a hard/soft tissue model that can mimic better the microenvironment of certain human cancers and may therefore be considered an appropriate model for anti-cancer drug discovery.

The specific hypotheses of this thesis are as follow:

Hypothesis 1- Electrospun 3D nanofibrous scaffolds modified by selected plasma treatments (both plasma functionalization and plasma polymer coating) can yield vastly improved (stromal) cell adhesion and growth.

Hypothesis 2- Electrospun 3D nanofibrous scaffolds fabricated with different morphologies (fiber diameters, random orientation) and materials (different bio-degradable polymers) can provide suitable fibrous microenvironments for 3D cell interactions and can influence cell adhesion and migration.

Hypothesis 3- The 3D hybrid co-culture model can portray different tissue-tumor microenvironments and a broad range of cancer cell lines with different aggressivity to predict their migratory behaviour and to treat with chemotherapeutics in drug screening experiments.

Hypothesis 4- The 3D interface model may perform similarly as a commercial product, Matrigel®, in terms of efficacy and range of applications.

Hypothesis 5- The 3D interface model can realistically simulate different tissue-tumor microenvironments by incorporating different primary stromal cells co-cultured with various patient-derived metastasized tumor cells; therefore, it can become a platform for drug screening in personalized cancer therapy.

The general objective of this thesis is:

To develop a biocompatible 3D co-culture interface model based on plasma-treated electrospun scaffolds seeded with stromal cells that is coupled with a thin overlayer of hydrogel embedded with tumor cells, representing a tissue-tumor interface; to assess migration and invasion of tumor cells across said tumour-like interface, and subsequently applied as a platform in drug screening applications for personalized medicine.

The specific objectives of the three papers published/submitted for this thesis are defined as follow:

Article 1-

Design and development of bioactive 3D co-culture models are important to reproduce the microenvironment of human cancer tissues and could considerably aid in advance of chemotherapy drugs discovery. Electrospun mats would be the best candidate to provide a nanofibrous scaffolds to better mimic the extracellular matrix of the tumor microenvironment with 3D fibrous structures. They can be made from various soft or stiff materials, have advantages of reproducibility, being inert, with tunable biodegradability, and more specifically, control on tuning chemical composition, mechanical properties, porosity, and fiber size for realistically mimicking the ECM of natural tissues. However, the surface of synthetic polymers is chemically quite inert, characterized by low surface energy and low wettability that leads to poor cells adhesion in subsequent biological tests. Plasma technique is one of the best solutions to treat the surface of polymeric scaffolds, making them bioactive to improve cell adhesion and better cellular activities. Therefore, we hypothesized that 3D electrospun nanofibrous scaffolds coupled with nitrogen- or oxygen-rich plasma reactive species through plasma functionalization and/or plasma coating can provide a biocompatible 3D system that is morphologically, mechanically, and biologically suitable for cell seeding and culture in different biological purposes. We also intended on implementing the model for drug screening applications and comparison of the efficiency with commercial product named Matrigel® which is commonly used as a 3D culture model in cancer study and following drug discovery testing.

Thus, the specific objectives of the first paper are:

1- **To produce 3D electrospun random nanofibrous scaffolds with three different polymeric materials (PLA, PCL, PU) and diameters (small, medium, large), followed by surface modification of the nanofibers with appropriate functional groups through plasma functionalization (O_2 and NH_3 plasma) or by coating them with thin bioactive films deposited by plasma polymerization (nitrogen-rich L-PPE:N coatings)**
2- **To characterize the 3D co-culture model for optimal plasma-modifying treatment, scaffolds materials and morphology, including fiber diameter and pore size, and evaluate their effect on initial cells adhesion as well as tumor cell migration and invasion in the co-culture model of fibroblast stromal cells and MDA-MB 231 aggressive breast cancer cells**
3- **To compare the efficacy of the developed 3D hybrid model with standard Matrigel® migration assays while screening two models with the same concentrations of an anti-cancer drug (Doxorubicin)**

Article 2-

Having previously developed a 3D co-culture interface model for migration assay and drug screening application using triple-negative aggressive breast cancer cell line co-cultured with stromal fibroblast cells, the main focus of the second paper was to represent a bone tissue-tumor interface model in which human osteoblasts (bone cells) were used as the stromal compartment and different more-or-less aggressive breast tumor cell lines and non-cancerous epithelial breast cells were applied to mimic the tumor tissue compartment. In this paper, we reproduced the microenvironment of metastasis in bone-like tissue, in fact, evaluating breast tumor cells metastasized to bone since this type of metastasis is quite common in patients with breast cancer. Further objectives of this paper were to investigate the performance of Doxorubicin against tumor migration/invasion, and additional different plasma treatments at low- and atmospheric pressure.

Thus, the specific objectives of the second paper are:

1- **To simulate a metastatic microenvironment by developing a 3D bone-tumor interface model for evaluating migratory behaviour of breast cancer cells with different levels of aggressivity, and to investigate the impact of Doxorubicin treatment against invasion of different tumor cell lines.**

2- **To compare the effect of various low- and atmospheric pressure plasma treatments of 3D PLA mesh on cancer cell invasion and metastasis across the bone-tumor interface model.**

Article 3-

Considering the data generated in the second paper, showing meaningful migratory behaviours and chemotherapeutics response of different breast tumor cell lines with varying aggressivity towards a stromal comportment within the 3D model, we expanded our earlier work through replication of a real cancerous tissue based on patient-derived spine-metastasis tumor cells in gel, like an organoid, having made an interface with human primary bone cells, osteoblasts, pre-seeded in plasma-treated 3D fibrous scaffolds. Evaluation of the 3D model through dose-response curves analysis was performed based on two well-known chemotherapy drugs, Doxorubicin and Cisplatin. We hypothesized that the model supports migration of different patient-derived primary metastasized tumor cell types, while challenging with the common chemotherapeutic drugs. We also examined the gene expression profiles of those aggressive breast tumor cells lines that had migrated to test the commonly accepted mechanism of the metastasis process, epithelial-mesenchymal transition (EMT).

Therefore, the specific objectives of the third paper are:

1- **Implementation of the hybrid co-culture system to simulate real cancerous tissue microenvironments based on primary cells, to quantify migration and chemotherapeutic responses of different patient-derived spine-metastasis tumor cells towards a stromal compartment of primary bone cells, osteoblasts.**

2- **Evaluation of gene expression profiles of immortalized cell line, MDA-MB 231, having migrated through the developed 3D interface model to test the generally accepted epithelial-mesenchymal transition (EMT) mechanism**

CHAPTER 4 ARTICLE 1: A NOVEL 3D CO-CULTURE PLATFORM FOR INTEGRATING TISSUE INTERFACES FOR TUMOR GROWTH, MIGRATION AND THERAPEUTIC SENSITIVITY: "PP-3D-S"

Mansoureh Mohseni Garakani[1,3], Pouyan Ahangar[4], Sean Watson[2], Bernard Nisol[2], Michael R. Wertheimer[2,3], Derek H. Rosenzweig[4,5,*], Abdellah Ajji[1,3,*]

[1]Chemical Engineering Department, Polytechnique Montreal

[2]Department of Engineering Physics, Polytechnique Montreal

[3]Institute of Biomedical Engineering, Polytechnique Montreal

[4]Department of Surgery, Division of Orthopaedic Surgery, McGill University

[5]Injury, Repair and Recovery Program, Research Institute of McGill University Health Center, Montreal, Canada

[*]These authors contributed equally.

Correspondence:

Derek H Rosenzweig, PhD, Montreal General Hospital, Room C10.148.4, 1650 Cedar Ave, Montreal, QC H3G 1A4, Telephone number: +1(514) 934-1934 Ext. 43238; Email: derek.rosenzweig@mcgill.ca

Abdellah Ajji, PhD, CREPEC, Chemical Engineering Department, Polytechnique Montreal, QC, Canada, H3T 1J4, Phone: +1(514) 340-4711 Ext. 3703; Fax: +1(514) 340-4159; Email: abdellah.ajji@polymtl.ca

This article has been published in "Materials Science and Engineering, 2021, p. 112566" [40].

Abstract

Metastatic cancers can be highly heterogeneous, show large patient variability and are typically hard to treat due to chemoresistance. Personalized therapies are therefore needed to suppress tumor growth and enhance patient's quality of life. Identifying appropriate patient-specific therapies remains a challenge though, due mainly to non-physiological in vitro culture systems. Therefore, more complex and physiological in vitro human cancer microenvironment tools could drastically aid in development of new therapies. We developed a plasma-modified, electro-spun 3D scaffold (PP-3D-S) that can mimic the human cancer microenvironment for customized-cancer therapeutic screening. The PP-3D-S were characterized for optimal plasma-modifying treatment and scaffolds morphology including fiber diameter and pore size. PP-3D-S was then seeded with human fibroblasts to mimic a stromal tissue layer; cell adhesion on plasma-modified poly (lactic acid), PLA, electrospun mats vastly exceeded that on untreated controls. The cell-seeded scaffolds were then overlaid with alginate/gelatin-based hydrogel embedded with MDA-MB231 human breast cancer cells, representing a tumor-tissue interface. Among three different plasma treatments, we found that NH_3 plasma promoted the most tumor cell migration to the scaffold surfaces after 7 days of culture. For all treated and non-treated mats, we observed a significant difference in tumor cell migration between small-sized and either medium- or large-sized scaffolds. In addition, we found that the PP-3D-S was highly comparable to the standard Matrigel® migration assays in two different sets of doxorubicin screening experiments, where 75% reduction in migration was achieved with 0.5μM doxorubicin for both systems. Taken together, our data indicate that PP-3D-S is an effective, low-cost, and easy-to-use alternate 3D tumor migration model which may be suitable as a physiological drug screening tool for personalized medicine against metastatic cancers.

Keywords: 3D Co-culture Systems, Nanofibrous Scaffolds, Plasma Surface Treatment, Interface Tissue Models, Drug Screening, Breast Cancer

4.1 Introduction

According to a recent report from Canadian Cancer Statistics [1], close to 50% of Canadians will develop cancer in their lifetime, and nearly half of these will die of the disease. While there are many existing treatments such as surgery, radio-therapy and chemotherapy, there is an urgent need to develop new improved therapies to treat cancer [5]. However, developing these is lengthy and costly, with 75-90% of new oncology drug candidates failing to pass phase 3 clinical trials [6-8]. Current methods to test new drug therapies include two-dimensional (2D) cell cultures that do not reproduce complexities of the extracellular matrix (ECM), including cell-ECM interactions and the three-dimensional (3D) environment of native tissues [9-11]. Interaction between cancer epithelial cells and the stromal compartment, which plays a crucial role in tumorigenesis and progression, is very difficult to recapitulate in 2D culture [12, 13]. 3D culture systems have been used to simulate the complexity and heterogeneity of tissues and organs in tissue engineering and regenerative medicine, and it has great potential to be used as in vitro 3D models for drug discovery [15-17]. Finally, 3D models can be tailored to portray hard-soft tissue interfaces, such as those in the bone-tumour microenvironment [12, 13].

There has been a rapid increase in research developing 3D culture and co-culture models of cancer microenvironments [10, 14]. Cancer cells in 3D systems better mimic in vivo tumor growth compared with 2D culture [9-11, 14], as already pointed out. This allows for medium throughput investigation and screening of novel therapeutics for anti-cancer efficacy, using either cell lines or patient derived cells [11, 12, 18]. Numerous 3D culture products have been developed in recent years to model the tumor microenvironment, namely scaffold-free and scaffold-based culture systems including hydrogels, sol gels, ceramic or polymeric 3D-printed scaffolds, expanded polystyrene supports, permeable membranes, and electrospun nanofiber layers [19]. Other approaches such as cell spheroids [20-23] or organoids [24] have also been trending in cancer research and have proven valuable in identifying differences in drug responses to new and existing therapeutics, opening doors for personalized medicine [25]. The current "gold standard" hydrogel in tumour models is basement membrane extract (BME), commercially known as Matrigel®, a gelatinous protein mixture secreted by certain murine sarcoma cells, which resembles the complex ECM environment found in many tissues [273-275]. These

products, however, are expensive, exhibit batch-to-batch variability, have limited mechanical strength and uncontrolled degradation. Furthermore, they do not truly mimic the biophysical and biochemical networks found in native ECM in vivo [274, 276]. Natural components of the ECM such as collagen, fibronectin and hyaluronic acid, as well as alternates such as gelatin, and alginate, have been used as 3D culture systems as they mimic the highly hydrated, 3D extracellular matrix of native tissues. These more cost-effective materials are commonly used to mimic soft tissues due to their inherent cytocompatibility and, in some cases, intrinsic cell adhesion properties and capability of being remodelled by cells [14, 38, 39].

Solid scaffolds for hard tissue engineering from synthetic materials such as polyethylene glycol (PEG), poly (lactide-co glycolide) (PLG), polycaprolactone (PCL) and poly (lactic acid) (PLA) are highly inert, with tunable biodegradability; through processing, mechanical properties and chemical composition can be tailored to mimic the ECM of tumors. Electrospinning is a powerful method to produce fibrous scaffolds based on those synthetic materials, and it has been widely used for biomedical applications, including in tissue engineering and in vitro 3D co-culture models of tumor microenvironment [28-33, 153, 216]. Electrospun mats are particularly attractive because they can be made from various soft or stiff materials to achieve desired mechanical properties, porosity and fiber sizes [26, 27]. However, the surfaces of synthetic materials are usually characterized by low surface energy and poor wettability [240]. This is overcome by plasma-based grafting of the fibre surfaces with appropriate functional groups or by coating them with thin bio-active plasma polymer films. As will clearly emerge, these lead to greatly enhanced cell colonization on the scaffold surfaces [27, 240, 271].

Commonly, 3D models are generated only from epithelial tumor cells; obviously, this cannot elucidate the molecular underpinnings of stromal-epithelial interactions in the tumor microenvironment. Therefore, 3D models that contain both stromal and epithelial tumor cells constitute an important development. In this study, we combine hydrogel and electrospun approaches of hard/soft tissue models to develop a 3D interface model comprised of both stromal and epithelial cancer cells. Referred to hereafter as PP-3D-S (for Plasma-Polymer coated, electro-spun 3D Scaffold), we use this novel 3D co-culture model to assess 3D migration and invasion of cells across a tumour-like interface. We hypothesize that plasma-bioactivated 3D scaffolds greatly improve cell adhesion and growth to stimulate invasive tumor cell migration. We start by

characterizing the materials, surface properties and morphological aspects, then followed by biological investigations such as cancer cell invasion and metastasis after interfacing scaffold and hydrogel.

4.2 Experimental Section

4.2.1 Preparation of plasma-treated electrospun nanofibrous scaffold

Figure 4.1 schematically portrays the various fabrication steps that characterize the preparation of the PP-3D-S plasma-treated electrospun nanofibrous scaffold technology being described in this present article.

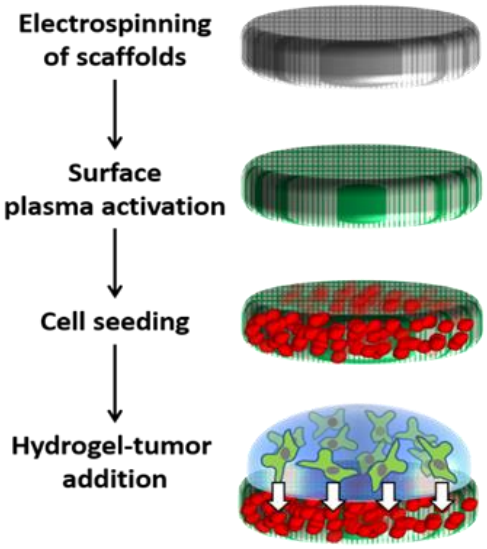

Figure 4.1 Schematic diagram of the main steps that comprise the current innovative methodology. Each of these is elaborated in successive sub-sections of the text in much greater detail

4.2.1.1 Fabrication of nanofibrous mat: electrospinning

As the first step, electrospinning was used to fabricate poly (lactic acid), PLA (NatureWorks 4032D, density of 1.24 g/cc) randomly oriented nanofibrous scaffolds with finely-tuned morphology, in three different sizes of fiber diameters, hereafter designated “Small”, “Medium” and “Large”. Briefly, to produce a “Medium” PLA mat, 16 wt.% polymer solution was prepared by dissolving PLA pellets in 2,2,2 trifluoroethanol, TFE, (M=100.04 g/mol, Merck) solvent

and stirring for 24h. Using a syringe pump placed in a chamber with a controlled temperature (21- 24 ^{0}C) and relative humidity of about 45%-50%, 10 ml of polymer solution (depending on the desired final mat thickness, which was intended to be about 250 μm) was electrospun with a flow rate of 1.6 ml/hr. The distance of the grounded needle tip (21G) and a rotating collector (25 rpm) was set at 15 cm, and the applied DC voltage of 20 kV between the needle tip and the rotating mandrel was provided by a stable DC high-voltage (HV) power supply. Nanofiber filaments were collected on the rotating metal drum, onto which an aluminum foil had been wrapped. The electrospun mats on the foil were then placed in ambient air to evaporate residual solvent for ca. 3 days, then gently detached, cut into smaller pieces, and stored in a desiccator for subsequent use. Two additional types of different medium-sized electro-spun polymer scaffolds, namely polyurethane, PU (MDI-polyester/polyether polyurethane, CAS 68084-39-9) and polycaprolactone, PCL (Sigma-Aldrich, Mn = 80 000) were also fabricated, to examine how versatile the methodology might be. For the case of PU a 1:1 mixture of tetrahydrofuran, THF, and N,N dimethylformamide, DMF, (both from Sigma) was used as solvent, while TFE was still that preferred for the PCL-based solution. In the "supplementary data section", details of the electrospinning parameters for each scaffold, based on size and type of polymers, are presented as a table.

4.2.1.2 Scaffold surface treatment: Plasma functionalization and plasma polymerization

It is known for many years that synthetic polymers are characterized by low surface energy and low wettability, leading to weak adhesion with other surfaces, including living cells. This can be remedied by modifying the polymer surface using exposure to low-temperature (non-equilibrium) plasma [240]. In this present work, cell adhesion to the hydrophobic surfaces of pristine electrospun scaffolds is generally very limited [27]. To correct this shortcoming, the surface compositions of scaffolds were modified by incorporating selected new functional groups using plasma treatment with different gases or gas mixtures. Treatment or coating uniformity throughout the (typically 250 μm-thick) 90% porous scaffolds are assured by the fact that its open volume facilitates diffusive transport of active precursor species from the plasma. This fact and details regarding plasma apparatus and methodology have been validated and presented elsewhere [27, 248, 252, 271, 277]. We have also shown previously that plasma activation of

electrospun scaffolds greatly enhances cellular interactions with those scaffolds that are highly favourable and conducive to tissue engineering applications [27, 271].

Here, the surfaces of the fibers were exposed to low-pressure radio frequency (rf) glow discharges in selected gases and also coated with an ultra-thin (< 100 nm) amine-rich plasma-polymer films symbolized by "L-PPE:N". Since the details have been described in previous work, we explain here only the most essential aspects. The surface of nanofiber mats was functionalized by using oxygen or ammonia gas (O_2 or NH_3, both from Air Liquide Canada Ltd., Montreal, QC) in a low-pressure (600 millitorr or 80 Pa) capacitively coupled radio-frequency (r.f., 13.56 MHz) glow discharge plasma reactor (cylindrical aluminum/steel chamber) with a gas flow rate of 15 standard cubic centimeters per minute (sccm) and plasma exposure time of 30 s for O_2 and 1 min for NH_3 under mild plasma condition (power: P=15 W and self-bias voltage: Vb=-40 V). Alternatively, plasma-polymerized "L-PPE:N" coating was deposited on the scaffold surface in the same low pressure (80 Pa) glow discharge plasma reactor by using ethylene (C2H4)/ammonia (NH_3) gas mixture (C2H4: 99.5%; NH_3: 99.99%), also under mild plasma conditions (P: 15 W, Vb: -40 V). The flow rates of the two high-purity feed gases, C_2H_4 and NH_3, were kept at 20 sccm and 15 sccm, respectively for a duration of 7.5 min for both sides of the scaffold samples. These conditions had been previously optimized to yield a thin layer of almost 100 nm of L-PPE:N on a glass microscope slide, with adequate nitrogen ([N]) and amine concentrations [NH_2] on the surface, and low solubility in cell culture media [252, 253]. The treated samples were finally sealed in sterilized Petri-dishes for the subsequent steps.

4.2.2 Scaffolds characterization

4.2.2.1 Scanning Electron Microscopy (SEM)

To evaluate electrospun nanofiber structure and morphology, the surface of polymeric mats was characterized by Scanning Electron Microscopy (SEM) using a Hitachi model TM3030plus instrument at a working distance of 2 mm and voltage of 15 kV, performed at different magnifications. Selected samples were mounted on a sample holder using double-sided adhesive tape and adjusted at the targeted distance. The diameters of 200 randomly selected fibers for each sample of large, medium and small fiber size (at least three different spots/sample in triplicate)

were measured either in situ or captured SE-micrographs were then analyzed using ImageJ analysis software.

4.2.2.2 Overall porosity and pore size distribution

Overall porosity of PLA electrospun mats of the three different fiber sizes (small, medium and large) was quantified using a liquid (ethanol) intrusion method [233, 278]: Dry mats were first weighed (W1) before being immersed in 100% ethanol overnight for complete wetting of the samples. Next day, the mats were gently wiped to remove excess ethanol and weighed again (W2). Porosity is defined as the volume of ethanol trapped in the mats (~ [W2-W1]) divided by that of the wet mats (~ W2). This technique, as well as mercury intrusion porosimetry, had been verified in previous studies [27, 277] and both had been found to yield very similar results. In addition, calculation of average pore size and its distribution in the nanofiber scaffolds for each fiber size, was performed by using a useful and practical plugin named "DiameterJ" in ImageJ software, through fitting an ellipse inside the pores' shape, and the mean pore size for each scaffold (from three different spots per sample in triplicates) was measured from the average of the long and the short axes for each fitted ellipse.

4.2.2.3 Mat thickness measurement

The thicknesses of nanofiber mats (targeted design values at 250 μm) were determined using a digital micrometer gauge for film thickness measurements (Film Master, Qualitest, 10 μm resolution). The samples were sandwiched between two rigid PET films to minimize errors resulting from compression during measurements.

4.2.2.4 Surface chemical analyses (XPS)

X-Ray photoelectron spectroscopy (XPS) analysis was performed on treated and non-treated scaffolds in a VG ESCALAB 3MkII instrument, using non-monochromatic Mg Kα radiation. The sampling depth, in the range of 1-5 nm, depends on the fiber geometries in the ca. $1mm^2$ analyzed area. To acquire spectra, emission angle was set at 00, normal to the mat surface, and charging was corrected by referencing to the C1s peak at binding energy BE=285.0 eV. The X-ray source's operation condition was at 15 kV, 20 mA and quantification of the constituent elements was performed using Avantage software (Thermo Electron Corporation) after Shirley-

type background subtraction, following which the concentrations of elements were determined from XPS survey spectra.

4.2.2.5 Static contact angle measurements

Static contact angles (SCA) of water droplets were measured at room temperature using a FDS tensiometer, OCA Data Physics, model TBU 90E. Treated and non-treated mat samples were fixed on glass slides; then 2µL droplets of MilliQ water were placed on the sample surfaces with a micro-syringe (at least four different spots/sample, carried out in triplicate) and average values along with standard deviations of SCAs were evaluated using SCA20-U software provided by the manufacturer.

4.2.3 Biological experiments

4.2.3.1 Cell culture, seeding and preparation of the 3D models

The epithelial breast cancer cell line MDA-MB231 (Green-fluorescent protein, GFP), and stromal connective tissue cells including IMR-90 mcherry Fibroblasts (Red-florescent protein, RFP) [279, 280], provided by the laboratories of Professor M. Park at McGill University, were cultured in high-glucose Dulbecco's modified Eagle medium (DMEM), supplemented with 10% fetal bovine serum (FBS), 1% Pen Strep (PS) antibiotic (all from Gibco, Thermofisher), at 37 ^{0}C in a humidified cell culture incubator with an atmosphere of 5% CO_2. After reaching 90% of confluency, cells (passage 3) were first washed with sterile phosphate buffered saline (PBS), detached using 0.25% trypsin (Gibco, Thermofisher), followed by adding fresh RPMI cell culture medium (Gibco, Thermofisher) supplemented with 10% FBS and 1% PS. Then, the cell suspensions were centrifuged at 1500 rpm for 5 min to collect cells at the bottom of vials, and finally suspended in 3 mL fresh complete media, counted, and diluted to 100,000 cells/mL for fibroblasts, ready to be seeded on the scaffolds and 500,000 cells/mL for cancer cells to be mixed with hydrogel. Treated and non-treated electrospun mat scaffolds were precisely cut into disks with a 9 mm punch, sterilized with RPMI media containing 1% antibiotic to remove possible contaminants, then finally placed into individual wells of non-adherent 48-well polystyrene culture plates, destined here for i) a tumor migration assay; ii) a high-throughput therapeutic screening test. Next, 200 µL of fibroblast cell suspension (20,000 cells/scaffold) was added to

each well and incubated for 30 min in the humidified atmosphere of 5% CO_2. Then, medium was aspirated from each well and rinsed with fresh media to remove non-adherent cells. Finally, a layer of (100 μL) of alginate (1%)/ gelatin (7%) hydrogel (A1G7), pre-impregnated with MDA-MB 231 tumor cells (50,000 cells in gel/well), was applied on top of each sample compartment, followed by adding 200 μL of $CaCl_2$ (100 mM) for ionic crosslinking. The rationale behind the choice of alginate or gelatin versus conventional hydrogels like collagen is that the alginate/gelatin-based type is more cost-effective. Each well was then aspirated, washed twice with fresh media to remove residual crosslinking agent and 500 μL of complete media was finally added per well. The plates were incubated for 1, 3 and 7 days, the culture medium being changed every three days.

4.2.3.2 Investigation of initial cell adhesion

Initial adhesion of fibroblasts seeded on the treated and non-treated scaffolds with different pore and fiber sizes was assessed after 30 min incubation of the cells. After this, the liquid was suctioned off, and the mats were washed twice to remove non-adhered cells. The mats with adhered cells were then fixed by PFA 4% for 15 min at room temperature, before washing twice with PBS solution. They were subsequently placed on glass slides for observation using an EVOS M5000 fluorescence microscope. Images of the whole surface of each 9 mm-disk were captured with a 4X-objective. The number of adhered fibroblasts were counted, and the percentage was calculated based on the total 20,000 cells initially seeded.

4.2.3.3 Tumor cell migration - observation and quantification

Movement and migration of cancer cells was assessed as a function of incubation time. The top surface and depth of treated and untreated scaffolds (nominal thickness 250 μm) were monitored after 1, 3 and 7 days, after scraping off the hydrogel and fixing the surface with 4% PFA. The samples had been placed onto microscope slides, first covered with a droplet of mounting medium (containing DAPI) to avoid dehydration, then with a protective glass cover slip. Images of green (tumor cells) and red (fibroblast) cells on the top surface and within the scaffolds were captured under different magnifications using a florescent and a confocal scanning microscope, namely EVOS M5000 (4X) and Olympus IX81 (10X), respectively. Images were analyzed and

the florescent intensity quantified and/or the number of migrated cells directly counted using ImageJ software. Each experiment was done in triplicate, with quantification from 20 spots to fully cover the surface of each sample.

4.2.3.4 Drug screening experiment

A drug screening experiment was devised using a well-known cancer drug, Doxorubicin (Sigma), to evaluate tumor migration in our 3D cell culture model. 48-well plates loaded with O_2 plasma-treated PLA mats (medium size), as before pre-cultured with fibroblasts and tumor cells, were treated either (i) with various concentrations of Doxorubicin, namely 0, 0.05, 0.1, 0.5, 1 and 2 μM; or (ii) with sterile PBS as control, in low-serum conditions (1% FBS) in triplicate for 7 days. The media loaded with the drug was replaced on day 4 for each well. An alternative drug screening experiment was also carried out, namely "Boyden Chamber Migration Assay" [274, 275] based on Matrigel®, with the aim of comparing the results with our present 3D model. Similar numbers of fibroblasts (20,000 cells/well) were seeded in a 24-well plate and 500 μL of complete media (10% FBS) were added to each well. In the second 24-well plate, Matrigel® with MDA-MB 231 breast cancer cells (50,000 cells/well), in triplicate, was loaded in the upper compartments of Boyden trans-well chambers with suitable transparent PET membranes (8 μm pore size; Corning, NY, USA); following this, 500 μL of complete media (10% FBS) was added and incubated at 37 oC, 5% CO_2. After 24 hours of incubation, PET membranes with Matrigel® and tumor cells were transferred to the first plate with the fibroblasts, and cells were then treated with combined PBS / Doxorubicin at concentrations of 0.05, 0.1, 0.5μM in RPMI media with low-serum conditions (1% FBS) in the upper compartment. Tumor cell migration was triggered over 7 days using RPMI supplemented with 2% FBS as a chemoattractant in the lower compartment.

4.2.4 Statistical analysis

All experiments reported here were carried out in triplicate to evaluate reproducibility and all data were expressed as mean values ± SD/SE. Statistical analysis was carried out using two (or three)-way ANOVA with Tukey's post hoc analysis for parametric data; in the case of having non-parametric data Kruskal-Wallis test was done, followed by Mann-Whitney post hoc analysis

to compare two independent groups of interest. Values of $p < 0.05$ were considered significant for all tests.

4.3 Results and Discussion

As illustrated in the schematic diagram, **Figure 4.1**, PP-3D-S fabrication involves several steps, namely (i) electrospinning of a suitable biodegradable polymer (herein mainly PLA) as scaffold; (ii) bio-activation via treatment of the nanofiber scaffold by plasma functionalization or ultra-thin plasma polymer (PP) coating; (iii) seeding stromal cells within the open 3D volume of treated scaffolds to mimic target tissues; and finally (iv) depositing a droplet of hydrogel pre-seeded with different types of tumor cells on top, to evaluate tumor cells migration and metastasis over specific time intervals. Results of experiments and discussion are presented in the following text.

4.3.1 Physical properties and morphology evaluation of nanofibrous mats

4.3.1.1 Fiber diameter and distribution

Electrospun (PLA) scaffolds have been used frequently in bone tissue engineering [281] and 3D cancer modeling [282]. These can be made from PLA, but also from other polymers like polyurethane (PU) or poly-caprolactone (PCL); they can be fabricated with different morphological features including pore size, porosity, and fiber diameters, as well as various mechanical properties, mimicking different target tissue matrices. We have previously developed these scaffolds for neuronal [283], cardiac [284], vascular [27, 271] tissue engineering applications, but now are developing this toward modelling a tumor microenvironment. **Figure 4.2** shows micrographs of electrospun mats captured by SEM, along with the plots of fiber diameter distribution and the average size (three individual experiments with triplicate samples), in which the red dotted line presents the average (at peak). The micrographs clearly demonstrate randomly interconnected network structures of the electrospun mats, which proves the desired smooth surfaces lacking “beads” (spheroidal-shaped defects), and thus witnessing favorable processing conditions. As targeted, the value of fiber diameter for PLA mats was mainly found to be in the range of 200-300 nm for “Small” (average diameter: 273±30 nm), 600-800 nm for “Medium” (average diameter: 730±75 nm), and 1-2 μm for “Large” (average diameter: 1.47±0.2 μm) scaffold size; for the cases of PU and PCL mats, the mean values for medium size were

820±40 nm and 910±86 nm, respectively. SEM characterization was also done on plasma-treated mats, and as expected (images not shown) no perceptible difference was observed between bare (non-treated) and treated ones, as also reported in previous work [27].

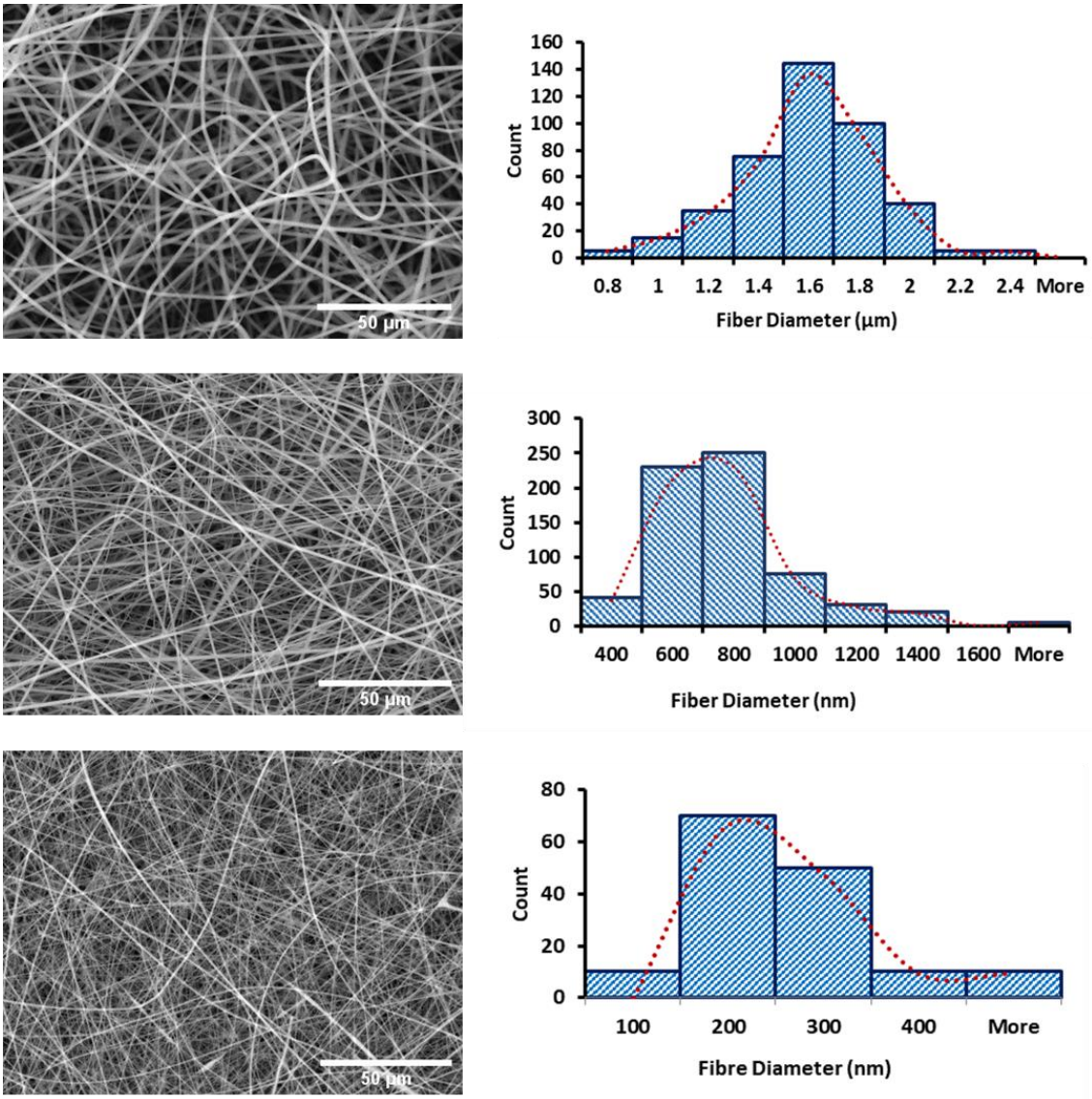

Figure 4.2 SEM micrographs and fiber diameter distribution curves of PLA electrospun mats of different fiber diameter sizes (small:200-400 nm, medium:600-800 nm, large:1-2 µm), scale bar: 50 µm

4.3.1.2 Thickness of nanofibrous scaffolds

The final product is an electrospun sheet with dimensions of 28 by 30 cm in length and width (mandrel diameter: 10 cm), respectively. Thickness measurements, using a digital micrometer, usually vary substantially from the center (max. 280 µm) to the edges (ca. 80 µm). Hence, samples (squares of 5 by 7 cm, 200-250 µm) were taken from central portions of the sheets for use in the subsequent experiments.

4.3.1.3 Porosity and pore size measurement

Table 4.1 and **Figure 4.3** show overall porosity and average pore sizes of PLA mats (small, medium, and large sizes) obtained by the methods in section 4.2.2.2 (liquid intrusion technique and ImageJ). The so-called "large" scaffolds possess larger pores and slightly smaller overall porosity than the other two; the observed high porosity of ca. 90% in all three cases is of course highly desirable for intended use, because it readily enables transport of oxygen and other gases, nutrients, metabolic wastes, etc. during metabolic activity in the biological microenvironment. Furthermore, the (multi-µm) pore sizes are clearly large enough to allow ready accommodation of stromal cells into the scaffolds. To verify data obtained by the two above-mentioned methods, we also resorted to others, including MIP (Mercury Intrusion Porosimetry) test; porosity (ε) was evaluated gravimetrically according to equation (1) [285], and average pore diameter (r) by equation (2) [286].

$$\varepsilon=1-[\rho_{mat}/\rho_{bulk}] \quad (1) \qquad\qquad r=-(D/\ln \varepsilon) \quad (2)$$

where ρ_{mat} is the electrospun mat's measured density, ρ_{bulk} is the bulk density of PLA (1.24 g/cm^3), and D the mean fiber diameter. As shown in Table 1, there are slight differences between average pore diameters obtained from ImageJ and eq. (2). Pore diameters for medium and large mats determined by the MIP test were found to differ little, possibly for the following reason: It seems that pores in the bulk differ in size from voids observed from SEM images. Possibly, during mercury intrusion into the mats, the latter can deform and enlarge the apparent pore size. Nevertheless, data from **Figure 4.3** and **Table 4.1** confirm that the present PLA mats are suitable 3D networks for accommodation and displacement of live cells through the nanofibrous structures, as they do in their natural ECM, both the stromal fibroblasts as well as MDA-MB 231 breast cancer cells, respectively 10-15 and 15-20 µm in average size [287, 288].

Table 4.1 Comparison of average pore size (µm) and porosity (%) of PLA electrospun mats in different sizes calculated by three techniques including ImageJ, eq. (2) and MIP test

Parameter	Scaffold	ImageJ	eq. (2)	MIP Test (30Kpsia)
Average Pore Diameter, r (µm)	Large	3.0 ± 0.32	5.2 ± 0.6	2.94
	Medium	2.1 ± 0.2	3.3 ± 0.5	2.91 ± 0.6
	Small	1.0 ± 0.05	1.3 ± 0.1	1.99
Porosity (%)	Large	90.3 ± 1.5	87.4 ± 0.45	84.2
	Medium	91.0 ± 1.6	87.2 ± 0.3	84.0 ± 1.05
	Small	91.3 ± 0.9	88.3 ± 0.25	86.1

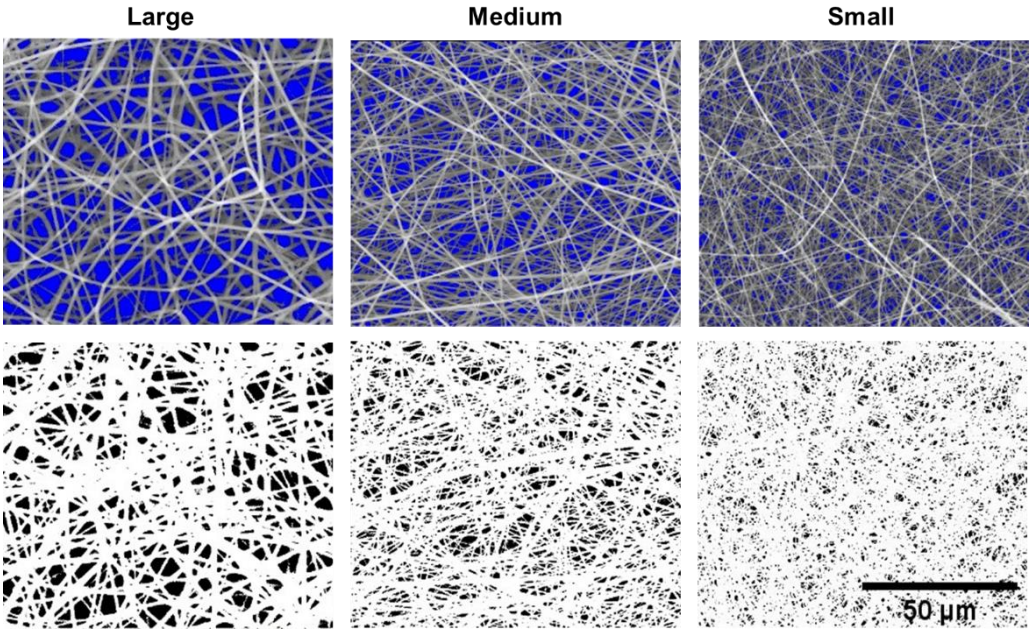

Figure 4.3 SEM micrographs of electrospun PLA mats with different fiber sizes and porosities (large, medium, and small fibers), scale bar: 50 µm

4.3.2 Surface characterization of bare and plasma-treated scaffolds

4.3.2.1 Surface-Chemical Analyses (XPS)

In section 4.2.1.2 we have already described the rationale for various plasma treatments used in the current context of 3D nanofibrous scaffolds. Following treatments, XPS analyses were used to evaluate surface chemical compositions of the substrates that had been treated with O_2 plasma or by L-PPE:N coating, alongside pristine PLA mats. XPS survey spectra (not shown) indicate surface-near heteroatom concentrations before and after treatments, as presented in **Table 4.2**. As expected, the results in this table show increases in the [O] and [N] concentrations of scaffolds treated with O_2 and L-PPE:N, respectively, in comparison with pure PLA mat, confirming the presence of oxygen- and/or nitrogen (amine)-rich functionalities on the surface of scaffolds. Detected fluorine (F) originated from the Teflon-sprayed aluminum foil used for collecting nanofiber mats while electrospinning; some bound F, like here, is considered to be safe, without danger of cytotoxicity and of no risk to cells during culture.

Table 4.2 Surface chemical compositions of pure PLA and PLA mats modified with L-PPE:N coating or O_2 plasma, determined from XPS survey spectra

Element	Pure PLA (At. %)	O_2 Plasma (At. %)	L-PPE:N Coating (At. %)
F1s[1]	13.3	13.2	2.2
O1s	36.6	39.8	4
N1s	-	-	12.7
C1s	50.1	47	81.2
[O]/[C]	0.73	0.85	0.05
[N]/[C]	-	-	0.16

4.3.2.2 Static Contact Angle (SCA) measurements

SCA results are summarized in **Table 4.3**. Although these must be considered only as qualitative in view of the porous, rough surface, it is obvious that medium PLA samples treated with O_2 and

[1] The source of fluorine is the Teflon spray applied to the Aluminium foil used to collect nanofibers during the electrospinning process.

NH_3 plasma dramatically change surface properties from hydrophobic to fully hydrophilic (0°) in comparison with the pristine PLA mat: Immediately upon contact, water droplets spread and diffused into the plasma-treated mats. Capillarity, surface roughness, porosity, and high polarity due to chemically-bonded oxygen (**Table 4.2**) all combined to cause the observed increase in wettability, but surprisingly this was not the case for samples coated with L-PPE:N, which is known to include desired bioactive nitrogen-rich functionalities such as primary amines.

Table 4.3 Static water contact angles of plasma-treated and non-treated PLA mats

Samples	**Static Contact Angle (º)**
Pure PLA	142 ± 2
O_2	0
NH_3	0
L-PPE:N	133

4.3.3 Investigation of initial cell adhesion

4.3.3.1 Effect of treatment type and scaffold size on stromal fibroblast adhesion

First, the effects of three different plasma treatments and three mesh sizes were studied with regard primarily to bonding of cancer-associated stromal fibroblasts, for both treated and non-treated PLA mats, after 30 minutes of incubation. Because pristine PLA mats are hydrophobic, they do not facilitate cell seeding and adhesion, unlike all plasma-treated scaffolds, as illustrated in **Figure 4.4**. Statistically significant differences are noted between the percentages of cells adhered to the scaffolds with different morphologies and plasma treatments (H=27.33, P=0.0041). The observed greatly improved cell adhesion on plasma-modified scaffolds (NH_3 and O_2, compared with Ctrl) can be respectively attributed to positively- or negatively-charged hydrophilic functional groups [271]. Indeed, we had already much earlier reported that cell adhesion and -proliferation on plasma-modified electro-spun 3D scaffolds greatly exceeded those on virgin control samples [27, 277]. The results shown in **Figure 4.4** present *surface-near* numbers of the cancer-associated fibroblasts, because merely 30 minutes after seeding no appreciable cell penetration deeper into the porous scaffold should be expected for small-, medium, or large-sized fiber scaffolds, plasma-modified or not. Interestingly, although L-PPE:N-coated samples displayed unexpected “hydrophobic” behaviour (see **Table 4.3**), their bioactive

amine groups nevertheless are seen to have promoted fibroblast adhesion, albeit less pronounced than for the O_2 and NH_3 plasma-modified cases. Finally, the medium and large-sized scaffolds displayed much higher cell counts than their small-sized counterparts, presumably owing to much larger pore sizes even near the surface (see **Table 4.1**).

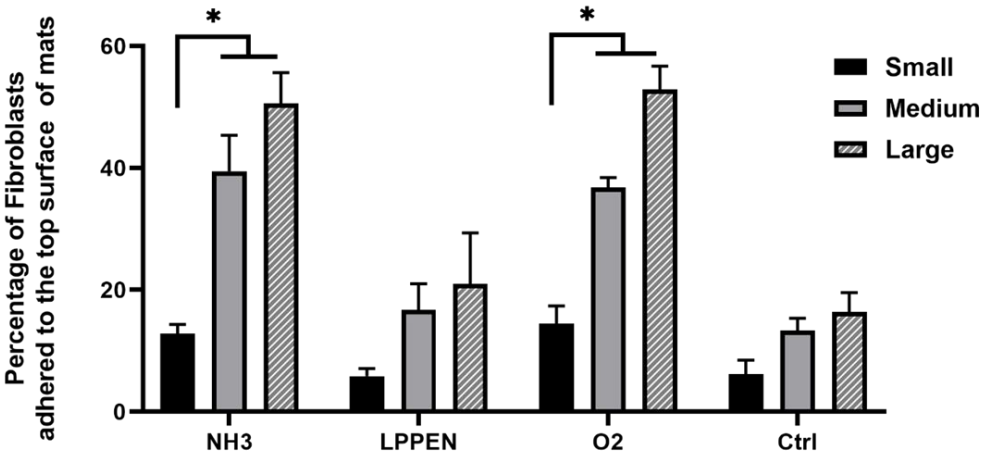

Large-NH_3 Vs. Large-Ctrl *	Med-NH_3 Vs. Small-NH_3 *
Med-NH_3 Vs. Med-Ctrl *	Large-NH_3 Vs. Small-NH_3 **
Large-O_2 Vs. Large-Ctrl *	Med-O_2 Vs. Small-O_2 *
Med-O_2 Vs. Med-Ctrl *	Large-O_2 Vs. Small-O_2 **

Figure 4.4 Percentages of initially-seeded RFP cancer-associated fibroblasts adhering to plasma (O_2, NH_3 and L-PPE:N)-treated and non-treated PLA scaffolds 30 minutes after seeding 20,000 cells (error bars: SE., n=3)

4.3.4 Tumor-cell migration

4.3.4.1 Effect of plasma treatment type on tumor cell migration

We next investigated migration of MDA-MB-231 breast cancer cells into the 3D microenvironment of our PP-3D-S model. Breast cancer commonly metastasizes to other organs or to bone, for example to the spine [289], so we have conducted a series of experiments that elegantly simulate breast cancer metastasis. Over 7 days, the GFP triple-negative breast cancer

cells, seeded within the upper hydrogel layer, readily migrate to the medium-sized PLA mat first seeded with IMR-90 mCherry fibroblasts (**Figure 4.5**).

Figure 4.5(A) presents microscopic images of invading and migrating (and proliferating) breast cancer cells (green) in the 3D scaffolds, in which the RFP fibroblasts (red) were pre-adhered to different plasma-treated (O_2, NH_3, L-PPE:N) and untreated medium-sized PLA scaffolds. The reader is reminded that the tumor cell-bearing hydrogel layer was removed by scraping just prior to acquisition of the images; therefore, these micrographs manifest greatly increasing presence of the (green) tumor cells well within the scaffold's volume, by having changed the type of treatment and also by increasing the incubation time (statistically proved: $H(12)=33.4$, $P=0.00045$). This is clearly observable in all four cases (including untreated controls), especially after 7 days, as also quantitatively illustrated in the lower portion, **Figure 4.5(B)**. Now, referring to **Figure 4.5(A)**, O_2 and NH_3 plasma-treated scaffolds very evidently show quite large (green) tumor cell populations after 7 days compared with untreated controls, especially NH_3 (O_2 displaying quite significant scatter among the n=3 data sets). But the unexpected, surprising result is that relating to the L-PPE:N coated scaffolds, which show only marginal improvement over corresponding untreated control samples. We shall return to this perplexing observation in the Discussion section later in this text.

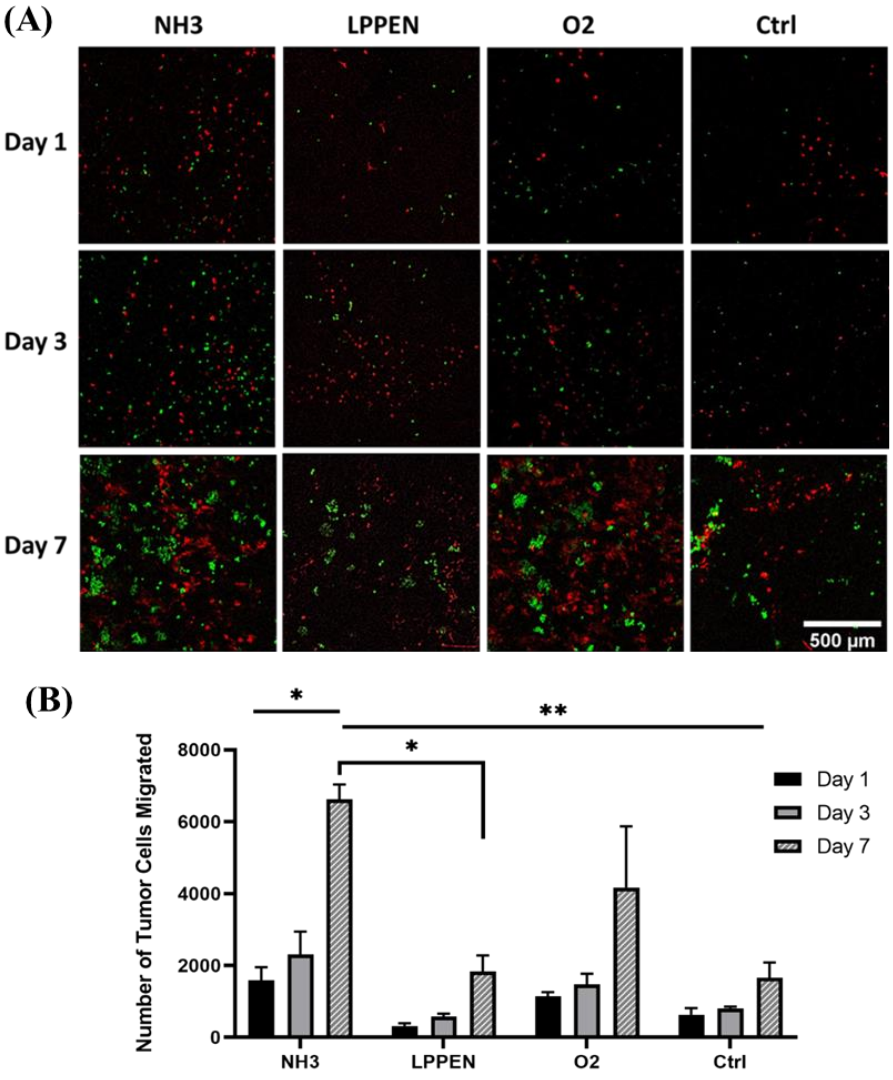

NH_3-D3 Vs. Ctrl-D3 *	Ctrl-D1 Vs. Ctrl-D7 *
NH_3-D3 Vs. L-PPE:N-D3 *	NH_3-D1 Vs. L-PPE:N-D1 *
L-PPE:N-D1 Vs. L-PPE:N-D7 *	NH_3-D1 Vs. Ctrl-D1 *
O_2-D1 Vs. O_2-D7 *	O_2-D3 Vs. L-PPE:N-D3 *

Figure 4.5 Tumor cell migration in the PP-3D-S model. (A): Representative images of RFP cancer-associated fibroblasts (red) adhering to untreated controls, and to L-PPE:N, O_2, NH_3 plasma-treated medium-sized PLA fiber scaffolds, along with increasing numbers of GFP breast cancer cells (green) having migrated over periods of up to 7 days. (B): histograms that quantitatively represent tumor cell migration following the different types of plasma treatments and durations (error bars: SE., n=3)

4.3.4.2 Effect of scaffold size on tumor cell migration

Figure 4.6 shows not only the effects of plasma treatment types on tumor cell migrations after different incubation periods (see **Figure 4.5(A,B)**), but here also that of the three different scaffold sizes, small, medium and large. Many of the comments made in preceding section 4.3.4.1 for the case of the medium-sized scaffolds are seen to apply here, too, namely large numbers of migrated / proliferated (green) tumor cells observed in the scaffold volumes, especially after 7 days for O_2 and NH_3 plasma treatments, while L-PPE:N results only marginally improved compared with their control counterparts. The principal new observations (statistically significant difference: $H(35)=96.95$, $P<0.00001$) that may be noted in **Figure 4.6** are: i) Small-sized scaffolds, even those corresponding to O_2 and NH_3 plasma treatments, display only very minor variations among themselves, compared with untreated control samples; ii) Large- and medium-sized scaffolds show rather similar numerical values, slightly higher for "large" in the NH_3 and L-PPE:N cases but not significantly different compared with "medium". Data from **Figure 4.6** indicates that the significantly reduced pore openings that characterize small-sized scaffolds (ca. 1 µm, compared with roughly 2 and 3 µm for medium- and large-size, respectively, see **Table 4.1**) evidently greatly hindered cell mobility through the open volumes of the "small" scaffolds, even though those free volumes were comparable in all three cases, roughly 90% (**Table 4.1**). Not even the much smaller fiber diameters (**Figure 4.2**) and correspondingly greater flexibility of the small-sized scaffolds' fibers could compensate for obstacles posed by the reduced pore volumes. This observation somewhat parallels that of fibroblast adhesion on the topmost surface layer of the three different-sized scaffolds (see section 4.3.3.1, **Figure 4.4**), where small scaffold size initially (first 30 minutes) led to much lesser numbers of adhering cells in all cases.

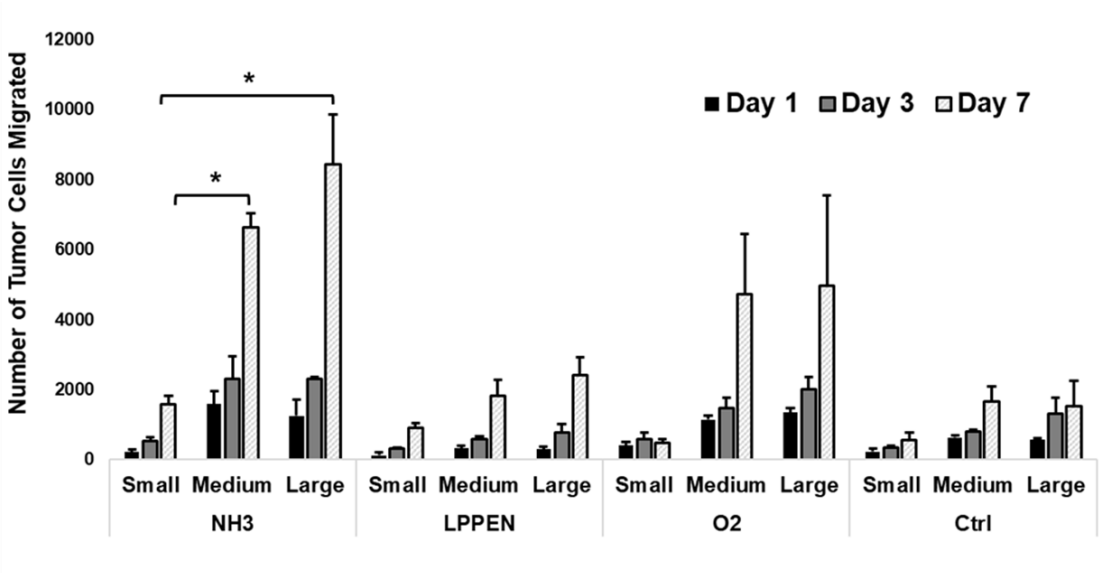

O_2-D7: Small Vs. Med & Large *	NH_3-D7 Med & Large Vs. Ctrl-D7 Med & Large **
L-PPE:N-D7: Small Vs. Large *	NH_3-D7 Med & Large Vs. L-PPE:N-D7 Med & Large **
NH_3-D3 Med & Large Vs. L-PPE:N-D3 Med & Large *	NH_3-D3 Med & Large Vs. Ctrl-D3 Med & Large *
O_2-D3 Med & Large Vs. L-PPE:N-D3 Med & Large *	NH_3-D1 Med & Large Vs. L-PPE:N-D1 & Ctrl-D1 Med & Large *

Figure 4.6 Numbers of tumor cells having migrated into the volume of different-sized and differently plasma-treated scaffolds (error bars: SE., n=3)

4.3.4.3 Effect of polymer type on tumor cell migration

As pointed out in section 4.2.1.1, electrospun mats of two other polymers besides PLA were also fabricated, namely polyurethane (PU) and poly(caprolactone) PCL, all of “medium” size (fiber diameters in the 800 – 900 nm range, and all having here undergone identical O_2 plasma treatments). Those three materials possess among themselves quite different mechanical stiffness characteristics in which tensile modulus (Young’s modulus as an index of stiffness) of electrospun mats based on PLA [153, 290-292], PCL [293-295], and PU [296-298] are approximately between 50-300 , 5-50, and 0.5-2 MPa, respectively, depends on their fiber sizes. In **Figure 4.7** are presented (A) micrographs that show the red- and green-fluorescent fibroblasts and tumor cells, respectively; and (B) the corresponding numbers of tumor cells found migrated / proliferated in the scaffold volumes after 1, 3 and 7 days. What most clearly emerges here is that after 7 days, no statistically significant differences ($F(2,1.7)=0.834$, $P=0.5593$; $W(2,1.5)=1.165$, $P=0.4950$) can be observed among the three cases, in spite of the appreciably differing fiber

stiffnesses. Comparing this outcome to that of preceding section 4.3.4.2, one may conclude that the main parameter which clearly dominated the tumor cells' mobilities / proliferations, hence their numbers within the scaffold interiors, was the scaffold morphology; by this is meant the combination of average pore and fiber sizes, free volumes and numbers of O-based surface-functional groups from plasma treatments presumably being very similar. In other words, mechanical stiffnesses of the electrospun polymers somewhat surprisingly appear to have played only a relatively minor role. This demonstrates that the present PP-3D-S tissue model can potentially be readily fabricated based on different (biodegradable) polymers having different mechanical and/or other physical properties, tuned to best match the targeted tissue types (bone, soft tissue, …).

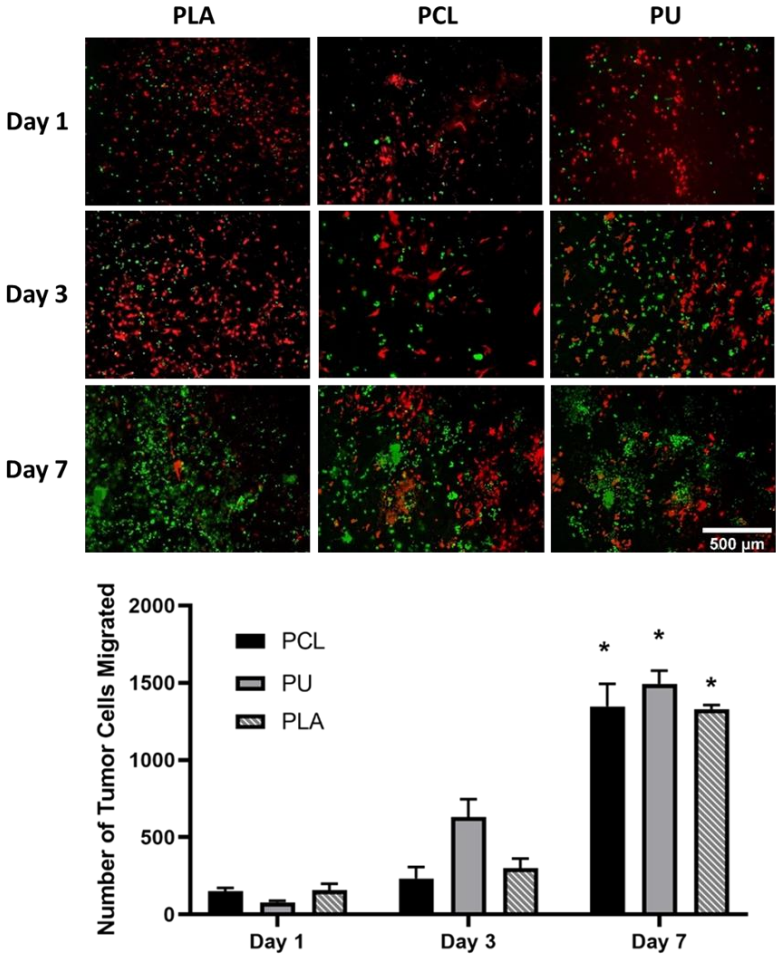

Figure 4.7 Effect of polymer type on tumor cell migration (A) optical micrographs showing (red) fibroblasts and (green) tumor cells; (B) Tumor-cell numbers after 7 days of migration and

proliferation in the volumes of “medium”-sized scaffolds of three different polymers, all O_2 plasma-treated (**The only pairs with P<0.05:** PCL: D1 Vs. D7; PU : D1 Vs. D7; PLA : D1 Vs. D7; error bars: SE., n=2)

4.3.5 Penetration depth of tumor cells

Top-view photomicrographs of red- and green-fluorescent cells shown in preceding sections give no indication how deep below the top surface of the ca. 250 µm-thick 3D scaffold those cells were located. However, that information can be derived from confocal microscopic observations portrayed in **Figure 4.8(A)**, where a 3-dimensional distribution is shown that also includes the z-direction (blue arrow), down to a maximum depth of ca. 120 µm below the original hydrogel-mat interface (z=0), for all plasma-treated and non-treated medium-sized scaffolds after 7 days. In **Figure 4.8(B)** the tumor cell migration into the depth of NH_3- and O_2 plasma-treated mats was significantly greater than that observed for L-PPE:N-coated and -untreated control samples after 7 days of culture (statistically proved by H(7)=22.451, P=0.002). Moreover, the depth of penetration rose substantially with increasing duration of culture for all cases, namely within the ranges of 50-70 µm, 80-90 µm and 90-120 µm (120 µm mostly for treated mats) from day 1 to day 7, respectively.

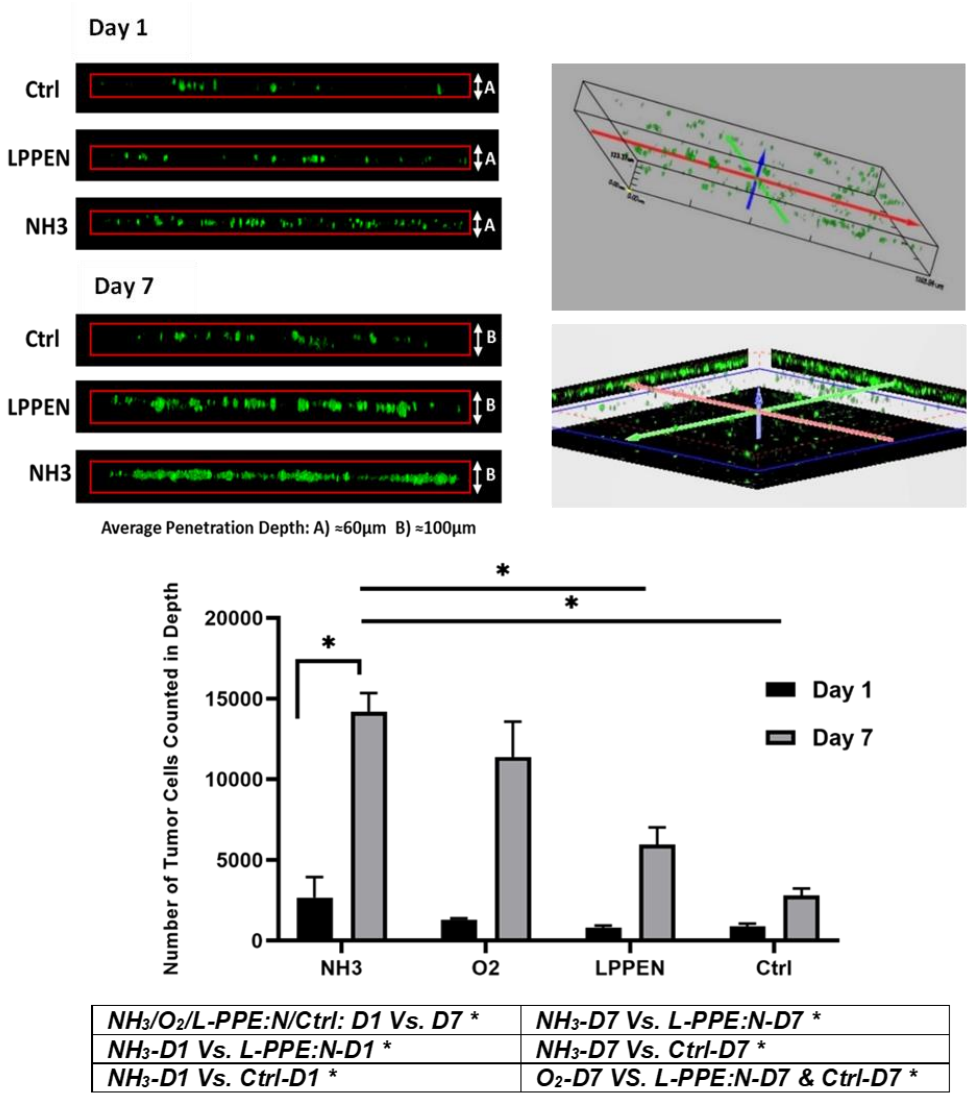

*NH_3/O_2/L-PPE:N/Ctrl: D1 Vs. D7 **	*NH_3-D7 Vs. L-PPE:N-D7 **
*NH_3-D1 Vs. L-PPE:N-D1 **	*NH_3-D7 Vs. Ctrl-D7 **
*NH_3-D1 Vs. Ctrl-D1 **	*O_2-D7 VS. L-PPE:N-D7 & Ctrl-D7 **

Figure 4.8 Tumor cell migration and growth in depth of the PP-3D-S model. (A): Representative 3D projections of stacked GFP breast cancer cells having migrated and proliferated through the depth of mats at day 1 and 7; (B) Number of GFP tumor cells quantified in depth of the 3D mat for different types of plasma treatments at day 1 and 7 (error bars: SE., n=3)

4.3.6 Drug screening experiments with PP-3D-S and Matrigel® models

Figure 4.9 shows images captured after 7 days, corresponding to increasing doses of Doxorubicin (Dox: 0, 0.05, 0.1, 0.5, 1 and 2 µM) with our PP-3D-S tumor interface model (see

section 4.3.4.1). Treatment with increasing amounts of Dox is seen to have blocked GFP-tumor cell migration to the target tissue, fibroblasts in the 3D mat. We have compared this with invasion and migration of the same tumor cell types, along with the same Dox treatment regime, but now across Matrigel®/Boyden chambers (images not shown). Quantitative data (histograms in **Figure 4.9**) show remarkably similar dose-dependent Dox-induced reductions of GFP-tumor cell migration in both models. Even though the two assays are clearly seen to have worked similarly, the PP-3D-S interface model is more advantageous because it can be set up far more rapidly (in roughly half the time), is adaptable to different tissue porosity and mechanics, and it avoids the characteristic batch-to-batch variation for which Matrigel® is known.

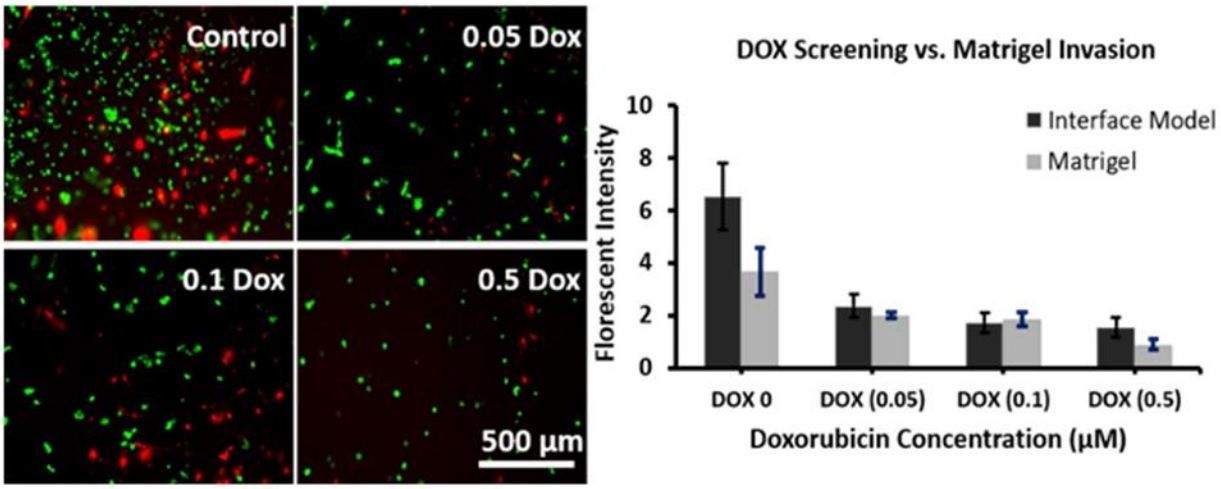

Figure 4.9 Drug screening experiments with PP-3D-S and Matrigel® models. Images: captured 7 days after treatment with increasing doses of Doxorubicin (Dox, µM) in our PP-3D-S tumor interface model. Graph: Comparison with invasion and migration of the same tumor cells across Matrigel®/Boyden chambers (images not shown), showing similar Dox-induced reduction of GFP-tumor cell migration in both models (error bars: SD., n=3)

4.4 General Discussion and Conclusions

In this article we have reported results obtained with novel plasma-treated electro-spun 3D scaffolds combined with hydrogel ("*PP-3D-S*") that can mimic various tissue types for general cell-biological research, including the human cancer microenvironment. This has significant potential value, including for customized cancer therapeutic screening; as a typical example of *PP-3D-S* use, designed to evaluate tumor cell migration, a breast-cancer tissue model has been simulated in this particular study. In more general terms, *PP-3D-S* has been found to enable mimicking "natural" cell interactions in a synthetic 3D environment that resembles the morphology of natural tissues in the human body, both in surface texture and chemistry as they affect the response by either benign or malignant living cells. It is also found to improve cell seeding and -adhesion capability of multi-cellular evaluation in 3D; controllable durability of the scaffold for predetermined duration, and improved controllable mechanical properties compared with commercially available 3D cell culture media such as Matrigel®. Mechanical characteristics can be made to vary over a wide range, to simulate softer or harder tissue types through choice of the electro-spun polymer scaffold, as demonstrated here by PLA, PCL and PU. PP-3D-S enables selecting the appropriate plasma treatment technique, either surface modification by grafting new functional groups (e.g. oxygen- or nitrogen-containing ones), or by coating the polymer fibre surfaces with thin plasma polymer films, both of which improve cell adhesion and -proliferation.

Regarding those plasma-induced surface treatments, the penetration of short-lived highly reactive species to large depths in the 3D scaffold, possibly exceeding 1000 µm, occurs thanks to their large mean-free-path lengths, especially in the case of the low-pressure plasmas used here. The beneficial result, of course, is uniform surface-chemical composition, hence uniform cell response throughout the scaffold volume. As clearly demonstrated, cell adhesion on plasma-modified mats greatly exceeds that on untreated controls. An unexpected and so far unexplained result has been the fact that L-PPE:N coatings only marginally improved performance with respect to the controls. Let us recall, first, that thin plasma polymer deposits *a priori* have an advantage over plasma modification (e.g. via O_2, NH_3, …), namely ability to avoid "hydrophobic recovery" (also known as aging), and second that L-PPE:N has performed very well in our past experience with a rather similar situation [27, 271, 277]; there is therefore a strong incentive to

understand and correct this problem. This is already in progress in our laboratories at this time, via new atmospheric-pressure plasma-based coating approaches and chemistries, and preliminary results appear very promising indeed.

The purpose of developing the PP-3D-S co-culture system was to reproduce or mimic the physiological metastatic tumor microenvironment. The generated migration/invasion model could then be used to incorporate patient derived tumor cells and matching stromal fibroblasts for screening personalized therapies. The driving force for this migration across the interface between the top (hydrogel) and bottom (electrospun) scaffold is directly related to the surface treatment (**Figure 4.5**) but may also be related to signalling among the two different cell types [299-301]. In fact, combining fibroblasts as stromal cells co-cultured with tumor cells in the 3D interface model leads to an appropriate biochemical environment and more accurately represents realistic tissue environment around the tumor cells; this is essential for drug therapy experiments described in the presented work. Ongoing studies in our group are seeking to address specific aspects relating to the *ab-initio* presence of fibroblasts and ensuing signaling pathways among the different cell types within the co-culture 3D model, including patient-derived cells.

In two different sets of cancer drug screening experiments, a) *PP-3D-S* and b) Matrigel®, numbers of migrated surviving tumor cells were compared after exposure to varying dosages of the well-known chemotherapeutic Doxorubicin; numerical outcomes, ca. 75% reduction with 0.5 µM drug concentration, were found to be very similar. These data indicate that *PP-3D-S* is an effective, economical and easy-to-use alternate 3D tumor migration model compared to standard Matrigel® assays. Furthermore, it supports the notion that the PP-3D-S system represents a physiological tumor microenvironment model. This has implications for studying different cancer types, both primary and metastatic, as well as being tailored to a high-throughput format. In such a system, both academic and industrial labs may find valuable use with this model. Future work will test the PP-3D-S system using cancer cells of other origins (i.e., prostate, lung and colorectal), or breast cancer cells, like here, but of differing degrees of aggressiveness, co-culturing patient-derived tumor cells and matching stomal cells, and a battery of alternate chemotherapeutics.

With the aim to provide a cell culture system of still lower cost, greater durability (shelf life) and reproducibility compared with existing commercial ones, we have carried out further research,

concentrating on medium-sized fiber PLA scaffolds, but attempting to optimize other fabrication variables, including the mentioned atmospheric-pressure plasma treatments. Future work will probe all of these aspects.

Acknowledgments: The authors gratefully acknowledge funding support from the Natural Sciences and Engineering Research Council (NSERC) of Canada (A.A. and M.R. W.), the Institute TransMedTech at Polytechnique Montreal (A.A., M.R.W. and D.H.R.), and Start-Up Funds from the Research Institute of McGill University Health Center and Fonds de Recherche du Quebec Sante (FRQS) Junior 2 Research Scholar Award (D.H.R.). The authors also gratefully acknowledge Professor Morag Park (McGill university) for kindly providing the fluorescent cell lines used in this study.

CHAPTER 5 ARTICLE 2: A NOVEL 3D *IN VITRO* TISSUE MODEL FOR BONE-METASTASIZED BREAST CANCER: A PRECLINICAL TOOL IN DRUG DISCOVERY AND TESTING

Mansoureh Mohseni Garakani[1,3], Megan E. Cooke[4,5], Michael R. Wertheimer[2,3], Derek H. Rosenzweig[4,5,*], Abdellah Ajji[1,3,*]

[1]Chemical Engineering Department, Polytechnique Montreal

[2]Department of Engineering Physics, Polytechnique Montreal

[3]Institute of Biomedical Engineering, Polytechnique Montreal

[4]Department of Surgery, Division of Orthopaedic Surgery, McGill University

[5]Injury, Repair and Recovery Program, Research Institute of McGill University Health Center, Montreal, Canada

[*]These authors contributed equally.

Correspondence:

Derek H Rosenzweig, PhD, Montreal General Hospital, Room C10.148.4, 1650 Cedar Ave, Montreal, QC H3G 1A4, Telephone number: +1(514) 934-1934 Ext. 43238; Email: derek.rosenzweig@mcgill.ca

Abdellah Ajji, PhD, CREPEC, Chemical Engineering Department, Polytechnique Montreal, QC, Canada, H3T 1J4, Phone: +1(514) 340-4711 Ext. 3703; Fax: +1(514) 340-4159; Email: abdellah.ajji@polymtl.ca

This article has been published in “Plasma Processes and Polymers, 2022, e2100206” [41].

Abstract

Bone metastasis is a frequent occurrence following breast cancer. The bone-tumor microenvironment is heterogeneous and complicated to recapitulate. Development of new chemotherapeutics is ineffective partly due to a lack of precise *in vitro* tissue models. We developed a 3D bone-tumor interface model for customized chemotherapeutic screening. It comprises a plasma-modified electrospun mat seeded with osteoblasts to mimic a bone tissue, with a cell-seeded hydrogel layer containing more- and less-aggressive or non-cancerous cells on top, mimicking the tumor compartment. By screening the model with Doxorubicin, we observed different migratory behaviors, with IC50 values that were largely in accordance with those cell lines' characteristics. Our 3D model reproduces the bone microenvironment and has great potential as a drug screening tool for personalized medicine.

Keywords: 3D Co-culture System, Nanofibrous Scaffolds, Plasma Surface Treatment, Interface Tissue Models, Drug Screening, Breast Cancer, Bone metastasis

5.1 Introduction

In vitro work in using cell cultures is a major first step often used in drug discovery, particularly in cancer research. However, it is known that cell culture on flat (2D) polystyrene culture dishes does not realistically portray the behaviour of living cells in their normal three-dimensional (3D) environment [9]. Due to the complexity of tumor microenvironments, it is challenging to mimic intercellular interaction *in vitro* [10, 11]; to do so requires realistic and/or physiologically-relevant tissue models. Additionally, the conventional two-dimensional (2D) cell cultures neither reproduce complexities of cell-extracellular matrix (ECM) interactions *in vivo*, nor those between cancer epithelial cells and the stromal compartment, which play a crucial role in tumorigenesis and progression. This has led to a shift toward more realistic 3D replacements for 2D commercial labware [10, 14]. Numerous 3D culture products have been developed in recent years, including hydrogels, ceramic or polymeric 3D-printed scaffolds, expanded polystyrene supports, permeable membranes, and electro-spun nanofiber scaffolds, to name but a few [19]. Commercially available basement membrane extract (BME), a gelatinous protein mixture secreted by certain murine sarcoma cells, resembles the complex ECM environment found in many tissues [273, 274]. The heterogeneous composition of these matrices allow for study of cell-migratory behavior, complex co-culture and organoid/tumoroid modeling of high importance to pharmaceutical small molecule screening [275]. However, these products are expensive, require multiple steps for implementation, exhibit batch-to-batch variability, have limited mechanical strength and uncontrolled degradation. Furthermore, they do not truly mimic the biophysical and biochemical networks found in native ECM *in vivo* [274, 276].

3D tumor models including spheroids [20, 22, 302] and organoids [24] have been extensively adopted for cancer research for over 2 decades. Yet many studies lack the cellular, biomolecular and biomechanical heterogeneity and complexity of the tumor microenvironment observed *in vivo*. Therefore, new pre-clinical drug screening platforms that better mimic the complex tumor physiological microenvironment are necessary to enhance regulatory approval and clinical translation. We recently developed a novel 3D tumor microenvironment model based on electrospinning that is customizable, reproducible and that closely resembles *in vivo* tissues and tumors; it is also more versatile and simpler to use than commercial BME materials such as Matrigel® or Cultrex®. Referred to as ***PP-3D-S*** (for **P**lasma-**P**olymer coated, electro-spun **3D**

Scaffold), this technology can mimic the microenvironment of human cancers, for example, to screen new anti-cancer therapeutics in a medium-throughput manner [40].

Bone is one of the most frequent sites of tumor metastasis, whereby primary tumors from breast and prostate (65-75%), thyroid (60%), lung (30-40%), and kidney (20-25%) spread to secondary sites [2, 4]. According to the American Cancer Society [52], it is estimated that among 750,000 Americans diagnosed with breast, lung, and prostate cancer in 2021, around 60% will then develop bone metastases, with the spine identified as the most common site. Understanding the effect of therapeutics on the bony environment, therefore, continues to be a particularly important area of research in the field of chemotherapeutic drug discovery. Drug development, a long, costly and complex process, with low success rates in clinical trials, remains one of the most challenging issues in oncology [140]. Many efforts have been devoted to the study of bone metastatic cancer by developing 3D *in vitro* models for chemotherapeutic discovery. Recent state-of-the-art tumor models of this type include 3D-bioprinted scaffolds based on natural polymeric hydrogels [303, 304], 3D microfluidic models [305, 306], 3D Bone-on-a-Chip [307], decellularized biological scaffolds [308], hydrogel microparticles/spheres [309, 310], 3D co-culture systems based on silk-fibroin [311, 312], and nanoclay scaffolds [313]. All these *in vitro* models of breast cancer metastasized to bone have served in attempts to assess efficacy of anti-cancer drugs. Despite promise in some cases, they are limited mostly by high cost and insufficient screening options; therefore, there is much scope to develop 3D models with greatly improved reproducibility, scalability, and cost.

In this present work, we extend our earlier findings with the so-called PP-3D-S technology, by electrospinning a nano-fibrous polylactic acid (PLA) scaffold that is then plasma-treated to greatly improve cell adhesion [40] at a bone-like stromal interface. The 3D scaffold (A) is then coupled with a thin overlayer of tumor cell-seeded alginate/gelatin hydrogel (A1G7) (B) representing the tumor interface. This generates a biocompatible 3D co-culture interface model between the two pseudo-tissues, (A) and (B), that respectively contain stromal (osteoblast) cells and breast tumor cells that here comprise several different types of aggressive or less-aggressive cell lines. We simulate the microenvironment of metastasis in bone-like tissue and test its ability to screen impact of therapeutic treatment against tumor migration/invasion. We hypothesize that plasma-bioactivated 3D scaffolds greatly improve cell adhesion and growth, and that they can

trigger and stimulate the migration and invasion of tumor cells; another important aspect of research presented here relates to improved PP-3D-S performance through several new, higher-performing plasma treatments.

5.2 Experimental Section

5.2.1 Fabrication of plasma-treated electro-spun nanofibrous scaffolds

5.2.1.1 Electrospinning of 3D scaffolds

Figure 5.1 schematically summarizes the main fabrication steps of our novel PP-3D-S scaffold, starting with electrospinning a nanofibrous (NF) mat [40]. We discuss here only poly (lactic acid), PLA (NatureWorks 4032D, density= 1.24 g/cc) randomly oriented NF scaffolds of three different fiber diameters, “Small”: 200-300 nm; “Medium”: 600-800 nm; and “Large”: 1-2 μm. Briefly, these were respectively electro-spun from 14, 16, and 19 wt.% polymer solutions containing PLA pellets dissolved in 2,2,2 trifluoroethanol, TFE, (M=100.04 g/mol, Merck). For example, a “Medium” scaffold (nominal mat thickness: 250 μm) required 10 ml of polymer solution, fed at a flow rate of 1.6 ml/hr using a syringe pump, all placed in a chamber with controlled temperature (21-24 °C) and relative humidity RH= 45%-50%. The distance between the grounded needle tip (21G) and the rotating mandrel (25 rpm) was 15 cm, with a stable DC high voltage (HV) of 20 kV between them. Nanofiber filaments were collected on the rotating metal drum onto which aluminum (Al) foil had been wrapped. The completed NF mats on Al foil were then placed in ambient air for ca. 3 days to evaporate residual solvent, then gently detached, cut into smaller pieces, and stored in a desiccator for subsequent use. More details and processing parameters can be found in reference [40], along with detailed methods for measuring mat thickness, mean NF diameters, pore sizes and porosities (see section 5.2.2 and **Table 5.1** further below).

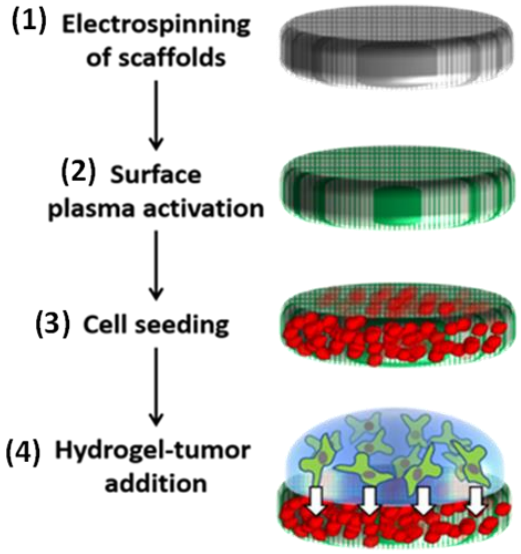

Figure 5.1 Schematic diagram of the four steps that comprise the current methodology: 1) Electrospinning of 3D PLA scaffold; 2) Plasma functionalization and/or plasma coating the scaffold surface; 3) Seeding with stromal cells; 4) Applying a layer of hydrogel pre-seeded with tumor cells on top of the 3D scaffold [40]

5.2.1.2 3D scaffold surface treatment by plasma: functionalization and coating

It has been known for many years that synthetic polymers are characterized by low surface energy and low wettability, leading to weak adhesion with other surfaces, including living cells. This can be remedied by modifying the polymer surface using exposure to low-temperature (non-equilibrium) plasma [240]. As already pointed out in reference [40] and elsewhere [27], cell adhesion to the hydrophobic surfaces of pristine electro-spun NF scaffolds is very limited. To correct this shortcoming, their surface compositions were modified by incorporating selected new functional groups using plasma treatment with different gases or gas mixtures. In [40] we had exclusively resorted to low-pressure (LP) radio-frequency (r.f., 13.56 MHz) glow discharge plasmas in O_2 and NH_3 to graft new O- and N-containing functional groups onto the PLA, but had also applied ultra-thin "L-PPE:N" coatings (**L**ow pressure- **P**lasma **P**olymerized **E**thylene, **N** doped), deemed to provide better long-term stability against so-called "hydrophobic recovery" [314]. As pointed out in [40], however, those coatings were found to perform quite poorly; this came much to our surprise, because they had earlier led to good outcomes in a quite similar context [27, 271, 277]. This latter fact motivated us to explore another LP plasma polymer, L-

PPE:O (**L**ow pressure- **P**lasma **P**olymerized **E**thylene, **O** doped) [315], but also ones prepared by an atmospheric-pressure (AP) dielectric barrier discharge (DBD) methodology we had recently perfected in this laboratory [316]. Low pressure plasma treatments or coating uniformity throughout (typically 250 µm-thick) 90% porous 3D scaffolds are assured by the fact that the vast open volume facilitates diffusive transport of active precursor species from the plasma thanks to their large mean free paths (mfp). For dielectric barrier discharges at atmospheric pressure (AP DBD), where the mean free path is orders of magnitude smaller, this is much less obvious; nevertheless, Kushner and coworkers [317] have shown by way of computational modeling that AP DBD plasma can propagate through interconnected open volumes in porous dielectric sheets, the propagation being controlled by a balance between retarding charging of the internal surfaces of the pores and photoionization that extends the plasma around corners. With those facts in mind, we have therefore used the same low pressure apparatus and methodologies described earlier [248] for O_2 and NH_3 plasma-induced surface modifications ("grafting" of functional groups), along with coating thin L-PPE:N and L-PPE:O deposits [315], on one hand. On the other hand, we have now also added AP DBD coating with ultra-thin layers of **P**lasma **P**olymerized-**E**thyl **L**actate, PP-EL, (from the oxygen-containing monomer, ethyl lactate, a volatile ester) [316] and **P**lasma **P**olymerized-**A**llyl **A**mine, PP-AAm, (from that nitrogen-containing volatile amine) [unpublished]. To avoid excessive duplication of published material, the reader is referred to earlier articles from this laboratory, where practically all necessary details can be found [316, 318]. Let us simply add here that PP-EL and PP-AAm, were both deposited with atmospheric pressure DBD plasma sustained by audio-frequency power at f = 20 kHz, high-voltage (8 kV, peak-to peak) in a large-area parallel-plate reactor with a 2 mm discharge gap, as first described in reference [39]. All such DBD polymerizations were carried out using mixtures of 10 standard liters per minute (slm) of pure argon (Ar) carrier gas (99.9 + % purity, Air Liquide Canada, Ltd., Montreal) into which were respectively mixed 5.5 sccm of the EL monomer vapor (at 60 deg C), or 8.5 sccm of AAm vapor at room temperature (both from Sigma–Aldrich, ≥ 98%). Prior gravimetric calibrations allowed us to accurately determine the "monomer" flow rates. Based on our previous low-pressure plasma polymerization work [252, 253], these processing parameters had been optimized to produce 100 nm layers on silicon wafers or glass microscope slides, for

characterization (see following sections). The 3D NF mats treated using the same sets of conditions were kept in sealed sterilized Petri-dishes for subsequent experiments.

5.2.2 Physico-chemical characterization of 3D NF scaffolds

A preceding article from these laboratories [40] already reported some detailed physico-chemical characterization results regarding 3D NF scaffolds. Below, we present certain selected extracts from those data, designed to familiarize the reader with the particular 3D PLA NF substrate materials exclusively used in this present context. Though, strictly speaking, these are "Results", it is deemed more logical for the sake of clarity to include them here in the Experimental section; only the small portion of aging-related measurements in Table 3 represent truly new "results".

5.2.2.1 Scanning Electron Microscopy (SEM)

To characterize their structure and morphology, NF mats were examined by Scanning Electron Microscopy (SEM) using a Hitachi model TM3030plus instrument at a working distance of 2 mm and voltage of 15 kV. Specimens were mounted on the sample holder using double-sided adhesive tape; the diameters of 200 randomly selected fibers of the large, medium and small groups (at least three different spots/sample in triplicate) were measured either *in situ* or captured SE-micrographs were then analyzed using ImageJ analysis software. **Figure 5.2** shows a typical SEM image of a medium-sized sample, along with a histogram of fiber diameters.

5.2.2.2 Porosity and pore size distribution

Overall porosity of samples representing the three different fiber size groups was quantified by a liquid (ethanol) intrusion method [233, 278], complemented by mercury intrusion porosimetry, as previously described [40]. In addition, average pore size distributions were determined using "DiameterJ" plugin in ImageJ software, based on averages of the long and short axes of each fitted ellipse (see **Figure 5.2** and **Table 5.1**).

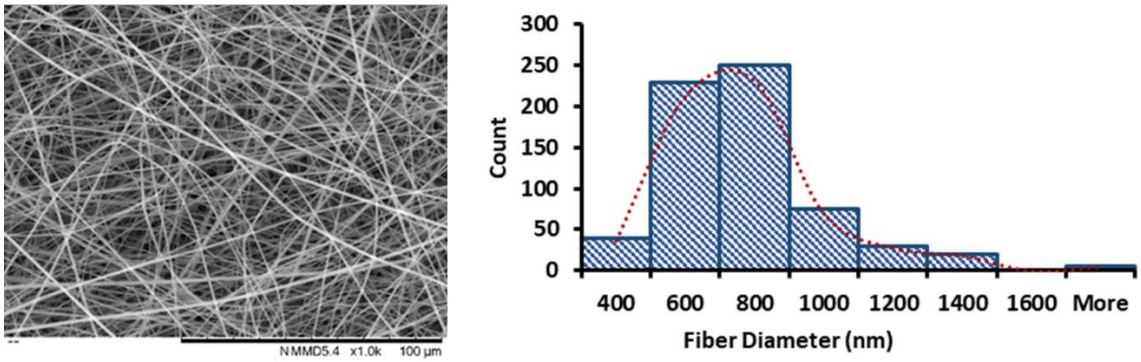

Figure 5.2 SEM micrograph and fiber diameter distribution curve of electrospun PLA NF mats of medium (600-800 nm) fiber diameter sizes; scale bar:100 µm (adapted from [40])

Table 5.1 Mean fiber diameter, pore size and overall porosity of PLA electrospun mats for small, medium and large nano-fiber sizes, n=3 (adapted from [40])

Scaffold	**Mean Fiber Diameter (nm/µm)**	**Average Pore Size (µm)**	**Porosity (%)**
Large	1.47 ± 0.2 µm	3.0 ± 0.32	90.3 ± 1.5
Medium	730 ± 75 nm	2.1 ± 0.2	91.0 ± 1.6
Small	273 ± 30 nm	1.0 ± 0.05	91.3 ± 0.9

5.2.2.3 Surface chemical analyses (XPS)

X-Ray photoelectron spectroscopy (XPS) analyses were performed on untreated and plasma-treated NF scaffold samples in a VG ESCALAB 3MkII instrument, using non-monochromatic Mg Kα radiation. The sampling depth, in the range of 1-5 nm, depends on fiber geometries in the ca. 1 mm^2 analyzed area. To acquire spectra, emission angle was set at 0°, normal to the mat surface, and charging was corrected by referencing to the C1s peak at binding energy BE = 285.0 eV. The operation condition of the X-ray source was at 15 kV, 20 mA; quantification of the constituent elements was performed using Avantage software (Thermo Electron Corporation) after Shirley-type background subtraction, following which the elemental concentrations were determined from XPS survey spectra. **Table 5.2** presents data for untreated PLA NF mats, along

with those of samples that had been modified by each of the plasma-treatments represented in this work.

Table 5.2 Surface chemical compositions of untreated and plasma-modified PLA mats; plasma treatments with O2 and NH3, or L-PPE:N, L-PPE:O, PP-EL and PP-AAm coatings (data from XPS survey spectra)

Element	**Pure PLA (%)**	**O_2 (%)**	**NH_3 (%)**	**L-PPE:N (%)**	**L-PPE:O (%)**	**PP-EL (%)**	**PP-AAm (%)**
F1s[2]	13.3	13.2	0	2.2	0	0	0
O1s	36.6	39.8	35.1	4	24.5	30.7	11.3
N1s	-	-	4.66	12.7	0.23	0.8	17.3
C1s	50.1	47	59.9	81.2	75.3	68.4	71.3
[O]/[C]	0.73	0.85	0.58	0.05	0.32	0.45	0.15
[N]/[C]	-	-	0.07	0.16	0.003	0.011	0.24

5.2.2.4 Static contact angle measurements

Static contact angles (SCA) of water droplets were measured at room temperature using a FDS tensiometer, OCA Data Physics, model TBU 90E. Untreated and plasma-treated NF mat samples were fixed on glass slides, following which 2 µL droplets of MilliQ water were placed on the surfaces with a micro-syringe (at least four different spots/sample, carried out in triplicate); average values along with standard deviations of SCAs were evaluated using SCA20-U software provided by the manufacturer.

In section 5.2.1.2 above we have already alluded to the potential problem of performance degradation with prolonged storage of plasma-treated NF mats, caused by well-documented, thermodynamically driven “hydrophobic recovery” associated with macromolecular “reptation” motion [242]. Hereby, polar functional groups, grafted to the polymer surface, become “buried”, resulting in a reduction in the material’s surface free energy. This is illustrated in **Table 5.3**, where such an aging effect is illustrated by gradual reduction in [O], the measured O content

[2] The source of fluorine is likely Teflon spray applied to the Aluminium foil used to collect nanofibers during the electrospinning process, or slight residue from TFE solvent.

within the topmost surface-near region, ca. 5 nm, probed by XPS analyses. In the case of plasma polymer coatings this is much reduced on account of their intrinsic cross-linked, disordered structure, on one hand, and by the fact that any "reptation" simply replaces burying polar moieties with identical ones that take their place. We return to this subtle topic of "aging" in the Results section further below.

Table 5.3 Aging effect in O2 plasma-treated NF mats over 7 days, from XPS survey scans

O_2 Plasma at	C1s (%)	O1s (%)	F1s (%)	[O]/[C]
Day 0	50.4	42.3	7.3	0.84
Day 1	52.4	41.8	5.8	0.79
Day 3	52.9	41.4	5.7	0.78
Day 7	53.2	37	9.8	0.69

5.2.3 Biological experiments

5.2.3.1 Cell seeding and culture in 3D NF scaffolds

IMR-90 mCherry fibroblasts or primary human osteoblasts isolated from the vertebral bodies of healthy organ donors (IRB# A04-M53-08B and A10-M113-13B approved by the institutional review board of McGill University), labelled with DiI (red) membrane labeling dye (Molecular Probes, Invitrogen, according to manufacturer's instructions), were used as the stromal component seeded onto the plasma-treated electrospun scaffolds (the mats were seeded with cells 24 hours after plasma treatment) (A). The following cell lines were labeled with DiO (green) membrane dye (Molecular Probes, Invitrogen) and used for the tumor component (B): aggressive epithelial breast cancer MDA-MB-231 (Green-fluorescent protein labelled, GFP), less-aggressive breast cancer MDA-MB 453 and MCF7, non-cancerous breast epithelial cells MCF 10A. Cells were cultured in high-glucose Dulbecco's modified Eagle medium (DMEM), supplemented with 10% fetal bovine serum (FBS) and 1% penicillin/streptomycin (PS) (all from Gibco, Thermofisher), at 37 °C in a humidified cell culture incubator with an atmosphere of 5% CO_2. Untreated and plasma-treated electrospun NF scaffolds were precisely cut into disks with a 9 mm-punch, sterilized with RPMI media containing 1% PS, and placed into the wells of untreated (non-adherent) 48-well culture plates. These were destined here for i) a tumor migration assay;

and ii) a high-throughput therapeutic screening test. For the stromal component (A, mCherry fibroblasts or DiI labelled osteoblasts) 20,000 cells in a volume of 100 μL were added to each well and incubated for 30 min at 37°C, following which the liquid was aspirated from each well and rinsed with fresh media to remove non-adherent cells. For the cancer cell lines, 500,000 cells/mL were mixed into an Alginate (1%)/Gelatin (7%) hydrogel (A1G7). 100 μL of cell-seeded A1G7 (50,000 cells/well), was applied on top of the NF scaffold, followed by addition of 200 μL of $CaCl_2$ (100 mM) for ionic crosslinking. After 10 min, the $CaCl_2$ was aspirated, and each scaffold washed twice with fresh media to remove residual crosslinking agent, and 500 μL of fresh media (RPMI with 10% FBS and 1% PS) was added per well. The plates were incubated for 1, 3, 5 and 7 days (depending upon the specific experimental design), the culture medium being changed every three days.

5.2.3.2 Observation and quantification of tumor migration

Tumor cell migration and invasion was evaluated as a function of incubation time. At different time points (1, 3, 5, and 7 days) the hydrogel was carefully removed from the NF scaffold and cells on the treated and untreated mats were fixed with 4% paraformaldehyde (PFA). The samples were then placed on microscope slides covered with a drop of mounting medium (Sigma, Fluoroshield with DAPI), along with a protective glass cover slip to avoid dehydration. The top surface and depth of mats (nominal thickness 250 μm) were imaged using florescent and/or confocal scanning microscopy (EVOS M5000 (4X) and Olympus IX81 (10X), respectively). The number of green (breast cancer) migrated cells on top or within the scaffolds were counted and quantified using ImageJ (National Institute of Health, US) (20 spots/sample of three replicated experiments).

5.2.3.3 Metabolic activity and proliferation assays

Metabolic activity and growth of cells were assessed using a commercial Alamar Blue® kit (Thermofisher). Briefly, at the required time-point, Alamar Blue dye was added to media at 1:10 dilution and incubated on the cells or scaffold at 37°C, 5% CO_2 for 4-6 h depending on the cell type. 100 μL from each well was transferred to a 96-well plate (Corning, black half-area) and fluorescence of Alamar Blue at Excitation/Emission wavelengths 540/585 nm were analyzed

using a Tecan Infinite M200 pro microplate reader (Tecan Trading, AG, Männedorf, Switzerland). The experiments were performed in triplicate for each cell type to test reproducibility.

5.2.3.4 Drug screening experiment

The effect of Doxorubicin (Dox), a well-known chemotherapy drug, was investigated in aggressive, less-aggressive tumor cell lines and non-cancerous cells seeded in the 3D cell culture model. 48-well plates containing medium-sized plasma-treated PLA NF mats (used 24 h after plasma treatment) pre-cultured with stromal and tumor cells incubated for 5 days, were exposed either to various concentrations of Doxorubicin (0.05, 0.1, 0.5 and 1 μM), or to sterile PBS as control (placebo) in RPMI media with low-serum conditions (1% FBS, 1% PS); this was prepared in triplicate, and media loaded with the drug was replaced after 3 days. After 5 days of treatment with Dox, the metabolic activity of cells was first analyzed by Alamar Blue, and IC50 values (50% inhibitory concentration) were calculated by constructing a dose-response curve and using non-linear regression (Equation: log(inhibitor) vs. normalized response) in GraphPad prism software. Finally, the numbers of migrated cells from the gel to the mats' surfaces were measured by microscopy.

5.2.4 Statistical analysis

All quantitative results reported here were obtained from at least three independent experiments to evaluate reproducibility, data being expressed as the mean values ± SE. Statistical analysis was carried out using two (or three)-way ANOVA with Tukey's post hoc analysis for parametric data; in the case of non-parametric data the Kruskal-Wallis test was employed, followed by Mann-Whitney post hoc analysis to compare two independent groups of interest. P values of less than 0.05 ($p < 0.05$) were considered significant for all tests.

5.3 Results and Discussion

5.3.1 Surface-related characteristics of 3D NF scaffolds

In section 5.2.2, entitled Physico-chemical Characterization of 3D NF Scaffolds, we already presented data relating to structural characteristics of the nano-fibrous mats, including their

morphologies, surface compositions and related properties, foremost their wettability (surface energy) and possible time-dependent ("aging") effects. For reasons outlined just before section 5.2.2.1., it was decided to include the figures and Tables presented there, rather than at this juncture of "Results", in order to better facilitate the reader's understanding. We pointed to surprisingly high static water contact angle (SCA) measurements observed for L-PPE:N [40], in spite of its quite respectable heteroatom (N) concentration (**Table 5.2**), and the fact that this plasma polymer had performed well in earlier studies of a comparable nature [27, 271, 277]. In the preceding report, however, L-PPE:N was found to perform far less satisfactorily that O_2 and NH_3 plasma-modified scaffolds [40]. These facts, coupled with aging of the O- and N-functionalized surfaces (see **Table 5.3**) led us to extend the present study to other plasma polymer coatings, deposited either at LP (L-PPE:O) or in AP DBD plasmas (PP-EL, PP-AAm). In other words, it will now be of great interest to examine measured data for possible (probable?) correlations between wettability (SCA values) and adhering cell populations / proliferation in the 3D NF matrices. To begin answering the foregoing question, we have performed SCA measurements for small, medium and large mat scaffolds after a 3-day period of (partial) aging, for plasma-modified or -coated samples with all six treatment types being studied in this present work, compared with untreated control samples (see **Figure 5.3**). As before, L-PPE:N is "hydrophobic", barely distinguishable from control samples. L-PPE:O shows somewhat improved wettability, but unexplained variation among the three fiber sizes. Also as before, O_2- and NH_3-plasma modified scaffolds display "super-hydrophilic" behaviour, in that the 2 μL water droplets almost instantaneously vanish beneath the sample surface. This is also found for the two AP-plasma deposited polymer coatings, PP-EL and PP-AAm.

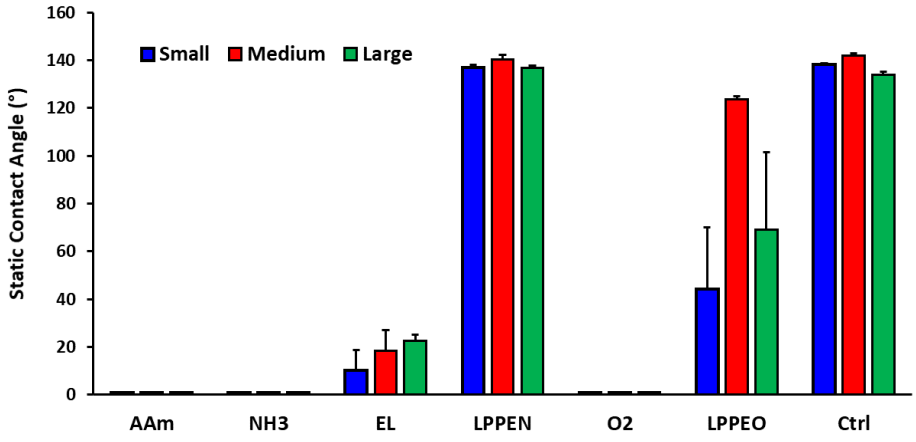

Figure 5.3 Static water contact angles of plasma-treated and untreated PLA mats with different fiber sizes, Small, Medium, and Large, measured 3 days after treatment (error bars: SE., n=3)

5.3.2 Biological test results

5.3.2.1 Effect of diverse plasma treatments on tumor cell migration and proliferation

Bone, especially the spine, is a frequent site of tumor metastasis, often originating from primary breast cancer [289]; this has led us to conduct experiments that aim to model bone metastasis secondary to breast cancer. Our previous work [40] showed pronounced migration of aggressive breast cancer cells into the 3D network of some low-pressure (LP) plasma-treated PLA mats and we have now employed different treatments to include atmospheric-pressure (AP) plasmas. We therefore reinvestigated the same MDA-MB-231 cell migration into the 3D NF mats of the three sizes (“Small”, “Medium”, and “Large”) treated with new types of coatings, PP:EL and PP:AAm (both AP), and L-PPE:O (LP), for comparison with data achieved by O_2, NH_3, and L-PPE:N treatments [40]. **Figure 5.4(A)** presents typical micrographs of invading /proliferating GFP breast cancer cells (green) after 7 days within the various PLA scaffolds in which RFP IMR-90 mCherry fibroblasts (red) pre-adhered. We demonstrated, using confocal microscopy, that cells had penetrated to depths exceeding half the 250 µm nominal scaffold thickness, i.e., > 100 µm. One clearly notes greatly increasing numbers of tumor cells for all plasma treatments, except in the case of L-PPE:N coating; this is also borne out quantitatively in **Figure 5.4(B)**, which in

addition presents data corresponding to days 1 and 3. Inspecting **Figure 5.4(B)** reveals several dominant features, namely the following:

(i) The best-performing plasma treatments are clearly PP-EL, PP-AAm and L-PPE:O coatings, especially the former two, along with surface modification by NH_3 plasma; L-PPE:N and O_2 plasma yield much lower performances, the former barely above untreated control samples;

(ii) Both O- and N-based functionalities are effective in promoting the desired effects;

(iii) Practically all of the tumor cell migration / proliferation occurs between days 3 and 7;

(iv) While data for medium- and large- diameter NF scaffolds are always quite comparable (large perhaps being slightly superior in general), cell numbers for small-diameter scaffolds are always much lower.

We shall return to these observations in the Discussion section further below; nevertheless, it is appropriate to comment that the "best" of these treatments appear to be well-suited for envisaged biological applications. A probable reason for (iv) is that the smaller average pore size (**Table 5.1**) obstructs cell entry and -mobility, despite 90% porosity for all three NF diameters, as already suggested earlier [40]. This important point will be elaborated in far more detail in the Discussion.

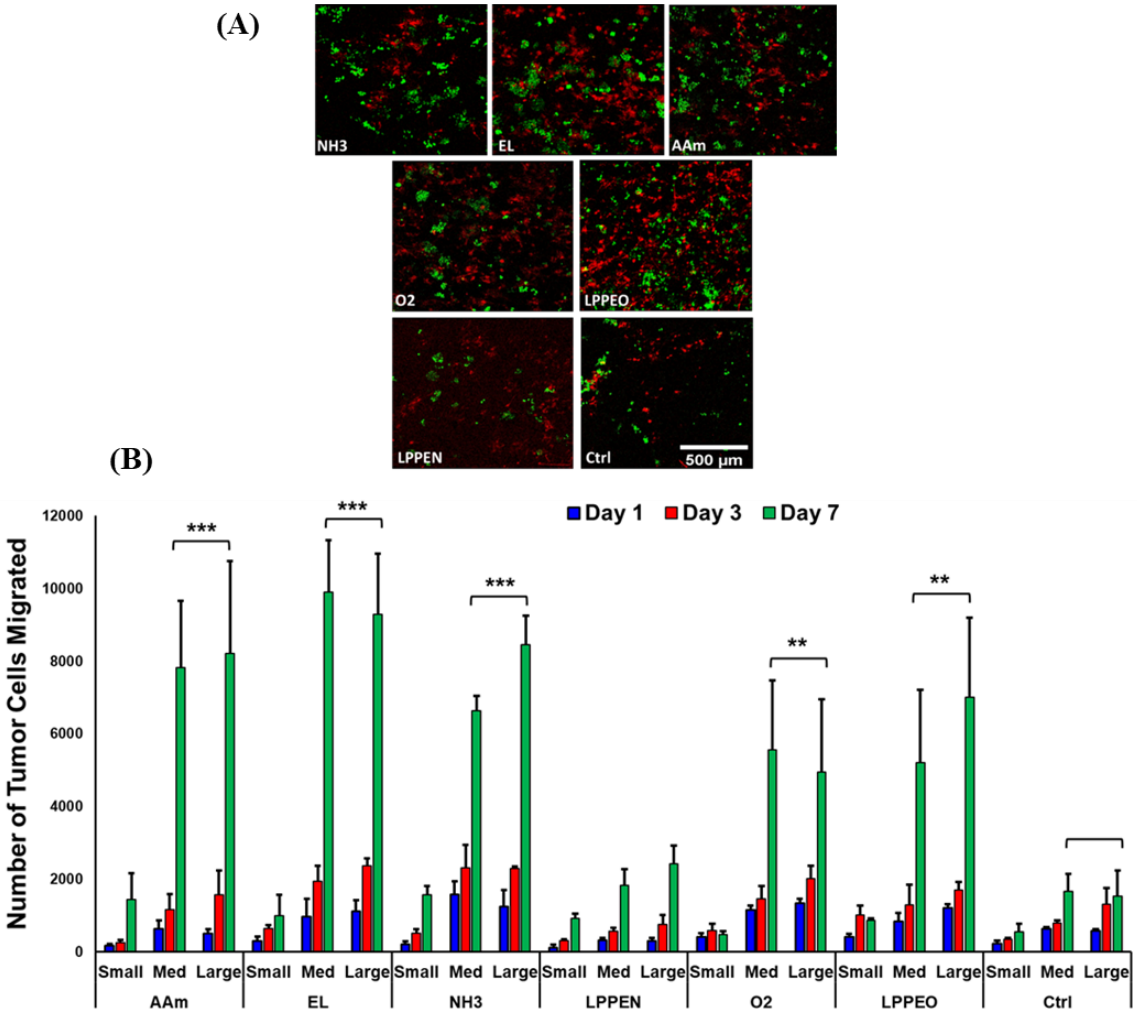

AAm-D7: Small Vs. Med & Large ***	NH_3, AAm, EL-D7 Med & Large Vs. Ctrl-D7 Med & Large ***
EL-D7: Small Vs. Med & Large ***	O_2, L-PPE:O-D7 Med & Large Vs. Ctrl-D7 Med & Large **
NH_3-D7: Small Vs. Med & Large **	NH_3, AAm, EL, O_2, L-PPE:O-D7 Med & Large Vs. L-PPE:N-D7 Med & Large **
O_2-D7: Small Vs. Med & Large **	NH_3, EL, AAm, O_2, L-PPE:O-D3 Med & Large Vs. L-PPE:N, Ctrl-D3 Med & Large *
L-PPE:N-D7: Small Vs. Med & Large *	NH_3, EL, O_2-D1 Med & Large Vs. L-PPE:N, Ctrl-D1 Med & Large *
L-PPE:O-D7: Small Vs. Med & Large **	Ctrl-D7: Small Vs. Med & Large *

Figure 5.4 Numbers of tumor cells having migrated/proliferated in the volume of different-sized and differently plasma-treated scaffolds (A): Typical confocal microscopic images of RFP cancer-associated fibroblasts (red) adhering to the various PLA scaffolds, along with accumulated numbers of GFP breast cancer cells (green), after 7 days. (B): Histograms representing tumor cell numbers for the different types of scaffolds over periods of up to 7 days (error bars: SE., n=3; significant differences for plasma-treated samples at day 7 compared to the

controls are presented by *, where *=P<0.05, **=P<0.01, ***=P<0.001; all pairs with significant differences are also listed in the table below the graph)

5.3.2.2 Migration behaviour of variably aggressive breast cancer cells

Our focus in this work is to model metastasis to bone tissue by primary breast cancer cells. In our previous work the PP-3D-S model was applied under very specific circumstances, combining MDA-MB 231 breast cancer cells with a fibroblast stromal compartment. We have now modelled the scenario using tumor cells of varying aggressiveness, and by replacing fibroblasts pre-adhered in the (medium-sized, NH_3 plasma-treated) PLA scaffolds with human primary osteoblasts.

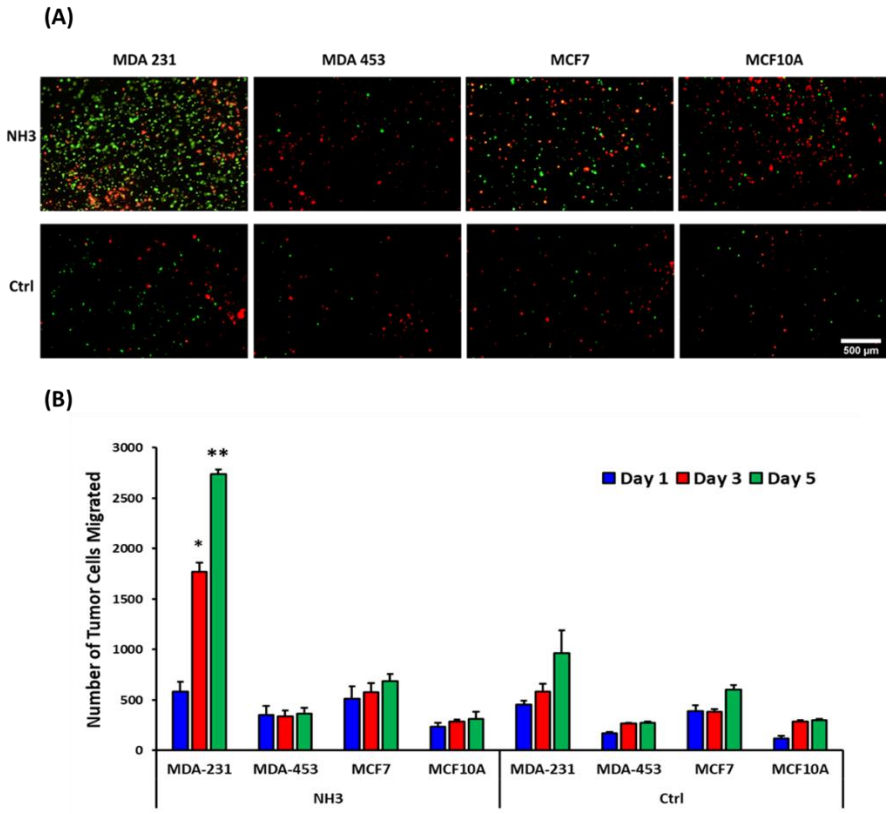

Figure 5.5 Numbers of variably-aggressive breast tumor cells and benign breast epithelial cells having migrated into osteoblast-seeded NH_3 plasma-treated medium-sized PLA scaffolds (A): Representative images of DiI-labelled red osteoblasts adhering to NH_3 plasma-modified mats, along with GFP or DiO-labelled breast cancerous and non-cancerous cells having migrated after 5 days. (B): Histograms representing more-or-less aggressive and non-aggressive tumor cell

numbers migrated to the mat after indicated culture durations
(error bars: SE., n=3, *=P<0.05, **=P<0.01)

Figure 5.5 shows that after 5 days of culture there is increased migration and proliferation of MDA-MB 231, a triple-negative aggressive cancer cell type (negative to human epithelial receptor 2 (HER2), progesterone receptor (PR), and estrogen receptor (ER)). In comparison, the less aggressive MDA-MB 453 (positive to HER2), MCF7 (positive to ER and PR markers) [319, 320], and non-cancerous (benign) MCF10A cells show reduced migration to the osteoblast-seeded scaffolds, compared to control values. Those latter cell lines being characterized as "less-aggressive" and/or "benign", their observed much reduced migratory behaviours are not unexpected. In other words, the hybrid (3D scaffold + overlaid hydrogel) model is found to retain the non- or less-aggressive cells within the gel layer, with only very limited migration from the "primary tumor" (hydrogel containing tumor cells) to the second ("bone") tissue, osteoblasts embedded in 3D NF scaffolds. On the other hand, the aggressive MDA-MB 231 tumor cell type readily invades the target "bone" tissue, manifesting substantially greater migratory behaviour within the same 5-day incubation time. Furthermore, to repeat, numerical values obtained with the untreated control mats are considerably lower than their (NH_3 plasma-treated) counterparts for the case of MDA-MB 231, but not significantly different for MDA-MB 453, MCF7, and MCF10A, as expected. In **Figure 5.5** we note that all but the MDA-MB 231 cell line display slight increases in numbers between days 1, 3 and 5; this raises the question whether these increases are attributable to migration, or to proliferation in the 3D NF structure, or to a combination of the two. We therefore performed a series of proliferation assays to investigate those cells' metabolic activities in different culture environments: (i) cells individually pre-seeded in 2D wells (in a 48-well plate); (ii) in 3D hydrogel (A1G7); and (iii) in 3D NF mats (NH_3-treated medium-sized PLA). The Alamar Blue assay was performed at different time points (1, 3, 5 and 7 days). **Figure 5.6** suggests that all four cell lines show comparable growth in 2D monolayer culture; however, MDA-MB 453 are seen to grow very slowly in hydrogel and in the 3D mats compared with the others. This means that they have lower tendency for both proliferation and migration, confirming corresponding data in **Figure 5.5**. Although MCF10A cells display significant proliferation both in gel and mats, quite similar to MDA-MB 231, they do not migrate much after 5 days (see **Figure 5.5**), unlike MDA-MB 231; this exactly expresses

the migratory behavior characteristics anticipated for non-cancerous MCF10A and aggressive MDA-MB 231. Also, while less aggressive MCF7 cells display reasonable growth in 3D mats, they do not migrate much compared with MDA-MB 231, see **Figure 5.5**. We can therefore conclude that MDA-MB 231 aggressive breast cancer cells both strongly migrate and proliferate, while the other three cell types tend more to proliferate than to migrate; this is fully in accordance with the migration assay outcome, **Figure 5.5**.

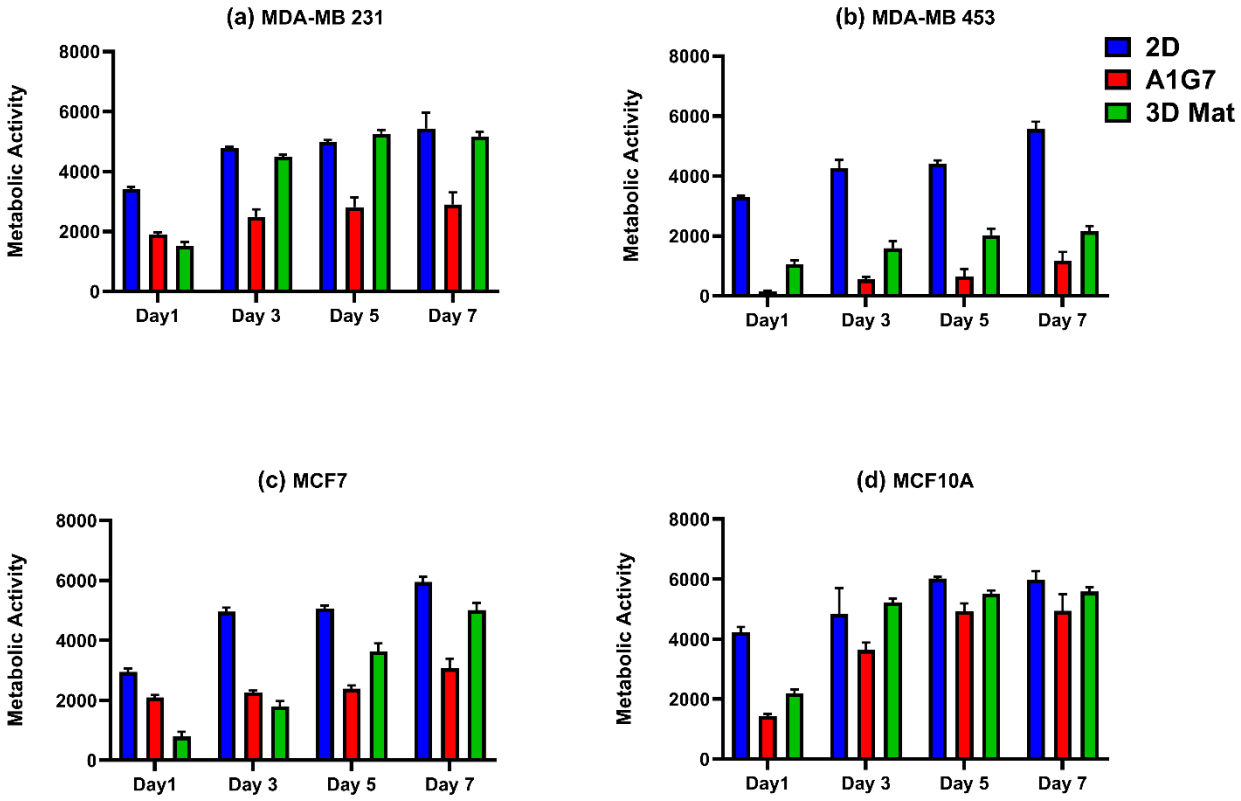

Figure 5.6 Metabolic activity/ proliferation evaluation of the different cancerous and benign breast cells growing in 2D, 3D hydrogel (A1G7), and 3D nano-fibrous mats (NH_3 plasma-treated, medium-sized PLA): over 1, 3, 5 and 7 days in which a) MDA-MB 231; b) MDA-MB 453; c) MCF7; d) MCF10A

5.3.2.3 Doxorubicin (Dox) screening on breast tumor cells and benign epithelial cells

As expected from immortalized cell lines, all breast cells showed reduced metabolic activity with increasing Dox concentration. Further, statistical analyses show that increasing Dox concentration has a significant effect on metabolic activity of all cell lines, particularly in MDA-MB 231 and MDA-MB 453 cells, with IC50 values (the concentration of Dox where metabolic activity is reduced by 50%) of 0.36 and 0.10 µM, respectively (**Figure 5.7)**. Compared with MDA-MB 231, the less aggressive MDA-MB 453 cells show higher drug sensitivity, or lower IC50 values, meaning that they are more sensitive to Dox, while more aggressive MDA-MB 231 cells are more resistant to Dox. Although both MCF7 and MDA-MB 453 are identified in the category of less-aggressive breast cancer cells, the former is much more resistant to the drug (IC50 = 0.48 µM) compared with MDA-MB 453 (IC50 = 0.10 µM). This may be attributed to them being HER2 negative [321], while MDA-MB 453 cells are HER2 positive. Finally, non-cancerous MCF10A breast epithelial cells were found to be the most Dox-resistant of the cell lines investigated, with an IC50 value of 0.67 µM.

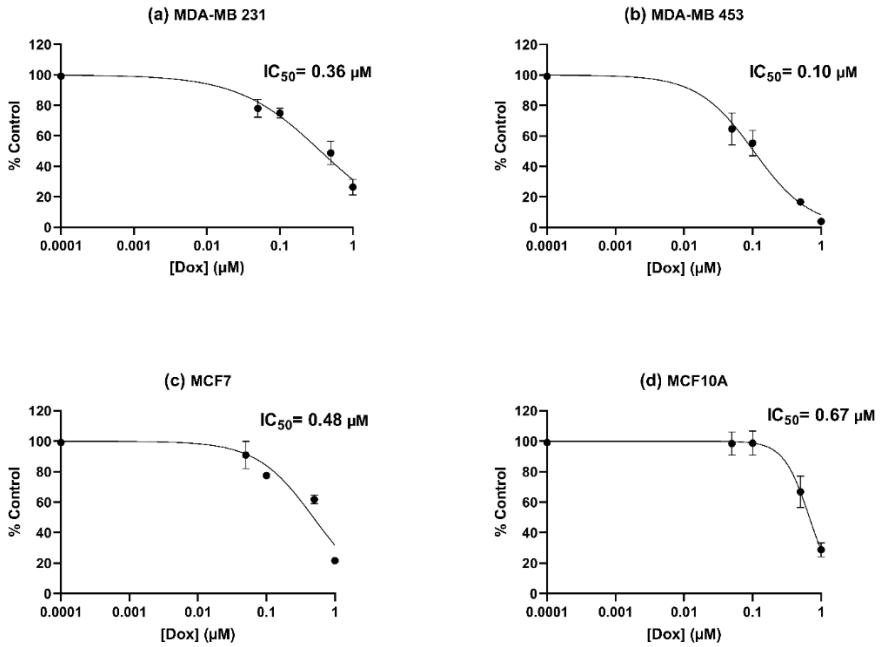

Figure 5.7 Metabolic activities of different cancer- and non-cancerous breast cells, in terms of increasing doses of Doxorubicin (Dox) after 5 days of culture in which a) MDA-MB 231; b) MDA-MB 453; c) MCF7; d) MCF10A (error bars: SE., n=3)

When considering the MDA-MB 231 cell line, the inhibition of migration occurs at much lower Dox concentrations compared to the inhibition of metabolic activity (**Figure 5.8**). The number of migrated cells is significantly decreased at 0.05 µM Dox (P<0.001), while 20 times the concentration of Dox is required to reach this level of significance for a reduction in metabolic activity. Doxorubicin has a greater effect on migration of MDA-MB 231 into the scaffolds compared to proliferation.

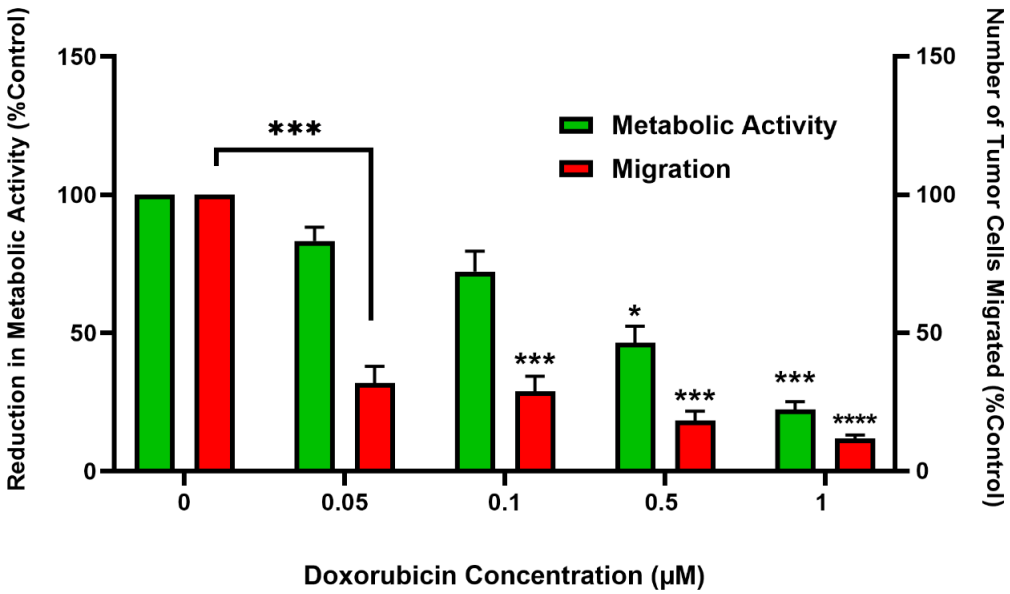

Figure 5.8 Effect of Doxorubicin on migration and metabolic activities of MDA-MB 231 cells after 5 days of culture (error bars: SE., n=3, *=P<0.05, **=P<0.01, ***=P<0.001, ****=P<0.0001)

5.4 General Discussion and Conclusion

In our previous work we presented a novel *in vitro* co-culture synthetic tissue model that we have termed "PP-3D-S", schematically shown in **Figure 5.1** [40]. It comprises two components, (A) a "stromal" tissue compartment made of an electrospun nano-fibrous (NF) 3D (3 Dimensional) mat; and (B) a thin layer of hydrogel impregnated with a cancer cell type under study, representing a cancerous "tumor" part; both provide cell-adhesive moieties and mechanical support/structure for 3D cell growth. The purpose here is to simulate the micro-environment of tumor cell behaviour, for example migration across the boundary between (A) and (B), and to

provide a flexible new tool for drug screening. For (A) to be able to host sufficient numbers of stromal cells, the NF structure's surface must first be rendered wettable and highly cell-adhesive by suitable surface modification, low- or atmospheric-pressure (LP or AP) plasma being the most convenient and logical means [36]. In earlier work [271], our group had examined a two-layer L-PPE:N coated mat sample, on top [a], 0 μm; in the middle, [b], 50 μm; and at the bottom, [c], 100 μm by XPS analyses. Although [N] decreased with increasing depth to roughly 70% and 50% of [a] in cases [b] and [c], respectively, this confirmed that active plasma species penetrated many tens of μm through the micro-porous structure. Domingos et al. [322] reported very uniform deposition of "L-PPE:N" through 8 mm deep 3D scaffolds of much coarser extruded cylindrical PCL fibres spaced 650 μm apart in a regular 0/90° pattern, creating interconnected pores of regular dimensions. It was found that this subsequently permitted uniform bulk colonization by osteoblast cells. In our first article, which successfully served to demonstrate feasibility of the PP-3D-S technology, stromal cells in (A) were selected to be fibroblasts, while an aggressive human breast cancer cell line, MDA-MB 231, was used in (B). Three different LP plasma treatments were tested, two (in O_2 or NH_3) leading to surface modification (grafting of new O- or N-based polar functional groups), the third being coating with ca. 100 nm ultra-thin L-PPE:N films. In this new article, the same approach has been extended and diversified by using (i) human spine-isolated osteoblasts in the stromal component; and (ii) each of four different human breast cells in the gel, three cancerous (including the same aggressive MDA-MB-231, the other two less aggressive MDA-MB 453 and MCF7) and one normal breast epithelial cell line, MCF 10A. The inventory of plasma pre-treatments of (A) has also been significantly extended, namely by adding to the above another LP plasma polymer coating, L-PPE:O, and two AP DBD coatings, PP-EL and PP-AAm. The specific aim has been to simulate metastasis to bone of the spinal column from primary breast cancer, unfortunately a rather common occurrence.

The reasons for adding plasma polymer coatings beside the (simpler) "grafting" is that the latter inevitably results in "hydrophobic recovery", also known as aging, whereby macromolecular rotational motion ("reptation") slowly buries the grafted polar groups below the surface [242]. They are then no longer "felt" by living cells; actually, cell interaction with a functionalized surface occurs more indirectly, via their adhesion to a thin layer of proteins that rapidly become chemically bonded on the functional groups after contact with a bio-fluid [323].

Table 5.3 revealed that the O/C surface ratio of O_2 plasma-treated PLA NF mats decreased about 17% over the first 7 days; data from this laboratory (unpublished) suggest that an asymptotic limit is approached within another week or so, a value at which the surface still remains quite wettable, with a low water contact angle. However, as shown by Siow et al. [36], ageing characteristics depend greatly upon types of materials and plasma conditions. It is also important to add that aging is a vital consideration for commercial products that may require storage over many months, even if suitably packaged; since cross-linked plasma polymers *a-priori* possess superior aging resistance, this is why so much effort has been devoted to their study here.

Figures 5.3 and **5.4** reveal that both O- and N-containing functional groups can result in high numbers of cells migrated (**Figure 5.4**), and that those values tend to correlate with wettability (**Figure 5.3**) quite strongly, low water contact angles leading to high cell counts. Considering that both chemical and electrostatic effects can help explain cell adhesion [254], this is obviously advantageous; O-type surfaces (particularly -COOH groups) are negatively charged, while N-type surfaces (with primary amine groups, C-NH_2) bear positive charge. However, it is known that the latter functionality slowly oxidizes to form amides when exposed to atmospheric O_2 [253], while O-functionalized surfaces tend to be more stable in air, already being at their highest level of oxidation. All this said, considering that PP-AAm and NH_3 treatments (amine-containing) and O-group yielding PP-EL, L-PPE:O and O_2 treatments all gave "good" results (**Figure 5.4**), the better longer-term stability of the latter (oxidized) surfaces should probably be preferred in potential commercial contexts.

In all preceding text we have so far left aside an explanation how those large cells, fibroblasts, osteoblasts, benign or malignant breast epithelial cells, with volumes of typically a few thousand μm^3 (ca. 10 µm radius), can accommodate into the much smaller electrospun scaffolds' cavities (see **Table 5.1**). Indeed, in defining material characteristics leading to superior biocompatibility, Ratner [324] proposed that interconnected micropores typically 30 µm in diameter might yield optimum outcomes, for example in terms of angiogenesis. Regarding the present pore size and cell penetration, the following may be said: spheroidal cells of ca. 10 µm radius can deform into spindle-like shape with much smaller minor-axis diameter, capable of penetrating through 3-or-less µm pores near the surface. While Domingos' [322] and Ratner's [324] scaffolds are rigid, the sub-µm-sized polymer fibrils of the present electrospun 3D mats are

flexible and can readily be deformed under the action of penetrating cells, thereby at least temporarily creating larger cavities through which inward cell displacement is possible. This, we believe, is the basis for explaining the apparently easy movement and final in-depth localization of cells that we unambiguously observed in [40], and in the microscopic images presented here.

Figure 5.5 shows that after 5 days of culture there was remarkably increased migration and invasive proliferation of the aggressive MDA-MB 231 cancer cell type, in comparison with less aggressive MDA-MB 453, MCF7, and non-cancerous MCF10A cells; those all displayed lower numbers, comparable to control values. In other words, the non- or less-aggressive cells were found to largely remain within the "primary tumor" gel layer, behaving like a benign tissue, with only very limited migration and invasion to the "bone" tissue, osteoblasts embedded in 3D NF scaffolds. The fact that the aggressive MDA-MB 231 tumor cells manifested substantially greater migratory/invasive behaviour within the same 5-day incubation time is fully in keeping with expected behaviour of this cell line. The question whether observed increases between days 1, 3 and 5 were attributable to migration or proliferation in the 3D NF structure, or a combination of the two, was examined by way of the cell proliferation assay results presented in **Figure 5.6**. It indicates that non- or less-aggressive cells tend to do more proliferation than migration, whereas aggressive MDA-MB 231 cells were found to undergo both migration and proliferation over the culture time, all in accordance with their characteristics. Further, non-cancerous cells are seen to be more resistant to Dox, indicating that they may enter a state of senescence and maintain some metabolic activities [325]. Overall, the experimental findings show that this innovative two-matrix PP-3D-S tissue model can be used as a simulation of cell migration in the metastatic microenvironment.

As in the preceding article [40], we have taken this experimental test program an important step further, by exposing the cancerous microenvironments to varying Doxorubicin (Dox) concentrations (**Figures 5.7** and **5.8**). In the earlier work we had carried out treatments of the aggressive MDA-MB 231 cell line with 0, 0.05, 0.1, 0.5 and 1 μM of Dox in the PP-3D-S model environment, but also compared results with those across Matrigel®/Boyden chambers. We quantitatively proved that both models have remarkably similar dose-dependent Dox-induced reductions of tumor cell migration. However, our interface model is more advantageous by offering the simplicity of manufacturing procedures and materials, so having low production

costs, fast and user-friendly compared with commercial Matrigel®. This has significant potential value for anti-cancer compound screening. Specifically, the platform's fully defined components (A) and (B) and controlled architecture help improve reproducibility, whereas its tunability for stiffness (with different NF materials [40]) or cell type being used makes it adaptable for different tissue types and assay set-ups. Lastly, the multi-well plate format on which the technology was built and the hydrogel's compatibility with liquid-handling equipment make of this novel platform a scalable *in-vitro* model that is ideally suited for compound testing workflows, compared with commercially available 3D cell culture matrices such as Matrigel®.

Acknowledgement

The authors thank Dr. Matt Kinsella and Dr. Morag Park for donations of cell lines used in this study. They also acknowledge the support of McGill ortho fellows and surgeons for assistance in obtaining primary human osteoblasts. The authors also gratefully acknowledge funding support from the Natural Sciences and Engineering Research Council (NSERC) of Canada, the Canadian Institutes of Health Research (CIHR, MEC Funding Ref. 171258), the Research Institute of McGill University Health Center (MUHC) and *Fonds de Recherche du Québec Santé* (FRQS) Junior 2 Research Scholar Award (to DHR).

CHAPTER 6 ARTICLE 3: A 3D, COMPARTMENTAL TUMOR-STROMAL MICROENVIRONMENT MODEL OF PATIENT-DERIVED BONE METASTASIS

Mansoureh Mohseni Garakani[1,3], Megan E. Cooke[4,5], Michael Weber[4,5], Michael R. Wertheimer[2,3], Abdellah Ajji[1,3,*], Derek H. Rosenzweig[4,5,*]

[1]Chemical Engineering Department, Polytechnique Montreal

[2]Department of Engineering Physics, Polytechnique Montreal

[3]Institute of Biomedical Engineering, Polytechnique Montreal

[4]Department of Surgery, Division of Orthopaedic Surgery, McGill University

[5]Injury, Repair and Recovery Program, Research Institute of McGill University Health Center, Montreal, Canada

[*]These authors contributed equally.

Correspondence:

Abdellah Ajji, PhD, CREPEC, Chemical Engineering Department, Polytechnique Montreal, QC, Canada, H3T 1J4, Phone: +1(514) 340-4711 Ext. 3703; Fax: +1(514) 340-4159; Email: abdellah.ajji@polymtl.ca

Derek H Rosenzweig, PhD, Montreal General Hospital, Room C10.148.4, 1650 Cedar Ave, Montreal, QC H3G 1A4, Telephone number: +1(514) 934-1934 Ext. 43238; Email: derek.rosenzweig@mcgill.ca

This article has been submitted to “Biomedical Engineering Advances”.

Abstract

Bone is a frequent site of metastasis secondary to breast cancer. The bone tumor microenvironment is heterogeneous and complex in nature. Such complexity is compounded by relations between the metastatic cells and bone cells influencing their sensitivity/resistance to chemotherapeutics. Standard chemotherapeutics may not show efficacy for every patient, and new therapeutics are slow to emerge owing to the limitations of existing in vitro/in vivo models. We previously developed a 3D interface model for personalized therapeutic screening. The model consists of an electrospun poly lactic acid, PLA, mesh activated with electric discharge plasma species and seeded with stromal cells. Tumor cells embedded in an alginate-gelatin hydrogel are overlaid to create a physiologic 3D interface. Here, we applied our 3D model as a migration assay tool to evaluate and verify the migratory behaviour of different patient-derived bone metastasized cells. We assessed the impact of two different chemotherapeutics, Doxorubicin and Cisplatin, on migration of patient cells as well as their immortalised cell line counterparts. We observed different migratory behaviours and cellular metabolic activities which could be blocked with both Doxorubicin and Cisplatin treatment; however, higher efficiency or lower IC50 was observed with Doxorubicin. Gene expression analysis of immortalized cell lines that migrated through our 3D hybrid model verified epithelial-mesenchymal transition through increased expression of mesenchymal markers and a reduction in epithelial markers involved in the metastasis process. Our findings indicate that we can model tumor migration *in vivo*, in line with different cell characteristics. Finally, our data indicates that the model may be a suitable drug screening tool for personalized medicine approaches in metastatic cancer treatment.

Keywords: 3D Co-culture System, Nanofibrous Scaffolds, Interface Tissue Models, Drug Screening, Bone metastasis, Personalized Medicine

6.1 Introduction

Bone is a frequent site of tumor metastasis when primary tumors spread from their original site to the bone. Bone metastasis is common following primary breast (65-75%), prostate (65-75%), thyroid (60%), lung (30-40%), bladder (40%), and kidney (20-25%) cancer [2, 326]; and among all the bones, spine is the most common site [327-331]. It was estimated by the American Cancer Society that among 750,000 Americans diagnosed with breast, lung, and prostate cancer in 2021, around 60% of them will then develop bone metastases, commonly occurring in the spine [52]. Bone metastases can be osteoblastic, osteolytic or a mixture of both, characterized by deposition of the new dense bone and destruction of the bone, respectively. Both are caused through factors secreted by cancer cells, affecting the normal homoeostasis of bone formation and resorption resulting in changes to the structure and function of the bone. Excessive bone formation or resorption leads to vertebral instability, fractures, high blood calcium levels, and spinal cord compression [51]. Current treatments are surgery, along with radiation therapy and systemic chemotherapy, which is associated with severe side effects. Overwhelmingly, with rare exceptions, bone or spine metastasis cannot be cured and long-term survival of patients with metastatic cancer is low [332]. Thus, more studies are necessary to have better understanding of the interaction between tumor cell and bone microenvironments, alongside better *in vitro* culture models to determine the best course of treatment based on a patient-to-patient approach.

General approaches of “one-size-fits-all” like the above-mentioned therapeutic strategies have been traditionally used to treat patients with cancer [333]. However, no two patients’ cancers are the same and will have variable responses to different chemotherapeutics and doses, as tumors may have different underlying genetic sources, and express various proteins from one patient to another. Precision or personalized medicine is an emerging predictive, preventive, and more tailored approach that can be unique to an individual patient’s needs based on the genetic profile of their cancer cells, overcoming limitations of standardised treatment [333-336]. Current personalised medicine approaches still effectively use 2D cell culture-based models in drug pre-clinical screening which cannot reflect the complexity and heterogeneity of the tumor microenvironments [139]. Also, animal xenografts, as commonly used models in pharmaceutical research, are poor predictors of drug safety in humans, along with other limitations including ethical concerns, high cost, and time-consuming processes which cause delays in drug approval

[337]. Thus, bridging *in vitro* cell culture and *in vivo* animal models by developing proper 3D culture technologies is essential. Advanced 3D culture models provide more physiologically relevant environments to assess tumor heterogeneity. 3D Bioprinting approaches for personalized treatment [338-341], human organoid/tumoroid models [342-349] and microfluidic modelling of the tumor microenvironment [350-353] are some examples of recent state-of-the-art tools adopted in anti-cancer drug discovery and personalized therapy. However, few such 3D cancer models enable one to separate stroma/tumor tissue compartments so as to better mimic the tumor microenvironment. For example, (i) a breast cancer model was fabricated by 3D bioprinting, in which a "tumor" in the center was surrounded by a stromal compartment [354]; (ii) co-extrusion produced a core-sell structure with immune cells in the core and tumor cells in the outer layer [355]; (iii) multi-channel microfluidic devices combined with hydrogels filled with different stromal and breast cancer cells in separate channels [305, 356-360], allowed mimicking the stroma-tumor environments of breast cancer and to subsequently assess their response to different chemotherapy drugs.

Numerous natural and synthetic biomaterials have been developed for 3D cell culture or co-culture models for studying cancer metastasis [139, 361-363]; however, only few have separated compartments with different mechanical characteristics mimicking soft-hard tissues interfaces. To close this gap, new strategies need to be introduced based on electrospinning combined with hydrogel, or 3D bioprinting of gradient-based material or multi-materials [362, 364]. Such advanced stroma-tumor 3D models may potentially replace animal-based studies for developing new therapeutics and improving treatment efficacy with higher success rates in pre-clinical trials. In previous work [40] we presented a 3D interface model of tissue-tumor microenvironment based on the combination of an electric discharge plasma-treated fibrous PLA scaffold pre-seeded with stromal cells, and an alginate/gelatin-based hydrogel embedded with tumor cells; this model enables quantifying migration and chemotherapeutic response of different tumor cell lines towards a stromal comportment. In this current study we greatly expand that earlier work: (i) we use patient-derived spine-metastasis tumor cells embedded in hydrogel, like an organoid; (ii) an interface is established with human primary bone cells, osteoblasts, pre-seeded in plasma-treated 3D fibrous scaffolds all together reproducing a real bone-tumor tissue model; (iii) subsequent tumor cell invasion/metastasis is assessed through the model; (iv) two different chemotherapy

drugs are used to screen the bone-tumor interface model, accompanied by studying gene expression profile of tumor cells. This can become a customizable, flexible platform (a) for oncologists to monitor and predict how the disease will progress; (b) to screen novel therapeutics or new repurposing chemotherapy combinations to help specific cancer patients.

6.2 Experimental Section

6.2.1 Fabrication of plasma-treated electrospun nanofibrous scaffold

6.2.1.1 Electrospinning of 3D electrospun mat

We fabricated poly (lactic acid), PLA (NatureWorks 4032D, density= 1.24 g/cc) randomly oriented nanofibrous scaffolds with fiber diameters between about 600-800 nm. Briefly, 16 wt.% polymer solution containing PLA pellets dissolved in 2,2,2 trifluoroethanol, TFE, (M=100.04 g/mol, Merck) solvent was electrospun; to fabricate mats of 250 μm nominal thickness, 10 ml of polymer solution was fed at a flow rate of 1.6 ml/hr using a syringe pump, all placed inside a chamber with controlled temperature (21-24 ^{0}C) and relative humidity of 45%-50%. The distance between the grounded needle tip (21G) and a rotating mandrel (25 rpm) was set at 15 cm, and a stable DC high-voltage (HV) power supply provided a voltage of 20 kV between them. The rotating metal drum mandrel, pre-wrapped with an aluminum foil, was used to collect nanofiber filaments, the finished electrospun mats on Al foil then being maintained in ambient air for 3 days to evaporate residual solvent, then gently detached, cut into smaller pieces, and stored in a desiccator for subsequent use.

6.2.1.2 Surface treatment of 3D scaffolds by plasma functionalization

The fiber surfaces throughout the highly porous (ca. 90%) open volume of the fabricated 3D electrospun mat were exposed to low-pressure radiofrequency (rf) glow discharge plasma in NH_3 gas; based on data from earlier work [40, 41] PLA mats so-treated were optimized for tumor cell migration / adhesion. Since much detail has already been described [27, 271, 277], we explain here only essential aspects. As stated above, the mats were functionalized using ammonia gas (Air Liquide Canada Ltd., Montreal, QC) in a low-pressure (600 millitorr or 80 Pa) capacitively coupled radiofrequency (r.f., 13.56 MHz) glow discharge plasma reactor (cylindrical

aluminum/steel chamber) with a gas flow rate of 15 standard cubic centimeters per minute (sccm) and plasma exposure time of 1 min under mild plasma conditions (power: 15W and Voltage: -40V). The treated mats were then stored in sealed sterilized Petri-dishes before subsequent experiments and analysis.

More details of processing parameters and methods for measuring mats thickness, fiber diameters, pore sizes and overall porosity of nanofibrous mats, along with surface physio-chemical characterization results for non-treated and variously plasma-treated 3D scaffolds were presented earlier [40]. **Figure 6.1** will familiarize the reader with (a) the overall process scheme, the "PP-3D-S" model; (b) the 3D mat type exclusively used in this present article.

(a) **(b)**

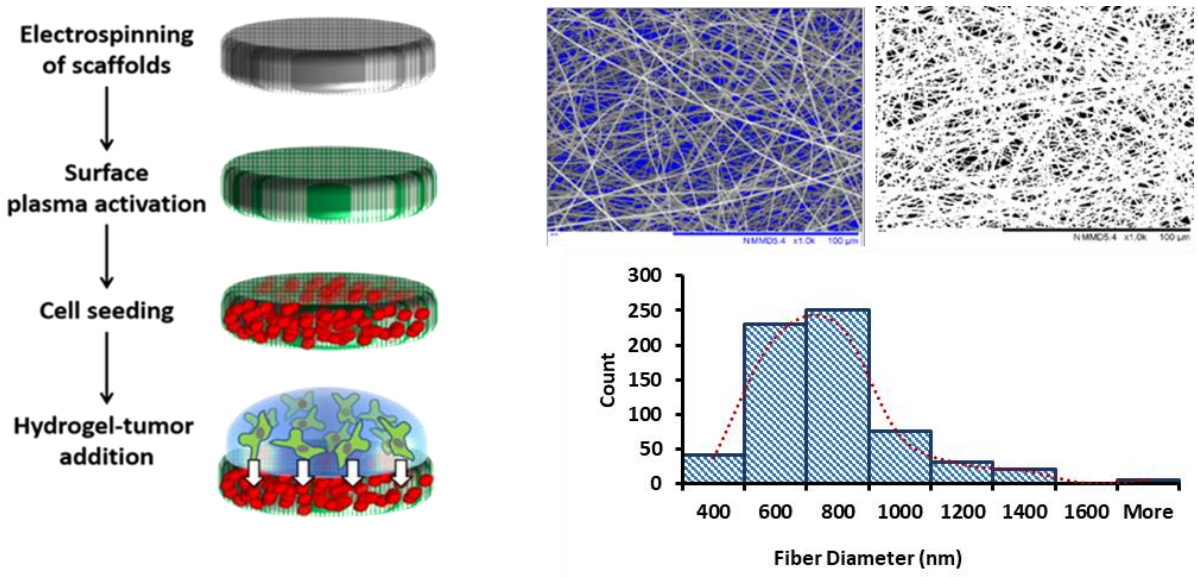

Figure 6.1 (a): Schematic diagram of the main steps of the current "PP-3D-S" 3D interface model; (b): SEM micrographs of medium-sized electrospun PLA mats (fiber diameter sizes: 730 ± 75 nm; Average pore size: 2.1 ± 0.2 µm; overall porosity: 91.0 ± 1.6 %) along w with fiber diameter distribution curve; scale bar:100 µm (adapted from [40])

6.2.2 Biological experiments

6.2.2.1 Cell culture and seeding in hybrid 3D scaffolds

Referring to (a) of **Figure 6.1**, the "stromal" (fibrous mat) component of the "PP-3D-S" model [40, 41] (hereafter part "A") was prepared as follows: primary human osteoblasts were isolated from the vertebral bodies of healthy organ donors (IRB# A04-M53-08B and A10-M113-13B approved by the institutional review board of McGill University) labelled with DiI (red) membrane labeling dye (Molecular Probes, Invitrogen, according to manufacturer's instructions) and IMR-90 mCherry-labelled fibroblasts (red florescent), provided by the laboratory of professor M. Park at McGill University, were seeded onto the sterile electrospun scaffolds 24 hours after plasma treatment. For the "tumor" component (hereafter, part "B" of the 3D model), triple negative epithelial breast cancer cell line MDA-MB231 (Green-fluorescent protein, GFP), donated by Park lab, as well as C42B prostate cancer cell line, and a series of the following patient-derived metastatic tumor cells all from consented donors at the MUHC (RI-MUHC, REB Extracellular Matrix Protocol # 2020-5647) were labeled with DiO (green) membrane dye (Molecular Probes, Invitrogen): patient-derived cells of bone metastasized secondary to breast (Bone Met Breast, BMB), to prostate (Bone Met Prostate, BMP), to lung (Bone Met Lung, BML), and to kidney (Bone Met Kidney, BMK). They were then embedded into an Alginate (1%)/Gelatin (7%) hydrogel (A1G7) to mimic a bone-metastasized tumor microenvironment. Cells were cultured in high-glucose Dulbecco's modified Eagle medium (DMEM), supplemented with 10% fetal bovine serum (FBS) and 1% penicillin/streptomycin (PS) (all from Gibco, Thermofisher), at 37 °C in a humidified incubator with an atmosphere of 5% CO_2. Plasma-treated electrospun mat scaffolds (Part A) were cut into disks with a 9 mm biopsy punch, sterilized with RPMI media containing 1% antibiotic, then placed into the wells of non-adherent 48-well polystyrene culture plates (SARSTEDT AG & Co.). 20,000 RFP-Fibroblasts or Dil-labeled osteoblasts were added to each well and incubated for 30 min at 37 °C and 5% CO_2, following which the liquid was aspirated from each well and scaffolds were rinsed with fresh media to remove non-adhering cells. Finally, (Part B) 50,000 cells/well (either breast cancer cell line or patient-derived bone-metastasized cells) in a volume of 100 μl A1G7 hydrogel, were applied on top of the pre-seeded nanofibrous mats (A), followed by addition of 200 μl of $CaCl_2$ (100 mM)

for ionic crosslinking. After 10 min $CaCl_2$ was aspirated, scaffolds were washed twice with fresh media to remove residual crosslinking agent, and 500 μl of complete media (RPMI with 10% FBS and 1% PS) was added per well. The scaffolds were incubated for 1, 3, and 5 days (depending upon the specific experimental design), and the culture medium was changed every three days.

6.2.2.2 Observation and quantification of tumor cell migration

Migration from (B) and invasion of tumor cells into (A) was assessed as a function of incubation time. At different time points (over the course of 1, 3, and 5 days), cells on the treated mats were fixed with 4% Paraformaldehyde (PFA) after carefully removing the hydrogel off the surface. The samples were then placed on microscope slides covered with a drop of mounting medium (Sigma, Fluoroshield with DAPI), along with a protective glass cover slip to avoid dehydration. The top surface of the mats was monitored using florescent scanning microscopy (EVOS M5000 (2X)). The number of GFP/DiO labelled tumor cells present on top of the scaffolds were counted (20 spots/sample of three replicated experiments) using ImageJ (National Institute of Health, US). Each experiment was done in triplicate, with quantification from 20 spots to fully cover the surface of each sample.

6.2.2.3 Drug screening experiment

Doxorubicin (Dox) and Cisplatin (Cis), well-known chemotherapy drugs, were used in screening experiments designed to evaluate their effect on cellular activities of patient-derived metastasized cells seeded in our 3D cell culture model. NH_3 plasma-treated PLA mats (used 24 h after plasma treatment) pre-cultured with stromal and tumor cells in 48-well plates were treated either with sterile PBS as control (placebo), or with Dox (0.05, 0.1, 0.5, 1, 2 and 5 μM) and/or Cis (1, 5, 50, 100, 150, 200 μM) in low-serum RPMI media (1% FBS, 1% PS) and incubated for 5 days. The experiment was performed with technical replicate of six and the media loaded with the drugs was replaced after 3 days. Cellular metabolic activity was analyzed by Alamar Blue assay after 5 days of treatment with Dox/Cis, and IC50 values (50% inhibitory concentration) were calculated by constructing a dose-response curve and using non-linear regression (Equation: log(inhibitor) vs. normalized response) in GraphPad prism. Finally, the numbers of migrated cells from the gel

(Part B) to the surface of mats were measured by florescent microscopy and quantified using ImageJ.

6.2.2.4 Metabolic activity measurement

Cellular metabolic activity was assessed using a commercial Alamar Blue® kit (Thermofisher), whereby resazurin dye (blue) is reduced to resorufin (pink). Briefly, stromal and tumor cells cultured in the 3D model and treated with Dox or Cis (for 5 days) were incubated with Alamar Blue dye added to media (RPMI, 1% FBS, 1% PS) at dilution of 1:10 at 37°C, 5% CO_2 for 4-8 h, depending on the cell type. After loading a volume of 100 µl from each well into 96-well plates (Corning, black half-area), fluorescence of Alamar Blue at Excitation/Emission wavelengths 540/585 nm were analyzed using a Tecan Infinite M200 pro microplate reader (Tecan Trading, AG, Männedorf, Switzerland). The experiments were performed in triplicate for each cell type to assure reproducibility.

6.2.2.5 Gene expression analysis: Real-time qPCR

After 5 days of incubation, RNA from tumor cells remaining in the hydrogel and from those migrated to the mat's surface were separately isolated using Trizol reagent (Ambion, Life technologies). The manufacturer's protocol was followed: Trizol was added, and the scaffold disrupted through mechanical homogenisation, before RNA was separated with chloroform, precipitated by isopropanol, washed with 75% ethanol (diluted in ultra-purified water), and finally dissolved in RNase-free water. RNA concentration and quality were determined by spectrophotometry (Tecan). 400 ng of total RNA was reverse transcribed into cDNA using a qscript cDNA synthesis kit, according to the manufacturer's instructions (Quanta bio). Synthesized cDNA was then amplified, and gene expression measured using real-time-quantitative PCR (Applied Biosystems). Housekeeping genes and genes of interest were purchased from Invitrogen and primer sequences are listed in **Table 6.1**. To prepare a total volume of 20 µl, 10 µl SYBR Green Master Mix qRT-PCR kit (Thermo Fisher), 1 µl of cDNA, 0.5 µl of forward primer, 0.5 µl of reverse primer, and 8 µl of RNase free water were mixed. Then, qPCR was performed as follows: pre-denaturation for 10 minutes at 95°C, denaturation for 15 seconds at 95°C, annealing for 1 min at 60°C, elongation/extension for 30 seconds at 72°C, 40 cycles. Quantitative data were analyzed by average of duplicate Ct values, normalized to β-actin

levels as an internal control, and target gene expression was calculated using the 2^(–ΔΔct) method. The results represent three independent experiments, and the final values compare MDA-MB 231 expression on mats relative to their expression in hydrogels.

Table 6.1 Detailed information of primer sequences used for qRT-PCR analyses

Full Name	**Forward primer 5'>3'**	**Reverse primer 5'>3'**	**Template size (base pairs)**
E-cadherin	CAAATCCAACAAAGACAAAGAAGGC	ACACAGCGTGAGAGAAGAGAGT	1 ea @ 25 (FWD), 22 (REV) bases
N-cadherin	CATCATCATCCTGCTTATCCTTGT	GGTCTTCTTCTCCTCCACCTTCT	1 ea @ 24 (FWD), 23 (REV) bases
TWIST1	ATGGCAAGCTGCAGCTATG	AGTTATCCAGCTCCAGAGTC	1 ea @ 19 (FWD), 20 (REV) bases
SLUG	AGCATTTCAACGCCTCCAA	ACACAGTGATGGGGCTGTAT	1 ea @ 19 (FWD), 20 (REV) bases
SNAIL1	GAAAGGCCTTCAACTGCAAA	TGACATCTGAGTGGGTCTGG	1 ea @ 20 (FWD), 20 (REV) bases
SOX2	CATCACCCACAGCAAATGAC	CAAAGCTCCTACCGTACCACT	1 ea @ 20 (FWD), 21 (REV) bases

6.2.3 Statistical analysis

All quantitative results reported here were obtained from at least three independent experiments to evaluate reproducibility, and data were expressed as the mean values ± SD/SE. Statistical analysis was carried out using one-way ANOVA with Tukey's post hoc analysis for parametric data; in the case of having non-parametric data, Kruskal-Wallis test was done, followed by Mann-Whitney post hoc analysis to compare two independent groups of interest. P values of less than 0.05 ($p < 0.05$) were considered significant for all tests. All statistical analysis was performed using Prism v 9.0 (GraphPad)

6.3 Results and Discussion

6.3.1 Invasion behavior of patient-derived spine-metastasized cells in the PP-3D-S model

Having previously examined our 3D model for migration and drug screening assay using different aggressive, less-aggressive, and non-cancerous breast epithelial cells lines [41], we sought to represent a real bone tissue-tumor interface model by reproducing it with patient-derived tumor cells, isolated from bony spinal metastases (BMX) including BMB, BMK, BML, and BMP. These BMX metastatic spine tumor cells all are aggressive, and we expected to see considerable migration and invasion over different time points. As illustrated in **Figure 6.2a**, we observed similar amounts of migration for all BMX samples, especially after 5 days, with no substantial difference between cells from different primary tumors individually at the certain time points. However, for each BMX sample, we found significant difference in the number of tumor cells migrated between day 1/3 and day 5. In addition, when they are compared with their equivalent cell lines, for example BMB cells to their counterparts of MDA-MB 231 (micrographs of **Figure 6.2b** and histograms of **Figure 6.2c**), there is appreciable variance in the rate of migration and potential growth of BMB and MDA-MB 231 cell lines at the same time point; because patient-derived BMX samples are primary cells, they do not proliferate, migrate, and generally behave the same way that immortalized cell lines do.

(a)

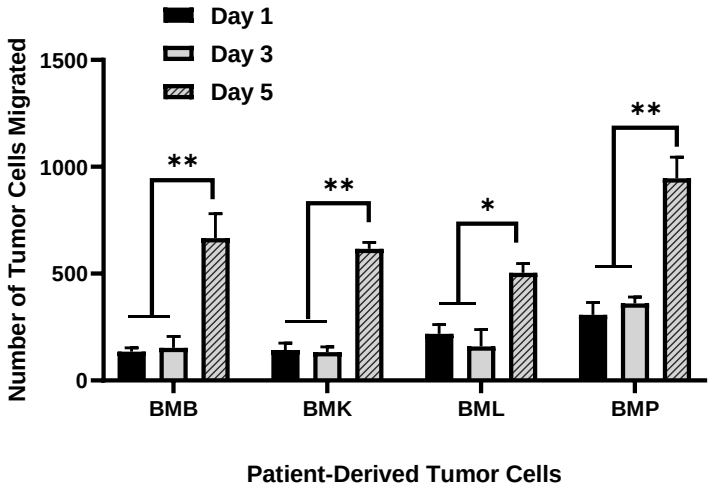

(b)

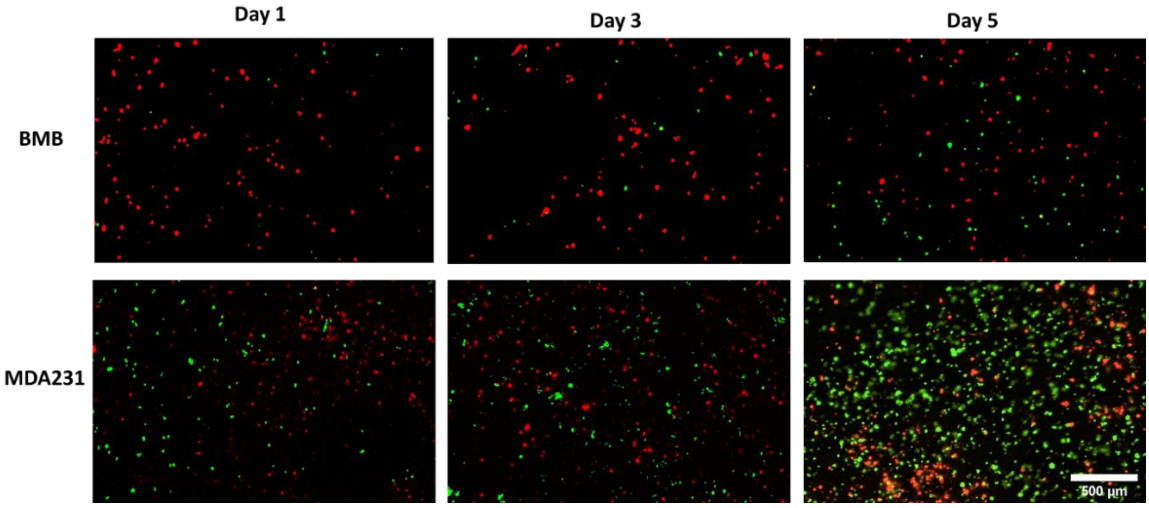

(c)

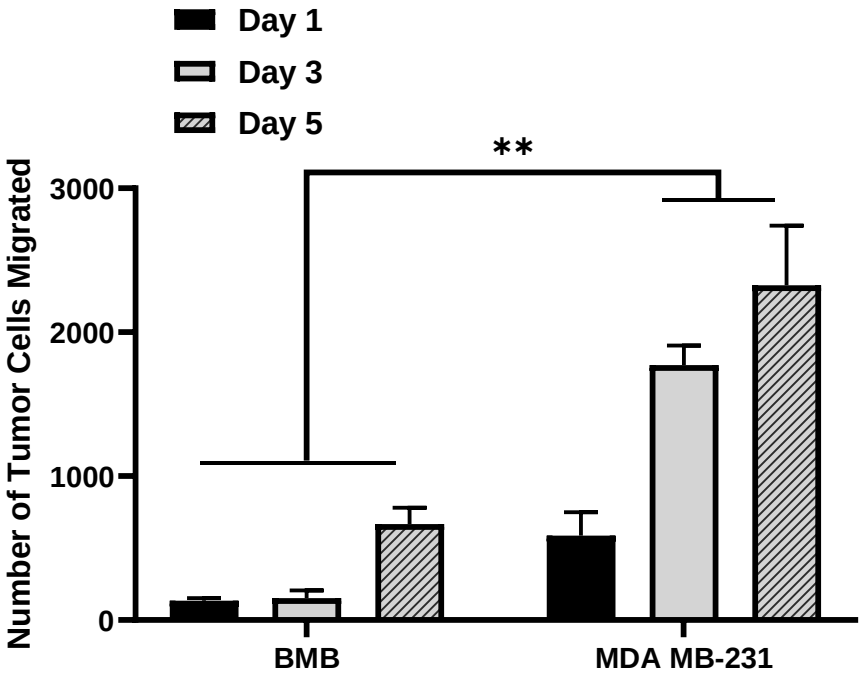

Figure 6.2 DiO-labeled patient-derived bone/spine-metastasized tumor cells secondary to Breast: Bone Met Breast (BMB), to kidney: Bone Met Kidney (BMK), to lung: Bone Met Lung (BML) and to prostate: Bone Met Prostate (BMP) cultured in hydrogel having migrated into osteoblast-seeded NH3 plasma-treated PLA scaffolds ; (a): Histograms representing patient-derived bone-

metastasized tumor cells numbers migrated to the bone interface, which is NH3-plasma treated PLA mats pre-seeded with DiI-labeled osteoblasts over the incubation time of 5 days; (b): Representative images of DiI-labelled red osteoblasts adhering to NH3 plasma-modified mats, along with DiO-labelled patient-derived metastasized cells and/or GFP-MDA-MB231 breast cancer cells having migrated after 5 days; (c): Comparison of patient-derived bone-metastasized breast cancer cells (BMB) with aggressive breast cancer cell line (MDA-MB 231) while migrating over 5 days [scale bar: 500 µm, error bars: SE., *=P<0.05, **=P<0.01, comparison indicated by lines]

6.3.2 Screening of patient-derived bone-metastasized cells with Doxorubicin

The end purpose of developing this bone or spine metastasis 3D model with primary patient-derived cells is their application in drug screening tests for personalized medicine, to screen novel chemotherapeutics or repurposing chemotherapy combinations, to help patients suffering from cancer. We conducted screening tests of above-mentioned patient-derived BMX cells with Doxorubicin (Dox) and compared the results with their equivalent cell lines at the similar range of drug concentration. From **Figure 6.3a**, we observed that BMX cells were protected from Dox-induced apoptosis, meaning that they were resistant to Dox at the same doses of 0, 0.05, 0.1, 0.5, and 1 µM which had been used earlier for the corresponding cell lines [41]. Further, we compared the differences between patient-derived cells and their equivalent cell lines including BMB and MDA-MB 231 breast cancer cells line and/or BMP and C42B prostate cancer cells line by assessing drug sensitivity, as shown in **Figure 6.3b**. The results indicated remarkable resistance of patient-derived bone metastasized tumor cells to Doxorubicin compared with consistent drug sensitivity of their counterpart cell lines at the same drug concentrations. This is meaningful data, achieved by applying our PP-3D-S model, showing substantial differences between the response to chemotherapeutics of immortalized cell lines versus patient-derived cells.

(a)

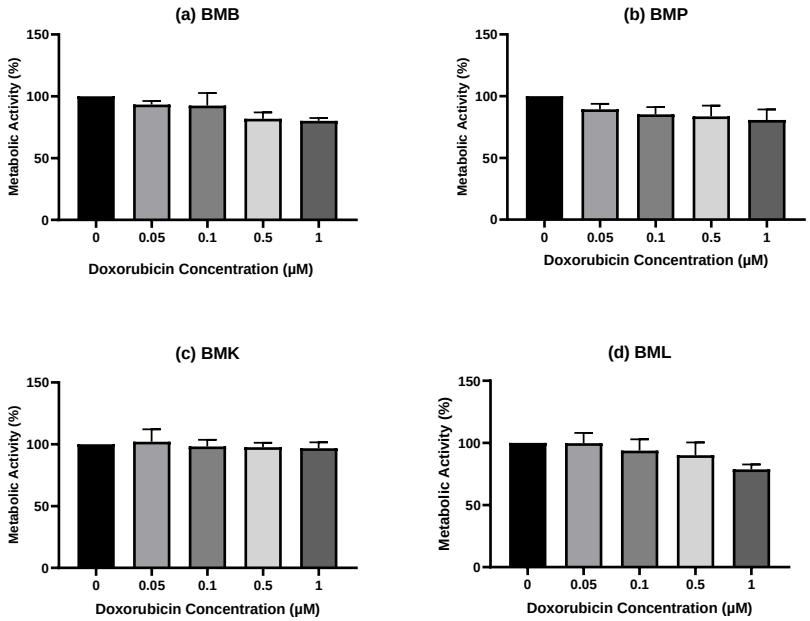

(b)

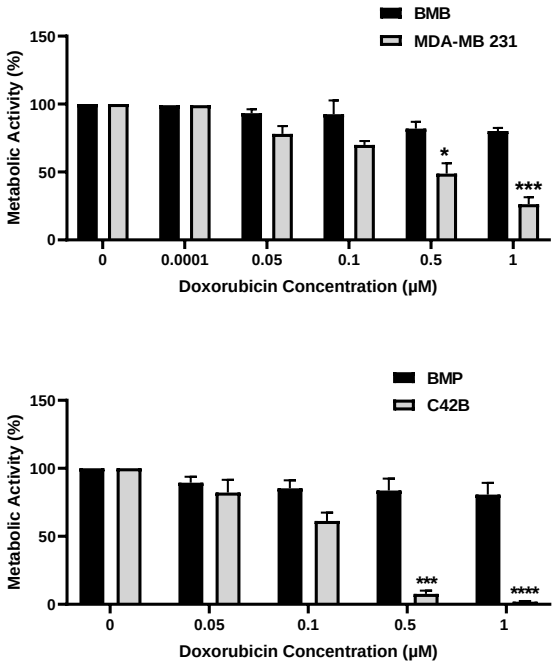

Figure 6.3 Metabolic activities of (a): Different patient-derived bone/spine-metastasized tumor cells secondary to Breast: BMB (a), to prostate: BMP (b), to kidney: BMK (c), and to lung: BML

(d) screened with Doxorubicin (0, 0.05, 0.1, 0.5, and 1 µM) after 5 days, (b): Two pairs of patient-derived cells and their equivalent immortalized cell lines including BMB & MDA-MB 231 and MBP & C42B after 5 days of culture; (error bars: SE., *=P<0.05, **=P<0.01, ***=P<0.001, ****=P<0.0001, bars with "*" are compared with control (Dox 0) and/or with their equivalent values of BMX samples)

6.3.3 Treatment of bone-metastasized secondary to breast tumor cells with different chemotherapy drugs

Metastasis and drug resistance are among the major issues to the treatment of advanced cancer, and the leading causes of death in cancer patients. Anti-cancer drugs discovery and development is still the main area of cancer research. It is clear that molecular and phenotypical changes induced by different chemotherapy drugs that have effect on intra-cellular signalling pathways, cell division and -proliferation, are specific for each particular cell type [365]. Doxorubicin and Cisplatin (Cis) are both considered to be effective, and they are commonly used chemotherapy drugs, among others, to treat cancer. With the aim of investigating drug resistance/sensitivity of the targeted tumor cells, we carried out a series of experiments on either patient's breast cancer cells metastasized to bone (BMB), or an equivalent cell line, MDA-MB 231, screened with both Dox and Cis at different doses. As shown above (**Figure 6.3a**), BMB cells were resistant to Dox concentrations between 0.05 to 1 µM. However, by increasing its concentration from 1 to 5 µM (**Figure 6.4a**), we observed a marked reduction in metabolic activity of BMB cells, with the relative IC50 value around 1.52 µM. It is interesting to compare this with the IC50 value of MDA-MB 231, 0.36 µM, which clearly shows an important difference in drug sensitivity between BMB patient-derived cells and their equivalent MDA-MB 231 breast cancer cell line. When compared to Cisplatin, the other chemotherapeutic drug used in this study, there was also a considerable difference in chemosensitivities between the two drugs after screening both MDA-MB-231 and BMB cells with Dox and Cis: Comparing the two curves shown in **Figure 6.4a**, it is clear that BMB cells are more sensitive to Dox (IC50 = 1.52 µM) than to Cis (IC50 = 28.37 µM) at the same drug concentrations, while **Figure 6.4b** reveals a similar trend for the immortalized MDA-MB 231 breast cancer cell line, namely IC50 values of 0.36 and 7.28 µM for Dox and Cis,

respectively. We believe that there might be a crucial connection between molecular states before drug treatment and cellular phenotypes induced by different chemotherapeutics after treatment, one that needs to be transcriptionally investigated in our future studies [366-373]. The results above clearly underline that our current 3D culture model is appropriate for screening not only cell lines, but also different patient-derived metastasis cells with a variety of existing or newly developed chemotherapy drugs for specific patients.

(a)

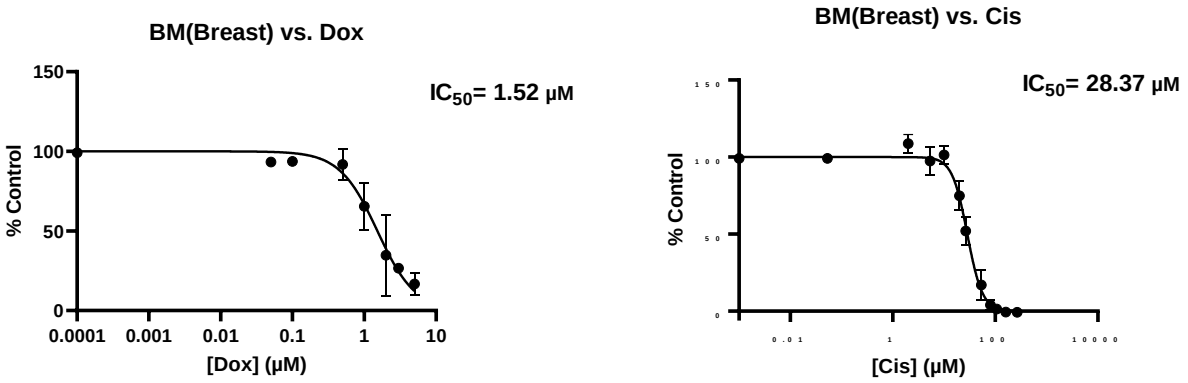

(b)

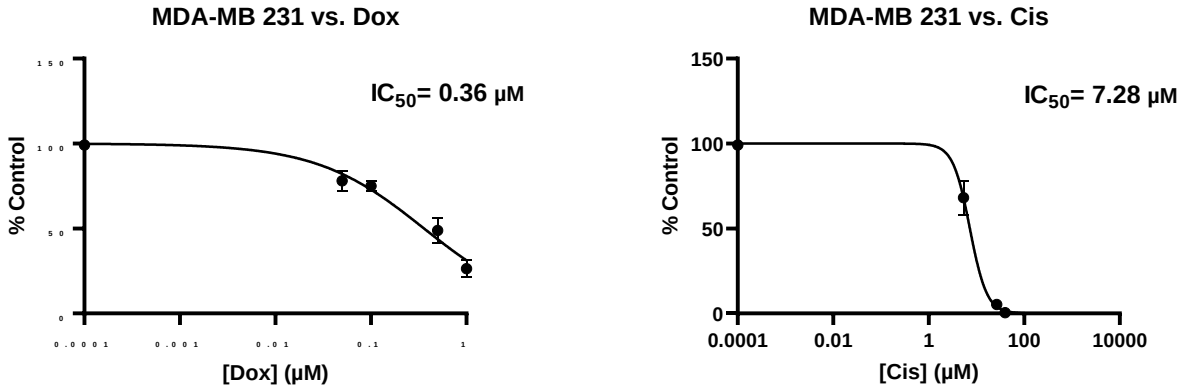

Figure 6.4 . Metabolic activities of (a) patient-derived bone-metastasized tumor cells secondary to Breast: BMB and (b) MDA-MB 231 breast cancer cell lines screened with Doxorubicin (0-5 µM) and Cisplatin (0-200 µM) after 5 days of culture; (error bars: SE.)

6.3.4 Gene expression profile of breast cancer cell lines in the PP-3D-S model

Epithelial-to-mesenchymal transition (EMT) and the reverse process (MET) have been widely discussed in the literature as key steps in cancer metastasis: They are biological processes by which cancer cells transit between epithelial and mesenchymal states [374]. Indeed, immotile epithelial cells undergo multiple biochemical changes and specific morphological alterations in which they lose their tight cell-cell adhesion, switch to mesenchymal phenotypes and eventually acquire enhanced motility, migratory properties, and invasiveness. Following travel (metastasis) to a new location, multiple steps occur for the metastatic cancer cells to recover to their epithelial characteristics, termed MET, and form a secondary tumor [374-376]. Several different biomarkers/signaling pathways and molecular processes involved in initiation of EMT have been proposed in the literature, including expression of cell-surface proteins/markers of EMT: E-cadherin, N-cadherin [377-379]; cytoskeletal markers of EMT: Vimentin [380]; extracellular proteins: Fibronectin [381]; and activation of transcription factors: Snail, Slug, Zeb, Twist, and Sox families [382-385]. These markers all are upregulated during cancer metastasis, known as mesenchymal markers, except E-cadherin (cell-cell attachment receptor) which is decreased during EMT as epithelial markers [375, 376]. Since we observed significant MDA-MB 231 migration after 5 days (quantitatively proved in **Figure 6.2c**), we investigated the possible role of EMT mechanisms through monitoring the expression of E-cadherin, N-cadherin, Twist1, Slug, Snail1, and Sox2 by real-time qPCR. **Figure 6.5** shows epithelial and mesenchymal markers expressed by MDA-MB 231 cells that migrated onto the mats, compared with the cells that remained in the hydrogel (data normalized to the gel). Clearly, an appreciable proportion of tumor cells that had migrated into the mats manifested increased expression of mesenchymal markers N-cadherin, Slug, and Sox2 compared with the values in the gel, the expected upregulation of those markers during EMT. However, we found that expression of E-cadherin, the epithelial marker, also showed great increase. This indicates that cells which readily migrated to the mats not only lost their E-cadherin receptors while leaving the gel and acquiring mesenchymal phenotype while undergoing EMT, but that they also might be able to revert to their original phenotype. Termed MET, this occurs in the secondary environment, the mat in this case, after cell growth and proliferation on the mat over 5 days of culture [386]. Nevertheless, some limitations remain as we only investigated one tumor cell line and one time point. Thus,

future work will have to explore a time course with several tumor cell types to fully understand the impact of EMT on our 3D model. Taken together, these findings highlight that this PP-3D-S *in vitro* 3D culture model indeed can realistically represent cancer cell migration/invasion processes; here, EMT was manifested by overexpression of mesenchymal markers. Nevertheless, besides numerous published reports in the literature proving that EMT is crucial in metastatic cancer, alternative mechanisms have also been proposed for spreading and metastases. These include collective or cluster-based migration, mesenchymal invasion, and amoeboid invasion (crawling-like cell movement) [387].

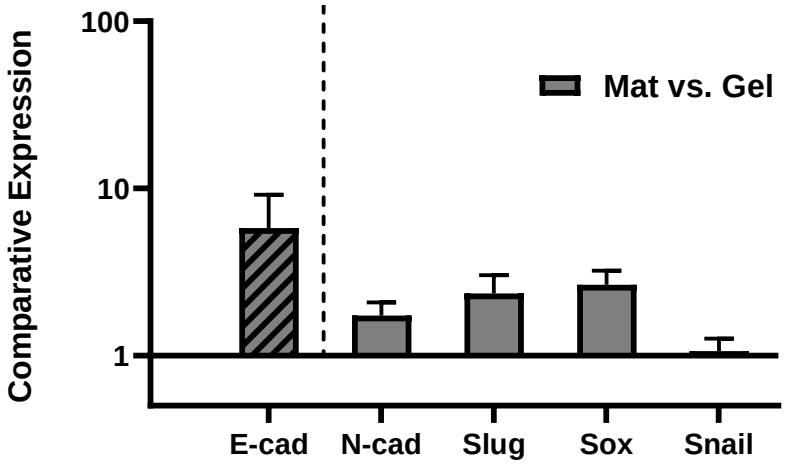

Figure 6.5 Gene expression profile of MDA-MB231 aggressive breast cancer cells cultured in PP-3D-S model for 5 days: expression of E-cadherin, N-cadherin, Twist1, Slug, Snail1, and Sox2 on the mat versus gel quantified by real-time qPCR assay; (error bars: SE.)

6.4 Conclusion

In this study we adopted our previously developed PP-3D-S co-culture tumor microenvironment model [40, 41] to investigate migration and metabolic activity of patient-derived spine metastases cell secondary to breast, prostate, lung, and kidney cancers. The model enables observing migration of patient derived cells to a stromal interface, although not to the same extent as

immortalised cell lines, likely due to their lower metabolic activity. When challenged with the commonly used chemotherapeutics, Doxorubicin (Dox) and Cisplatin (Cis), patient-derived cells were found to be significantly more resistant to these drugs compared to immortalized cell lines. Patient-derived bone-metastasized breast cancer cells and breast cancer cell lines were both more resistant to Cis than to Dox, displaying higher IC50 values. Furthermore, we assessed common EMT markers (N-Cadherin, Snail, Slug, Sox2 and E-Cadherin) comparing expression levels in cell which migrated to the stomal compartment versus those remining behind in the gel after 5 days culture. Compared to the non-migrated cells, the migrated cells displayed higher expression N-cad, Slug and Sox2, indicating the EMT status of the migrated MDA-MB-231 cells. However, there was also higher E-cad detection (epithelial marker), indicating that caution should be exercised since only one tumor cell line and one time point was probed. Taken all together, we have demonstrated that this 3D co-culture model, PP-3D-S, is sensitive to different immortalized and primary cell types, and that it provides a powerful environment in which patient-derived cells can be screened with different chemotherapeutics. It has strong potential as a tool to assess effectiveness of new drugs or drug combinations, to move towards the goal of personalized cancer treatment.

Acknowledgments

The authors thank Dr. Matt Kinsella and Dr. Morag Park for donations of cell lines used in this study. They also acknowledge the support of McGill ortho fellows and surgeons for assistance in obtaining primary human osteoblasts and express thanks to Mr. Sean Watson for his valuable assistance in plasma functionalization of scaffolds. The authors also gratefully acknowledge funding support from the Natural Sciences and Engineering Research Council (NSERC) of Canada, the Canadian Institutes of Health Research (CIHR, MEC Funding Ref. 171258), the Research Institute of McGill University Health Center (RI-MUHC) and Fonds de Recherche du Québec - Santé (FRQS) Junior 2 Research Scholar Award (to DHR).

CHAPTER 7 GENERAL DISCUSSION

In this PhD thesis, we proposed to develop a novel 3D hybrid cancer model based on a plasma-treated electrospun 3D scaffold combined with an alginate-gelatine (AG) hydrogel, termed here as “PP-3D-S”. This has been done in order to address a current gap in the literature, namely, the lack of appropriate interface 3D models to study cancer metastasis and invasion between separate sections of the tumor microenvironment, namely the stroma and tumor mass. Moreover, literature data indicate that interface 3D cancer models based on patient-derived cells or primary clinical samples, mimicking a real tumor microenvironment, are more accurate for screening of anti-cancer drugs for personalized treatments, now an emerging and promising approach in cancer studies. Thus, our approach was to create an interface 3D model based on two compartments:(A) stromal/normal and (B) cancerous tissues that is compatible with broad ranges of either patient-derived primary cells or immortalized cell lines.

This research has been performed in four different steps: (1) combine electrospun random nanofibrous mats with two different plasma treatment techniques (plasma functionalization and plasma polymerization) to generate biocompatible 3D scaffolds and to optimize them for cell culture applications; (2) combine the (A) plasma-treated nanofibrous scaffolds with (B) alginate-gelatin based hydrogels to develop a novel 3D co-culture (A)-(B) interface model applied for migration/invasion assays and drug screening applications; (3) evaluate migration and drug sensitivity of several immortalized cell lines with different aggressiveness through the 3D model; (4) evaluate migration and drug sensitivity/resistance of patient-derived metastasized cancer cells using the 3D model.

7.1 Combination of electrospinning, plasma treatment, and hydrogel technologies for 3D culture applications

In order to create a biocompatible, bioactive 3D scaffold for 3D cell culture applications, we first combined electrospinning with low-pressure (LP) plasma functionalization or low- and atmospheric-pressure (AP) plasma polymerization, as explained in detail in **Chapter 4 & 5**, to enhance biological properties of the 3D scaffolds in terms of cell adhesion, growth and migration.

Our first hypothesis was that electrospun 3D nanofibrous scaffolds modified by selected plasma treatments (both plasma functionalization and plasma polymer coating) can yield vastly improved (stromal) cell adhesion and growth.

Contrary to wet-chemical approaches (e.g., hydrolysis with NaOH [232, 388]) which entrain issues of toxicity, loss of mechanical properties, and environmental impact [225], we know that plasma is a rapid, clean, highly reproducible, free-solvent, and environmentally-friendly technique that can offer an attractive alternative to fine-tune and modify the surface properties of scaffolds even complex shaped ones without compromising bulk properties of the substrate [235, 277].

Thus, initial adhesion of stromal fibroblast cells on PLA electrospun mats treated with low-pressure O_2 and NH_3 plasma (functionalization) and L-PPE:N (plasma polymer, ca. 100 nm ultra-thin films) and non-treated (control) mats was examined (**Chapter 4**). Initial cell attachment, within 30 min after seeding, increased on the mats with oxygen- and nitrogen-containing functional groups, unlike pristine PLA mats. This improvement in cell adhesion on plasma-modified scaffolds, proven by previous works [27, 271, 277], can be explained by the positively- or negatively-charged hydrophilic functional groups, respectively provided by NH_3 and O_2 plasma, which first bind proteins in culture systems, in turn followed by cell surface integrin receptors [221, 222, 323]. However, although we observed unexpected hydrophobic characteristics for samples with L-PPE:N coating (confirmed by contact angle tests in **Chapters 4, 5**), fibroblasts nevertheless adhered to the coated surfaces (via amine groups), more than on virgin samples, but less than the O_2 and NH_3 plasma-modified ones.

In order to simulate breast cancer metastasis, the plasma-treated scaffold was combined with AG hydrogel, following which migration of MDA-MB 231 breast cancer cells was monitored over 7 days. We examined different plasma treatments including LP plasma in O_2 and NH_3, and several different thin plasma polymer coatings, namely L-PPE:N (LP) , L-PPE:O (LP), PP-EL (AP), and PP-AAm (AP) (results of the three latter only in **Chapter 5**). According to the microscopic images and quantitative data in **Chapter 5**, greatly increased numbers of the aggressive tumor cells had migrated into the scaffolds for all plasma treatments, except L-PPE:N coating, over the course of 7 days, particularly between days 3 and 7. This is believed due to their surface wettability; in other words, lower water contact angles lead to higher cell counts. The “best”

performance was observed for NH_3, PP-AAm, PP-EL; but L-PPE:O and O_2 were quite comparable. It can be concluded that both oxygen- (e.g. -COOH groups) and nitrogen-based (e.g. $-NH_2$ groups) functionalities are effective in promoting tumor cell migration and adhesion due mainly to their negatively- and positively-charged characteristics, respectively [254]. Moreover, plasma-polymerized coatings have proven to be highly bioactive, reproducible, and sufficiently stable over time (much slower hydrophobic recovery than plasma modification) [249-251, 255, 256, 389-391]; thus, with such better long-term stability they might be preferred in potential commercial contexts.

However, an unexpected and so far unexplained result was that L-PPE:N coating showed only marginal improvement over the untreated control samples, despite the fact that it had earlier performed satisfactorily in quite similar situations [27, 271, 277]. A possible **recommendation** is to change the gas mixture ratio of ethylene and ammonia to reach optimum conditions of desirable hydrophilicity and further improved biological performance. In addition, it is also worth it to provide new PLA pellets from alternate sources to fabricate the mats accordingly, since batches can vary by different manufacturers.

The second hypothesis was that electrospun 3D nanofibrous scaffolds fabricated with different morphologies (fiber diameters, random orientation) and materials (different bio-degradable polymers) can provide suitable fibrous microenvironments for 3D cell interactions and can influence cell adhesion and migration.

We demonstrated by confocal microscopy that our PP-3D-S model enables mimicking the natural interaction of cells in a synthetic 3D network that recapitulates many features of natural human tissues, because electrospun nanofiber mats resemble the morphology of fibrous ECM of tissues in the human body. Electrospun random PLA mats with average fiber diameters of 700 nm (medium) and 1.5 μm (large) presented much higher numbers of fibroblasts bonded to the surface than the small-sized scaffolds (mean fiber diameter of 300 nm), after 30 minutes of incubation, because the latter have smaller voids that obstruct cell infiltration. The outcomes for medium- and large-sizes were quite comparable, slightly higher for large. Thus, we proved that cells are able to readily enter into and adhere to the surfaces of 3D scaffolds with fibers size both less and higher than ca. 1 μm. However, the literature is controversial, with some studies showing better performance with fibers diameter <1 μm [189-191], and others proved for >1 μm [192-194].

Regarding tumor cell migration and growth, the result was somewhat similar to that of fibroblasts adhesion on the mats, in that both medium- and large-diameter scaffolds manifested large numbers of migrated/proliferated tumor cells in the volumes of scaffolds, especially after 7 days of culture and for the best-performing plasma treatments (PP-EL, PP-AAm, NH_3), far more than in small-sized ones. It indicates that even though all three sizes are highly porous, roughly 90% porosity, the small-sized mat (average pore size ca 1 µm, compared with 2 and 3 µm for medium- and large-size, respectively) significantly hindered cell entry and movement through the open volume, even after 7 days.

Z-stack confocal images (**Chapter 4**) revealed how cells interacted with each other, with the underlying 3D fibrous structure in a coherent manner, and how they penetrated to the depths about half the scaffold's nominal thickness, 250 µm, 60 to 120 µm from day 1 to day 7, respectively; these depths of penetration were substantially greater than for untreated samples.

Nanofiber mats based on polymers with different mechanical stiffnesses (PLA, PCL, PU) revealed no statistically significant differences in the numbers of migrated tumor cells over 7 days of incubation. In other words, the electrospun mats can be tuned to best match the targeted tissues (softer or harder types) through choice of proper polymers. It is also possible to fabricate 3D scaffolds with controllable predetermined durability. Therefore, by selecting a polymer with desired mechanical properties, using optimized processing parameters for fiber diameter of scaffolds and plasma treatment, one can achieve a system with the best possible cellular performance, lowest cost, best durability and reproducibility, all these in comparison with commercial products such as Matrigel®.

<u>Research Contributions</u>

The originality of this Ph.D. thesis has been to prove feasibility of combining three different technologies to generate a 3D interface culture system, and to demonstrate it as a migration/invasion model to study human cancer metastasis. It is the first of its kind to examine the combination of electrospinning, plasma, and hydrogel for such 3D cell culture applications. The results of this part of the research were published in the peer-reviewed journal of "Materials Science and Engineering: C", p. 112566, 2021, under the title "A novel 3D co-culture platform

for integrating tissue interfaces for tumor growth, migration and therapeutic sensitivity: PP-3D-S"[40].

It was also filed as a patent in 2020 and was internationally published by WIOP (PCT) in 2021 with the application number of "WO 2021/087613A1" under the title of "Customizable 3D cell culture system comprising hydrogel-embedded cells and uses thereof".

7.2 Evaluation of migration and drug sensitivity/resistance of immortalized cancer cell lines with different aggressivity through the PP-3D-S model

The aim of developing the PP-3D-S co-culture system was to produce a physiologically relevant model of the human cancer microenvironment for migration/invasion assays and drug screening applications.

Thus, *our third hypothesis has been that the 3D hybrid co-culture model can portray different tissue-tumor microenvironments and a broad range of cancer cell lines with different aggressivity to predict their migratory behaviour and to treat with chemotherapeutics in drug screening experiments.*

We examined the model (**Chapter 5**) by incorporating a series of breast cancer cell lines of varying aggressivity (MDA-MB 231, MDA-MB 453, MCF7) and non-cancerous normal epithelial breast cells (MCF10A) separately encapsulated in the gel layer, along with matching stromal cells, human primary osteoblasts, embedded in the nanofibrous mats. This mimicked a bone-tumor interface since bone is a frequent site of metastasis particularly from primary breast tumors [2, 4, 51, 331]. We observed different meaningful migratory behaviours of the above-mentioned cells, namely considerably increased migration, and invasion by the aggressive MDA-MB 231 over 5 days, compared with the less-aggressive MDA-MB 453, MCF7 and normal non-cancerous MCF10A. In other words, the non- or less-aggressive cells tended to mainly remain within the ("primary tumor") gel layer, behaving like benign tissue, whereas aggressive cells readily invaded the target "bone" tissue, showing significantly greater migratory behaviour toward the bone-like environment, like highly malignant tissue. This was in accordance with their intrinsic characteristics and expectations [319, 320], namely that non- or less-aggressive cells

tend more to proliferate than migrate, while aggressive cells showed both over the course of 5 days.

By screening those cancerous and normal breast cell lines with varying Doxorubicin (Dox) concentrations (0.05, 0.1, 0.5 and 1 µM) over 5 days, we observed a statistically significant reduction in metabolic activity of all, as expected from these immortalized cell lines. By increasing Dox concentration, less-aggressive MDA-MB 453 showed higher drug sensitivity or lower IC50 values (IC50 = 0.10 µM) than aggressive MDA-MB 231 (IC50 = 0.36 µM). However, MCF7, a less-aggressive cancer cell line, is much more resistant to Dox (IC50 = 0.48 µM) compared with MDA-MB 453; this might be attributed to their different HER-2 marker responses, the former being HER-2 negative, the latter HER-2 positive [321]. Moreover, non-cancerous MCF10A breast epithelial cells were seen to be the most Dox-resistant (IC50 = 0.67 µM), possibly that these benign cells may go into a state of senescence while preserving some metabolic activity [325].

We concluded from these experimental findings that the PP-3D-S model has the potential to accurately simulate migration of variably aggressive cancer cell lines in this pseudo-metastatic microenvironment, and to manifest different cellular responses to the chemotherapy drug Dox in screening experiments.

Our fourth hypothesis was that the 3D interface model may perform similarly as a commercial product, Matrigel®, in terms of efficacy and range of applications

We also aimed the 3D co-culture model to be more durable, reproducible, and cost-effective than an existing commercial product, Matrigel® (**Chapter 4**). Thus, we screened the aggressive MDA-MB 231 cells with different doses of Dox over 7 days, both via our PP-3D-S model and via Matrigel®/Boyden chamber to compare the two. Migration and invasion of tumor cells to the target tissue were blocked by increasing amounts of Dox, and we quantitatively proved that both models have remarkably similar outcomes, ca. 75% reduction of tumor cell migration with 0.5 µM drug concentration. However, compared to standard Matrigel®, PP-3D-S is more advantageous for the following reasons:

It can truly represent a physiological tumor microenvironment by creating an (stroma-tumor) interface, which is adaptable to different tissue porosity and mechanics for studying a broad

range of cancer types; it helps improve reproducibility since it avoids the characteristic batch-to-batch variation for which Matrigel® is known; it is cost-effective, fast, and user-friendly by offering the simplicity of manufacturing procedures and materials manipulation; this model can also be tailored to a high-throughput setup because the methodology is built on the multi-well plate format along with the hydrogel which is compatible with liquid-handling equipment. Thus, all these factors taken together make this 3D platform a scalable *in-vitro* model that is ideal for drug discovery and testing and can be valuable for use in both academic and industrial labs.

Research Contributions

The originality of this Ph.D. thesis has been to investigate migration and drug response of varyingly aggressive breast cancer cell lines and non-cancerous breast epithelial cells by utilizing the innovative PP-3D-S model. The results of this part of the research were published in the journal of "Plasma Processes and Polymers-", 2022, p. e2100206, under the title of "A novel 3D in vitro tissue model for bone-metastasized breast cancer: A preclinical tool in drug discovery and testing" [41].

7.3 Evaluation of migration and drug sensitivity/resistance of patient-derived metastasized cancer cells using the PP-3D-S model

Treatment of advanced cancer is challenging due to metastasis and drug resistance; thus, chemotherapy drug discovery and development are essential. In this research, with the aim of developing a realistic bone-tumor tissue interface model, we examined our PP-3D-S model for migration and drug screening assays using patient-derived spine-metastasis tumor cells (isolated from bony spinal metastases including Bone Met Breast (BMB), Bone Met Kidney (BMK), Bone Met Lung (BML) and Bone Met Prostate (BMP)). All were embedded in AG hydrogel, like an organoid, while having an interface with human primary osteoblasts pre-seeded into the plasma-treated nanofibrous scaffolds (details in **Chapter 6**).

Therefore, *the fifth hypothesis was that the 3D interface model can realistically simulate different tissue-tumor microenvironments by incorporating different primary stromal cells co-cultured*

with various patient-derived metastasized tumor cells; therefore, it can become a platform for drug screening in personalized cancer therapy.

We carried out a series of migration assays for all of the above-mentioned BMX bone-metastasized cells and observed considerable degrees of migration and invasion toward the target bone tissue after 5 days of incubation time; similar migratory behaviour was observed for breast, prostate, lung, kidney cases individually at certain time points, as expected from very aggressive tumor cells. However, the rate of migration and potential growth of patient-derived BMX cells were found to be less than their equivalent cell lines at the same time points, such as the bone-metastasized breast cells compared with their counterpart MDA-MB 231, due to the intrinsically different physiological characteristics of primary cells and immortalized cell lines.

The end goal of the PP-3D-S model's use with patient-derived metastasized tumor cells is drug screening tests for personalized treatment. Thus, we first screened BMX cells with Dox and found remarkable resistance of those patient-derived bone metastasized tumor cells to Dox compared with their counterpart cell lines at the same drug concentrations. In other words, Dox was not able to induce patient-derived cells to initiate apoptosis by increasing the doses of Dox by 1 µM, while their equivalent cell lines indicated consistent drug sensitivity at the same range of drug concentration. Thus, we observed substantial differences in response to chemotherapeutics of the immortalized cell lines versus patient-derived cells.

We also changed the type of drugs to investigate and compare their respective efficacy in screening experiments on either BMB or MDA-MB 231, with increasing concentrations of Dox and Cisplatin (Cis). First, by increasing Dox concentrations from 1 to 5 µM, BMB cells showed a drug sensitivity IC50 value of 1.52 µM while the MDA-MB 231 value was IC50=0.36 µM by exposure to the same Dox concentrations. This large difference in IC50 values proved clear differences in drug sensitivity/resistance of specific patient cells and their counterpart cell line. We observed a similar trend when repeating the test with Cis, but IC50 shifted to much higher values, 7.28 and 28.37 µM for MDA-MB 231 and BMB cells, respectively. These results evidently confirmed that those two drugs have substantially different chemosensitivities, both cells being much more sensitive to Dox than to Cis at the same drug concentrations.

Consequently, chemotherapy drugs that have influence on cell division, proliferation, and intra-cellular signalling pathways, have potential to induce specific molecular and phenotypical changes for each particular cell type [365], and this fact should be both transcriptionally and biochemically verified in future studies, especially for cell crosstalk.

The literature extensively reported about well-known and critical biological mechanisms occurring in cancer metastasis, namely Epithelial-to-Mesenchymal Transition (EMT) and the reverse process (MET), in which epithelial cells go through multiple biochemical and morphological changes; eventually a transition between epithelial and mesenchymal phenotypes take place for those cells during invasion and metastasis [374-376]. Among the various EMT biomarkers proposed in the literature, including cell-surface proteins (E-cadherin, N-cadherin) [377-379], cytoskeletal markers (Vimentin) [380], extracellular proteins (Fibronectin) [381], and transcription factors (Snail, Slug, Zeb, Twist, Sox) [382-385], we examined possible expression of E-cadherin, N-cadherin, Twist1, Slug, Snail1, and Sox2 in our 3D model cultured with MDA-MB 231 breast cancer cells for 5 days, to validate the possible role of EMT mechanism. All those markers are typically upregulated as mesenchymal markers through cancer metastasis except E-cadherin (known as an epithelial indicator) [375, 376]. However, even though we observed increased expression of mesenchymal markers (N-cadherin, Slug, and Sox2) by tumor cells that had migrated onto the mats, compared with the cells that remained in the hydrogel, the epithelial marker (E-cadherin) was also greatly expressed. It might be attributed to the fact that those migrated tumor cells not only lose their E-cadherin receptors while leaving the gel (gaining mesenchymal phenotype during EMT), but that they also may have reverted to their origins, (epithelial characteristics, termed MET mechanism) which occur in the second environment (mat) and started to grow and proliferate there over 5 days of culture [386]. One major limitation is that we only examined one tumor cell line and one time point. Future work will therefore have to investigate a time course with several tumor cell types to better understand the impact of EMT on our 3D model, an important process for physiological representation. However, besides EMT/MET, alternative mechanisms for tumor invasion and metastases (collective or cluster-based migration, mesenchymal invasion, and crawling-like cell movement) [387] have also been proposed in the literature, which therefore represents an interesting avenue to explore.

Thus, genetic and epigenetic screening under the different conditions may also be appropriate in this case.

The outcomes above clearly highlight that our 3D bone-metastasized model (PP-3D-S), a customizable and flexible platform, is compatible with a broad range of either immortalized cell lines or patient-derived metastatic cells. It can monitor and possibly predict cancer progression and realistically represent cancer cell migration/invasion processes like EMT. Our model has also significant potential value for customized/personalized cancer therapy through screening different patient-derived metastasis cells with a variety of current or newly established chemotherapeutic drugs for specific cancer patients.

Research Contributions

The originality of this part of the current Ph.D. thesis was to simulate a realistic bone-tumor tissue microenvironment utilizing the developed PP-3D-S model, to present an interface between bone stroma and tumor tissue, so as to investigate migration and drug response of varying patient-derived bone-metastasized cells. The results of this part of the research have been submitted to the journal of "Biomedical Engineering Advances", under the title of "A 3D, compartmental tumor-stromal microenvironment model of patient-derived bone metastasis".

CHAPTER 8 CONCLUSIONS AND RECOMMENDATIONS

To conclude, this study draws on an interdisciplinary approach, at the interface of materials science, engineering, and biology, mainly focused on cancer studies. In this PhD thesis, we demonstrated the strong potential of combining electrospinning, plasma treatment and hydrogel technologies to develop an innovative 3D *in vitro* co-culture model, so-called PP-3D-S, which can quite accurately mimic the complexity and heterogeneity of human tumor microenvironment. The model enables observing motility and invasion of metastatic cancer cells in migration assays and is also considered a suitable tool for anti-cancer drug screening applications. The improvements proposed in this research will create significant contributions to overcome knowledge gaps in current 3D cancer models, which lack the capability to engineer separate stromal compartments and tumor masses. Indeed, our invented 3D model is based upon two compartments comprising separated stromal and tumor cells which simulate a biomimetic stroma-tumor interface, hence a more realistic human cancer microenvironment. The PP-3D-S model has also significant potential as a customizable, flexible platform with finely tailored morphological, biophysical, mechanical, and surface properties suited to a variety of tissues and cancer types. We proved that this 3D co-culture model is sensitive to a broad range of immortalized and primary cell types through a proof-of-concept using two different chemotherapeutics: it has enabled screening primary clinical samples such as patient-derived metastasized cells with two anti-cancer drugs. Therefore, it will prove to have great value to assess effectiveness of current and newly developed chemotherapeutic drugs, to approach the goal of personalized cancer therapy and improve clinical outcomes for patients suffering from cancer.

Recommendation for future research

Although the results of the current PhD research are promising and encouraging, some important subjects have been highlighted and warrant further research.

- Investigation of specific biological aspects concerning the presence of either fibroblasts or osteoblasts used as stromal cells in the model and subsequent signaling pathways between

stromal and tumor cells within the co-culture 3D interface model is a priority for further study.

- It is also necessary to address the induction effect of chemotherapy drugs on the molecular and phenotypical states of both immortalized cell lines and patient-derived cells before and after treatment by conducting more biological assays in depth, including evaluation of targeted proteins and gene expression profiles.

- In order to accurately present a realistic tissue-tumor model and to obtain a more physiologically relevant tumor microenvironment, we would recommend modifying the PP-3D-S model specially to have more efficient drug screening experiments as follows:

  i. Beside fibroblasts/osteoblasts, two more stromal cell types, endothelial and immune cells, can be seeded in the stromal compartment of the 3D system, co-cultured with tumor cells in the second compartment (in the case of using patient-derived tumor cells, including matched patient derived stromal cells may be of benefit here as well); this might more accurately replicate the tumor microenvironment, having diverse population of stromal cells around tumor cells. In the case of seeding mats with osteoblasts, it might be beneficial to increase the culture time to 3 weeks before adding the hydrogel containing tumor cells, so as to encounter a mature bone tissue with desired mineralization and calcified matrix.

  ii. A thin layer of collagen type IV (the main collagen component of the basement membrane) could be coated onto the pre-seeded mat as a barrier to separate the epithelium (tumor mass) from the stromal compartment, as in a natural tumor microenvironment.

  iii. As primary cells, particularly the patient-derived ones in our case, are difficult to grow in 3D culture, it is worth using more specifically developed media suitable

for all cell types in our co-culture model, by either incorporating appropriate growth factors, cytokines, and soluble factors into the stroma/tumor compartments to support cell growth or immobilization of those reagents to the hydrogel/mat parts, and/or encapsulation in carriers to sustainably release them in the culture system.

iv. It might be beneficial to fabricate the hydrogel (tumor compartment) by electrospinning, producing electrospun nanofiber mats based on alginate-gelatin or even other specific proteins such as laminin, fibronectin, collagen, etc. to better mimic the natural ECM environment of tumor cells.

v. Since the PP-3D-S model is applied under static cell culture conditions, it might be more realistic to place it in a bioreactor with fluid flow-induced shear stress, so as to better mimic the dynamic physiological conditions of the natural microenvironment. Also, to ensure mimicking the right interface in the model, at the same time, a broader range of substrate stiffness may be examined and then their effect on gene expression profile of the "stromal" compartment can be investigated.

REFERENCES

[1] C. Public Health Agency of, C. Statistics, S. Canadian Cancer, and r. provincial/territorial cancer, "Release notice - Canadian Cancer Statistics 2019," (in engfre), *Health Promot Chronic Dis Prev Can*, vol. 39, no. 8-9, p. 255, Sep 2021, doi: 10.24095/hpcdp.39.8/9.04. Avis de publication - Statistiques canadiennes sur le cancer 2019.

[2] R. Coleman, "Metastatic bone disease: clinical features, pathophysiology and treatment strategies," *Cancer treatment reviews*, vol. 27, no. 3, pp. 165-176, 2001.

[3] B. R. Zetter, "Angiogenesis and tumor metastasis," *Annual review of medicine*, vol. 49, no. 1, pp. 407-424, 1998.

[4] R. E. Coleman, "Skeletal complications of malignancy," *Cancer: Interdisciplinary International Journal of the American Cancer Society*, vol. 80, no. S8, pp. 1588-1594, 1997.

[5] C. L. Shapiro and A. Recht, "Side effects of adjuvant treatment of breast cancer," *New England Journal of Medicine*, vol. 344, no. 26, pp. 1997-2008, 2001.

[6] D. W. Thomas, J. Burns, J. Audette, A. Carroll, C. Dow-Hygelund, and M. Hay, "Clinical development success rates 2006–2015," *BIO Industry Analysis*, vol. 1, p. 16, 2016.

[7] H. Dowden and J. Munro, "Trends in clinical success rates and therapeutic focus," *Nature Reviews Drug Discovery*, vol. 18, no. 7, pp. 495-497, 2019.

[8] S. Pretorius, "Phase III trial failures: costly, but preventable," *Applied Clinical Trials*, vol. 25, no. 8/9, p. 36, 2016.

[9] K. Duval *et al.*, "Modeling physiological events in 2D vs. 3D cell culture," *Physiology*, vol. 32, no. 4, pp. 266-277, 2017.

[10] J. B. Kim, "Three-dimensional tissue culture models in cancer biology," in *Seminars in cancer biology*, 2005, vol. 15, no. 5: Elsevier, pp. 365-377.

[11] D. Herrmann *et al.*, "Three-dimensional cancer models mimic cell–matrix interactions in the tumour microenvironment," *Carcinogenesis*, vol. 35, no. 8, pp. 1671-1679, 2014.

[12] E. Knight and S. Przyborski, "Advances in 3D cell culture technologies enabling tissue-like structures to be created in vitro," *Journal of anatomy*, vol. 227, no. 6, pp. 746-756, 2015.

[13] J. W. Haycock, "3D cell culture: a review of current approaches and techniques," in *3D cell culture*: Springer, 2011, pp. 1-15.

[14] J. B. Kim, R. Stein, and M. J. O'hare, "Three-dimensional in vitro tissue culture models of breast cancer—a review," *Breast cancer research and treatment*, vol. 85, no. 3, pp. 281-291, 2004.

[15] V. Mironov, T. Trusk, V. Kasyanov, S. Little, R. Swaja, and R. Markwald, "Biofabrication: a 21st century manufacturing paradigm," *Biofabrication*, vol. 1, no. 2, p. 022001, 2009.

[16] L. Moroni *et al.*, "Biofabrication: a guide to technology and terminology," *Trends in biotechnology,* vol. 36, no. 4, pp. 384-402, 2018.

[17] L. Moroni *et al.*, "Biofabrication strategies for 3D in vitro models and regenerative medicine," *Nature Reviews Materials,* vol. 3, no. 5, pp. 21-37, 2018.

[18] L. Gu and D. J. Mooney, "Biomaterials and emerging anticancer therapeutics: engineering the microenvironment," *Nature Reviews Cancer,* vol. 16, no. 1, p. 56, 2016.

[19] M. P. Nikolova and M. S. Chavali, "Recent advances in biomaterials for 3D scaffolds: A review," *Bioactive materials,* vol. 4, pp. 271-292, 2019.

[20] E. Gottfried, L. A. Kunz-Schughart, R. Andreesen, and M. Kreutz, "Brave little world: spheroids as an in vitro model to study tumor-immune-cell interactions," *Cell Cycle,* vol. 5, no. 7, pp. 691-695, 2006.

[21] L. A. Kunz-Schughart, J. P. Freyer, F. Hofstaedter, and R. Ebner, "The use of 3-D cultures for high-throughput screening: the multicellular spheroid model," *Journal of biomolecular screening,* vol. 9, no. 4, pp. 273-285, 2004.

[22] P. Zhuang, A. X. Sun, J. An, C. K. Chua, and S. Y. Chew, "3D neural tissue models: From spheroids to bioprinting," *Biomaterials,* vol. 154, pp. 113-133, 2018.

[23] T. Ishiguro, H. Ohata, A. Sato, K. Yamawaki, T. Enomoto, and K. Okamoto, "Tumor-derived spheroids: relevance to cancer stem cells and clinical applications," *Cancer science,* vol. 108, no. 3, pp. 283-289, 2017.

[24] P. S. Thakuri, C. Liu, G. D. Luker, and H. Tavana, "Biomaterials-Based Approaches to Tumor Spheroid and Organoid Modeling," *Adv Healthc Mater,* Dec 4 2017, doi: 10.1002/adhm.201700980.

[25] J. Kondo and M. Inoue, "Application of Cancer Organoid Model for Drug Screening and Personalized Therapy," *Cells,* vol. 8, no. 5, May 17 2019, doi: 10.3390/cells8050470.

[26] Y. H. Xu, A. Ajji, and M. C. Heuzey, "Response behaviors and mechanical strength of thermal responsive hydrogels fabricated by electrospinning," (in English), *Polymer,* vol. 183, Nov 21 2019, doi: UNSP 12188010.1016/j.polymer.2019.121880.

[27] H. Savoji, A. Hadjizadeh, M. Maire, A. Ajji, M. R. Wertheimer, and S. Lerouge, "Electrospun nanofiber scaffolds and plasma polymerization: a promising combination towards complete, stable endothelial lining for vascular grafts," *Macromol Biosci,* vol. 14, no. 8, pp. 1084-95, Aug 2014, doi: 10.1002/mabi.201300545.

[28] J. C. Bridge *et al.*, "Electrospun gelatin-based scaffolds as a novel 3D platform to study the function of contractile smooth muscle cells in vitro," *Biomedical Physics & Engineering Express,* vol. 4, no. 4, p. 045039, 2018.

[29] S. Chen, S. K. Boda, S. K. Batra, X. Li, and J. Xie, "Emerging roles of electrospun nanofibers in cancer research," *Advanced healthcare materials,* vol. 7, no. 6, p. 1701024, 2018.

[30] S. Chen, R. Li, X. Li, and J. Xie, "Electrospinning: An enabling nanotechnology platform for drug delivery and regenerative medicine," *Advanced drug delivery reviews,* vol. 132, pp. 188-213, 2018.

[31] D. R. Nisbet, J. S. Forsythe, W. Shen, D. I. Finkelstein, and M. K. Horne, "A review of the cellular response on electrospun nanofibers for tissue engineering," *Journal of biomaterials applications,* vol. 24, no. 1, pp. 7-29, 2009.

[32] Q. P. Pham, U. Sharma, and A. G. Mikos, "Electrospinning of polymeric nanofibers for tissue engineering applications: a review," *Tissue engineering,* vol. 12, no. 5, pp. 1197-1211, 2006.

[33] Y. Zhou, J. Chyu, and M. Zumwalt, "Recent progress of fabrication of cell scaffold by electrospinning technique for articular cartilage tissue engineering," *International journal of biomaterials,* vol. 2018, 2018.

[34] H. Tian, Z. Tang, X. Zhuang, X. Chen, and X. Jing, "Biodegradable synthetic polymers: Preparation, functionalization and biomedical application," *Progress in Polymer Science,* vol. 37, no. 2, pp. 237-280, 2012.

[35] J. M. Goddard and J. Hotchkiss, "Polymer surface modification for the attachment of bioactive compounds," *Progress in polymer science,* vol. 32, no. 7, pp. 698-725, 2007.

[36] K. S. Siow, L. Britcher, S. Kumar, and H. J. Griesser, "Plasma methods for the generation of chemically reactive surfaces for biomolecule immobilization and cell colonization-a review," *Plasma processes and polymers,* vol. 3, no. 6-7, pp. 392-418, 2006.

[37] T. Zhou *et al.,* "Surface functionalization of biomaterials by radical polymerization," *Progress in Materials Science,* vol. 83, pp. 191-235, 2016.

[38] M. W. Tibbitt and K. S. Anseth, "Hydrogels as extracellular matrix mimics for 3D cell culture," *Biotechnology and bioengineering,* vol. 103, no. 4, pp. 655-663, 2009.

[39] P. Worthington, D. J. Pochan, and S. A. Langhans, "Peptide hydrogels–versatile matrices for 3D cell culture in cancer medicine," *Frontiers in oncology,* vol. 5, p. 92, 2015.

[40] M. M. Garakani *et al.,* "A novel 3D co-culture platform for integrating tissue interfaces for tumor growth, migration and therapeutic sensitivity:“PP-3D-S”," *Materials Science and Engineering: C,* p. 112566, 2021.

[41] M. Mohseni Garakani, M. E. Cooke, M. R. Wertheimer, D. H. Rosenzweig, and A. Ajji, "A novel 3D in vitro tissue model for bone-metastasized breast cancer: A preclinical tool in drug discovery and testing," *Plasma Processes and Polymers,* p. e2100206.

[42] K. Ganesh and J. Massagué, "Targeting metastatic cancer," *Nature medicine,* vol. 27, no. 1, pp. 34-44, 2021.

[43] J. Fares, M. Y. Fares, H. H. Khachfe, H. A. Salhab, and Y. Fares, "Molecular principles of metastasis: a hallmark of cancer revisited," *Signal transduction and targeted therapy,* vol. 5, no. 1, pp. 1-17, 2020.

[44] T. N. Seyfried and L. C. Huysentruyt, "On the origin of cancer metastasis," *Critical Reviews™ in Oncogenesis,* vol. 18, no. 1-2, 2013.

[45] M. Bacac and I. Stamenkovic, "Metastatic cancer cell," *Annu. Rev. Pathol. Mech. Dis.*, vol. 3, pp. 221-247, 2008.

[46] F. R. Balkwill, M. Capasso, and T. Hagemann, "The tumor microenvironment at a glance," *Journal of cell science*, vol. 125, no. 23, pp. 5591-5596, 2012.

[47] M. Wang *et al.*, "Role of tumor microenvironment in tumorigenesis," *Journal of Cancer*, vol. 8, no. 5, p. 761, 2017.

[48] R. Baghban *et al.*, "Tumor microenvironment complexity and therapeutic implications at a glance," *Cell Communication and Signaling*, vol. 18, no. 1, pp. 1-19, 2020.

[49] D. Hanahan and L. M. Coussens, "Accessories to the crime: functions of cells recruited to the tumor microenvironment," *Cancer cell*, vol. 21, no. 3, pp. 309-322, 2012.

[50] J. A. Joyce and J. W. Pollard, "Microenvironmental regulation of metastasis," *Nature reviews cancer*, vol. 9, no. 4, pp. 239-252, 2009.

[51] F. Macedo *et al.*, "Bone metastases: an overview," *Oncology reviews*, vol. 11, no. 1, 2017.

[52] C. S. C. American Cancer Society. http://cancerstatisticscenter.cancer.org. (accessed 2021).

[53] G. D. Roodman, "Mechanisms of bone metastasis," *New England journal of medicine*, vol. 350, no. 16, pp. 1655-1664, 2004.

[54] B. Cady, "Basic principles in surgical oncology," *Archives of Surgery*, vol. 132, no. 4, pp. 338-346, 1997.

[55] Q. D. Chu, J. F. Gibbs, and G. B. Zibari, *Surgical oncology: a practical and comprehensive approach*. Springer, 2014.

[56] F. Riedel *et al.*, "Is mastectomy oncologically safer than breast-conserving treatment in early breast cancer," *Breast Care*, vol. 12, no. 6, pp. 385-390, 2017.

[57] G. Delaney, S. Jacob, C. Featherstone, and M. Barton, "The role of radiotherapy in cancer treatment: estimating optimal utilization from a review of evidence-based clinical guidelines," *Cancer: Interdisciplinary International Journal of the American Cancer Society*, vol. 104, no. 6, pp. 1129-1137, 2005.

[58] P. Nygren, "What is cancer chemotherapy?," *Acta Oncologica*, vol. 40, no. 2-3, pp. 166-174, 2001.

[59] B. Liu, L. Ezeogu, L. Zellmer, B. Yu, N. Xu, and D. Joshua Liao, "Protecting the normal in order to better kill the cancer," *Cancer medicine*, vol. 4, no. 9, pp. 1394-1403, 2015.

[60] X. Lou, J. Zhang, S. Liu, X. Lou, and D. J. Liao, "The other side of the coin: The tumor-suppressive aspect of oncogenes and the oncogenic aspect of tumor-suppressive genes, such as those along the CCND–CDK4/6–RB axis," *Cell Cycle*, vol. 13, no. 11, pp. 1677-1693, 2014.

[61] A. E. Kayl and C. A. Meyers, "Side-effects of chemotherapy and quality of life in ovarian and breast cancer patients," *Current opinion in obstetrics and gynecology*, vol. 18, no. 1, pp. 24-28, 2006.

[62] N. E. Avis, S. Crawford, and J. Manuel, "Quality of life among younger women with breast cancer," *Journal of Clinical Oncology,* vol. 23, no. 15, pp. 3322-3330, 2005.

[63] E. Dickens and S. Ahmed, "Principles of cancer treatment by chemotherapy," *Surgery (Oxford),* vol. 36, no. 3, pp. 134-138, 2018.

[64] A. Arina, S. I. Gutiontov, and R. R. Weichselbaum, "Radiotherapy and immunotherapy for cancer: From “systemic” to “multisite”," *Clinical Cancer Research,* vol. 26, no. 12, pp. 2777-2782, 2020.

[65] J. A. Trapani and P. K. Darcy, "Immunotherapy of cancer," *Australian family physician,* vol. 46, no. 4, pp. 194-198, 2017.

[66] M. Drãgãnescu and C. Carmocan, "Hormone therapy in breast cancer," *Chirurgia,* vol. 112, no. 4, pp. 413-17, 2017.

[67] C.-N. Qian, Y. Mei, and J. Zhang, "Cancer metastasis: issues and challenges," (in eng), *Chin J Cancer,* vol. 36, no. 1, pp. 38-38, 2017, doi: 10.1186/s40880-017-0206-7.

[68] W.-Z. Qiu, P.-Y. Huang, J.-L. Shi, H.-Q. Xia, C. Zhao, and K.-J. Cao, "Neoadjuvant chemotherapy plus intensity-modulated radiotherapy versus concurrent chemoradiotherapy plus adjuvant chemotherapy for the treatment of locoregionally advanced nasopharyngeal carcinoma: a retrospective controlled study," (in eng), *Chin J Cancer,* vol. 35, pp. 2-2, 2016, doi: 10.1186/s40880-015-0076-9.

[69] S. Breslin and L. O'Driscoll, "Three-dimensional cell culture: the missing link in drug discovery," *Drug Discov Today,* vol. 18, no. 5-6, pp. 240-9, Mar 2013, doi: 10.1016/j.drudis.2012.10.003.

[70] W. N. Hait, "Anticancer drug development: the grand challenges," *Nat Rev Drug Discov,* vol. 9, no. 4, pp. 253-4, Apr 2010, doi: 10.1038/nrd3144.

[71] A. B. Kunnumakkara *et al.*, "Cancer drug development: The missing links," *Exp Biol Med (Maywood),* vol. 244, no. 8, pp. 663-689, May 2019, doi: 10.1177/1535370219839163.

[72] H. HogenEsch and A. Y. Nikitin, "Challenges in pre-clinical testing of anti-cancer drugs in cell culture and in animal models," *J Control Release,* vol. 164, no. 2, pp. 183-6, Dec 10 2012, doi: 10.1016/j.jconrel.2012.02.031.

[73] Y. Imamura *et al.*, "Comparison of 2D- and 3D-culture models as drug-testing platforms in breast cancer," *Oncol Rep,* vol. 33, no. 4, pp. 1837-43, Apr 2015, doi: 10.3892/or.2015.3767.

[74] A. M. K. Law, L. Rodriguez de la Fuente, T. J. Grundy, G. Fang, F. Valdes-Mora, and D. Gallego-Ortega, "Advancements in 3D Cell Culture Systems for Personalizing Anti-Cancer Therapies," *Front Oncol,* vol. 11, p. 782766, 2021, doi: 10.3389/fonc.2021.782766.

[75] N. T. Elliott and F. Yuan, "A review of three-dimensional in vitro tissue models for drug discovery and transport studies," *J Pharm Sci,* vol. 100, no. 1, pp. 59-74, Jan 2011, doi: 10.1002/jps.22257.

[76] S. Martinez-Pacheco and L. O'Driscoll, "Pre-Clinical In Vitro Models Used in Cancer Research: Results of a Worldwide Survey," *Cancers (Basel),* vol. 13, no. 23, Nov 30 2021, doi: 10.3390/cancers13236033.

[77] G. Damia and M. D'Incalci, "Contemporary pre-clinical development of anticancer agents--what are the optimal preclinical models?," *Eur J Cancer,* vol. 45, no. 16, pp. 2768-81, Nov 2009, doi: 10.1016/j.ejca.2009.08.008.

[78] M. Suggitt and M. C. Bibby, "50 years of preclinical anticancer drug screening: empirical to target-driven approaches," *Clin Cancer Res,* vol. 11, no. 3, pp. 971-81, Feb 1 2005. [Online]. Available: https://www.ncbi.nlm.nih.gov/pubmed/15709162.

[79] M. W. Lee *et al.*, "Current methods in translational cancer research," *Cancer Metastasis Rev,* vol. 40, no. 1, pp. 7-30, Mar 2021, doi: 10.1007/s10555-020-09931-5.

[80] S. A. Langhans, "Three-Dimensional in Vitro Cell Culture Models in Drug Discovery and Drug Repositioning," *Front Pharmacol,* vol. 9, p. 6, 2018, doi: 10.3389/fphar.2018.00006.

[81] Y. Fang and R. M. Eglen, "Three-Dimensional Cell Cultures in Drug Discovery and Development," *SLAS Discov,* vol. 22, no. 5, pp. 456-472, Jun 2017, doi: 10.1177/1087057117696795.

[82] E. T. Verjans, J. Doijen, W. Luyten, B. Landuyt, and L. Schoofs, "Three-dimensional cell culture models for anticancer drug screening: Worth the effort?," *J Cell Physiol,* vol. 233, no. 4, pp. 2993-3003, Apr 2018, doi: 10.1002/jcp.26052.

[83] J. B. Kim, R. Stein, and M. J. O'Hare, "Three-dimensional in vitro tissue culture models of breast cancer-- a review," *Breast Cancer Res Treat,* vol. 85, no. 3, pp. 281-91, Jun 2004, doi: 10.1023/B:BREA.0000025418.88785.2b.

[84] J. B. Kim, "Three-dimensional tissue culture models in cancer biology," *Semin Cancer Biol,* vol. 15, no. 5, pp. 365-77, Oct 2005, doi: 10.1016/j.semcancer.2005.05.002.

[85] I. Szadvari, O. Krizanova, and P. Babula, "Athymic nude mice as an experimental model for cancer treatment," *Physiol Res,* vol. 65, no. Suppl 4, pp. S441-S453, Dec 21 2016, doi: 10.33549/physiolres.933526.

[86] A. H. Jinnah, B. C. Zacks, C. U. Gwam, and B. A. Kerr, "Emerging and Established Models of Bone Metastasis," *Cancers (Basel),* vol. 10, no. 6, Jun 1 2018, doi: 10.3390/cancers10060176.

[87] C. P. Day, G. Merlino, and T. Van Dyke, "Preclinical mouse cancer models: a maze of opportunities and challenges," *Cell,* vol. 163, no. 1, pp. 39-53, Sep 24 2015, doi: 10.1016/j.cell.2015.08.068.

[88] Q. E. Yang, "Human cancer xenografts in immunocompromised mice provide an advanced genuine tumor model for research and drug development-A revisit of murine models for human cancers," *Biochim Biophys Acta Gen Subj,* vol. 1865, no. 8, p. 129929, Aug 2021, doi: 10.1016/j.bbagen.2021.129929.

[89] E. Yada, S. Wada, S. Yoshida, and T. Sasada, "Use of patient-derived xenograft mouse models in cancer research and treatment," *Future Sci OA,* vol. 4, no. 3, p. FSO271, Mar 2018, doi: 10.4155/fsoa-2017-0136.

[90] L. Thibaudeau *et al.*, "A tissue-engineered humanized xenograft model of human breast cancer metastasis to bone," *Dis Model Mech,* vol. 7, no. 2, pp. 299-309, Feb 2014, doi: 10.1242/dmm.014076.

[91] R. Laranga, S. Duchi, T. Ibrahim, A. N. Guerrieri, D. M. Donati, and E. Lucarelli, "Trends in Bone Metastasis Modeling," *Cancers (Basel),* vol. 12, no. 8, Aug 17 2020, doi: 10.3390/cancers12082315.

[92] J. Ding *et al.*, "Electrospun polymer biomaterials," *Progress in Polymer Science,* vol. 90, pp. 1-34, 2019.

[93] V. E. Santo, S. P. Rebelo, M. F. Estrada, P. M. Alves, E. Boghaert, and C. Brito, "Drug screening in 3D in vitro tumor models: overcoming current pitfalls of efficacy read-outs," *Biotechnol J,* vol. 12, no. 1, Jan 2017, doi: 10.1002/biot.201600505.

[94] E. L. S. Fong, T. B. Toh, H. Yu, and E. K. Chow, "3D Culture as a Clinically Relevant Model for Personalized Medicine," *SLAS Technol,* vol. 22, no. 3, pp. 245-253, Jun 2017, doi: 10.1177/2472630317697251.

[95] P. Krzyszczyk *et al.*, "The growing role of precision and personalized medicine for cancer treatment," *Technology (Singap World Sci),* vol. 6, no. 3-4, pp. 79-100, Sep-Dec 2018, doi: 10.1142/S2339547818300020.

[96] K. Tanner and M. M. Gottesman, "Beyond 3D culture models of cancer," *Sci Transl Med,* vol. 7, no. 283, p. 283ps9, Apr 15 2015, doi: 10.1126/scitranslmed.3009367.

[97] H. K. Dhiman, A. R. Ray, and A. K. Panda, "Three-dimensional chitosan scaffold-based MCF-7 cell culture for the determination of the cytotoxicity of tamoxifen," *Biomaterials,* vol. 26, no. 9, pp. 979-86, Mar 2005, doi: 10.1016/j.biomaterials.2004.04.012.

[98] H. Karlsson, M. Fryknas, R. Larsson, and P. Nygren, "Loss of cancer drug activity in colon cancer HCT-116 cells during spheroid formation in a new 3-D spheroid cell culture system," *Exp Cell Res,* vol. 318, no. 13, pp. 1577-85, Aug 1 2012, doi: 10.1016/j.yexcr.2012.03.026.

[99] O. Candini *et al.*, "A Novel 3D In Vitro Platform for Pre-Clinical Investigations in Drug Testing, Gene Therapy, and Immuno-oncology," *Sci Rep,* vol. 9, no. 1, p. 7154, May 9 2019, doi: 10.1038/s41598-019-43613-9.

[100] Y. Miki, K. Ono, S. Hata, T. Suzuki, H. Kumamoto, and H. Sasano, "The advantages of co-culture over mono cell culture in simulating in vivo environment," *J Steroid Biochem Mol Biol,* vol. 131, no. 3-5, pp. 68-75, Sep 2012, doi: 10.1016/j.jsbmb.2011.12.004.

[101] S. Sieh, A. V. Taubenberger, M. L. Lehman, J. A. Clements, C. C. Nelson, and D. W. Hutmacher, "Paracrine interactions between LNCaP prostate cancer cells and bioengineered bone in 3D in vitro culture reflect molecular changes during bone metastasis," *Bone,* vol. 63, pp. 121-31, Jun 2014, doi: 10.1016/j.bone.2014.02.001.

[102] F. Amirghasemi, E. Adjei-Sowah, B. A. Pockaj, and M. Nikkhah, "Microengineered 3D Tumor Models for Anti-Cancer Drug Discovery in Female-Related Cancers," *Ann Biomed Eng,* vol. 49, no. 8, pp. 1943-1972, Aug 2021, doi: 10.1007/s10439-020-02704-9.

[103] N. Gupta, J. R. Liu, B. Patel, D. E. Solomon, B. Vaidya, and V. Gupta, "Microfluidics-based 3D cell culture models: Utility in novel drug discovery and delivery research," *Bioeng Transl Med,* vol. 1, no. 1, pp. 63-81, Mar 2016, doi: 10.1002/btm2.10013.

[104] L. B. Tofani, J. P. Abriata, M. T. Luiz, J. M. Marchetti, and K. Swiech, "Establishment and characterization of an in vitro 3D ovarian cancer model for drug screening assays," *Biotechnol Prog,* vol. 36, no. 6, p. e3034, Nov 2020, doi: 10.1002/btpr.3034.

[105] E. Knight and S. Przyborski, "Advances in 3D cell culture technologies enabling tissue-like structures to be created in vitro," *J Anat,* vol. 227, no. 6, pp. 746-56, Dec 2015, doi: 10.1111/joa.12257.

[106] E. C. Costa, A. F. Moreira, D. de Melo-Diogo, V. M. Gaspar, M. P. Carvalho, and I. J. Correia, "3D tumor spheroids: an overview on the tools and techniques used for their analysis," *Biotechnol Adv,* vol. 34, no. 8, pp. 1427-1441, Dec 2016, doi: 10.1016/j.biotechadv.2016.11.002.

[107] E. Gheytanchi *et al.,* "Morphological and molecular characteristics of spheroid formation in HT-29 and Caco-2 colorectal cancer cell lines," *Cancer Cell Int,* vol. 21, no. 1, p. 204, Apr 13 2021, doi: 10.1186/s12935-021-01898-9.

[108] T. Das *et al.,* "Empirical chemosensitivity testing in a spheroid model of ovarian cancer using a microfluidics-based multiplex platform," *Biomicrofluidics,* vol. 7, no. 1, p. 11805, 2013, doi: 10.1063/1.4774309.

[109] V. Brancato, J. M. Oliveira, V. M. Correlo, R. L. Reis, and S. C. Kundu, "Could 3D models of cancer enhance drug screening?," *Biomaterials,* vol. 232, p. 119744, Feb 2020, doi: 10.1016/j.biomaterials.2019.119744.

[110] D. Herrmann *et al.,* "Three-dimensional cancer models mimic cell-matrix interactions in the tumour microenvironment," *Carcinogenesis,* vol. 35, no. 8, pp. 1671-9, Aug 2014, doi: 10.1093/carcin/bgu108.

[111] M. Shang, R. H. Soon, C. T. Lim, B. L. Khoo, and J. Han, "Microfluidic modelling of the tumor microenvironment for anti-cancer drug development," *Lab Chip,* vol. 19, no. 3, pp. 369-386, Jan 29 2019, doi: 10.1039/c8lc00970h.

[112] C. W. Chi, A. R. Ahmed, Z. Dereli-Korkut, and S. Wang, "Microfluidic cell chips for high-throughput drug screening," *Bioanalysis,* vol. 8, no. 9, pp. 921-37, May 2016, doi: 10.4155/bio-2016-0028.

[113] M. Marimuthu *et al.,* "Multi-size spheroid formation using microfluidic funnels," *Lab Chip,* vol. 18, no. 2, pp. 304-314, Jan 16 2018, doi: 10.1039/c7lc00970d.

[114] H. C. Chang *et al.,* "Multilayer architecture microfluidic network array for combinatorial drug testing on 3D-cultured cells," *Biofabrication,* vol. 11, no. 3, p. 035024, Jun 4 2019, doi: 10.1088/1758-5090/ab1f52.

[115] F. Eduati *et al.*, "A microfluidics platform for combinatorial drug screening on cancer biopsies," *Nat Commun*, vol. 9, no. 1, p. 2434, Jun 22 2018, doi: 10.1038/s41467-018-04919-w.

[116] N. Dhiman, P. Kingshott, H. Sumer, C. S. Sharma, and S. N. Rath, "On-chip anticancer drug screening - Recent progress in microfluidic platforms to address challenges in chemotherapy," *Biosens Bioelectron*, vol. 137, pp. 236-254, Jul 15 2019, doi: 10.1016/j.bios.2019.02.070.

[117] E. A. Aisenbrey and W. L. Murphy, "Synthetic alternatives to Matrigel," *Nat Rev Mater*, vol. 5, no. 7, pp. 539-551, Jul 2020, doi: 10.1038/s41578-020-0199-8.

[118] G. Benton, I. Arnaoutova, J. George, H. K. Kleinman, and J. Koblinski, "Matrigel: from discovery and ECM mimicry to assays and models for cancer research," *Adv Drug Deliv Rev*, vol. 79-80, pp. 3-18, Dec 15 2014, doi: 10.1016/j.addr.2014.06.005.

[119] L. Gu and D. J. Mooney, "Biomaterials and emerging anticancer therapeutics: engineering the microenvironment," *Nat Rev Cancer*, vol. 16, no. 1, pp. 56-66, Jan 2016, doi: 10.1038/nrc.2015.3.

[120] M. A. Badea *et al.*, "Influence of Matrigel on Single- and Multiple-Spheroid Cultures in Breast Cancer Research," *SLAS Discov*, vol. 24, no. 5, pp. 563-578, Jun 2019, doi: 10.1177/2472555219834698.

[121] Y. L. Wang and D. Li, "Creating Complex Polyacrylamide Hydrogel Structures Using 3D Printing with Applications to Mechanobiology," *Macromol Biosci*, vol. 20, no. 7, p. e2000082, Jul 2020, doi: 10.1002/mabi.202000082.

[122] T. Li *et al.*, "Preparation and Characterization of Thermoresponsive PEG-Based Injectable Hydrogels and Their Application for 3D Cell Culture," *Biomacromolecules*, vol. 21, no. 3, pp. 1254-1263, Mar 9 2020, doi: 10.1021/acs.biomac.9b01743.

[123] S. S. Majidi, P. Slemming-Adamsen, M. Hanif, Z. Zhang, Z. Wang, and M. Chen, "Wet electrospun alginate/gelatin hydrogel nanofibers for 3D cell culture," *Int J Biol Macromol*, vol. 118, no. Pt B, pp. 1648-1654, Oct 15 2018, doi: 10.1016/j.ijbiomac.2018.07.005.

[124] T. Andersen, P. Auk-Emblem, and M. Dornish, "3D Cell Culture in Alginate Hydrogels," *Microarrays (Basel)*, vol. 4, no. 2, pp. 133-61, Mar 24 2015, doi: 10.3390/microarrays4020133.

[125] E. L. Fong *et al.*, "Hydrogel-based 3D model of patient-derived prostate xenograft tumors suitable for drug screening," *Mol Pharm*, vol. 11, no. 7, pp. 2040-50, Jul 7 2014, doi: 10.1021/mp500085p.

[126] M. Cavo, M. Caria, I. Pulsoni, F. Beltrame, M. Fato, and S. Scaglione, "A new cell-laden 3D Alginate-Matrigel hydrogel resembles human breast cancer cell malignant morphology, spread and invasion capability observed "in vivo"," *Sci Rep*, vol. 8, no. 1, p. 5333, Mar 28 2018, doi: 10.1038/s41598-018-23250-4.

[127] Y. Li and E. Kumacheva, "Hydrogel microenvironments for cancer spheroid growth and drug screening," *Sci Adv,* vol. 4, no. 4, p. eaas8998, Apr 2018, doi: 10.1126/sciadv.aas8998.

[128] C. R. Lam, H. K. Wong, S. Nai, C. K. Chua, N. S. Tan, and L. P. Tan, "A 3D biomimetic model of tissue stiffness interface for cancer drug testing," *Mol Pharm,* vol. 11, no. 7, pp. 2016-21, Jul 7 2014, doi: 10.1021/mp500059q.

[129] Y. Wang, J. Qian, T. Liu, W. Xu, N. Zhao, and A. Suo, "Electrospun PBLG/PLA nanofiber membrane for constructing in vitro 3D model of melanoma," *Mater Sci Eng C Mater Biol Appl,* vol. 76, pp. 313-318, Jul 1 2017, doi: 10.1016/j.msec.2017.03.098.

[130] T. Sun, D. Norton, R. J. McKean, J. W. Haycock, A. J. Ryan, and S. MacNeil, "Development of a 3D cell culture system for investigating cell interactions with electrospun fibers," *Biotechnol Bioeng,* vol. 97, no. 5, pp. 1318-28, Aug 1 2007, doi: 10.1002/bit.21309.

[131] M. A. Brennan *et al.*, "3D cell culture and osteogenic differentiation of human bone marrow stromal cells plated onto jet-sprayed or electrospun micro-fiber scaffolds," *Biomed Mater,* vol. 10, no. 4, p. 045019, Aug 4 2015, doi: 10.1088/1748-6041/10/4/045019.

[132] N. Bhardwaj and S. C. Kundu, "Electrospinning: a fascinating fiber fabrication technique," *Biotechnology advances,* vol. 28, no. 3, pp. 325-347, 2010.

[133] O. Hartman *et al.*, "Microfabricated electrospun collagen membranes for 3-D cancer models and drug screening applications," *Biomacromolecules,* vol. 10, no. 8, pp. 2019-2032, 2009.

[134] M. T. Nelson *et al.*, "Preferential, enhanced breast cancer cell migration on biomimetic electrospun nanofiber 'cell highways'," *BMC Cancer,* vol. 14, p. 825, Nov 10 2014, doi: 10.1186/1471-2407-14-825.

[135] X. Ma *et al.*, "3D bioprinting of functional tissue models for personalized drug screening and in vitro disease modeling," *Adv Drug Deliv Rev,* vol. 132, pp. 235-251, Jul 2018, doi: 10.1016/j.addr.2018.06.011.

[136] K. Ling *et al.*, "Bioprinting-based high-throughput fabrication of three-dimensional MCF-7 human breast cancer cellular spheroids," *Engineering,* vol. 1, no. (2), pp. 269-274, 2015, doi: 10.15302/J-ENG-2015062.

[137] A. Gebeyehu *et al.*, "Polysaccharide hydrogel based 3D printed tumor models for chemotherapeutic drug screening," *Sci Rep,* vol. 11, no. 1, p. 372, Jan 11 2021, doi: 10.1038/s41598-020-79325-8.

[138] S. Knowlton, S. Onal, C. H. Yu, J. J. Zhao, and S. Tasoglu, "Bioprinting for cancer research," *Trends Biotechnol,* vol. 33, no. 9, pp. 504-13, Sep 2015, doi: 10.1016/j.tibtech.2015.06.007.

[139] S. A. Langhans, "Three-dimensional in vitro cell culture models in drug discovery and drug repositioning," *Frontiers in pharmacology,* vol. 9, p. 6, 2018.

[140] Y. Fang and R. M. Eglen, "Three-dimensional cell cultures in drug discovery and development," *Slas discovery: Advancing Life Sciences R&D,* vol. 22, no. 5, pp. 456-472, 2017.

[141] Y.-F. Goh, I. Shakir, and R. Hussain, "Electrospun fibers for tissue engineering, drug delivery, and wound dressing," *Journal of Materials Science,* vol. 48, no. 8, pp. 3027-3054, 2013.

[142] D. Li and Y. Xia, "Electrospinning of nanofibers: reinventing the wheel?," *Advanced materials,* vol. 16, no. 14, pp. 1151-1170, 2004.

[143] I. Yalcin Enis and T. Gok Sadikoglu, "Design parameters for electrospun biodegradable vascular grafts," *Journal of Industrial Textiles,* vol. 47, no. 8, pp. 2205-2227, 2018.

[144] C. P. Barnes, S. A. Sell, E. D. Boland, D. G. Simpson, and G. L. Bowlin, "Nanofiber technology: designing the next generation of tissue engineering scaffolds," *Advanced drug delivery reviews,* vol. 59, no. 14, pp. 1413-1433, 2007.

[145] S. Ramakrishna, *An introduction to electrospinning and nanofibers*. World scientific, 2005.

[146] Z.-M. Huang, Y.-Z. Zhang, M. Kotaki, and S. Ramakrishna, "A review on polymer nanofibers by electrospinning and their applications in nanocomposites," *Composites science and technology,* vol. 63, no. 15, pp. 2223-2253, 2003.

[147] S.-H. Shin, O. Purevdorj, O. Castano, J. A. Planell, and H.-W. Kim, "A short review: Recent advances in electrospinning for bone tissue regeneration," *Journal of tissue engineering,* vol. 3, no. 1, p. 2041731412443530, 2012.

[148] P. Katta, M. Alessandro, R. Ramsier, and G. Chase, "Continuous electrospinning of aligned polymer nanofibers onto a wire drum collector," *Nano letters,* vol. 4, no. 11, pp. 2215-2218, 2004.

[149] A. Eatemadi, H. Daraee, N. Zarghami, H. Melat Yar, and A. Akbarzadeh, "Nanofiber: Synthesis and biomedical applications," *Artificial cells, nanomedicine, and biotechnology,* vol. 44, no. 1, pp. 111-121, 2016.

[150] J. Xue, T. Wu, Y. Dai, and Y. Xia, "Electrospinning and electrospun nanofibers: Methods, materials, and applications," *Chemical reviews,* vol. 119, no. 8, pp. 5298-5415, 2019.

[151] A. Greiner and J. H. Wendorff, "Electrospinning: a fascinating method for the preparation of ultrathin fibers," *Angewandte Chemie International Edition,* vol. 46, no. 30, pp. 5670-5703, 2007.

[152] Z. Li and C. Wang, *One-dimensional nanostructures: electrospinning technique and unique nanofibers*. Springer, 2013.

[153] T. Haddad, S. Noel, B. Liberelle, R. El Ayoubi, A. Ajji, and G. De Crescenzo, "Fabrication and surface modification of poly lactic acid (PLA) scaffolds with epidermal growth factor for neural tissue engineering," *Biomatter,* vol. 6, no. 1, p. e1231276, 2016.

[154] M. Liu *et al.*, "Injectable hydrogels for cartilage and bone tissue engineering," *Bone research,* vol. 5, no. 1, pp. 1-20, 2017.

[155] F. Costa, R. Silva, and A. Boccaccini, "Fibrous protein-based biomaterials (silk, keratin, elastin, and resilin proteins) for tissue regeneration and repair," *Peptides and proteins as biomaterials for tissue regeneration and repair*, pp. 175-204, 2018.

[156] D. P. Bhattarai, L. E. Aguilar, C. H. Park, and C. S. Kim, "A review on properties of natural and synthetic based electrospun fibrous materials for bone tissue engineering," *Membranes,* vol. 8, no. 3, p. 62, 2018.

[157] A. P. Tiwari, M. K. Joshi, C. H. Park, and C. S. Kim, "Nano-nets covered composite nanofibers with enhanced biocompatibility and mechanical properties for bone tissue engineering," *Journal of nanoscience and nanotechnology,* vol. 18, no. 1, pp. 529-537, 2018.

[158] M. Carrabba and P. Madeddu, "Current strategies for the manufacture of small size tissue engineering vascular grafts," *Frontiers in bioengineering and biotechnology,* vol. 6, p. 41, 2018.

[159] R. M. Domingues, S. Chiera, P. Gershovich, A. Motta, R. L. Reis, and M. E. Gomes, "Fabrication of anisotropically aligned nanofibrous scaffolds based on natural/synthetic polymer blends reinforced with cellulose nanocrystals for tendon tissue engineering," *Front. Bioeng. Biotechnol,* vol. 4, 2016.

[160] K. Sun, H. Li, R. Li, Z. Nian, D. Li, and C. Xu, "Silk fibroin/collagen and silk fibroin/chitosan blended three-dimensional scaffolds for tissue engineering," *European Journal of Orthopaedic Surgery & Traumatology,* vol. 25, no. 2, pp. 243-249, 2015.

[161] A. P. Tiwari *et al.*, "Heterogeneous electrospun polycaprolactone/polyethylene glycol membranes with improved wettability, biocompatibility, and mineralization," *Colloids and Surfaces A: Physicochemical and Engineering Aspects,* vol. 520, pp. 105-113, 2017.

[162] Q. Yao *et al.*, "Three dimensional electrospun PCL/PLA blend nanofibrous scaffolds with significantly improved stem cells osteogenic differentiation and cranial bone formation," *Biomaterials,* vol. 115, pp. 115-127, 2017.

[163] P. Gentile, V. Chiono, I. Carmagnola, and P. V. Hatton, "An overview of poly (lactic-co-glycolic) acid (PLGA)-based biomaterials for bone tissue engineering," *International journal of molecular sciences,* vol. 15, no. 3, pp. 3640-3659, 2014.

[164] M. Singhvi, S. Zinjarde, and D. Gokhale, "Polylactic acid: synthesis and biomedical applications," *Journal of applied microbiology,* vol. 127, no. 6, pp. 1612-1626, 2019.

[165] K. A. Athanasiou, G. G. Niederauer, and C. M. Agrawal, "Sterilization, toxicity, biocompatibility and clinical applications of polylactic acid/polyglycolic acid copolymers," *Biomaterials,* vol. 17, no. 2, pp. 93-102, 1996.

[166] Z. Yuan *et al.*, "Synergistic mediation of tumor signaling pathways in hepatocellular carcinoma therapy via dual-drug-loaded pH-responsive electrospun fibrous scaffolds," (in eng), *Journal of materials chemistry. B,* vol. 3, no. 17, pp. 3436-3446, May 7 2015, doi: 10.1039/c5tb00206k.

[167] T. J. Sill and H. A. Von Recum, "Electrospinning: applications in drug delivery and tissue engineering," *Biomaterials,* vol. 29, no. 13, pp. 1989-2006, 2008.

[168] A. Haider, S. Haider, and I.-K. Kang, "A comprehensive review summarizing the effect of electrospinning parameters and potential applications of nanofibers in biomedical and biotechnology," *Arabian Journal of Chemistry,* vol. 11, no. 8, pp. 1165-1188, 2018.

[169] J. M. Deitzel, J. Kleinmeyer, D. Harris, and N. B. Tan, "The effect of processing variables on the morphology of electrospun nanofibers and textiles," *Polymer,* vol. 42, no. 1, pp. 261-272, 2001.

[170] K. Matabola and R. Moutloali, "The influence of electrospinning parameters on the morphology and diameter of poly (vinyledene fluoride) nanofibers-effect of sodium chloride," *Journal of Materials Science,* vol. 48, no. 16, pp. 5475-5482, 2013.

[171] S. Megelski, J. S. Stephens, D. B. Chase, and J. F. Rabolt, "Micro-and nanostructured surface morphology on electrospun polymer fibers," *Macromolecules,* vol. 35, no. 22, pp. 8456-8466, 2002.

[172] S. Haider *et al.*, "Highly aligned narrow diameter chitosan electrospun nanofibers," *Journal of Polymer Research,* vol. 20, no. 4, pp. 1-11, 2013.

[173] V. Pillay *et al.*, "A review of the effect of processing variables on the fabrication of electrospun nanofibers for drug delivery applications," *Journal of Nanomaterials,* vol. 2013, 2013.

[174] R. E. Benavides, S. C. Jana, and D. H. Reneker, "Nanofibers from scalable gas jet process," *ACS Macro Letters,* vol. 1, no. 8, pp. 1032-1036, 2012.

[175] W. K. Son, J. H. Youk, T. S. Lee, and W. H. Park, "The effects of solution properties and polyelectrolyte on electrospinning of ultrafine poly (ethylene oxide) fibers," *polymer,* vol. 45, no. 9, pp. 2959-2966, 2004.

[176] A. G. Kanani and S. H. Bahrami, "Effect of changing solvents on poly (ε-caprolactone) nanofibrous webs morphology," *J. Nanomater,* vol. 2011, no. 724153, pp. 1-724153, 2011.

[177] J. Lannutti, D. Reneker, T. Ma, D. Tomasko, and D. Farson, "Electrospinning for tissue engineering scaffolds," *Materials Science and Engineering: C,* vol. 27, no. 3, pp. 504-509, 2007.

[178] W. Zuo, M. Zhu, W. Yang, H. Yu, Y. Chen, and Y. Zhang, "Experimental study on relationship between jet instability and formation of beaded fibers during electrospinning," *Polymer Engineering & Science,* vol. 45, no. 5, pp. 704-709, 2005.

[179] S. Huan *et al.*, "Effect of experimental parameters on morphological, mechanical and hydrophobic properties of electrospun polystyrene fibers," *Materials,* vol. 8, no. 5, pp. 2718-2734, 2015.

[180] J. Pelipenko, J. Kristl, B. Janković, S. Baumgartner, and P. Kocbek, "The impact of relative humidity during electrospinning on the morphology and mechanical properties of nanofibers," *International journal of pharmaceutics,* vol. 456, no. 1, pp. 125-134, 2013.

[181] C. L. Casper, J. S. Stephens, N. G. Tassi, D. B. Chase, and J. F. Rabolt, "Controlling surface morphology of electrospun polystyrene fibers: effect of humidity and molecular

weight in the electrospinning process," *Macromolecules,* vol. 37, no. 2, pp. 573-578, 2004.

[182] S. De Vrieze, T. Van Camp, A. Nelvig, B. Hagström, P. Westbroek, and K. De Clerck, "The effect of temperature and humidity on electrospinning," *Journal of materials science,* vol. 44, no. 5, pp. 1357-1362, 2009.

[183] J.-Y. Park and I.-H. Lee, "Relative humidity effect on the preparation of porous electrospun polystyrene fibers," *Journal of nanoscience and nanotechnology,* vol. 10, no. 5, pp. 3473-3477, 2010.

[184] H.-S. Bae, A. Haider, K. Selim, D.-Y. Kang, E.-J. Kim, and I.-K. Kang, "Fabrication of highly porous PMMA electrospun fibers and their application in the removal of phenol and iodine," *Journal of Polymer Research,* vol. 20, no. 7, pp. 1-7, 2013.

[185] J. L. Lowery, N. Datta, and G. C. Rutledge, "Effect of fiber diameter, pore size and seeding method on growth of human dermal fibroblasts in electrospun poly (ε-caprolactone) fibrous mats," *Biomaterials,* vol. 31, no. 3, pp. 491-504, 2010.

[186] A. S. Badami, M. R. Kreke, M. S. Thompson, J. S. Riffle, and A. S. Goldstein, "Effect of fiber diameter on spreading, proliferation, and differentiation of osteoblastic cells on electrospun poly (lactic acid) substrates," *Biomaterials,* vol. 27, no. 4, pp. 596-606, 2006.

[187] G. T. Christopherson, H. Song, and H.-Q. Mao, "The influence of fiber diameter of electrospun substrates on neural stem cell differentiation and proliferation," *Biomaterials,* vol. 30, no. 4, pp. 556-564, 2009.

[188] A. Lopez Marquez, I. E. Gareis, F. J. Dias, C. Gerhard, and M. F. Lezcano, "How Fiber Surface Topography Affects Interactions between Cells and Electrospun Scaffolds: A Systematic Review," *Polymers,* vol. 14, no. 1, p. 209, 2022.

[189] M. Chen, P. K. Patra, M. L. Lovett, D. L. Kaplan, and S. Bhowmick, "Role of electrospun fibre diameter and corresponding specific surface area (SSA) on cell attachment," *Journal of Tissue Engineering and Regenerative Medicine,* vol. 3, no. 4, pp. 269-279, 2009.

[190] B. M. Whited and M. N. Rylander, "The influence of electrospun scaffold topography on endothelial cell morphology, alignment, and adhesion in response to fluid flow," *Biotechnology and bioengineering,* vol. 111, no. 1, pp. 184-195, 2014.

[191] S. G. Kumbar, S. P. Nukavarapu, R. James, L. S. Nair, and C. T. Laurencin, "Electrospun poly (lactic acid-co-glycolic acid) scaffolds for skin tissue engineering," *Biomaterials,* vol. 29, no. 30, pp. 4100-4107, 2008.

[192] S. De Valence *et al.*, "Advantages of bilayered vascular grafts for surgical applicability and tissue regeneration," *Acta biomaterialia,* vol. 8, no. 11, pp. 3914-3920, 2012.

[193] J. Zhao, H. Qiu, D.-l. Chen, W.-x. Zhang, D.-c. Zhang, and M. Li, "Development of nanofibrous scaffolds for vascular tissue engineering," *International journal of biological macromolecules,* vol. 56, pp. 106-113, 2013.

[194] C. Huang, S. Wang, L. Qiu, Q. Ke, W. Zhai, and X. Mo, "Heparin loading and pre-endothelialization in enhancing the patency rate of electrospun small-diameter vascular

grafts in a canine model," *ACS applied materials & interfaces,* vol. 5, no. 6, pp. 2220-2226, 2013.

[195] M. Norouzi, S. M. Boroujeni, N. Omidvarkordshouli, and M. Soleimani, "Advances in skin regeneration: application of electrospun scaffolds," *Advanced healthcare materials,* vol. 4, no. 8, pp. 1114-1133, 2015.

[196] E. D. Boland, T. A. Telemeco, D. G. Simpson, G. E. Wnek, and G. L. Bowlin, "Utilizing acid pretreatment and electrospinning to improve biocompatibility of poly (glycolic acid) for tissue engineering," *Journal of Biomedical Materials Research Part B: Applied Biomaterials: An Official Journal of The Society for Biomaterials, The Japanese Society for Biomaterials, and The Australian Society for Biomaterials and the Korean Society for Biomaterials,* vol. 71, no. 1, pp. 144-152, 2004.

[197] E. Tanzli and A. Ehrmann, "Electrospun nanofibrous membranes for tissue engineering and cell growth," *Applied Sciences,* vol. 11, no. 15, p. 6929, 2021.

[198] A. K. Gaharwar, M. Nikkhah, S. Sant, and A. Khademhosseini, "Anisotropic poly (glycerol sebacate)-poly (ϵ-caprolactone) electrospun fibers promote endothelial cell guidance," *Biofabrication,* vol. 7, no. 1, p. 015001, 2014.

[199] D. E. Heath, J. J. Lannutti, and S. L. Cooper, "Electrospun scaffold topography affects endothelial cell proliferation, metabolic activity, and morphology," *Journal of Biomedical Materials Research Part A,* vol. 94, no. 4, pp. 1195-1204, 2010.

[200] M. Doostmohammadi, H. Forootanfar, and S. Ramakrishna, "New Strategies for Safe Cancer Therapy Using Electrospun Nanofibers: A Short Review," *Mini reviews in medicinal chemistry,* vol. 20, no. 13, pp. 1272-1286, 2020.

[201] M. Cavo, F. Serio, N. R. Kale, E. D'Amone, G. Gigli, and L. Loretta, "Electrospun nanofibers in cancer research: from engineering of in vitro 3D cancer models to therapy," *Biomaterials Science,* vol. 8, no. 18, pp. 4887-4905, 2020.

[202] T. Hussain, S. Ramakrishna, and S. Abid, "Nanofibrous drug delivery systems for breast cancer: a review," *Nanotechnology,* 2021.

[203] P. I. Soares and J. P. Borges, "Recent advances in magnetic electrospun nanofibers for cancer theranostics application," *Progress in Natural Science: Materials International,* 2021.

[204] B. Pant, M. Park, and S.-J. Park, "Drug delivery applications of core-sheath nanofibers prepared by coaxial electrospinning: A review," *Pharmaceutics,* vol. 11, no. 7, p. 305, 2019.

[205] X. Shan, C. Liu, F. Li, C. Ouyang, Q. Gao, and K. Zheng, "Nanoparticles vs. nanofibers: a comparison of two drug delivery systems on assessing drug release performance in vitro," *Designed Monomers and Polymers,* vol. 18, no. 7, pp. 678-689, 2015.

[206] U. Akpan *et al.*, "Prodigiosin-loaded electrospun nanofibers scaffold for localized treatment of triple negative breast cancer," *Materials Science and Engineering: C,* vol. 114, p. 110976, 2020.

[207] M. H. Jouybari, S. Hosseini, K. Mahboobnia, L. A. Boloursaz, M. Moradi, and M. Irani, "Simultaneous controlled release of 5-FU, DOX and PTX from chitosan/PLA/5-FU/g-C3N4-DOX/g-C3N4-PTX triaxial nanofibers for breast cancer treatment in vitro," *Colloids and Surfaces B: Biointerfaces,* vol. 179, pp. 495-504, 2019.

[208] R. Sedghi, M. Gholami, A. Shaabani, M. Saber, and H. Niknejad, "Preparation of novel chitosan derivative nanofibers for prevention of breast cancer recurrence," *European Polymer Journal,* vol. 123, p. 109421, 2020.

[209] Y. J. Kim, M. Ebara, and T. Aoyagi, "A smart hyperthermia nanofiber with switchable drug release for inducing cancer apoptosis," *Advanced Functional Materials,* vol. 23, no. 46, pp. 5753-5761, 2013.

[210] G.-D. Fu, L.-Q. Xu, F. Yao, G.-L. Li, and E.-T. Kang, "Smart nanofibers with a photoresponsive surface for controlled release," *ACS applied materials & interfaces,* vol. 1, no. 11, pp. 2424-2427, 2009.

[211] S. Saha, X. Duan, L. Wu, P.-K. Lo, H. Chen, and Q. Wang, "Electrospun fibrous scaffolds promote breast cancer cell alignment and epithelial–mesenchymal transition," *Langmuir,* vol. 28, no. 4, pp. 2028-2034, 2012.

[212] K. Guiro, S. A. Patel, S. J. Greco, P. Rameshwar, and T. L. Arinzeh, "Investigating breast cancer cell behavior using tissue engineering scaffolds," *PloS one,* vol. 10, no. 4, p. e0118724, 2015.

[213] Y. K. Girard *et al.*, "A 3D fibrous scaffold inducing tumoroids: a platform for anticancer drug development," *PloS one,* vol. 8, no. 10, p. e75345, 2013.

[214] T.-E. Kim *et al.*, "Three-dimensional culture and interaction of cancer cells and dendritic cells in an electrospun nano-submicron hybrid fibrous scaffold," *International journal of nanomedicine,* vol. 11, p. 823, 2016.

[215] Y.-J. Kim, H.-I. Bae, O. K. Kwon, and M.-S. Choi, "Three-dimensional gastric cancer cell culture using nanofiber scaffold for chemosensitivity test," *International journal of biological macromolecules,* vol. 45, no. 1, pp. 65-71, 2009.

[216] O. Hartman *et al.*, "Biofunctionalization of electrospun PCL-based scaffolds with perlecan domain IV peptide to create a 3-D pharmacokinetic cancer model," *Biomaterials,* vol. 31, no. 21, pp. 5700-5718, 2010.

[217] H. Rangaswami, A. Bulbule, and G. C. Kundu, "Osteopontin: role in cell signaling and cancer progression," *Trends in cell biology,* vol. 16, no. 2, pp. 79-87, 2006.

[218] J.-H. Zhang *et al.*, "Over-expression of bone sialoprotein enhances bone metastasis of human breast cancer cells in a mouse model," *International journal of oncology,* vol. 23, no. 4, pp. 1043-1048, 2003.

[219] E. L. S. Fong *et al.*, "Modeling Ewing sarcoma tumors in vitro with 3D scaffolds," *Proceedings of the National Academy of Sciences,* vol. 110, no. 16, pp. 6500-6505, 2013.

[220] M. Santoro, S.-E. Lamhamedi-Cherradi, B. A. Menegaz, J. A. Ludwig, and A. G. Mikos, "Flow perfusion effects on three-dimensional culture and drug sensitivity of Ewing

sarcoma," *Proceedings of the National Academy of Sciences,* vol. 112, no. 33, pp. 10304-10309, 2015.

[221] M. Tirrell, E. Kokkoli, and M. Biesalski, "The role of surface science in bioengineered materials," *Surface Science,* vol. 500, no. 1-3, pp. 61-83, 2002.

[222] S. Yoshida, K. Hagiwara, T. Hasebe, and A. Hotta, "Surface modification of polymers by plasma treatments for the enhancement of biocompatibility and controlled drug release," *Surface and Coatings Technology,* vol. 233, pp. 99-107, 2013.

[223] H. Chen, L. Yuan, W. Song, Z. Wu, and D. Li, "Biocompatible polymer materials: role of protein–surface interactions," *Progress in Polymer Science,* vol. 33, no. 11, pp. 1059-1087, 2008.

[224] N. R. Richbourg, N. A. Peppas, and V. I. Sikavitsas, "Tuning the biomimetic behavior of scaffolds for regenerative medicine through surface modifications," *Journal of tissue engineering and regenerative medicine,* vol. 13, no. 8, pp. 1275-1293, 2019.

[225] T. Desmet, R. Morent, N. De Geyter, C. Leys, E. Schacht, and P. Dubruel, "Nonthermal plasma technology as a versatile strategy for polymeric biomaterials surface modification: a review," *Biomacromolecules,* vol. 10, no. 9, pp. 2351-2378, 2009.

[226] P. K. Chu, "Surface engineering and modification of biomaterials," *Thin Solid Films,* vol. 528, pp. 93-105, 2013.

[227] R. Förch *et al.*, "Recent and expected roles of plasma-polymerized films for biomedical applications," *Chemical Vapor Deposition,* vol. 13, no. 6-7, pp. 280-294, 2007.

[228] G. Wu, P. Li, H. Feng, X. Zhang, and P. K. Chu, "Engineering and functionalization of biomaterials via surface modification," *Journal of Materials Chemistry B,* vol. 3, no. 10, pp. 2024-2042, 2015.

[229] M. C. Boivin, P. Chevallier, S. Turgeon, J. Lagueux, and G. Laroche, "Micropatterning polymer materials to improve endothelialization," in *Advanced Materials Research,* 2012, vol. 409: Trans Tech Publ, pp. 777-782.

[230] J. H. Collier and T. Segura, "Evolving the use of peptides as components of biomaterials," *Biomaterials,* vol. 32, no. 18, pp. 4198-4204, 2011.

[231] C. A. Hoesli, A. Garnier, P.-M. Juneau, P. Chevallier, C. Duchesne, and G. Laroche, "A fluorophore-tagged RGD peptide to control endothelial cell adhesion to micropatterned surfaces," *Biomaterials,* vol. 35, no. 3, pp. 879-890, 2014.

[232] A. Hadjizadeh, A. Ajji, and M. N. Bureau, "Preparation and characterization of NaOH treated micro-fibrous polyethylene terephthalate nonwovens for biomedical application," *Journal of the mechanical behavior of biomedical materials,* vol. 3, no. 8, pp. 574-583, 2010.

[233] H. Savoji, D. Rana, T. Matsuura, S. Tabe, and C. Feng, "Development of plasma and/or chemically induced graft co-polymerized electrospun poly (vinylidene fluoride) membranes for solute separation," *Separation and Purification Technology,* vol. 108, pp. 196-204, 2013.

[234] Z. Ma, Y. Guan, X. Liu, and H. Liu, "Synthesis of magnetic chelator for high-capacity immobilized metal affinity adsorption of protein by cerium initiated graft polymerization," *Langmuir,* vol. 21, no. 15, pp. 6987-6994, 2005.

[235] P. Cools, N. De Geyter, and R. Morent, *Plasma modified textiles for biomedical applications*. Intech, 2015.

[236] F. S. Denes and S. Manolache, "Macromolecular plasma-chemistry: an emerging field of polymer science," *Progress in polymer science,* vol. 29, no. 8, pp. 815-885, 2004.

[237] N. Inagaki, *Plasma surface modification and plasma polymerization*. CRC Press, 1996.

[238] K. R. Kull, M. L. Steen, and E. R. Fisher, "Surface modification with nitrogen-containing plasmas to produce hydrophilic, low-fouling membranes," *Journal of membrane science,* vol. 246, no. 2, pp. 203-215, 2005.

[239] R. Morent, N. De Geyter, T. Desmet, P. Dubruel, and C. Leys, "Plasma Surface Modification of Biodegradable Polymers: A Review," *Plasma Processes and Polymers,* vol. 8, no. 3, pp. 171-190, 2011, doi: 10.1002/ppap.201000153.

[240] E. Liston, L. Martinu, and M. Wertheimer, "Plasma surface modification of polymers for improved adhesion: a critical review," *Journal of adhesion science and technology,* vol. 7, no. 10, pp. 1091-1127, 1993.

[241] N. De Geyter, R. Morent, and C. Leys, "Influence of ambient conditions on the ageing behaviour of plasma-treated PET surfaces," *Nuclear Instruments and Methods in Physics Research Section B: Beam Interactions with Materials and Atoms,* vol. 266, no. 12-13, pp. 3086-3090, 2008.

[242] S. Guimond and M. R. Wertheimer, "Surface degradation and hydrophobic recovery of polyolefins treated by air corona and nitrogen atmospheric pressure glow discharge," *Journal of Applied Polymer Science,* vol. 94, no. 3, pp. 1291-1303, 2004.

[243] T. Jacobs, R. Morent, N. De Geyter, P. Dubruel, and C. Leys, "Plasma surface modification of biomedical polymers: influence on cell-material interaction," *Plasma chemistry and plasma processing,* vol. 32, no. 5, pp. 1039-1073, 2012.

[244] H. S. Yoo, T. G. Kim, and T. G. Park, "Surface-functionalized electrospun nanofibers for tissue engineering and drug delivery," *Advanced drug delivery reviews,* vol. 61, no. 12, pp. 1033-1042, 2009.

[245] V. M. Donnelly and A. Kornblit, "Plasma etching: Yesterday, today, and tomorrow," *Journal of Vacuum Science & Technology A: Vacuum, Surfaces, and Films,* vol. 31, no. 5, p. 050825, 2013.

[246] N. Gomathi, A. Sureshkumar, and S. Neogi, "RF plasma-treated polymers for biomedical applications," *Current science,* pp. 1478-1486, 2008.

[247] P. L. Girard-Lauriault, F. Mwale, M. Iordanova, C. Demers, P. Desjardins, and M. R. Wertheimer, "Atmospheric pressure deposition of micropatterned nitrogen-rich plasma-polymer films for tissue engineering," *Plasma Processes and Polymers,* vol. 2, no. 3, pp. 263-270, 2005.

[248] F. Truica-Marasescu and M. R. Wertheimer, "Nitrogen-rich plasma-polymer films for biomedical applications," *Plasma processes and polymers,* vol. 5, no. 1, pp. 44-57, 2008.

[249] A. Gigout, J. C. Ruiz, M. R. Wertheimer, M. Jolicoeur, and S. Lerouge, "Nitrogen-rich plasma-polymerized coatings on PET and PTFE surfaces improve endothelial cell attachment and resistance to shear flow," *Macromolecular bioscience,* vol. 11, no. 8, pp. 1110-1119, 2011.

[250] P. L. Girard-Lauriault *et al.*, "Adhesion of human U937 monocytes to nitrogen-rich organic thin films: Novel insights into the mechanism of cellular adhesion," *Macromolecular bioscience,* vol. 9, no. 9, pp. 911-921, 2009.

[251] S. Lerouge *et al.*, "Nitrogen-rich coatings for promoting healing around stent-grafts after endovascular aneurysm repair," *Biomaterials,* vol. 28, no. 6, pp. 1209-1217, 2007.

[252] J. C. Ruiz, A. St-Georges-Robillard, C. Thérésy, S. Lerouge, and M. R. Wertheimer, "Fabrication and characterisation of amine-rich organic thin films: Focus on stability," *Plasma Processes and Polymers,* vol. 7, no. 9-10, pp. 737-753, 2010.

[253] A. St-Georges-Robillard *et al.*, "Adhesion of U-937 Monocytes on Different Amine-functionalised Polymer Surfaces," *Plasma Processes and Polymers,* vol. 9, no. 3, pp. 243-252, 2012.

[254] M. R. Wertheimer *et al.*, "Amine-rich organic thin films for cell culture: possible electrostatic effects in cell–surface interactions," *Japanese Journal of Applied Physics,* vol. 51, no. 11S, p. 11PJ04, 2012.

[255] A. Contreras-García and M. R. Wertheimer, "Low-pressure plasma polymerization of acetylene–ammonia mixtures for biomedical applications," *Plasma Chemistry and Plasma Processing,* vol. 33, no. 1, pp. 147-163, 2013.

[256] C. Charbonneau *et al.*, "Chondroitin sulfate and epidermal growth factor immobilization after plasma polymerization: a versatile anti-apoptotic coating to promote healing around stent grafts," *Macromolecular bioscience,* vol. 12, no. 6, pp. 812-821, 2012.

[257] P. Lequoy *et al.*, "In vitro and pilot in vivo evaluation of a bioactive coating for stent grafts based on chondroitin sulfate and epidermal growth factor," *Journal of Vascular and Interventional Radiology,* vol. 27, no. 5, pp. 753-760. e3, 2016.

[258] N. De Geyter, R. Morent, and C. Leys, "Penetration of a dielectric barrier discharge plasma into textile structures at medium pressure," *Plasma Sources Science and Technology,* vol. 15, no. 1, p. 78, 2006.

[259] J.-P. Chen and C.-H. Su, "Surface modification of electrospun PLLA nanofibers by plasma treatment and cationized gelatin immobilization for cartilage tissue engineering," *Acta biomaterialia,* vol. 7, no. 1, pp. 234-243, 2011.

[260] C. Sarra-Bournet, S. Turgeon, D. Mantovani, and G. Laroche, "Comparison of atmospheric-pressure plasma versus low-pressure RF plasma for surface functionalization of PTFE for biomedical applications," *Plasma Processes and Polymers,* vol. 3, no. 6-7, pp. 506-515, 2006.

[261] I. Unalan, O. Colpankan, A. Z. Albayrak, C. Gorgun, and A. S. Urkmez, "Biocompatibility of plasma-treated poly (3-hydroxybutyrate-co-3-hydroxyvalerate) nanofiber mats modified by silk fibroin for bone tissue regeneration," *Materials Science and Engineering: C*, vol. 68, pp. 842-850, 2016.

[262] E. Stoleru, M. C. Baican, A. Coroaba, G. E. Hitruc, M. Lungu, and C. Vasile, "Plasma-activated fibrinogen coatings onto poly (vinylidene fluoride) surface for improving biocompatibility with tissues," *Journal of Bioactive and Compatible Polymers*, vol. 31, no. 1, pp. 91-108, 2016.

[263] K. Park, Y. M. Ju, J. S. Son, K.-D. Ahn, and D. K. Han, "Surface modification of biodegradable electrospun nanofiber scaffolds and their interaction with fibroblasts," *Journal of Biomaterials Science, Polymer Edition*, vol. 18, no. 4, pp. 369-382, 2007.

[264] S. François, N. Chakfé, B. Durand, and G. Laroche, "A poly (L-lactic acid) nanofibre mesh scaffold for endothelial cells on vascular prostheses," *Acta Biomaterialia*, vol. 5, no. 7, pp. 2418-2428, 2009.

[265] X. Zhu, K. S. Chian, M. B. E. Chan-Park, and S. T. Lee, "Effect of argon-plasma treatment on proliferation of human-skin–derived fibroblast on chitosan membrane in vitro," *Journal of Biomedical Materials Research Part A: An Official Journal of The Society for Biomaterials, The Japanese Society for Biomaterials, and The Australian Society for Biomaterials and the Korean Society for Biomaterials*, vol. 73, no. 3, pp. 264-274, 2005.

[266] S. Siri, P. Wadbua, V. Amornkitbamrung, N. Kampa, and S. Maensiri, "Surface modification of electrospun PCL scaffolds by plasma treatment and addition of adhesive protein to promote fibroblast cell adhesion," *Materials Science and Technology*, vol. 26, no. 11, pp. 1292-1297, 2010.

[267] Z. Ma, M. Kotaki, T. Yong, W. He, and S. Ramakrishna, "Surface engineering of electrospun polyethylene terephthalate (PET) nanofibers towards development of a new material for blood vessel engineering," *Biomaterials*, vol. 26, no. 15, pp. 2527-2536, 2005.

[268] R. Wyrwa *et al.*, "Design of plasma surface-activated, electrospun polylactide non-wovens with improved cell acceptance," *Advanced Engineering Materials*, vol. 13, no. 5, pp. B165-B171, 2011.

[269] K. A. Meade *et al.*, "Immobilization of Heparan Sulfate on Electrospun Meshes to Support Embryonic Stem Cell Culture and Differentiation*[S]," *Journal of Biological Chemistry*, vol. 288, no. 8, pp. 5530-5538, 2013.

[270] H. Savoji, A. Hadjizadeh, M. Maire, A. Ajji, M. R. Wertheimer, and S. Lerouge, "Electrospun Nanofiber Scaffolds and Plasma Polymerization: A Promising Combination Towards Complete, Stable Endothelial Lining for Vascular Grafts," vol. 14, no. 8, pp. 1084-1095, 2014, doi: https://doi.org/10.1002/mabi.201300545.

[271] H. Savoji *et al.*, "Combining Electrospun Fiber Mats and Bioactive Coatings for Vascular Graft Prostheses," *Biomacromolecules*, vol. 18, no. 1, pp. 303-310, Jan 9 2017, doi: 10.1021/acs.biomac.6b01770.

[272] M. Bouchet, "Conception et évaluation in vivo de prothèses vasculaires compliantes de petit diamètre par électrofilage avec revêtement bioactif," École de technologie supérieure, 2020.

[273] C. S. Hughes, L. M. Postovit, and G. A. Lajoie, "Matrigel: a complex protein mixture required for optimal growth of cell culture," *Proteomics,* vol. 10, no. 9, pp. 1886-90, May 2010, doi: 10.1002/pmic.200900758.

[274] G. Benton, I. Arnaoutova, J. George, H. K. Kleinman, and J. Koblinski, "Matrigel: from discovery and ECM mimicry to assays and models for cancer research," *Advanced drug delivery reviews,* vol. 79, pp. 3-18, 2014.

[275] G. Benton, H. K. Kleinman, J. George, and I. Arnaoutova, "Multiple uses of basement membrane-like matrix (BME/Matrigel) in vitro and in vivo with cancer cells," *International journal of cancer,* vol. 128, no. 8, pp. 1751-1757, 2011.

[276] M. Czerwinski and J. R. Spence, "Hacking the matrix," *Cell stem cell,* vol. 20, no. 1, pp. 9-10, 2017.

[277] H. Savoji, S. Lerouge, A. Ajji, and M. R. Wertheimer, "Plasma-etching for controlled modification of structural and mechanical properties of electrospun PET scaffolds," *Plasma Processes and Polymers,* vol. 12, no. 4, pp. 314-327, 2015.

[278] S. de Valence *et al.*, "Advantages of bilayered vascular grafts for surgical applicability and tissue regeneration," *Acta Biomater,* vol. 8, no. 11, pp. 3914-20, Nov 2012, doi: 10.1016/j.actbio.2012.06.035.

[279] C. V. Rajadurai *et al.*, "5'-Inositol phosphatase SHIP2 recruits Mena to stabilize invadopodia for cancer cell invasion," *J Cell Biol,* vol. 214, no. 6, pp. 719-34, Sep 12 2016, doi: 10.1083/jcb.201501003.

[280] S. Flores-Torres *et al.*, "Alginate-gelatin-Matrigel hydrogels enable the development and multigenerational passaging of patient-derived 3D bioprinted cancer spheroid models," *Biofabrication,* vol. 13, no. 2, p. 025001, Mar 10 2021, doi: 10.1088/1758-5090/abdb87.

[281] C. Zhou *et al.*, "Electrospun bio-nanocomposite scaffolds for bone tissue engineering by cellulose nanocrystals reinforcing maleic anhydride grafted PLA," *ACS Appl Mater Interfaces,* vol. 5, no. 9, pp. 3847-54, May 2013, doi: 10.1021/am4005072.

[282] E. Polonio-Alcala *et al.*, "PLA Electrospun Scaffolds for Three-Dimensional Triple-Negative Breast Cancer Cell Culture," (in English), *Polymers,* vol. 11, no. 5, May 2019, doi: ARTN 91610.3390/polym11050916.

[283] L. Binan, C. Tendey, G. De Crescenzo, R. El Ayoubi, A. Ajji, and M. Jolicoeur, "Differentiation of neuronal stem cells into motor neurons using electrospun poly-L-lactic acid/gelatin scaffold," *Biomaterials,* vol. 35, no. 2, pp. 664-74, Jan 2014, doi: 10.1016/j.biomaterials.2013.09.097.

[284] A. Hadjizadeh, A. Ajji, M. Jolicoeur, B. Liberelle, and G. De Crescenzo, "Effects of electrospun nanostructure versus microstructure on human aortic endothelial cell behavior," *J Biomed Nanotechnol,* vol. 9, no. 7, pp. 1195-209, Jul 2013, doi: 10.1166/jbn.2013.1622.

[285] P. R. C. Tornello, P. C. Caracciolo, T. R. Cuadrado, and G. A. Abraham, "Structural characterization of electrospun micro/nanofibrous scaffolds by liquid extrusion porosimetry: a comparison with other techniques," *Materials Science and Engineering: C,* vol. 41, pp. 335-342, 2014.

[286] S. Soliman, S. Sant, J. W. Nichol, M. Khabiry, E. Traversa, and A. Khademhosseini, "Controlling the porosity of fibrous scaffolds by modulating the fiber diameter and packing density," *Journal of Biomedical Materials Research Part A,* vol. 96, no. 3, pp. 566-574, 2011.

[287] A. M. Andrew, "NANOMEDICINE, VOLUME 1: BASIC CAPABILITIES, by Robert A. Freitas Jr., Landes Bioscience, Austin, Texas, 1999, xxi+ 509 pp., ISBN 1-57059-645-X Index (Hardback, $89.000)," *Robotica,* vol. 18, no. 6, pp. 687-689, 2000.

[288] S. Connolly, K. McGourty, and D. Newport, "The in vitro inertial positions and viability of cells in suspension under different in vivo flow conditions," *Scientific reports,* vol. 10, no. 1, pp. 1-13, 2020.

[289] P. Ahangar, M. Aziz, D. H. Rosenzweig, and M. H. Weber, "Advances in personalized treatment of metastatic spine disease," (in English), *Ann Transl Med,* vol. 7, no. 10, May 2019, doi: ARTN 22310.21037/atm.2019.04.41.

[290] Y. Tertyshnaya, S. Karpova, M. Moskovskiy, and A. Dorokhov, "Electrospun Polylactide/Natural Rubber Fibers: Effect Natural Rubber Content on Fiber Morphology and Properties," *Polymers,* vol. 13, no. 14, p. 2232, 2021.

[291] A. R. Cho *et al.*, "Effect of annealing on the crystallization and properties of electrospun polylatic acid and nylon 6 fibers," *Journal of applied polymer science,* vol. 120, no. 2, pp. 752-758, 2011.

[292] N. Stoyanova *et al.*, "Poly (L-lactide) and poly (butylene succinate) immiscible blends: From electrospinning to biologically active materials," *Materials Science and Engineering: C,* vol. 41, pp. 119-126, 2014.

[293] S. Gao *et al.*, "Fabrication and characterization of electrospun nanofibers composed of decellularized meniscus extracellular matrix and polycaprolactone for meniscus tissue engineering," *Journal of Materials Chemistry B,* vol. 5, no. 12, pp. 2273-2285, 2017.

[294] N. Jirofti, D. Mohebbi-Kalhori, A. Samimi, A. Hadjizadeh, and G. H. Kazemzadeh, "Fabrication and characterization of a novel compliant small-diameter PET/PU/PCL triad-hybrid vascular graft," *Biomedical Materials,* vol. 15, no. 5, p. 055004, 2020.

[295] S. Saudi *et al.*, "Nanonet-nano fiber electrospun mesh of PCL–chitosan for controlled and extended release of diclofenac sodium," *Nanoscale,* vol. 12, no. 46, pp. 23556-23569, 2020.

[296] R. Sen *et al.*, "Preparation of single-walled carbon nanotube reinforced polystyrene and polyurethane nanofibers and membranes by electrospinning," *Nano letters,* vol. 4, no. 3, pp. 459-464, 2004.

[297] S. Bahrami, A. Solouk, H. Mirzadeh, and A. M. Seifalian, "Electroconductive polyurethane/graphene nanocomposite for biomedical applications," *Composites Part B: Engineering,* vol. 168, pp. 421-431, 2019.

[298] Z. E. Zadeh, A. Solouk, M. Shafieian, and M. H. Nazarpak, "Electrospun polyurethane/carbon nanotube composites with different amounts of carbon nanotubes and almost the same fiber diameter for biomedical applications," *Materials Science and Engineering: C,* vol. 118, p. 111403, 2021.

[299] S.-A. Kim, E. K. Lee, and H.-J. Kuh, "Co-culture of 3D tumor spheroids with fibroblasts as a model for epithelial–mesenchymal transition in vitro," *Experimental cell research,* vol. 335, no. 2, pp. 187-196, 2015.

[300] C. Arrigoni, S. Bersini, M. Gilardi, and M. Moretti, "In Vitro Co-Culture Models of Breast Cancer Metastatic Progression towards Bone," *Int J Mol Sci,* vol. 17, no. 9, p. 1405, Aug 25 2016, doi: 10.3390/ijms17091405.

[301] H. Dolznig *et al.*, "Modeling colon adenocarcinomas in vitro: A 3D co-culture system induces cancer-relevant pathways upon tumor cell and stromal fibroblast interaction," *The American journal of pathology,* vol. 179, no. 1, pp. 487-501, 2011.

[302] T. Ishiguro, H. Ohata, A. Sato, K. Yamawaki, T. Enomoto, and K. Okamoto, "Tumor-derived spheroids: Relevance to cancer stem cells and clinical applications," *Cancer Sci,* vol. 108, no. 3, pp. 283-289, Mar 2017, doi: 10.1111/cas.13155.

[303] T. Q. Huang, X. Qu, J. Liu, and S. Chen, "3D printing of biomimetic microstructures for cancer cell migration," *Biomedical microdevices,* vol. 16, no. 1, pp. 127-132, 2014.

[304] C. Zhu, L. He, X. Zhou, X. Nie, and Y. Gu, "Sulfatase 2 promotes breast cancer progression through regulating some tumor-related factors," *Oncology reports,* vol. 35, no. 3, pp. 1318-1328, 2016.

[305] S. Bersini *et al.*, "A microfluidic 3D in vitro model for specificity of breast cancer metastasis to bone," *Biomaterials,* vol. 35, no. 8, pp. 2454-2461, 2014.

[306] C. S. Shin, B. Kwak, B. Han, and K. Park, "Development of an in vitro 3D tumor model to study therapeutic efficiency of an anticancer drug," *Molecular pharmaceutics,* vol. 10, no. 6, pp. 2167-2175, 2013.

[307] S. Hao *et al.*, "A Spontaneous 3D bone-on-a-chip for bone metastasis study of breast cancer cells," *Small,* vol. 14, no. 12, p. 1702787, 2018.

[308] G. Rijal and W. Li, "A versatile 3D tissue matrix scaffold system for tumor modeling and drug screening," *Science advances,* vol. 3, no. 9, p. e1700764, 2017.

[309] S. Pradhan, J. M. Clary, D. Seliktar, and E. A. Lipke, "A three-dimensional spheroidal cancer model based on PEG-fibrinogen hydrogel microspheres," *Biomaterials,* vol. 115, pp. 141-154, 2017.

[310] J. L. Horning *et al.*, "3-D tumor model for in vitro evaluation of anticancer drugs," *Molecular pharmaceutics,* vol. 5, no. 5, pp. 849-862, 2008.

[311] S. Talukdar and S. C. Kundu, "Engineered 3D silk-based metastasis models: Interactions between human breast adenocarcinoma, mesenchymal stem cells and osteoblast-like cells," *Advanced functional materials,* vol. 23, no. 42, pp. 5249-5260, 2013.

[312] B. Subia, T. Dey, S. Sharma, and S. C. Kundu, "Target specific delivery of anticancer drug in silk fibroin based 3D distribution model of bone–breast cancer cells," *ACS applied materials & interfaces,* vol. 7, no. 4, pp. 2269-2279, 2015.

[313] S. Kar, D. R. Katti, and K. S. Katti, "Bone interface modulates drug resistance in breast cancer bone metastasis," *Colloids and Surfaces B: Biointerfaces,* vol. 195, p. 111224, 2020.

[314] M. Vandenbossche and D. Hegemann, "Recent approaches to reduce aging phenomena in oxygen-and nitrogen-containing plasma polymer films: An overview," *Current Opinion in Solid State and Materials Science,* vol. 22, no. 1, pp. 26-38, 2018.

[315] G. Boespflug, M. Maire, G. De Crescenzo, S. Lerouge, and M. R. Wertheimer, "Characterization and comparison of N-, O-, and N+ O-functionalized polymer surfaces for efficient (HUVEC) endothelial cell colonization," *Plasma Processes and Polymers,* vol. 14, no. 7, p. 1600139, 2017.

[316] B. Nisol, S. Watson, S. Lerouge, and M. R. Wertheimer, "Energetics of reactions in a dielectric barrier discharge with argon carrier gas: IV ethyl lactate," *Plasma Processes and Polymers,* vol. 13, no. 10, pp. 965-969, 2016.

[317] M. Wang, J. E. Foster, and M. J. Kushner, "Plasma propagation through porous dielectric sheets," *IEEE Transactions on Plasma Science,* vol. 39, no. 11, pp. 2244-2245, 2011.

[318] B. Nisol, H. Gagnon, S. Lerouge, and M. R. Wertheimer, "Energy of Reactions in Atmospheric-Pressure Plasma Polymerization with Inert Carrier Gas," *Plasma Processes and Polymers,* vol. 13, no. 3, pp. 366-374, 2016.

[319] D. L. Holliday and V. Speirs, "Choosing the right cell line for breast cancer research," *Breast cancer research,* vol. 13, no. 4, pp. 1-7, 2011.

[320] X. Dai, H. Cheng, Z. Bai, and J. Li, "Breast cancer cell line classification and its relevance with breast tumor subtyping," *Journal of Cancer,* vol. 8, no. 16, p. 3131, 2017.

[321] X. J. Fang, H. Jiang, Y. Q. Zhu, L. Y. Zhang, Q. H. Fan, and Y. Tian, "Doxorubicin induces drug resistance and expression of the novel CD44st via NF-κB in human breast cancer MCF-7 cells," *Oncology reports,* vol. 31, no. 6, pp. 2735-2742, 2014.

[322] M. Domingos *et al.*, "Improved osteoblast cell affinity on plasma-modified 3-D extruded PCL scaffolds," *Acta biomaterialia,* vol. 9, no. 4, pp. 5997-6005, 2013.

[323] B. D. Ratner, A. S. Hoffman, F. J. Schoen, and J. E. Lemons, *Biomaterials science: an introduction to materials in medicine*. Elsevier, 2004.

[324] B. D. Ratner, "A pore way to heal and regenerate: 21st century thinking on biocompatibility," *Regenerative biomaterials,* vol. 3, no. 2, pp. 107-110, 2016.

[325] M. Jia, N. Souchelnytskyi, U. Hellman, M. O'Hare, P. S. Jat, and S. Souchelnytskyi, "Proteome profiling of immortalization-to-senescence transition of human breast

epithelial cells identified MAP2K3 as a senescence-promoting protein which is downregulated in human breast cancer," *PROTEOMICS–Clinical Applications,* vol. 4, no. 10-11, pp. 816-828, 2010.

[326] R. E. Coleman, "Skeletal complications of malignancy," *Cancer,* vol. 80, no. 8 Suppl, pp. 1588-94, Oct 15 1997, doi: 10.1002/(sici)1097-0142(19971015)80:8+<1588::aid-cncr9>3.3.co;2-z.

[327] E. Akoury *et al.*, "Low-dose zoledronate for the treatment of bone metastasis secondary to prostate cancer," *Cancer Cell International,* vol. 19, no. 1, pp. 1-11, 2019.

[328] E. Akoury, P. Ahangar, A. S. R. Luna, A. Nour, M. Weber, and D. Rosenzweig, "3D-PRINTED SCAFFOLDS LOADED WITH THERAPEUTICS FOR THE TREATMENT OF BONE METASTASES," in *Orthopaedic Proceedings,* 2020, vol. 102, no. SUPP_7: The British Editorial Society of Bone & Joint Surgery, pp. 101-101.

[329] E. Akoury *et al.*, "Anti-tumor effects of low dose zoledronate on lung cancer-induced spine metastasis," *Journal of clinical medicine,* vol. 8, no. 8, p. 1212, 2019.

[330] E. Akoury, M. H. Weber, and D. H. Rosenzweig, "3D-Printed nanoporous scaffolds impregnated with zoledronate for the treatment of spinal bone metastases," *MRS Advances,* vol. 4, no. 21, pp. 1245-1251, 2019.

[331] P. Ahangar, M. Aziz, D. H. Rosenzweig, and M. H. Weber, "Advances in personalized treatment of metastatic spine disease," *Ann Transl Med,* vol. 7, no. 10, p. 223, May 2019, doi: 10.21037/atm.2019.04.41.

[332] D. Liu *et al.*, "Prognosis of prostate cancer and bone metastasis pattern of patients: a SEER-based study and a local hospital based study from China," *Scientific reports,* vol. 10, no. 1, pp. 1-11, 2020.

[333] P. Krzyszczyk *et al.*, "The growing role of precision and personalized medicine for cancer treatment," *Technology,* vol. 6, no. 03n04, pp. 79-100, 2018.

[334] F. R. Vogenberg, C. I. Barash, and M. Pursel, "Personalized medicine: part 1: evolution and development into theranostics," *Pharmacy and Therapeutics,* vol. 35, no. 10, p. 560, 2010.

[335] K. K. Jain, "Personalized medicine," *Current opinion in molecular therapeutics,* vol. 4, no. 6, pp. 548-558, 2002.

[336] V. Gambardella *et al.*, "Personalized medicine: recent progress in cancer therapy," *Cancers,* vol. 12, no. 4, p. 1009, 2020.

[337] G. A. Van Norman, "Limitations of animal studies for predicting toxicity in clinical trials: is it time to rethink our current approach?," *JACC: Basic to Translational Science,* vol. 4, no. 7, pp. 845-854, 2019.

[338] X. Ma *et al.*, "3D bioprinting of functional tissue models for personalized drug screening and in vitro disease modeling," *Advanced drug delivery reviews,* vol. 132, pp. 235-251, 2018.

[339] E. Maloney *et al.*, "Immersion bioprinting of tumor organoids in multi-well plates for increasing chemotherapy screening throughput," *Micromachines,* vol. 11, no. 2, p. 208, 2020.

[340] S. Mao *et al.*, "Bioprinting of in vitro tumor models for personalized cancer treatment: a review," *Biofabrication,* vol. 12, no. 4, p. 042001, 2020.

[341] J. Nie, Q. Gao, J. Fu, and Y. He, "Grafting of 3D bioprinting to in vitro drug screening: a review," *Advanced healthcare materials,* vol. 9, no. 7, p. 1901773, 2020.

[342] M. Takasato *et al.*, "Kidney organoids from human iPS cells contain multiple lineages and model human nephrogenesis," *Nature,* vol. 526, no. 7574, pp. 564-568, 2015.

[343] J. F. Dekkers *et al.*, "A functional CFTR assay using primary cystic fibrosis intestinal organoids," *Nature medicine,* vol. 19, no. 7, pp. 939-945, 2013.

[344] A. D. Gracz *et al.*, "A high-throughput platform for stem cell niche co-cultures and downstream gene expression analysis," *Nature cell biology,* vol. 17, no. 3, pp. 340-349, 2015.

[345] X. Xu, M. C. Farach-Carson, and X. Jia, "Three-dimensional in vitro tumor models for cancer research and drug evaluation," *Biotechnology advances,* vol. 32, no. 7, pp. 1256-1268, 2014.

[346] M. Stadler *et al.*, "Increased complexity in carcinomas: Analyzing and modeling the interaction of human cancer cells with their microenvironment," in *Seminars in Cancer Biology*, 2015, vol. 35: Elsevier, pp. 107-124.

[347] C. Pauli *et al.*, "Personalized in vitro and in vivo cancer models to guide precision medicine," *Cancer discovery,* vol. 7, no. 5, pp. 462-477, 2017.

[348] F. Weeber, S. N. Ooft, K. K. Dijkstra, and E. E. Voest, "Tumor organoids as a pre-clinical cancer model for drug discovery," *Cell chemical biology,* vol. 24, no. 9, pp. 1092-1100, 2017.

[349] M. van de Wetering *et al.*, "Prospective derivation of a living organoid biobank of colorectal cancer patients," *Cell,* vol. 161, no. 4, pp. 933-945, 2015.

[350] M. Shang, R. H. Soon, C. T. Lim, B. L. Khoo, and J. Han, "Microfluidic modelling of the tumor microenvironment for anti-cancer drug development," *Lab on a Chip,* vol. 19, no. 3, pp. 369-386, 2019.

[351] N. Alépée *et al.*, "t4 workshop report: State-of-the-art of 3D cultures (organs-on-a-chip) in safety testing and pathophysiology," *Altex,* vol. 31, no. 4, p. 441, 2014.

[352] D. Pamies, T. Hartung, and H. T. Hogberg, "Biological and medical applications of a brain-on-a-chip," *Experimental biology and medicine,* vol. 239, no. 9, pp. 1096-1107, 2014.

[353] H. Abaci, Z. Guo, Y. Doucet, J. Jacków, and A. Christiano, "Next generation human skin constructs as advanced tools for drug development," *Experimental Biology and Medicine,* vol. 242, no. 17, pp. 1657-1668, 2017.

[354] Y. Wang *et al.*, "3D bioprinting of breast cancer models for drug resistance study," *ACS Biomaterials Science & Engineering,* vol. 4, no. 12, pp. 4401-4411, 2018.

[355] J. M. Grolman, D. Zhang, A. M. Smith, J. S. Moore, and K. A. Kilian, "Rapid 3D extrusion of synthetic tumor microenvironments," *Advanced Materials,* vol. 27, no. 37, pp. 5512-5517, 2015.

[356] L. L. Bischel, D. J. Beebe, and K. E. Sung, "Microfluidic model of ductal carcinoma in situ with 3D, organotypic structure," *BMC cancer,* vol. 15, no. 1, pp. 1-10, 2015.

[357] Y.-C. Toh, A. Raja, H. Yu, and D. Van Noort, "A 3D microfluidic model to recapitulate cancer cell migration and invasion," *Bioengineering,* vol. 5, no. 2, p. 29, 2018.

[358] Y. Choi *et al.*, "A microengineered pathophysiological model of early-stage breast cancer," *Lab on a Chip,* vol. 15, no. 16, pp. 3350-3357, 2015.

[359] F. Gioiella, F. Urciuolo, G. Imparato, V. Brancato, and P. A. Netti, "An Engineered Breast Cancer Model on a Chip to Replicate ECM-Activation In Vitro during Tumor Progression," *Advanced healthcare materials,* vol. 5, no. 23, pp. 3074-3084, 2016.

[360] J. S. Jeon *et al.*, "Human 3D vascularized organotypic microfluidic assays to study breast cancer cell extravasation," *Proceedings of the National Academy of Sciences,* vol. 112, no. 1, pp. 214-219, 2015.

[361] D. M. van Marion, U. M. Domanska, H. Timmer-Bosscha, and A. M. Walenkamp, "Studying cancer metastasis: existing models, challenges and future perspectives," *Critical reviews in oncology/hematology,* vol. 97, pp. 107-117, 2016.

[362] G. Bahcecioglu, G. Basara, B. W. Ellis, X. Ren, and P. Zorlutuna, "Breast cancer models: Engineering the tumor microenvironment," *Acta biomaterialia,* vol. 106, pp. 1-21, 2020.

[363] J. Pape, M. Emberton, and U. Cheema, "3D Cancer Models: The Need for a Complex Stroma, Compartmentalization and Stiffness," *Frontiers in Bioengineering and Biotechnology,* vol. 9, p. 276, 2021.

[364] P. Datta, M. Dey, Z. Ataie, D. Unutmaz, and I. T. Ozbolat, "3D bioprinting for reconstituting the cancer microenvironment," *NPJ precision oncology,* vol. 4, no. 1, pp. 1-13, 2020.

[365] M. Niepel *et al.*, "Common and cell-type specific responses to anti-cancer drugs revealed by high throughput transcript profiling," *Nature communications,* vol. 8, no. 1, pp. 1-11, 2017.

[366] V. C. Ramani *et al.*, "Chemotherapy induces expression and release of heparanase leading to changes associated with an aggressive tumor phenotype," *Matrix biology,* vol. 55, pp. 22-34, 2016.

[367] L. Sun *et al.*, "MiR-200b and miR-15b regulate chemotherapy-induced epithelial-mesenchymal transition in human tongue cancer cells by targeting BMI1," *Oncogene,* vol. 31, no. 4, pp. 432-445, 2012.

[368] G. S. Karagiannis, J. S. Condeelis, and M. H. Oktay, "Chemotherapy-induced metastasis: molecular mechanisms, clinical manifestations, therapeutic interventions," *Cancer research,* vol. 79, no. 18, pp. 4567-4576, 2019.

[369] H. Lu *et al.*, "Chemotherapy triggers HIF-1–dependent glutathione synthesis and copper chelation that induces the breast cancer stem cell phenotype," *Proceedings of the National Academy of Sciences,* vol. 112, no. 33, pp. E4600-E4609, 2015.

[370] H. Lu *et al.*, "Chemotherapy-induced Ca2+ release stimulates breast cancer stem cell enrichment," *Cell reports,* vol. 18, no. 8, pp. 1946-1957, 2017.

[371] C. A. Tonnessen-Murray *et al.*, "Chemotherapy-induced senescent cancer cells engulf other cells to enhance their survival," *Journal of Cell Biology,* vol. 218, no. 11, pp. 3827-3844, 2019.

[372] S.-C. Lee *et al.*, "Chemotherapy-induced tumor gene expression changes in human breast cancers," *Pharmacogenetics and genomics,* vol. 19, no. 3, pp. 181-192, 2009.

[373] Q. Li *et al.*, "Involvement of NF-κB/miR-448 regulatory feedback loop in chemotherapy-induced epithelial–mesenchymal transition of breast cancer cells," *Cell Death & Differentiation,* vol. 18, no. 1, pp. 16-25, 2011.

[374] R. Kalluri and R. A. Weinberg, "The basics of epithelial-mesenchymal transition," *The Journal of clinical investigation,* vol. 119, no. 6, pp. 1420-1428, 2009.

[375] S. Heerboth *et al.*, "EMT and tumor metastasis," *Clinical and translational medicine,* vol. 4, no. 1, pp. 1-13, 2015.

[376] M. Zeisberg and E. G. Neilson, "Biomarkers for epithelial-mesenchymal transitions," *The Journal of clinical investigation,* vol. 119, no. 6, pp. 1429-1437, 2009.

[377] P. T. Nguyen, Y. Kudo, M. Yoshida, N. Kamata, I. Ogawa, and T. Takata, "N-cadherin expression is involved in malignant behavior of head and neck cancer in relation to epithelial-mesenchymal transition," *Histology and histopathology, Vol. 26, nº 2 (2011),* 2011.

[378] Z. Ye, M. Zhou, B. Tian, B. Wu, and J. Li, "Expression of lncRNA-CCAT1, E-cadherin and N-cadherin in colorectal cancer and its clinical significance," *International journal of clinical and experimental medicine,* vol. 8, no. 3, p. 3707, 2015.

[379] C.-Y. Loh *et al.*, "The E-cadherin and N-cadherin switch in epithelial-to-mesenchymal transition: signaling, therapeutic implications, and challenges," *Cells,* vol. 8, no. 10, p. 1118, 2019.

[380] C.-Y. Liu, H.-H. Lin, M.-J. Tang, and Y.-K. Wang, "Vimentin contributes to epithelial-mesenchymal transition cancer cell mechanics by mediating cytoskeletal organization and focal adhesion maturation," *Oncotarget,* vol. 6, no. 18, p. 15966, 2015.

[381] B. Li *et al.*, "Fibronectin 1 promotes melanoma proliferation and metastasis by inhibiting apoptosis and regulating EMT," *OncoTargets and therapy,* vol. 12, p. 3207, 2019.

[382] N. Yang, L. Hui, Y. Wang, H. Yang, and X. Jiang, "Overexpression of SOX2 promotes migration, invasion, and epithelial-mesenchymal transition through the Wnt/β-catenin

pathway in laryngeal cancer Hep-2 cells," *Tumor Biology,* vol. 35, no. 8, pp. 7965-7973, 2014.

[383] Q.-Q. Zhu, C. Ma, Q. Wang, Y. Song, and T. Lv, "The role of TWIST1 in epithelial-mesenchymal transition and cancers," *Tumor Biology,* vol. 37, no. 1, pp. 185-197, 2016.

[384] A. M. Haslehurst *et al.*, "EMT transcription factors snail and slug directly contribute to cisplatin resistance in ovarian cancer," *BMC cancer,* vol. 12, no. 1, pp. 1-10, 2012.

[385] P. Zhang, Y. Sun, and L. Ma, "ZEB1: at the crossroads of epithelial-mesenchymal transition, metastasis and therapy resistance," *Cell cycle,* vol. 14, no. 4, pp. 481-487, 2015.

[386] Y. L. Chao, C. R. Shepard, and A. Wells, "Breast carcinoma cells re-express E-cadherin during mesenchymal to epithelial reverting transition," *Molecular cancer,* vol. 9, no. 1, pp. 1-18, 2010.

[387] M. K. Jolly, K. E. Ware, S. Gilja, J. A. Somarelli, and H. Levine, "EMT and MET: necessary or permissive for metastasis?," *Molecular oncology,* vol. 11, no. 7, pp. 755-769, 2017.

[388] A. Hadjizadeh, A. Ajji, M. Jolicoeur, B. Liberelle, and G. De Crescenzo, "Effects of electrospun nanostructure versus microstructure on human aortic endothelial cell behavior," *Journal of biomedical nanotechnology,* vol. 9, no. 7, pp. 1195-1209, 2013.

[389] X. Liu, Q. Feng, A. Bachhuka, and K. Vasilev, "Surface modification by allylamine plasma polymerization promotes osteogenic differentiation of human adipose-derived stem cells," *ACS applied materials & interfaces,* vol. 6, no. 12, pp. 9733-9741, 2014.

[390] H. Testrich, H. Rebl, B. Finke, F. Hempel, B. Nebe, and J. Meichsner, "Aging effects of plasma polymerized ethylenediamine (PPEDA) thin films on cell-adhesive implant coatings," *Materials Science and Engineering: C,* vol. 33, no. 7, pp. 3875-3880, 2013.

[391] M. Ramiasa *et al.*, "Plasma polymerised polyoxazoline thin films for biomedical applications," *Chemical Communications,* vol. 51, no. 20, pp. 4279-4282, 2015.

APPENDIX A SUPPLEMENTARY DATA

Table 8.1 Process parameters applied to fabricate electrospun mats

Materials		Process Parameters				Collector	Ambient
Mat Type	**Polymer Solution Concentration (%w/v)**	**Needle size (G)**	**Tip-collector Distance (cm)**	**Voltage (kV)**	**Flow rate (ml/hr)**	**Mandrel Velocity (rpm)**	**RH (%)** **Tem. (ºC)**
PLA-Small	14 in TFE	26	20	22	0.6	25	40-50 21-24
PLA-Medium	16 in TFE	21	15	20	1.6	25	40-50 21-24
PLA-Large	19 in TFE	18	15	20	1.5	25	40-50 21-24
PCL-Medium	14 in TFE	21	15	20	1.3	25	40-50 21-24
PU-Medium	12 in THF+DMF	21	15	15	1	25	40-50 21-24

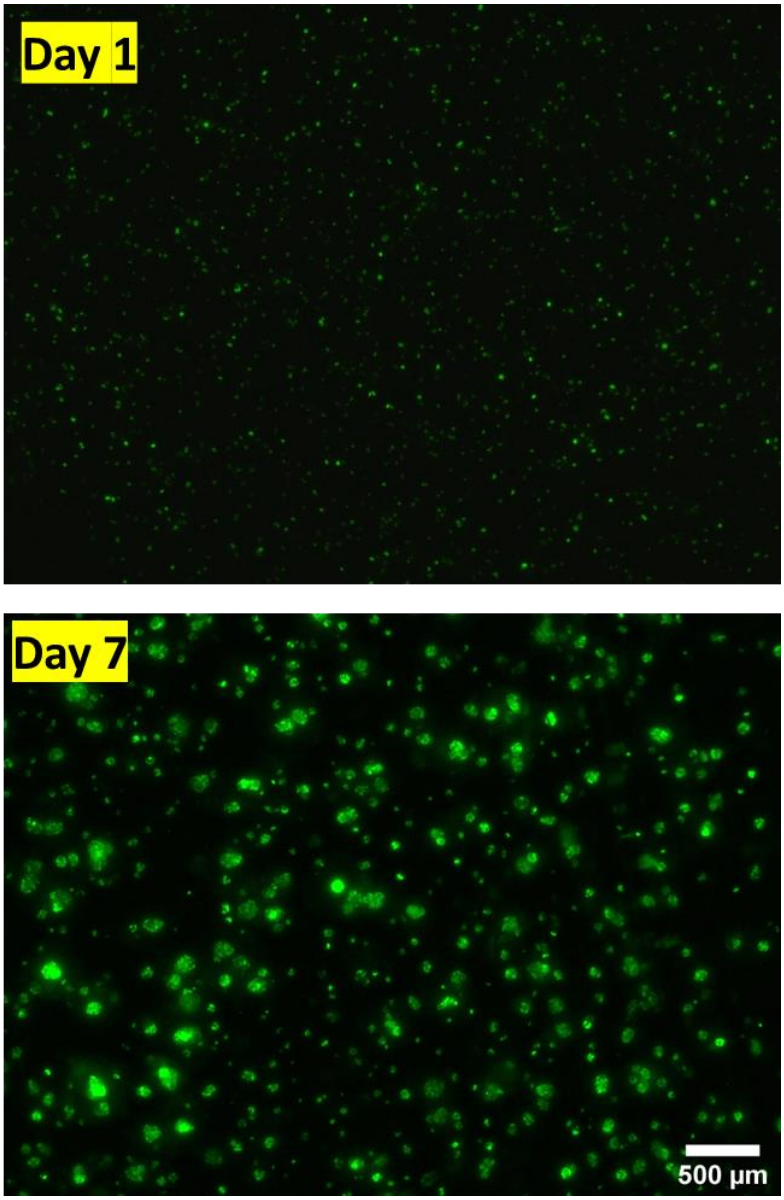

Figure A.1 Spheroid formation in hydrogel over 7 days of culture of MDA-MB 231

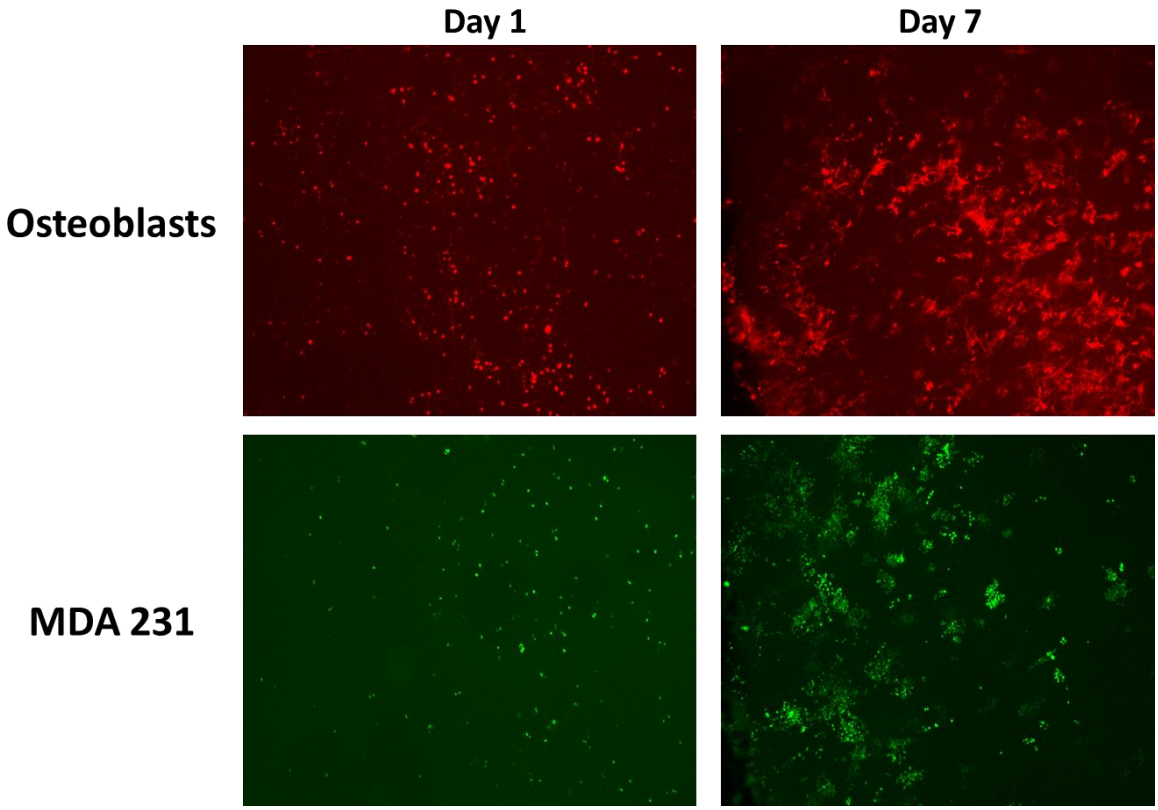

Figure A.2 Cell proliferation over 7 days of culture in plasma-treated PLA electrospun mats

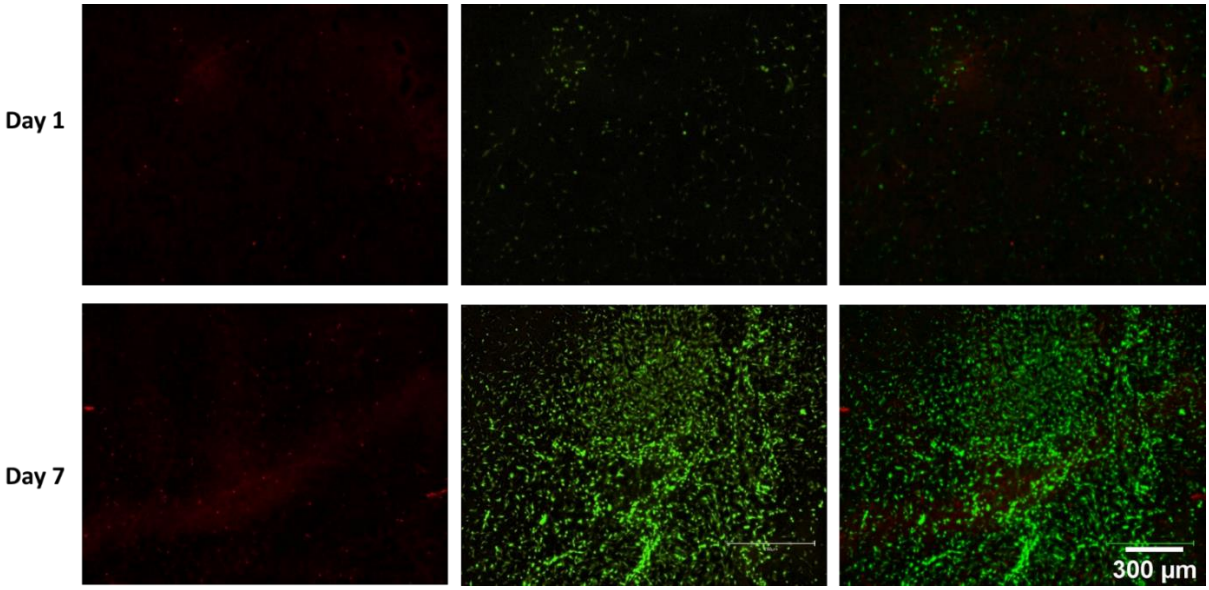

Figure A.3 Live/Dead assay on Osteoblasts culture on NH3 plasma-treated PLA mats over 7 days

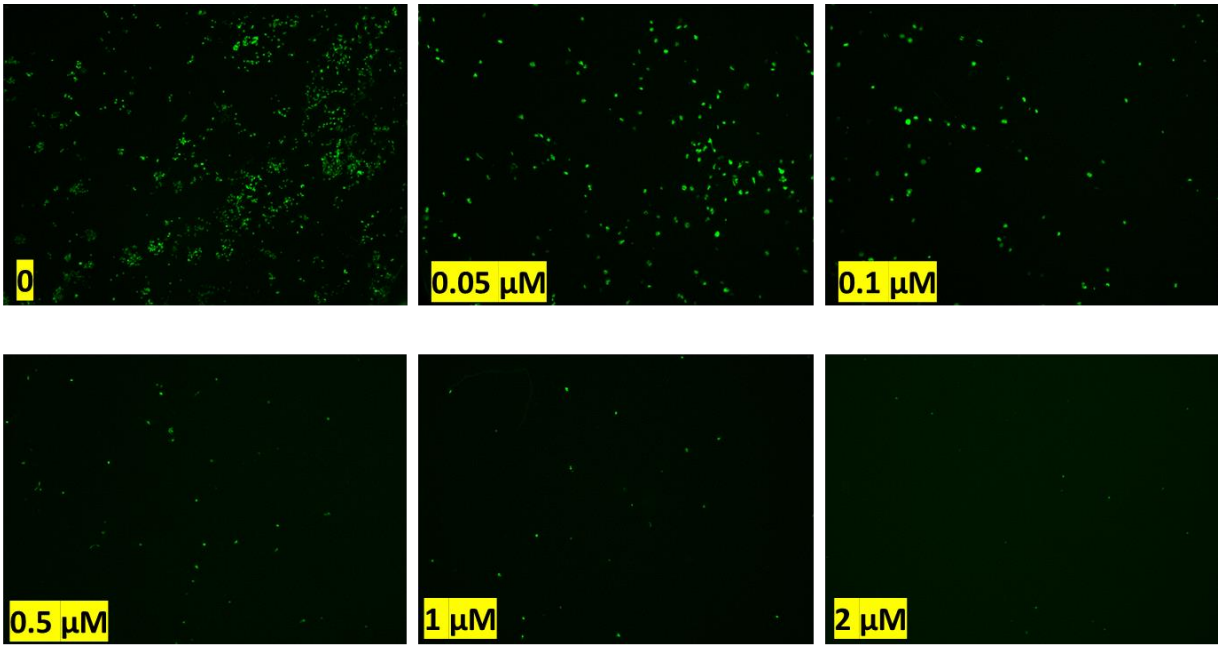

Figure A.4 Effect of Doxorubicin on tumor cell (MDA-MB 231) migration after 5 days

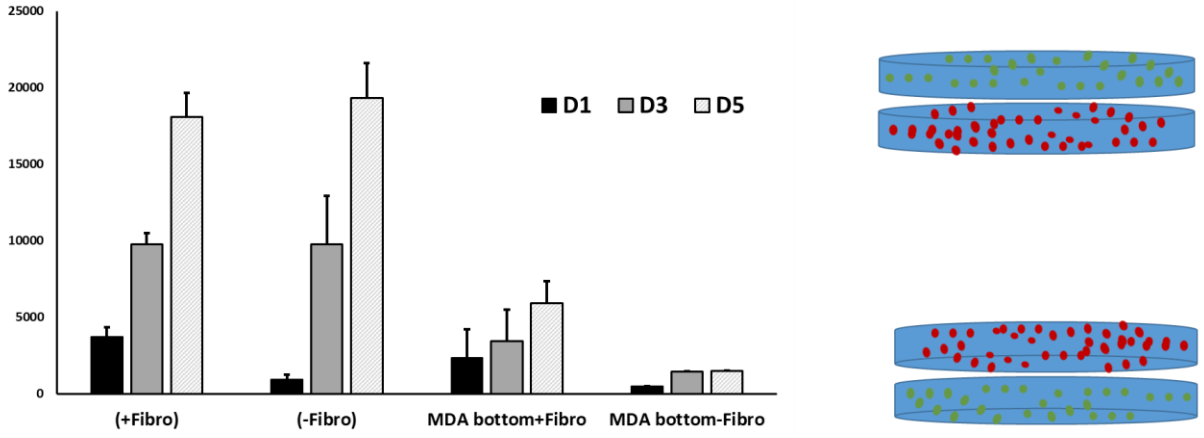

Figure A.5 applying two mats technique to investigate tumor cell (MDA-MB 231) migration across the 3D model (NH3 plasma-treated mats) after 5 days

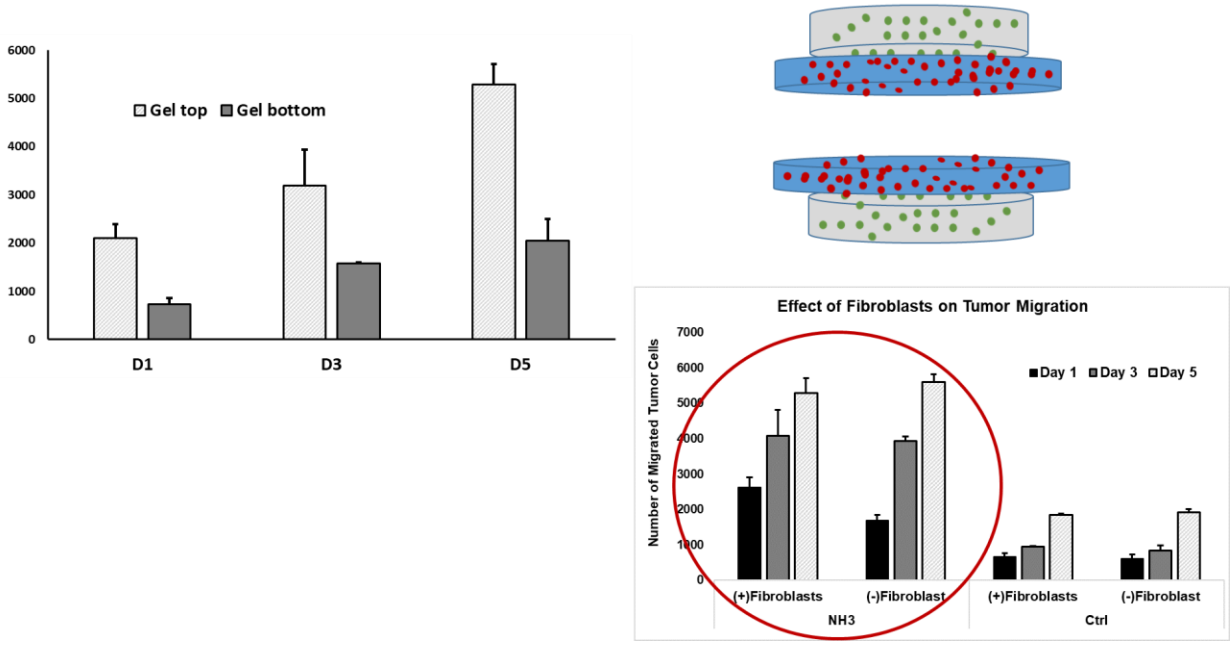

Figure A.6 Effect of gravity and presence/lack of fibroblast on tumor cell (MDA-MB 231) migration by inverting the PP-3D-S model

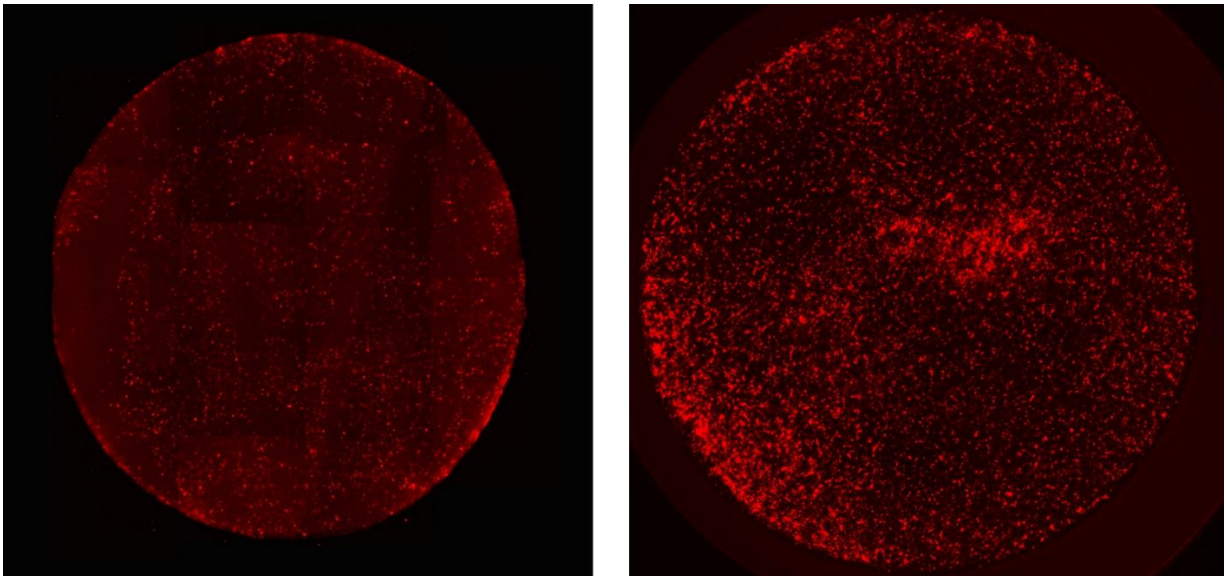

Figure A.7 A representative images of fully covered cell adhesion on the NH3 plasma-treated PLA mats

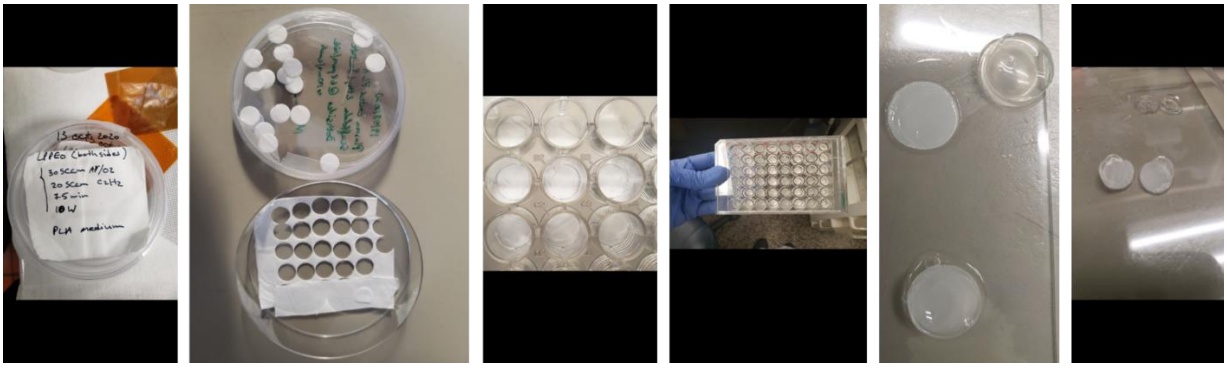

Figure A.8 Photographs of the scaffolds and hydrogels used in this thesis